Bis(N-heterocyclic carbene) carbazolide pincer complexes of s- and p-block metals and related studies

Author:
Buys, Kai

Publication Date:
2017

DOI:
https://doi.org/10.26190/unsworks/19604

UNSW AUSTRALIA

Bis(*N*-Heterocyclic Carbene)Carbazolide Pincer Complexes of *s*- and *p*-Block Metals and Related Studies

A thesis in partial fulfilment of the requirements for the degree of

Doctor of Philosophy (Chemistry)

by

Kai N. Buys

Supervisor: **Assoc. Prof. Marcus L. Cole**

School of Chemistry

The University of New South Wales

Sydney, Australia

April 2017

THE UNIVERSITY OF NEW SOUTH WALES
Thesis/Dissertation Sheet

Surname or Family name: **BUYS**

First name: **KAI** Other name/s: **NICHOLAS**

Abbreviation for degree as given in the University calendar: **PhD**

School: **CHEMISTRY** Faculty: **SCIENCE**

Title: **Bis(N Heterocyclic Carbene)Carbazolide Pincer Complexes of *s*- and *p*-Block Metals and Related Studies**

Abstract 350 words maximum:

This work presents synthetic investigations into main group organometallic chemistry, placing particular emphasis on the study of bis-*N*-heterocyclic carbene (NHC) carbazolide coordination environments. Complexes of high and low oxidation state metals from the *s*- and *p*-blocks were targeted and these comprise the content of the experimental chapters two through five.

Chapter one serves as a general introduction to rationalise the intent of this work. Herein focus is drawn to the nascent field of organometallic main group chemistry in the form of a discussion of its history using pertinent recent examples from the literature.

Chapter two details the synthesis of an emerging class of versatile bis(NHC)carbazolide pincer ligands; bimca^R, and their complexation to *s*-block metals. The development of a new zwitterionic bis(imidazolium)carbazolide proligand is discussed, as well as the structural metrics of new lithium and magnesium bimca^R derivatives. Specifically, a new iodomagnesium complex is probed for its synthetic utility as a ligand-transfer agent and catalytic precursor in conjunction with attempts to access a reduced Mg(I) derivative.

Chapter three focuses on the stabilising effect of the flanking bis(NHC) moieties of bimca^R on high valent group 13 metals and thusly presents a series of exceptionally stable bimca^R supported diiodides from aluminium to thallium. The indium- and thallium diiodides are subjected to iodide-hydride exchange reactions to assess the stability of the resulting dihydrides, whilst efforts are also made to access low valent heavy group 13 congeners.

Chapter four concentrates on the extension of this methodology to accessing heavy low valent group 14 complexes with the aim of creating highly activated metal centres to harness main group redox chemistry. To this end, a number of attempts are made to access low valent tin and lead halides with a view toward accessing the corresponding, highly reactive metallohydrides.

Chapter five presents an alternative approach to accessing such reactive group 14 species with the bulky triazenide ligand class, and thereby details the synthesis and steric characterisation of a new super bulky, unsymmetrical *N*-2,6-terphenyl triazenide ligand.

FOR OFFICE USE ONLY Date of completion of requirements for Award:

Originality Statement

‘I hereby declare that this submission is my own work and to the best of my knowledge it contains no materials previously published or written by another person, or substantial proportions of material which have been accepted for the award of any other degree or diploma at UNSW or any other educational institution, except where due acknowledgement is made in the thesis. Any contribution made to the research by others, with whom I have worked at UNSW or elsewhere, is explicitly acknowledged in the thesis. I also declare that the intellectual content of this thesis is the product of my own work, except to the extent that assistance from others in the project's design and conception or in style, presentation and linguistic expression is acknowledged.’

Signed …….

Date …….

Acknowledgments

My biggest expression of gratitude must go to my supervisor, Marcus Cole, who was always supportive of my work - through thick and thirsty - and in his own way, he has kindly taught me some of life's valuable lessons. Specifically, I must thank him for his patience and guidance in teaching me the delicate arts of wordsmithing and single crystal X-ray diffraction. With regard to the latter, I would also like to acknowledge Mohan Bhadbhade for his uncanny expertise in taming the machine spirits of our, at times, temperamental diffractometer.

To all the residents of the 1003 laboratory, please accept my humble thanks for creating such an animated workplace. Christoph, Pete, Tom, Skimmo, Niamh, and Kirsty, you have exceptional tastes in lifestyle! Sam, know that your help throughout my project was invaluable, especially when I was but a young pup (and thanks for all the free stuff).

I am equally thankful for the truly special opportunity to visit Doris Kunz and her research group at the University of Tübingen. My stay was made all the better by her friendly group members. Special mentions go to Bucki, Eva, Therry, and Domme for welcoming me into their extracurricular mischiefs and odd traditions.

Of course, none of this work would have been possible without the unwavering love of my dear friends and family at home: Pig, Jay, G, and obviously the members of the Super Deluxe Dream Team; Bunk, Bogdan, Thud, and Spicy. Many of you I have known since my very beginning, may we have countless more floats and quick pumps.

Mama and Pops, your ceaseless support often materialised as food and coffee donations, these were always welcome, especially towards the end. Brother dearest, sorry for eating your food during my times of need.

Finally, I would like to thank you, the kind reader, for at least making it this far. *Great job!*

Table of Contents

Abstract

This work presents synthetic investigations into main group organometallic chemistry, placing particular emphasis on the study of bis-*N*-heterocyclic carbene (NHC) carbazolide coordination environments. Complexes of high and low oxidation state metals from the *s*- and *p*-blocks were targeted and these comprise the content of the experimental chapters two through five.

Chapter one serves as a general introduction to rationalise the intent of this work. Herein focus is drawn to the nascent field of organometallic main group chemistry in the form of a discussion of its history using pertinent recent examples from the literature.

Chapter two details the synthesis of an emerging class of versatile bis(NHC)carbazolide pincer ligands; bimca^{R}, and their complexation to *s*-block metals. The development of a new zwitterionic bis(imidazolium)carbazolide proligand is discussed, as well as the structural metrics of new lithium and magnesium bimca^{R} derivatives. Specifically, a new iodomagnesium complex is probed for its synthetic utility as a ligand-transfer agent and catalytic precursor in conjunction with attempts to access a reduced Mg(I) derivative.

Chapter three focuses on the stabilising effect of the flanking bis(NHC) moieties of bimca^{R} on high valent group 13 metals and thusly presents a series of exceptionally stable bimca^{R} supported diiodides from aluminium to thallium. The indium- and thallium diiodides are subjected to iodide-hydride exchange reactions to assess the stability of the resulting dihydrides, whilst efforts are also made to access low valent heavy group 13 congeners.

Chapter four concentrates on the extension of this methodology to accessing heavy low valent group 14 complexes with the aim of creating highly activated metal centres to harness main group redox chemistry. To this end, a number of attempts are made to access low valent tin and lead halides with a view toward accessing the corresponding, highly reactive metallohydrides.

Chapter five presents an alternative approach to accessing such reactive group 14 species with the bulky triazenide ligand class, and thereby details the synthesis and steric characterisation of a new superbulky, unsymmetrical *N*-2,6-terphenyl triazenide ligand.

List of abbreviations

#	Denotes symmetry generated atom
°	Symbol for degrees
7Dipp	1,3-bis(2,6-diisopropylphenyl)-4,5,6,7-tetrahydro-1,3-diazepin-2-ylidene)
A	Symbol for area - in the context of G parameter calculations ($Å^2$)
Å	Symbol for Ångström ($1 \cdot 10^{-10}$ m)
Ac	Acetyl
***a*IDipp**	Abnormally (C4/5) bound IDipp (see IDipp)
Ar	Substituted aryl
Ar'	Shorthand for 2,6-bis(2,6-diisopropylphenyl)phenyl
Ar"	Shorthand for 2,4,6-tri-*tert*-butylphenyl
Ar*	Shorthand for 2,6-bis(2,4,6-triisopropylphenyl)phenyl
Ar$^{\#}$	Shorthand for 2,6-bis(2,4,6-trimethylphenyl)phenyl
atm	Symbol for atmospheres (101325 Pa)
AUD	Australian Dollars
Avg.	Average
bimca^{R}	Shorthand for 3,6-di-*tert*-butyl-1,8-bis(imidazol-2,2'-yliden-1,1'-yl)carbazolide where R = *N*-substituent at both 3,3'-imidazol-2-ylidenyl positions
br	Broad – in the context of NMR data
br	Broad – in the context of IR data
BTEA	Benzyltriethylammonium
BTMA	Benzyltrimethylammonium
°C	Symbol for degrees Celsius
ca.	*circa,* Latin for 'approximately'

Calcd.	Calculated
cf.	*confer*, Latin for ‘compare’
cis	Cisoid
cm	Symbol for centimetre ($1 \cdot 10^{-2}$ m)
cm^{-1}	Symbol for wavenumber (ν/c)
COSY	Correlation spectroscopy
Cp*	Pentamethylcyclopentadienyl
CSD	Cambridge structural database
D	Deuterium
d	Symbol for days
d	Doublet – in the context of NMR data
Δ	Denotes heating in a reaction scheme
δ	Symbol for chemical shift – in the context of NMR data
DBA	Dibenzylideneacetone
DCM	Dichloromethane
dec.	Decomposes
7Dipp	Shorthand for 1,3-bis(2,6- diisopropylphenyl)-4,5,6,7-tetrahydro-1,3-diazepin-2-ylidene)
Dipp	2,6-Diisopropylphenyl
Dipp*	2,6-Dibenzhydryl-4-methylphenyl
DME	Dimethoxyethane
DMF	Dimethylformamide
Dmp	2,6-Dimesitylphenyl
DMSO	Dimethylsulfoxide

d_n	Denotes number of (n) deuterium atoms – in the context of NMR data
E	Element
e.g.	*exempli gratia*, Latin for ‘for example’
eq.	Equivalent(s)
Et	Ethyl
et al.	*et alii*, Latin for ‘and others’
eV	Symbol for electronvolts ($1.602 \cdot 10^{-19}$ J)
eq.	Equivalents
FAB	Fast atom bombardment
fwhm	Full width at half maximum – in the context of NMR data
G	Symbol for the *G* parameter – in the context of *G* parameter calculations
Goof	Goodness-of-fit – in the context of single crystal X-ray diffraction data
h	Symbol for hours
HMBC	Heteronuclear multiple-bond correlation spectroscopy
HMDS	Hexamethyldisilazide
HOMO	Highest occupied molecular orbital
HSQC	Heteronuclear single-quantum correlation spectroscopy
Hz	Symbol for Hertz (s^{-1})
i.e.	*id est*, Latin for ‘it is,’ understood as ‘that is’
IDipp	Shorthand for 1,3-Bis(2,6-diisopropylphenyl)imidazol-2-ylidene
I*i*Pr	Shorthand for 1,3-Bis(diisopropyl)imidazol-2-ylidene
IMe$_4$	Shorthand for 1,3,4,5-tetramethylimidazol-2-ylidene
IMes	Shorthand for 1,3-Bis(2,4,6-trimethylphenyl)imidazol-2-ylidene
in situ	Latin for ‘in place,’ understood as ‘not isolated’ or ‘in the reaction mixture’
in vacuo	Latin for ‘in a vacuum’

***i*Pr**	Isopropyl
IR	Infrared
I*t*Bu	Shorthand for 1,3-Bis-*tert*-butylimidazol-2-ylidene
I*t*BuC$_2$H$_4$I*t*Bu	Shorthand for 1,2-ethylene-3,3'-di-*tert*-butyl-diimidazole-2,2'-diylidene
κ	Denotes binding mode for polydentate ligands
L	General shorthand notation for ligand or specifically a neutral donor ligand
λ	Symbol for wavelength – in the context of single crystal X-ray diffraction data
LA	Lewis acid
LDA	Lithium diisopropyl amide
LEP	Lone electron pair
lit.	Literature value
LUMO	Lowest unoccupied molecular orbital
M	Metal
M	Symbol for Molarity (mol l^{-1})
m	Medium – in the context of IR data
m	Multiplet – in the context of NMR data
m/z	Symbol for mass to charge ratio – in the context of MS data
μ	Symbol for absorption coefficient (mm^{-1}) – in the context of single crystal X-ray diffraction data
μ	Denotes a bridging ligand
MCPBA	*meta*-Chloroperoxybenzoic acid
Me	Methyl
Mes	1,3,5-Trimethylphenyl
MHz	Symbol for megahertz (see Hertz)

min Symbol for minute(s)

mL Symbol for millilitre ($1 \cdot 10^{-3}$ L)

mmol Symbol for millimoles ($1 \cdot 10^{-3}$ mol)

MO Molecular orbital

mp Melting point

MS Mass spectrometry

NacNac Shorthand for *N*-substituted β-diketiminate ligand

NB *Nota bene*, Latin for 'note well'

***n*Bu** *n*-Butyl

NHC *N*-Heterocyclic carbene

NHO *N*-Heterocyclic olefin

$^{n}J_{EE}$ Denotes coupling constant (*J*) of two elements (E) through number of (n) bonds

NMR Nuclear magnetic resonance

NOE Nuclear Overhauser effect

NOESY Nuclear Overhauser effect spectroscopy

O=PR$_3$ *P*-trisubstituted phosphineoxide

OTf Trifluoromethanesulfonate

Ph Phenyl

pK_a Acid dissociation constant

pm Symbol for picometer ($1 \cdot 10^{-12}$ m)

ppm Symbol for parts per million

R Generally an alkyl substituent

r Symbol for radius – in the context of *G* parameter calculations (Å)

r.t. Room temperature

R_f	Retention factor
ρ	Symbol for density (g cm^{-3})
refl.	Reflection – in the context of single crystal X-ray diffraction data
Rock*N_3	Shorthand for the unsymmetrical Dipp*N_3Dmp triazenide
s	Strong – in the context of IR data
s	Singlet – in the context of NMR data
***sec*Bu**	*sec*-Butyl
sept	Septet – in the context of NMR data
sh	Sharp – in the context of IR data
t	Triplet – in the context of NMR data
t	Time – in the context of reaction conditions
***t*Bu**	*tert*-butyl
THF	Tetrahydrofuran
TLC	Thin layer chromatography
TMEDA	*N*,*N*,*N*′,*N*′-Tetramethylethane-1,2-diamine
TOCSY	Total correlation spectroscopy
Tos	*p*-Toluenesulfonate
trans	Transoid
Tripp	2,4,6-Triisopropylphenyl
Trityl	Triphenylmethyl
UV	Ultraviolet
versus	Latin for ‘against’
via	Latin for ‘road,’ understood as ‘by way of’
vide infra	Latin for ‘see below’

vide supra	Latin for ‘see above’
vis-à-vis	French for ‘in relation to’
viz.	*Videlicet*, Latin for ‘namely’
vs.	*versus* (see *versus*)
w	Weak – in the context of IR data
w/v	Shorthand for mass per volume
Ω	Symbol for solid angles – in the context of *G* parameter calculations
X	Halide or pseudo-halide
xs	Excess
Y	Halide

List of Compounds – Chapter 2

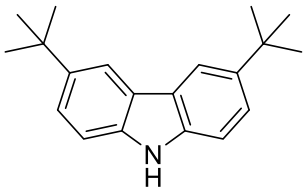

1

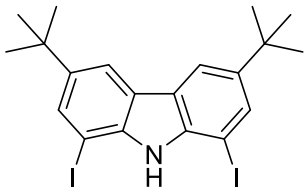

2

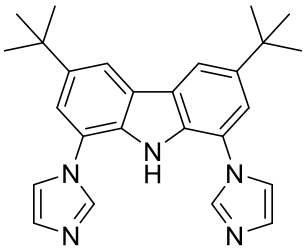

3

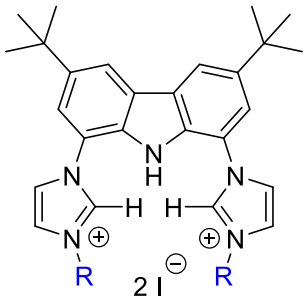

4^{Me}; R = Me
4^{iPr}; R = *i*Pr
4^{Ph}; R = Ph

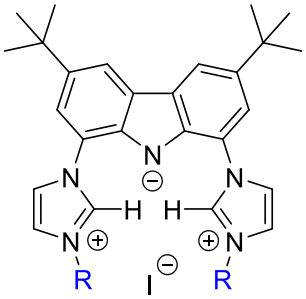

5^{Me}; R = Me
5^{iPr}; R = *i*Pr

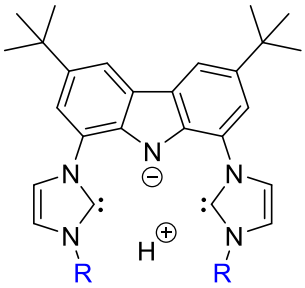

6^{Me}; R = Me
6^{iPr}; R = *i*Pr

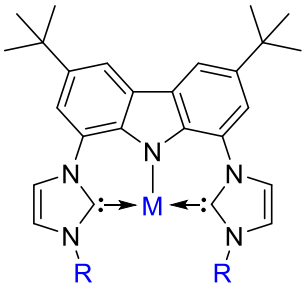

M**7^{Me}**; R = Me
M**7^{iPr}**; R = *i*Pr
(M = Li or K)

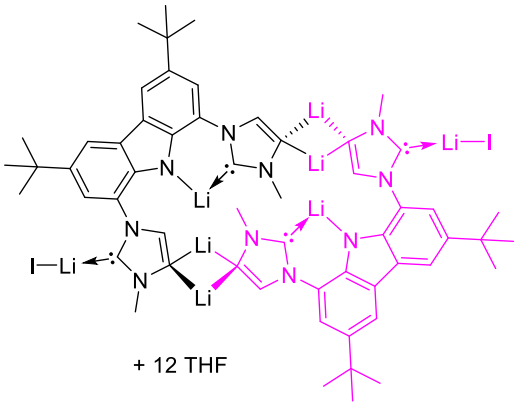

8

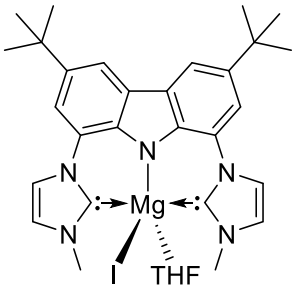

9^{Me}

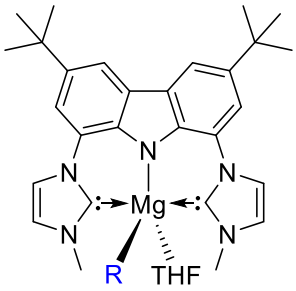

9^{Me}-HMDS; R = HMDS
9^{Me}-N*i*Pr$_2$; R = N*i*Pr$_2$
9^{Me}-OEt; R = OEt
9^{Me}-H; R = H

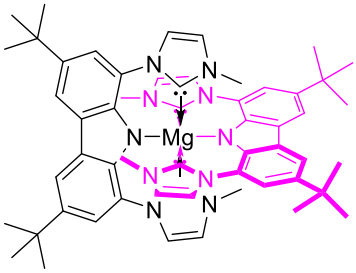

10^{Me}

List of compounds – Chapter 3

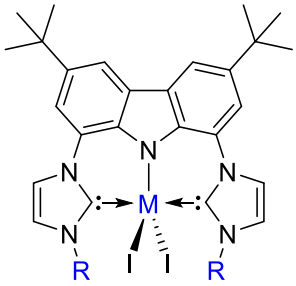

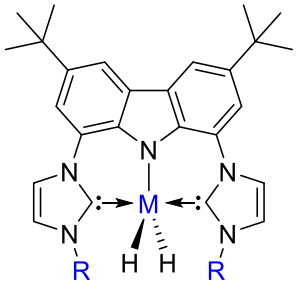

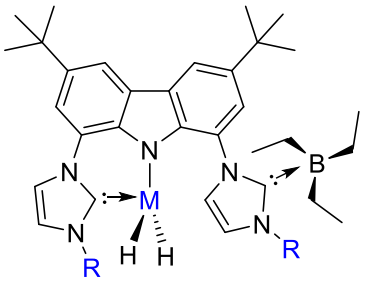

11^{iPr}; M = Al, R = *i*Pr

12^{iPr}; M = Ga, R = *i*Pr
12^{Me}; M = Ga, R = Me

13^{iPr}; M = In, R = *i*Pr
13^{Me}; M = In, R = Me

14^{iPr}; M = Tl, R = *i*Pr
14^{Me}; M = Tl, R = Me

15^{iPr}; M = In, R = *i*Pr
15^{Me}; M = In, R = Me

19^{iPr}; M = Tl, R = *i*Pr
19^{Me}; M = Tl, R = Me

15^{iPr}·BEt_3; M = In, R = *i*Pr
15^{Me}·BEt_3; M = In, R = Me

19^{iPr}·BEt_3; M = Tl, R = *i*Pr
19^{Me}·BEt_3; M = Tl, R = Me

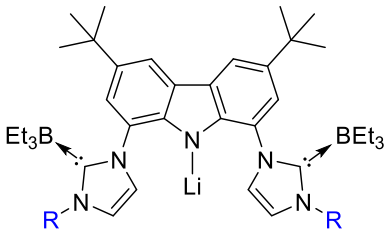

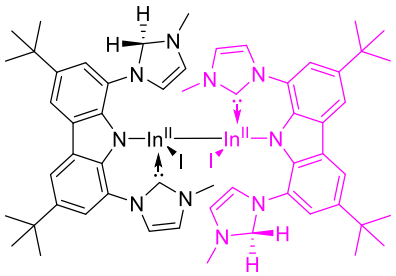

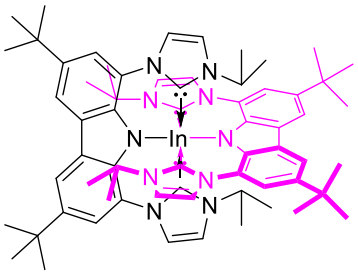

16^{iPr}; R = *i*Pr
16^{Me}; R = Me

17

18

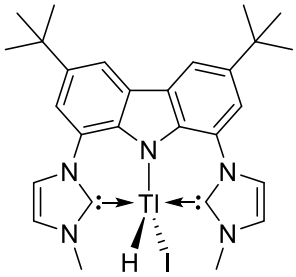

20^{Me}

List of compounds – Chapter 4

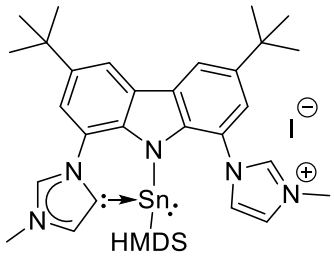

21^{Me}

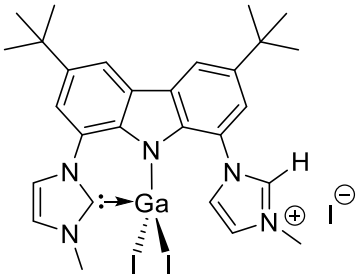

22^{Me}

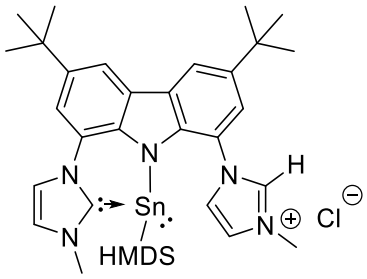

23^{Me}

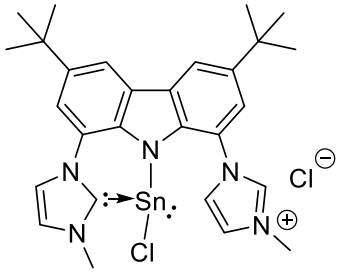

24^{Me}

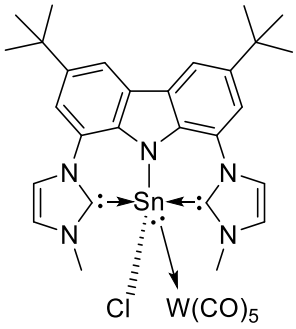

25^{Me}

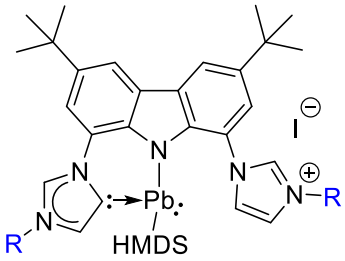

26^{iPr}; R = *i*Pr
26^{Me}; R = Me

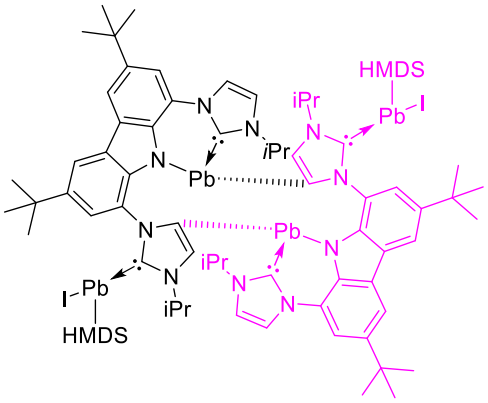

27^{iPr}

List of compounds – Chapter 5

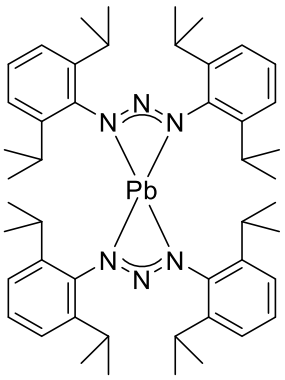

28

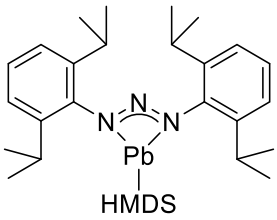

29

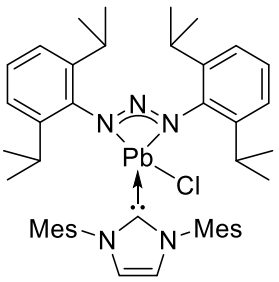

30

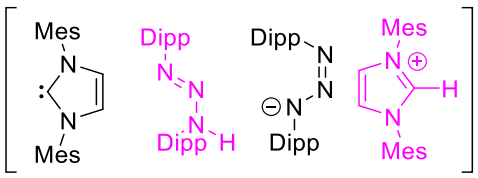

31

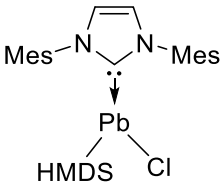

32

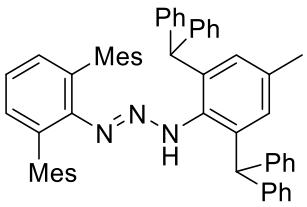

33

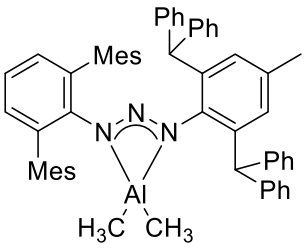

34

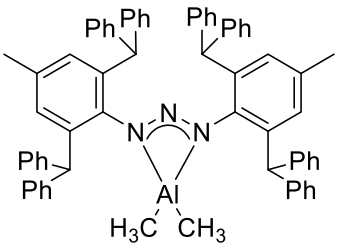

35

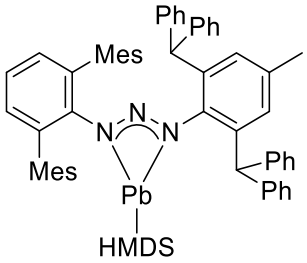

36

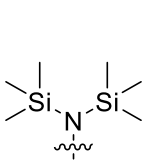

= HMDS

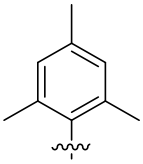

= Mes

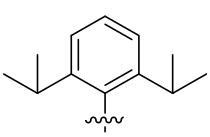

= Dipp

Chapter 1 – General Introduction

1.1 Introduction to main group organometallics

The organometallic chemistry of the heavy main group elements, comprising *s*- and *p*--block metals, is at times overshadowed by advances in related *d*-block studies. This notion is often sustained by the perceived flexibility, and thus utility, of transition metals, which have closely separated, partially filled *d*-valence orbitals.

Conversely, main group metals often assume more inert and segregated electronic configurations, owing to the stability of their unhybridised *s*- or *p*-valence orbitals, consequenced by the relativistic "inert pair effect" in heavy *p*-block metals specifically.[1-3] Furthermore, the isolation and thus study of electron deficient organometallic *s*- and *p*-block systems has historically been hampered by the extreme air- and moisture sensitivity of the M-C bond, which is susceptible to hydrolysis, leading to more stable M-O and C-H fragments, driven by the frequently oxophilic nature of most main group elements.[4]

Despite this, advances in air-free synthetic methods and characterisation techniques have allowed for the successful isolation of many previously intangible compounds, thereby spurring investigations into the chemical potential of main group elements, promoting them from curiosities to a growing and worthwhile branch of organometallic synthesis.[5] Accordingly, the desire to pursue syntheses previously thought to be impossible has dismantled the preconception that transition metal organometallics, and to some extent their early transition metal relatives including *f*-block metals,[6] possess richer chemistries. Indeed, many studies have exemplified that main group systems can behave like or

produce outcomes analogous to their *d*-block counterparts including catalytic applications.[7]

1.2 Introduction to p-block organometallics

Within the growing field of *p*-block organometallics, exceptional examples of developments over the past three decades include, amongst other examples, multiply bonded heavy main group analogues of lighter elements,[8,9] and low valent complexes with open coordination sites.[10] The latter is of major importance for the development of redox- or frustrated Lewis pair based catalytic applications.[11] These have gained considerable traction since low valent complexes have been shown to activate small molecules such as H_2,[12] NH_3,[13] CO_2,[14,15] and C_2H_4;[16] once thought to be the exclusive domain of transition metals (Schemes 1.1 and 1.2).

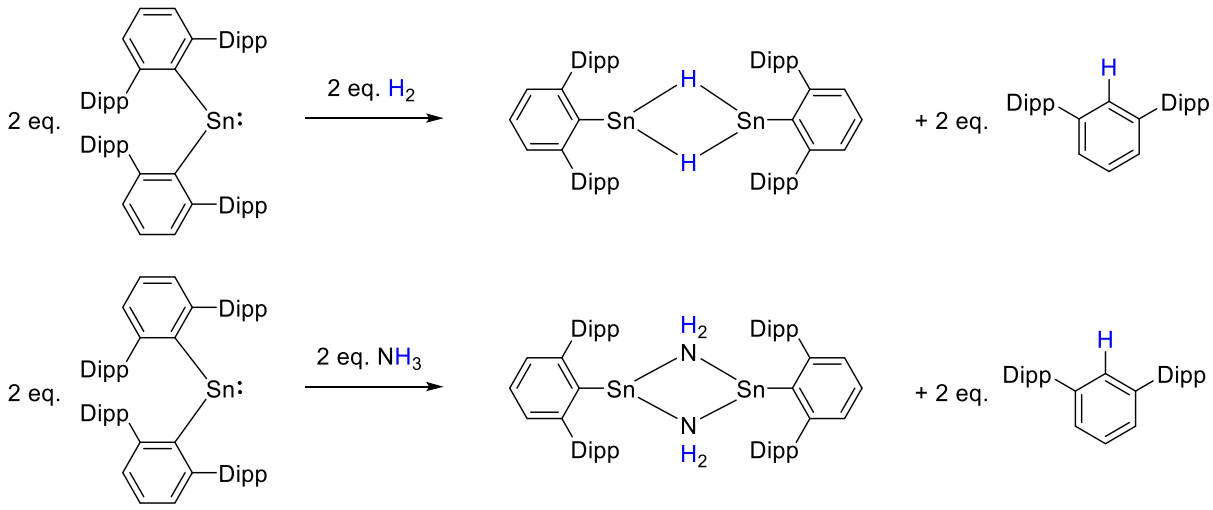

Scheme 1.1 Examples of main group elements activating H_2 and NH_3.

Dipp = 2,6-diisopropylphenyl.[13]

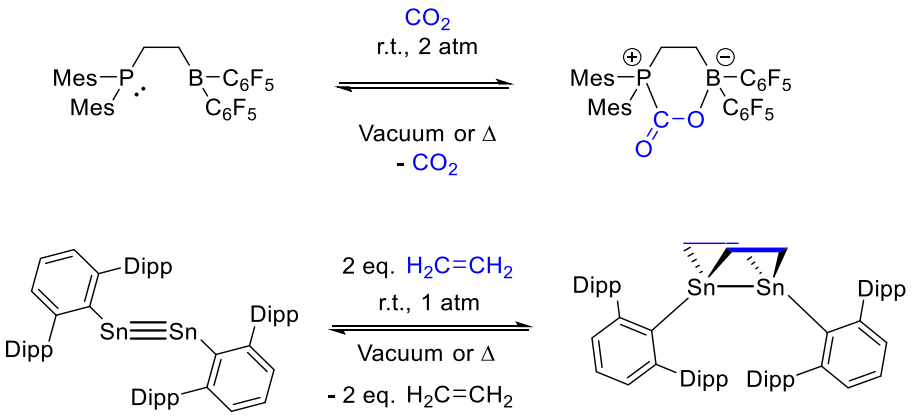

Scheme 1.2 Examples of main group elements activating CO_2, and C_2H_4.[14,16]

Mes = 2,4,6-trimethylphenyl.

Examination of the electronic effects involved between the frontier orbitals that dictate these processes helps to rationalise their outcomes, whilst also providing insight into their similarity to traditional transition metal mediated transformations.[17,18] In 2005 Power and co-workers demonstrated the facile addition of H_2(g) across a Ge-Ge triple bond to afford a mixture of reduced germanium hydride species (Scheme 1.3).[19]

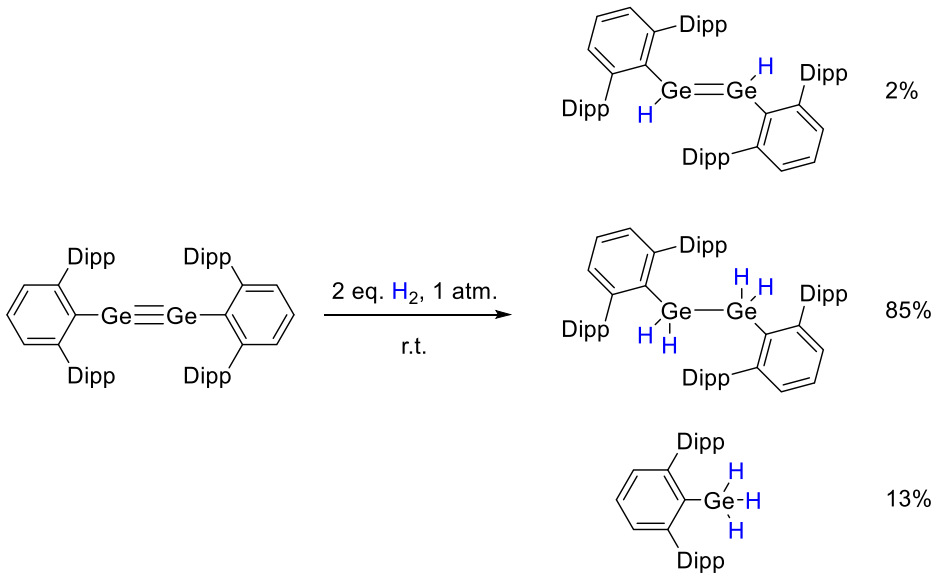

Scheme 1.3 Reduction of germanium alkyne analogue with H_2(g) to afford a mixture of germanium hydride species.[19]

Through theoretical calculations,[17] the authors suggest that this unprecedented reactivity results from the near perfect overlap (*ca.* 2 eV) of the germanium dimer LUMO with the σ-bonding molecular orbital (MO) of the H_2 molecule (red and purple lobes, Figure 1.1), which leads to a spatial and symmetric disposition of the germanium dimer π-orbital HOMO and the σ^*-antibonding MO of the H_2 molecule (blue and green lobes in Figure 1.1). These orbital interactions activate the dihydrogen molecule, leading to reduction of the germanium dimer.

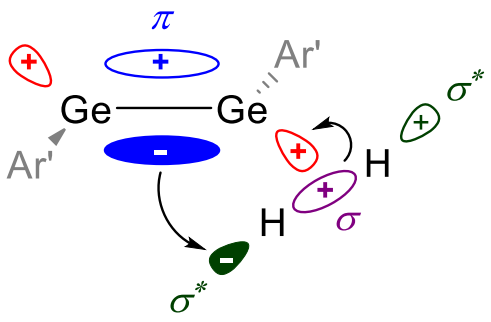

Figure 1.1 Illustration of frontier orbitals involved in the activation of dihydrogen by the germanium dimer Ar'GeGeAr', where blue = Ge dimer π-bonding MO, red = partial LUMO of Ge dimer, purple = H_2 σ-bonding MO, and green = H_2 σ-antibonding MO.

This noteworthy oxidative addition of H_2 to a low valent main group metal centre has been followed by related reports with other *p*-block metals,[9] including an analogous Sn(II) system[12] referred to in Scheme 1.1 above.[13] It is noteworthy that these reactions form stable hydride products. Such species can be unstable with respect to reductive dehydrogenation particularly for heavy main group systems, indicating that the aryl co-ligands are sterically and electronically conducive of metallohydride stabilisation.[20,21] This general reactivity is comparable to some transition metal systems, which have been known to undergo such additions for decades, albeit with different metal frontier orbitals,

namely *d*-orbitals, for which well understood backdonation rationales have been developed (Figure 1.2).[22]

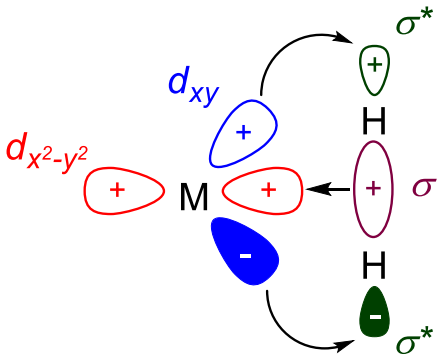

Figure 1.2 Illustration of some representative frontier orbital lobes typically involved in the oxidative addition of H_2 to a transition metal centre, where blue = partial metal d_{xy} orbital, red = partial metal $d_{x^2-y^2}$ orbital, purple = H_2 σ-bonding MO, and green = H_2 σ*-antibonding MO.

The formation of multiply bonded main group elements, such as the aforementioned Ge and Sn alkyne analogues, owe their genesis to the serendipitous isolation of the first heavy *p*-block metal-metal bonded compounds, which involved a low valent tin dimer; the alkene analogue R_2SnSnR_2 (R = $CH(SiMe_3)_2$) reported by Lappert and co-workers in 1973, for whom the mononuclear, dialkyl tin(II) species, or heavy "carbene" analogue, was the synthetic target and for which it had been established that smaller R-groups led to polymeric $(R_2Sn)_n$ species.[23] From these studies, it was reasoned that greater steric bulk was necessary for the separation of such species into stable constituent monomers with non-bonding metal valence electrons remaining on the metal centre as, for example, lone pairs.[24]

Historically, the steric tuning to effect these outcomes began with derivatisation of large monoanionic ligand scaffolds such as tertiary alkyls or silylamides, or substituted aryls.

Over time, this led to ligands that would ultimately stabilise mono-ligated alkyne analogues (see Schemes 1.2 and 1.3), including bulky amides.[8,24-27] The following section provides an overview of the development of these ligands.

1.2.1 Monoanionic ligands

To afford monomeric compounds of the type originally targeted by Lappert, it was found necessary to have ligands with large steric profiles, *e.g.* Ar" (2,4,6-tri-*tert*-butylphenyl) with heavier more inert metals such as Pb(II), as well as ideal stereoelectronic properties for the resulting complexes. Lappert and co-workers characterised several bis(amido) plumbylenes that met these requirements in 1977,[24] and comprehensive studies into the determining factors of the nuclearity and donicity of related species followed later.[28] Noteworthy examples include the diaryl carbene analogues presented by Klinkhammer and Weidenbruch,[29,30] and Jutzi[31] in Figure 1.3.

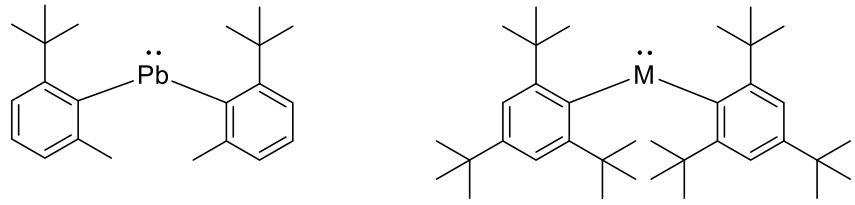

Figure 1.3 Monomeric plumbylene[29] and a related germylene and stannylene, where M = Ge or Sn, respectively. [30,31]

Subsequent reports showed that low valent heavy carbene analogues possess donor abilities and complexes with *N*-heterocyclic germylene, -stannylene, and -plumbylene donors have all been structurally characterised.[32-34] Indeed, much of our appreciation of these ligands is based on extensive research begun in the 1990s and early 2000s into the steric- and electronic properties of such complexes, supported by physical characterisation methods and theoretical calculations.[35,36] These provided a number of

guiding principles for targeting and acquiring either monomeric or dimeric metal-metal bonded species (Table 1.1). For example, with respect to accessing dimers (i) non-bonding electrons, present as a lone electron pair, must be available on the low valent metal centre, (ii) there must be a small energy gap between the molecular orbital that the non-bonding electrons occupy in the monomer and the envisaged π-orbital of the dimer (< 4 eV), and (iii) ligands must possess a steric profile big enough to preclude oligomerisation but small enough to allow a single homobonding interaction to occur.[5]

Property	Monomer	Dimer
Available metal LEP	Yes	Yes
Energy gap between metal LEP and M-M bonding MO	Large	Small
Steric profile of ligands	Large enough to inhibit dimerisation	Large enough to inhibit oligomerisation, small enough to allow dimerisation

Table 1.1 Determining factors of nuclearity in low valent main group complexes.

1.2.2 The "Gallyne" debate

In 1997 Robinson and co-workers reported the landmark [Na_2(Ar*GaGaAr*)] (Ar* = 2,6-(2,4,6-triisopropylphenyl)phenyl) complex and sparked a debate over the bond order between the two gallium atoms, which the authors provocatively termed a "gallyne," thereby implying a Ga-Ga bond order of three (Figure 1.4).[37] The initial report focused primarily on the experimentally determined and extraordinarily short Ga-Ga bond distance (2.320(4) Å, *cf.* 2.44 Å in metallic gallium).[38] However, although this intermetal distance is the shortest ever reported in a gallium compound, it is now thought the short contact is induced by sodium-arene interactions, which pull the two gallium atoms closer together, as substantiated by independent syntheses and theoretical studies by Power and

co-workers that targeted some similarly substituted Ga-Ga complexes of the general form ArGaGaAr, including Ar*GaGaAr*.[28]

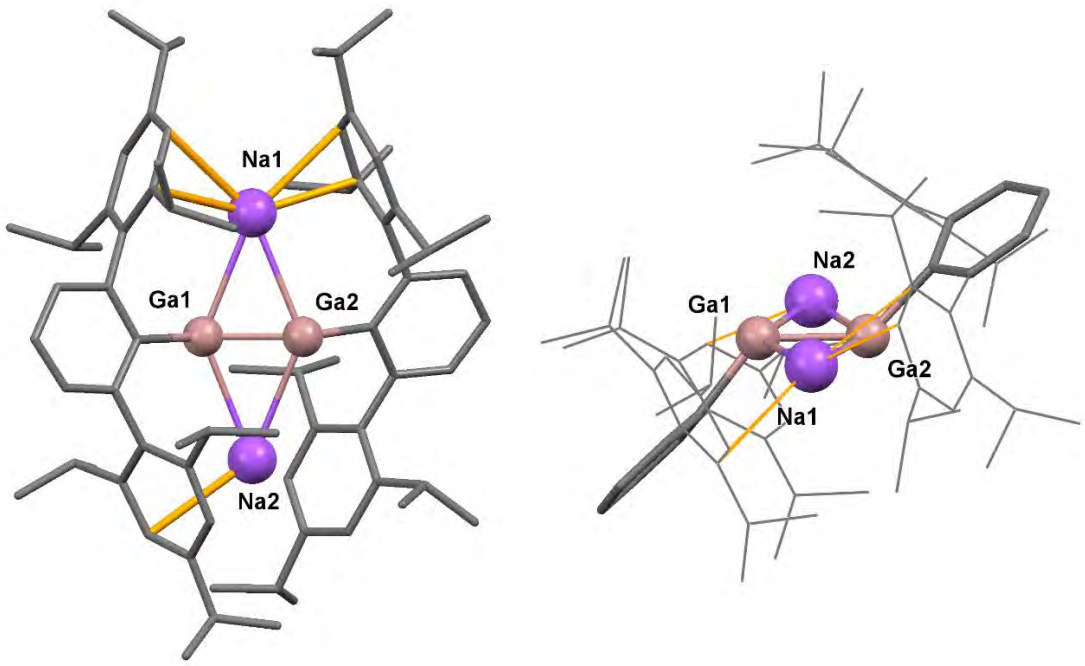

Figure 1.4 The disputed "gallyne" reported by Robinson; Ga-Ga: 2.320(4) Å (hydrogen atoms omitted for clarity, aryl-Na contacts highlighted in orange).[37]

While the exact nature of the bonding in this complex is not directly pertinent to the content of this thesis, the interest that the debate into Ga-Ga bonding generated led to rapid developments in the field of low oxidation state *p*-block chemistry. A notable example is the solution state monomer; :GaAr' (Ar' = 2,6-bis(2,6-diisopropylphenyl) phenyl), which bears accessible non-bonding electrons on the metal, also reported by Power and co-workers. [39] This is activated towards the oxidative addition of H_2 to produce a hydride bridged bis-Ga(III) tetrahydride (Scheme 1.4), comparable to the previously discussed Ge dimer.[12]

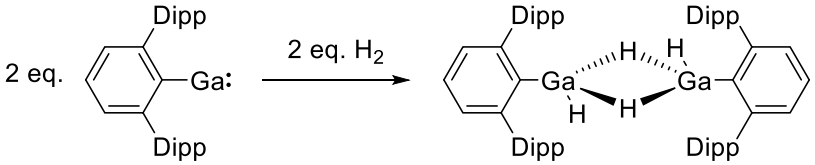

Scheme 1.4 Oxidative addition of H_2 to the monomeric GaAr' complex reported by Power and co-workers.[39]

1.3 Heavy p-block metallohydrides

The oxidative addition of H_2 to low valent *p*-block metal species has corollaries with earlier investigations into main group hydride chemistry, some of which were identified as potential entry points to multiply bonded metal-metal species *via* the reductive elimination of dihydrogen (Scheme 1.5), *i.e.* the reverse of the process reported by Power in Figure 1.1 above.

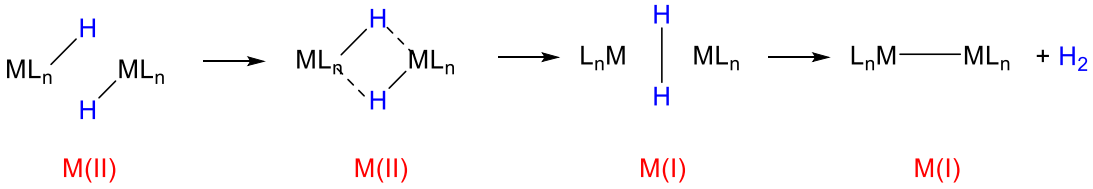

Scheme 1.5 Example of reductive dehydrogenation from a metallohydride to generate a metal-metal bonded product.

Beside this application, low valent main group metallohydrides are promising synthetic targets for specialist applications or as reactive sources of hydride since the related high valent (conventional oxidation state) main group metallohydrides make up a considerable proportion of the commercially available reducing agents for synthetic and industrial applications, *e.g.* $HSnR_3$, $Li[AlH_4]$, and the numerous boranes and borates.

The stabilisation of low valent metallohydrides is challenged by the tendency of such species to preferentially undergo reductive dehydrogenation in the absence of ligands with suitably large steric demand to generate dimers, trimers and further oligomeric species (Scheme 1.5 above).[18] Such decomposition reactions often yield reduced products that include elemental metal and dihydrogen gas in the absence of alternative reaction coupling partners.[18]

Although many researchers have contributed to this research field, the contributions of Power and Roesky have set a particularly sound foundation.[18,40] For example, the preparation of tin(II) hydrides through halide-hydride exchange at organotin chlorides using hydroborate or hydroaluminate salts gives the hydride bridged tin(II) dimer [Ar*Sn(μ-H)$_2$SnAr*] (Scheme 1.6),[21] identical to those later accessed by the oxidative addition of hydrogen to Sn-Sn bonded species (*vide supra*). Extension of this approach to [PbAr*Br] proved unsuccessful, instead affording a Pb-Pb containing Pb(I) dimer (Scheme 1.6).[27] As briefly commented on earlier, this product is consistent with a fleeting organolead hydride intermediate that reductively eliminates dihydrogen (Scheme 1.5). Of note, the related conversion of the bismuth(III) species, [BiAr$^{\#}{}_2$Cl] to [BiAr$^{\#}{}_2$H], affords one of the few known 6th period *p*-block hydrides that does not reductively dehydrogenate (Scheme 1.7).[41]

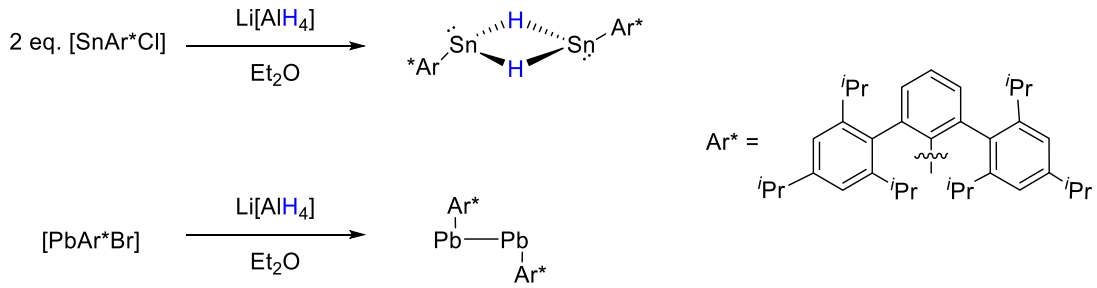

Scheme 1.6 Power's terphenyl stabilised tin(II) hydride, and a lead(I) species formed by related reactions.[21,27]

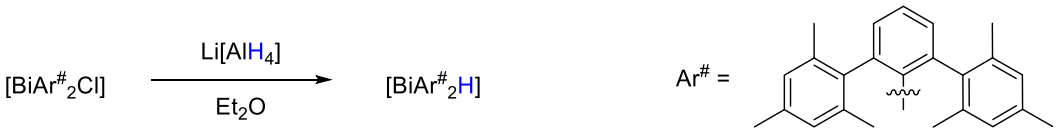

Scheme 1.7 Power's synthesis of the terphenyl stabilised Bi(III) hydride species.[41]

In 2006, Roesky and co-workers reported the first mononuclear divalent group 14 hydrides of germanium and tin using sterically hindered *β*-diketiminate (NacNac) ligand supports.[42] These species are able to exist as monomers by virtue of the greater steric demands of the *N*-aryl ligand *vis-à-vis* Power's terphenyl systems (*vide supra*). The chloride-hydride exchange method used by Roesky extends Power's original approach by use of a non-aluminate aluminohydride; the alane [$AlH_3{\cdot}NMe_3$]. However, K-selectride™, KHB*sec*Bu_3, was later found to afford superior yields (Scheme 1.8).[43] (*NB*: L-selectride™ had been used previously by Power and co-workers).[20]

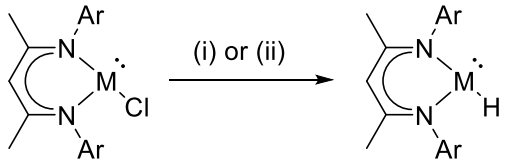

Scheme 1.8 Roesky's preparation of germanium(II) and tin(II) hydrides (M = Ge or Sn, Ar = 2,6-*i*$Pr_2C_6H_3$: (i) [$AlH_3{\cdot}NMe_3$];[42] (ii) K-selectride™.[43]

Application of the same approach to the synthesis of a lead(II) analogue resulted in metal deposition and NacNac ligand protonation. Presumably the inability of an ensuing Pb(I) product to homocouple (*cf.* Scheme 1.5), as is consistent with the increased bulk of the *N*-donor ligand, stymies the reductive elimination of hydrogen and formation of a stable Pb-Pb bonded Pb(I) decomposition product.

More recently, related highly air- and moisture sensitive *s*-block organometallic coordination complexes have also enjoyed a spate of interest, encouraged by advances in

air-free manipulation and characterisation techniques.[44,45] The development of these systems have led to a wide range of applications, particularly as reagents and catalysts.[7,46] This branch of main group chemistry clearly warrants its own discussion and pertinent examples are introduced in the following section.

1.4 Introduction to s-Block organometallics

Similar to the organometallic chemistries of the heavy *p*-block elements, the study of *s*-block organometallics is founded on the stabilising properties of large, monoanionic ligands that permit the reactivity of these "hard" oxophilic metal cations to be controlled or spatially limited.[47-50]

The synthetic applications of these metals, outside of the rich catalogue of organolithium and Grignard reagents, are relatively young compared to those of the *p*-block metals discussed above. In particular, they have been developed toward such applications by Hill and co-workers.[51] Amongst the ligand classes most successfully deployed, the previously discussed NacNacs have been used prodigiously,[52] as have 1,8-disubstituted carbazolides, which have presented themselves as good alternatives to bulky 2,6-terphenyls in the *s*-block field owing to their similar steric profile and more electronegative *N*-donors relative to the aforementioned carbanions, like 2,6-terphenyls[53] (Figure 1.5).

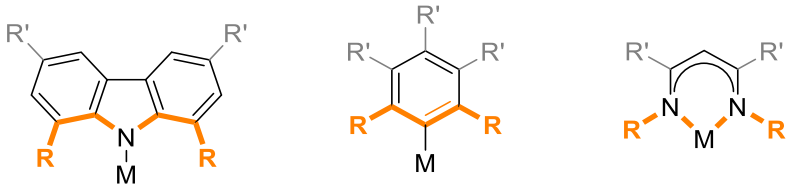

Figure 1.5 Comparison of 1,8-disubstituted carbazolides and NacNacs with the ubiquitous 2,6-terphenyl ligand class (where M = *s*- or *p*-block metal, R = substituted phenyl or bulky alkyl, and R' = alkyl, aryl, or hydrogen substituent).

1.4.1 1,8-Disubstituted carbazolides as support ligands

The projection of the 1- and 8-carbazolide substituents near parallel to the M-N donor vector (assuming M lies in the carbazolide plane) have potential to provide excellent facial shielding to metals coordinated at the anionic nitrogen. These substituents can also exhibit donor based directing ability that retains the metal within the pincer plane. For example, carbazolides decorated with 1,8-diimines,[54] -diphenyls,[53] -diphosphines,[55] and -diNHCs[56] have all been reported.

In the absence of donor groups at the 1,8-positions, or in the presence of blocking groups such as bulky alkyls, it is generally found that the diffuse nature of the negative charge at the carbazolide nitrogen leads the metal to bind facially to the heterocycle. This is particularly the case for "hard" metal cations, as demonstrated by Kays with alkaline earth metals (Figure 1.6).[57]

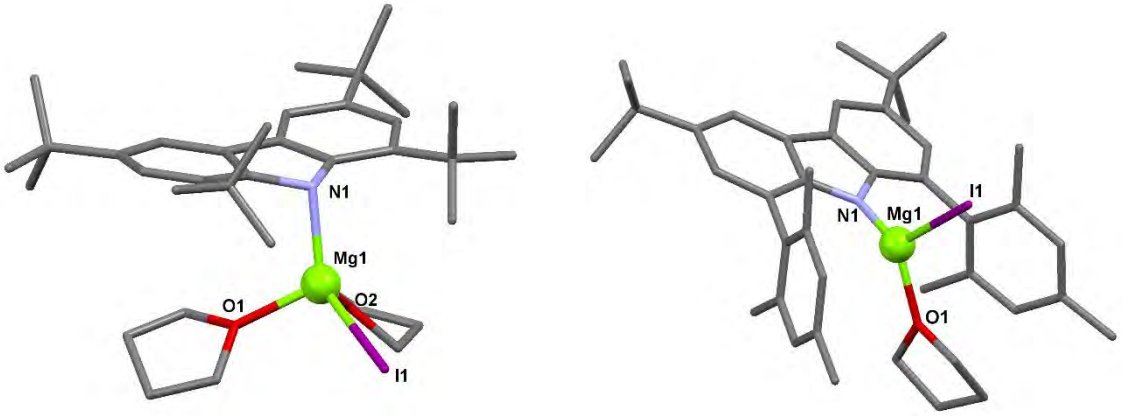

Figure 1.6 Magnesium 1,3,6,8-tetra-*tert*-butylcarbazolide (left) and magnesium 3,6-di-*tert*-butyl-1,8-dimesitylcarbazolide (right) reported by Kays, contrasting the effects of blocking and donor groups at the 1,8-positions on metal placement facially or in the carbazolide plane.[57]

1.4.2 β-Diketiminates

The less parallel oriented *N*-substituents of *β*-diketiminates (NacNacs) relative to the M-L vector have enabled the synthesis of alkaline earth metal-metal bonded dimers,[58] notably the Mg(I) compounds popularised by Jones and co-workers.[59] In general, these are accessed by chemical reduction of the iodomagnesium complex [Mg(NacNac)I] with elemental potassium or sodium to give the corresponding dimer (i, Scheme 1.9).[59] For the Mg(I) systems, these have proven their utility as rare soluble one electron organometallic reducing agents (ii, Scheme 1.9).[60]

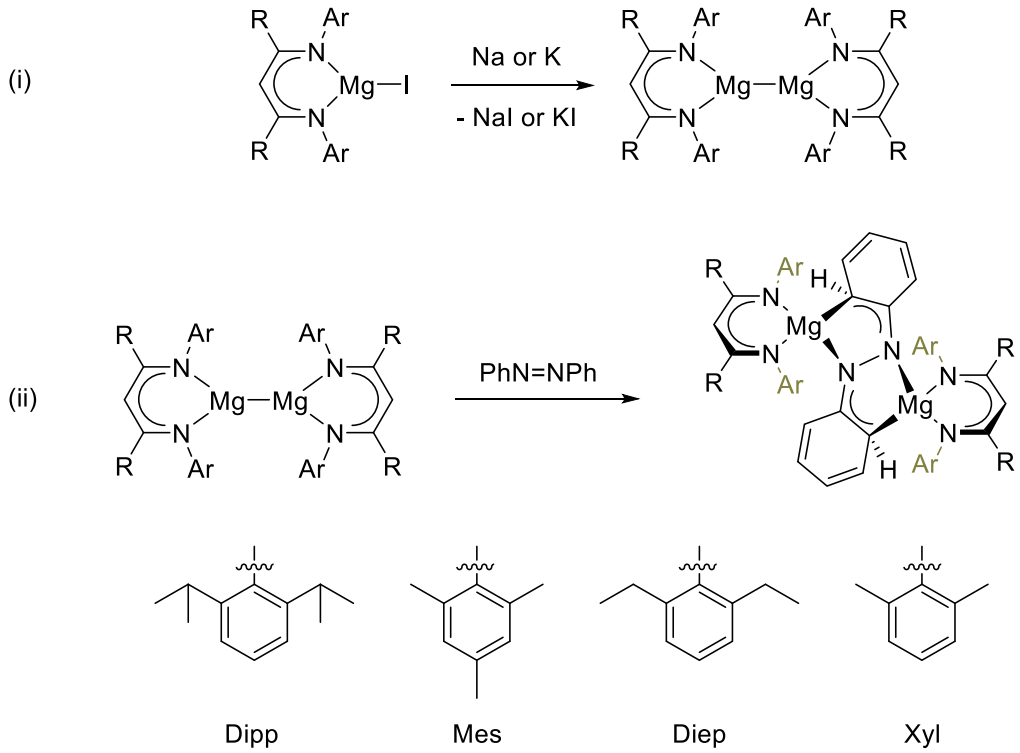

Scheme 1.9 (i) Mg(I) dimer synthesis (ii) use of Mg(I) dimer as a chemical reductant.[59,60] (i) Ar = Dipp, Mes, Diep, Xyl, R = Me, *t*Bu; (ii) Ar = Dipp, Mes, R = Me.

According to Jones, these Mg(I) dimers are best described as anionically stabilised covalent Mg_2^{2+} cations rather than discrete Mg(I) ions.[61] This is borne out by extensive theoretical calculations coupled with high resolution X-ray crystallographic data, which have substantiated that the two magnesium atoms share diffuse electron density that experiences a local maximum near the centre of the Mg-Mg bond, as is consistent with a covalent bond with a bond order of one.

These highly reactive alkaline earth species have been shown to be thermodynamically unstable with respect to disproportionation (*e.g.* $2\ Mg^{I} \rightarrow Mg^{0} + Mg^{II}$) and are therefore stabilised by the ligand steric bulk that confines the Mg_2^{2+} subunit and stymies redox processes in the absence of suitably small molecules.[61]

Despite the reactivity of the Mg_2^{2+} unit, the oxidative addition of H_2 has remained elusive with respect to these *s*-block systems, unlike their *p*-block analogues discussed above (*vide supra*).[59,62]

1.5 Neutral σ-donors as support ligands for low oxidation state main group compounds

1.5.1 p-Block NHC complexes

Well established monodentate neutral Lewis basic ligands (L), *e.g.* amines, phosphines, NHCs, have also been used to great effect to stabilise low valent metal-metal bonded *p*-block species. These low valent complexes are often accessed by chemical reduction of suitably ligated, higher oxidation state halides or hydrides, as exemplified by Jones and co-workers who used the Mg(I)-Mg(I) complex discussed previously to reduce the NHC stabilised aluminium trihydride [AlH_3IDipp] (IDipp = 1,3-bis(2,6diisopropylphenyl) imidazole-2-ylidene) to form a highly stable symmetrical Al(II) dihydride dimer with concomitant access to the magnesium hydride (Scheme 1.10), viewed as inaccessible *via* direct reaction with dihydrogen, *vide supra*.[63]

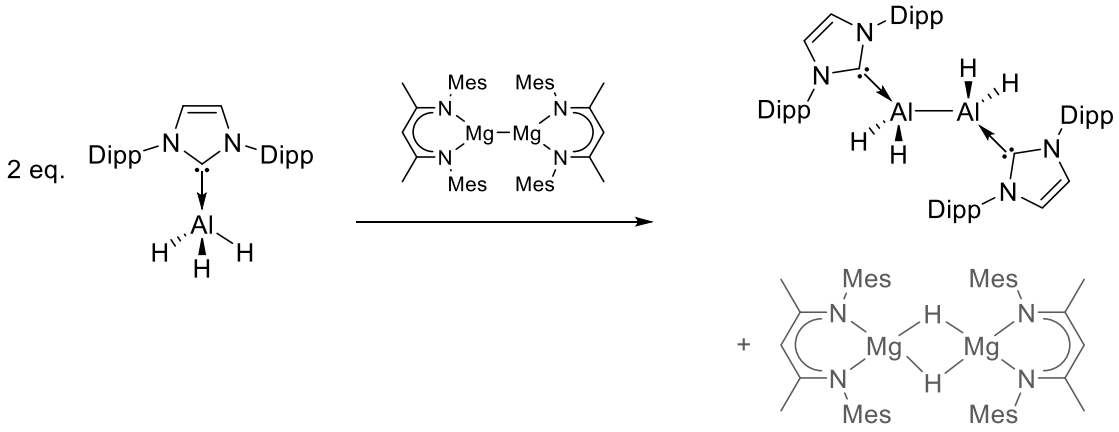

Scheme 1.10 Preparation of [{AlH_2(IDipp)}$_2$] from [AlH_3(IDipp)] using a one electron Mg(I) reductant.[63]

The stability of the Al(II) dihydride dimer is attributable in part to the steric protection provided by the large, shielding substituents on the NHC donor and, importantly, its high nucleophilicity. The formation of this low valent product is noteworthy since, prior to this report, the unadorned parent Al_2H_4 species had previously only been observed spectroscopically during matrix isolation studies at 5 K.[64,65]

The strong nucleophilicity of NHC donors is also apparent in the monomeric aluminium-telluride reported by Inoue and co-workers who, through the use of strongly donating alkyl substituted NHC ligands, were able to isolate the first monotopic aluminium chalcogenide (Figure 1.7).[66] The unique stability of this monomeric species is afforded by the Lewis basicity of the NHC support ligands.

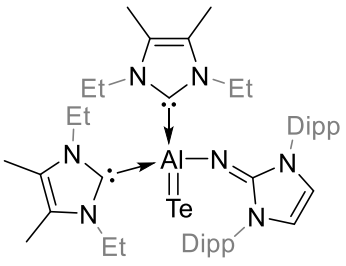

Figure 1.7 Monotopic aluminium telluride supported by two small NHCs.[66]

Typically, high valent group 13 metals (M = Al, Ga, In, Tl) are "hard", highly electropositive cations that, in combination with group 16 elements (E = O, S, Se, Te), form strongly polarised M-E bonds. The highly electrophilic sites on the metal atoms strongly attract electron density on the chalcogenide atoms, causing self-oligomerisation.[67] Inoue and co-workers thusly demonstrated that the electrophilicity of an aluminium metal centre could be effectively quenched by the binding of small alkyl substituted NHCs, in turn inhibiting the normally observed oligomerisation (Figure 1.8).[68,69]

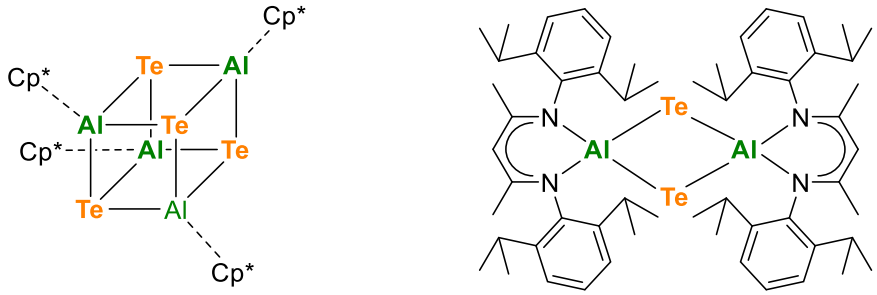

Figure 1.8 Oligomeric aluminium tellurides reported by Roesky and co-workers.[68,69]

Cp* = pentamethylcyclopentadienyl

Despite their noted stabilising ability, bis(NHC) complexes of *p*-block elements like that in Figure 1.7 are extremely rare.[70] This confounds the expectation that their electronic configurations, *i.e.* with vacant or partially filled *p*-orbitals, will accommodate multiple NHC donors, as per weaker Lewis bases such as tertiary amines and phosphines.[71,72] Steric effects have been noted as possible causes for the stubborn reactivities of trivalent group 13 metal complexes, whereby the spatial requirements of up to three anionic co-ligands must also be taken into account. This consideration is less important for the aforementioned NR_3 or PR_3 ligand systems, which direct their steric bulk away from the metal centre unlike NHCs (Figure 1.9).[72,73]

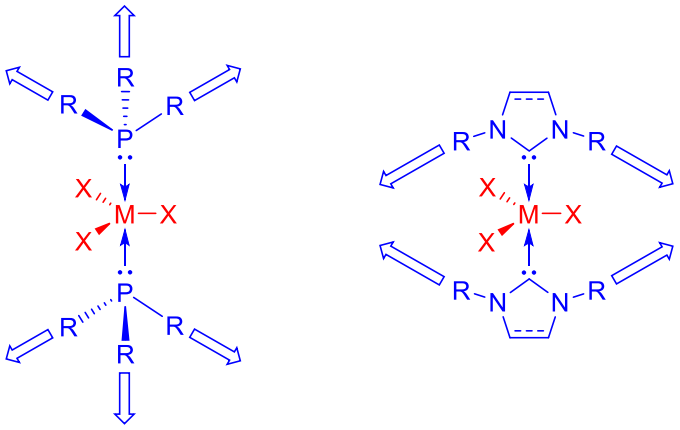

Figure 1.9 Steric bulk projection by bis-tertiary phosphine *vs*. bis(NHC) complexes.

From the few examples that exist, it is apparent that bis(NHC) coordination with monodentate NHCs at a trivalent metal centre necessitates at least one small, usually alkyl substituted NHC, suggesting that steric effects are a key factor in the successful bis(NHC) coordination (Figure 1.10).[73]

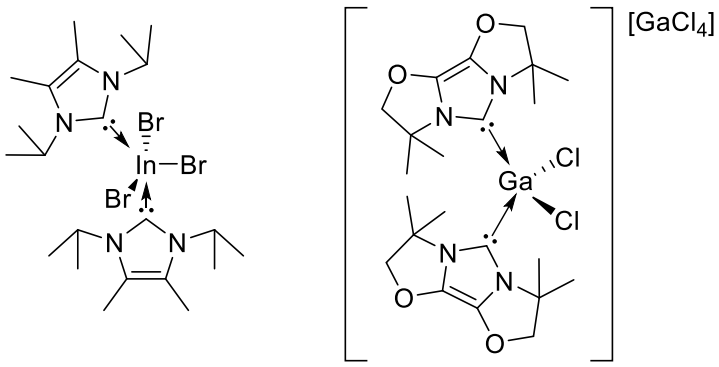

Figure 1.10 Some examples of bis(NHC) complexes of trivalent group 13 metals.[73,74]

In light of the proclivity for mono(NHC) donation, tethered, multidentate NHC ligands have been used to overcome lability by providing additional entropic stability to the resulting complex (Figure 1.11).[75,76]

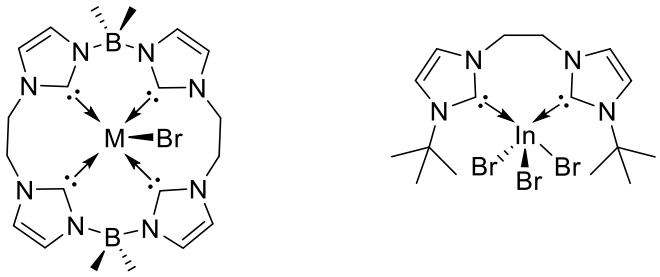

Figure 1.11 (i) Macrocyclic tetra(NHC)borate complexes (where M = Al or In)[75] and (ii) $[InBr_3(ItBuC_2H_4ItBu)]$.[76]

1.5.2 s-Block NHC complexes

Mono- and multidentate NHC ligands have recently been used to great effect in the isolation of reactive *s*-block organometallics, notably by Hill and co-workers who have produced NHC adducts of alkaline earth metal (Mg, Ca, Sr, and Ba) hexamethyldisilazides (HMDS) (Figure 1.12) with the intention to develop the Ca and Sr congeners into precatalysts (*vide infra*).[77]

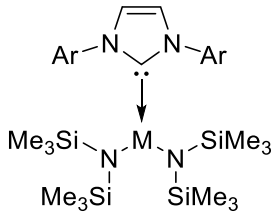

Figure 1.12 NHC adducts of alkaline earth NHC adducts reported by Hill and co-workers, (Ar = 2,6-diisopropylphenyl, M = Mg, Ca; M-C = 2.276(2) Å and 2.6285(16) Å, respectively; Ar = mesityl, M = Ca, Sr, Ba; M-C = 2.598(2) Å, 2.731(3) Å, and 2.915(4) Å, respectively).[51,77]

When comparing the metrics of the simple bis(amide) NHC adducts, the M-C bond length increases ranging from 2.276(2) Å in the magnesium IDipp complex to 2.915(4) Å in the barium IMes complex (IMes = 1,3-bis(2,4,6-trimethylphenyl)imidazol-2-ylidene).[51] This bond elongation leads to lability of the NHC ligand in the presence of "harder" oxygen

donors *e.g.* triphenylphosphine oxide, $O{=}PPh_3$, which readily displaces the NHC ligand to rapidly form the corresponding bis($O{=}PPh_3$) complex, as described in the case of [$Ca(HMDS)_2$(IDipp)] below (Scheme 1.11).[51]

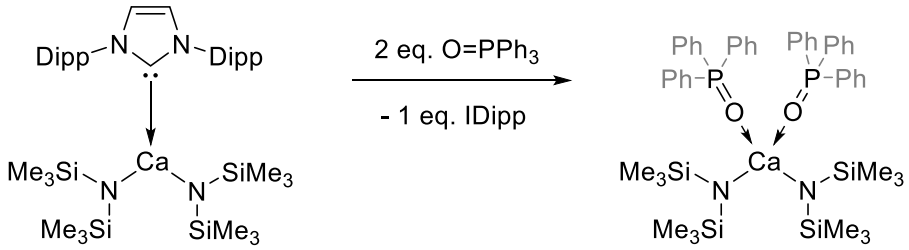

Scheme 1.11 Facile displacement of NHC ligand by phosphine oxide at $Ca(HMDS)_2$.

The general solution state lability of the NHC ligand under catalytically relevant conditions, as demonstrated here in the presence of $O{=}PPh_3$, precluded further studies into the catalytic potential of those heavier alkaline earth complexes.[51] To address lability, a monoanionic bis(NHC)borate ligand was envisaged to enhance coordination of the NHC ligand to the metal centre (Scheme 1.12, i).

The use of a bis(NHC)borate ligand provides a suitable entropic barrier with respect to ligand dissociation, and affords rare examples of bis(NHC) ligated Ca- and Sr(HMDS) complexes (Scheme 1.12, i). These were deployed to achieve a range of catalytic intramolecular hydroaminations, although high reaction temperatures (> 50 °C) were noted to induce Schlenk-type ligand redistribution to homoleptic species.[78] As shown in Scheme 1.12, deprotonation of the aminoalkene substrate by the HMDS co-ligand of the precatalyst generates the catalytically active species which affords the cyclic hydroaminated product following proton transfer from a second molecule of substrate in transition state (A) shown in Scheme 1.12, ii.[79,80]

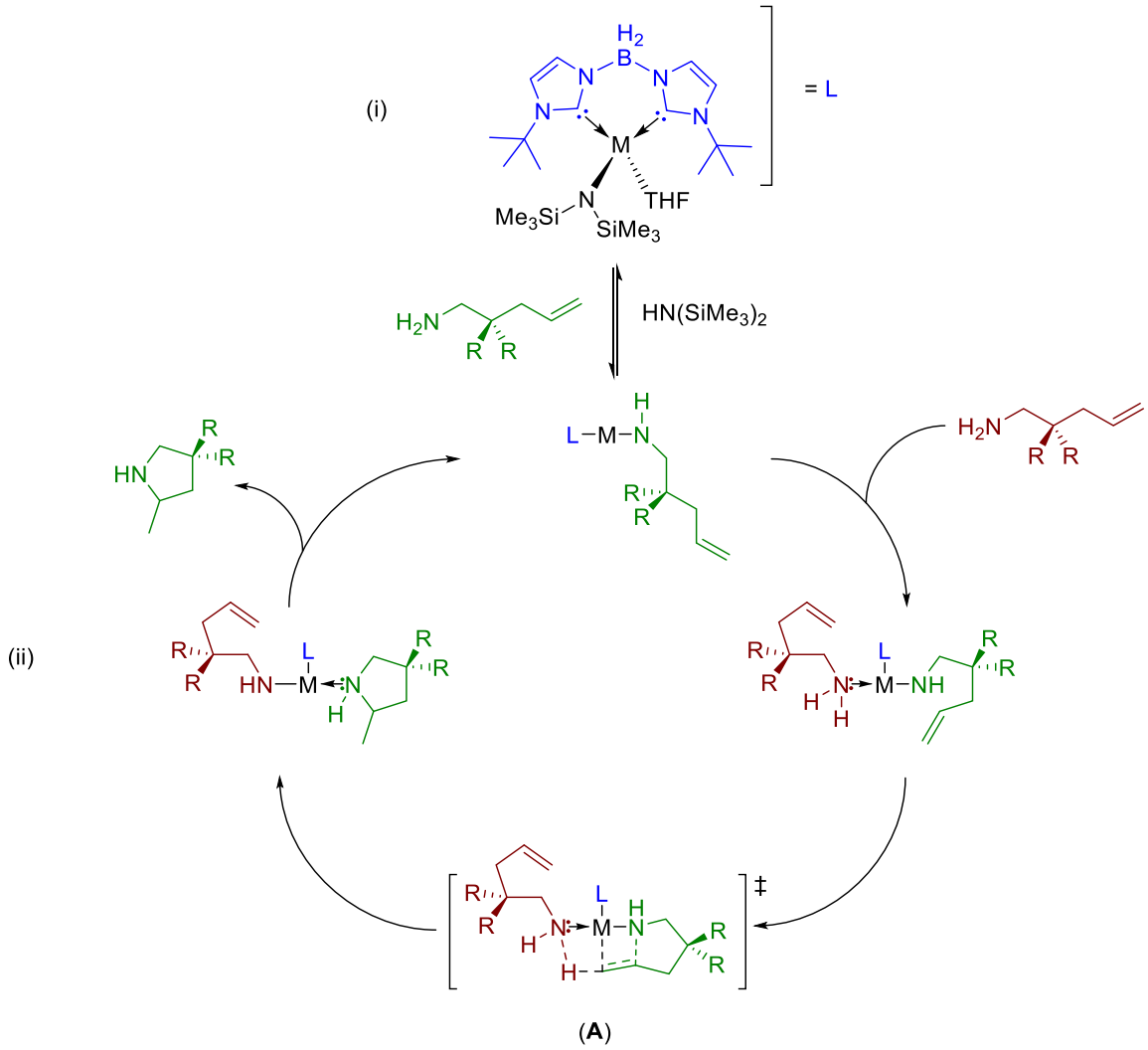

Scheme 1.12 (i) Bis(NHC)borate complexes (M = Ca or Sr) (ii) used to catalyse hydroamination reactions.[80]

Interestingly, the magnesium to carbon bond of the non-anionic mono(NHC) complex, [Mg(HMDS)$_2$(I*t*Bu)] (I*t*Bu = 1,3-bis-*tert*-butylimidazol-2-ylidene), reported by Nembenna and co-workers proves robust to displacement.[81] As a result, this NHC supported magnesium precatalyst effects intermolecular hydroguanylations from the insertion of a carbodiimide substrate across the Mg-NHR bond in a similar fashion to the calcium and strontium bis(NHC)borate complexes reported by Hill in Scheme 1.12.[81] The authors also note that the hydroguanylation proceeds with catalytic amounts of

[Mg(HMDS)$_2$], but with lower turnover frequencies,[81] which is consistent with the findings of Hill's earlier investigations using [M(HMDS)$_2$] (M = Ca, Sr).[82]

1.6 Purpose of this work

This thesis seeks to bolster and draw further attention to the rapidly developing field of main group coordination chemistry and its application, as stimulated by the emergent trends in the preceding discussions. The unique electronic configurations produced by mono- or bis(NHC) coordination clearly enable fine tuning of the electronic properties and reactivities of main group metal centres. To date, such complexes have demonstrated their potential to replace transition metals in a number of important synthetic applications.

As alluded to before, the preparation of *s*- and *p*-block bis(NHC) coordination complexes has proved difficult, owing to the diffuse *s*-valence orbital and relatively low positive charge for the former, and lower propensity to support high coordination numbers for the latter. Consequently, there is a scarcity of reports characterising these species and little is known about their synthetic potential. To bridge this gap, bis(NHC) coordination of the earthly abundant metals that comprise groups 1 and 2 (Chapter 2), 13 (Chapter 3), and 14 (Chapters 4 and 5) will be the key focus of this work.

Heeding this, the monoanionic bis(NHC)carbazolide pincer ligand class, bimca^R (where bimca = 3,6-di-*tert*-butyl-1,8-bis(imidazol-2,2'-yliden-1,1'-yl)carbazolide, and R = *N*-substituent at both 3,3'-imidazol-2-ylidenyl positions), originally reported by Kunz and co-workers,[56] provides an ideal stage from which to study the consequences of bis(NHC) coordination on bound metal centres (Figure 1.13), and will be used as the principal entry into the study of this chemistry.

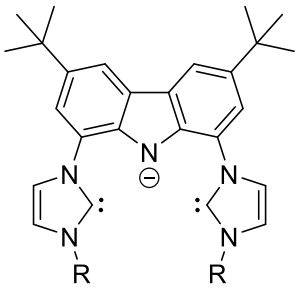

Figure 1.13 General bimca^{R} ligand framework.

The bimca^{R} ligand framework comprises a fully sp^2 hybridised, rigid carbazolide backbone that directs two flanking NHC σ-donors toward a meridional coordination geometry. The relatively labile monoanionic carbazolide serves as a tethering site for the central metal atom.

These donor properties are of particular interest for the purposes of this thesis since they include the donor characteristics of ligands used extensively by the Cole group (Figure 1.14) in a single tridentate ligand, namely an organoamide and two NHC donors.

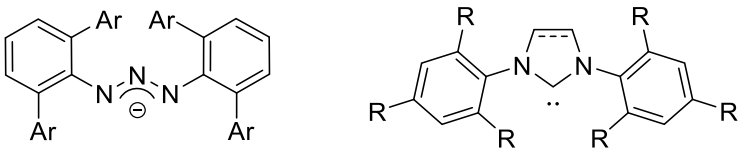

(i) (ii)

Figure 1.14 General structure of some bulky ligands used in the Cole group and in this thesis (i) triazenides and (ii) NHCs.

1.6.1 Disclosure of related preliminary studies

Indeed, a series of bimca^{Me} supported gallium, indium, and thallium dihalide complexes have been synthesised in the Cole group prior to the work presented herein.[83] These preliminary investigations, conducted by Dr Samantha Furfari, demonstrated that

tridentate bis(NHC) carbazolide coordination may be achieved through salt metathesis reactions of the Li(bimca^{Me}) transfer reagent with MX_3 trihalide precursors, M = Ga, or Tl; X = Cl, or M = In; X = Br) to afford the corresponding [M(bimca^{Me})X_2] complexes *via* the elimination of LiX. However, these syntheses were met with several unforeseeable difficulties, namely the solubility profiles of the precursor materials and [M(bimca^{Me})X_2] complexes, which resulted in impure reaction products. These and low yielding preparations of bimca^{R} precursors hampered further study. With this in mind, this project seeks to address the shortcomings of our previous studies, to extend bimca^{R} complex synthesis to a wider range of main group metals, and to develop more expedient access paths to bimca^{R} precursors in collaboration with the group of Prof D. Kunz.

These studies are supplemented by the development of a large, sterically encumbered triazenide ligand, the establishment of its steric profile, and pilot deployment to the study of lead(II) species.

Chapter 2 – Bimca^{R} ligand synthesis and s-block derivatives

2.1 Introduction

As alluded to in Chapter 1, examples of bis(NHC) complexes of *s*-block elements are few. This scarcity of reports provides an opening for their further study. Our attention was drawn to the bimca^{R} ligand scaffold, of which the original report by Kunz and co-workers details the synthesis of an exceptionally nucleophilic [Rh(bimca^{Me})CO] oxidative addition catalyst (Scheme 2.1),[56] which exploits the donor properties discussed in Chapter 1.

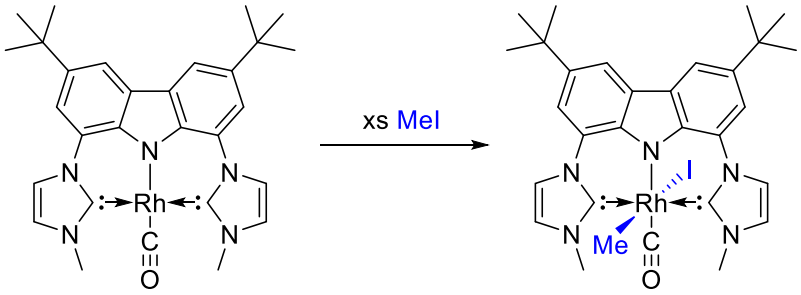

Scheme 2.1 Oxidative addition of methyl iodide to [Rh(bimca^{Me})CO].

Subsequent reports have demonstrated the ability of this ligand system to accommodate different metal cations, most prominently transition metals.[84] Such complexes are typically accessed *via* a lithio ligand-transfer agent, Li(bimca^{R}), of which the solid state structures have not been characterised.

2.1.1 Purpose of this chapter

This chapter seeks to structurally elucidate lithium bimca^{R} complexes to address the absence of structural data in the literature. It aims to extend this chemistry to heavier alkali metals such as potassium, and to expand the known *s*-block bimca^{R} complexes to the alkaline earth metals.

In doing so, the bimca^{R} ligand scaffold has great promise for studying the effects of bis(NHC) coordination because of the presence of two flanking NHC donor moieties which are expected to bind *s*-block metals in the carbazolide donor cavity, and act as transfer species to *p*-block elements (Chapters 3 and 4).

This chapter seeks to revise the synthetic strategy for constructing this ligand in collaboration with the Kunz group.[85] As such, the successful revised preparation of bis(imidazolium)carbazole proligand salts, **4^{R}**, (Scheme 2.2 for retrosynthetic approach to bimca^{R}) is presented in the following sections.

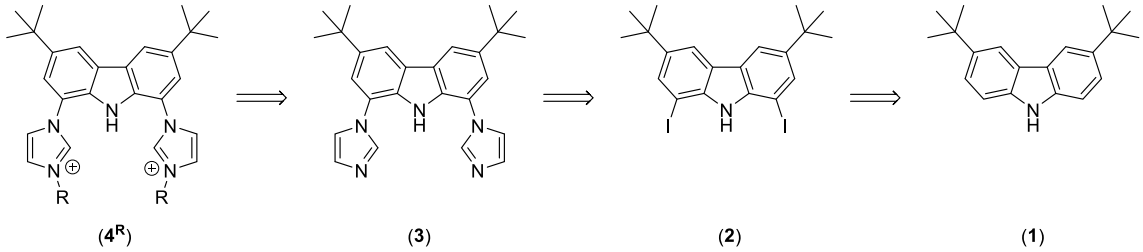

Scheme 2.2 Retrosynthetic analysis of the Hbimca^{R}(2H)$^{2+}$ proligand showing the synthetic disconnects at **1**-**3**

2.2 Results and discussion

2.2.1 Carbazole 3,6-di-protection

The carbazole heterocycle is the foundation upon which the bimca^{R} scaffold is built. The key locations for bis(imidazole) derivatisation of the precursor heterocycle are the 1- and 8-carbazole positions (Figure 2.1).

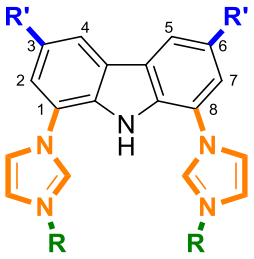

Figure 2.1 Functionalisation sites of carbazole for generating the bimca^{R} scaffold where imidazole substituents at the 1,8-positions form the binding cavity (orange), the steric and donor properties of which are tuned by *N*-R substituents (green) and R' substituents at the 3,6-positions serve as protecting and solubilising groups (blue)

Exclusive imidazole functionalisation at these positions *via* halogenation and subsequent C-N coupling (*vide infra*) necessitates pre-substitution of the more reactive 3- and 6-carbazole positions. This is most readily achieved through a facile Friedel-Crafts alkylation with *tert*-butyl chloride using either an $AlCl_3$ or $ZnCl_2$ Lewis acid catalyst in DCM or $MeNO_2$ respectively (Scheme 2.3).

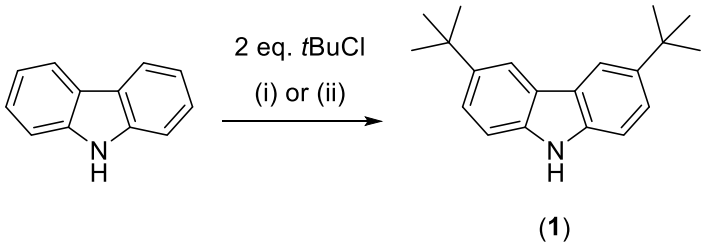

Scheme 2.3 Synthesis of 3,6-di-tert-butylcarbazole (**1**) from carbazole; (i) $AlCl_3$, DCM (79%), (ii) $ZnCl_2$, $MeNO_2$ (52%).

During these reactions it was established that although $ZnCl_2$ in $MeNO_2$ gives more consistent moderate yields, cleaner workups are achieved with newly purchased $AlCl_3$ in DCM. An added benefit of the $AlCl_3$ reactions is the easy removal of the more volatile DCM solvent. Despite stoichiometric additions of the alkylating reagent, contamination of the intended 3,6-di-*tert*-butylcarbazole product with the 1,3,6,8-tetra-*tert*-butyl

substituted species and unreacted carbazole was observed under all reaction conditions, as indicated by an additional *tert*-butyl alkyl proton signal at 1.40 ppm (DMSO-d_6) in all ^{1}H NMR spectra of the crude reaction mixtures. The undesired tetra-alkylated product and residual unreacted carbazole can be separated chromatographically by eluting the crude reaction solids with neat ethyl acetate or recrystallisation from a saturated hexane solution at room temperature placed at -24 °C. Both methods afford spectroscopically pure 3,6-di-*tert*-butylcarbazole, **1**.

The ^{1}H NMR (DMSO-d_6 or $CDCl_3$) spectra of **1** are consistent with literature reports for this compound,[86] including second order multiplets at 7.39 ppm and 8.13 ppm attributable to the 1,2,7,8- and 4,5-carbazole positions respectively, as well as the appearance of a singlet at 1.41 ppm, attributable to the newly introduced *tert*-butyl groups, which serve to confirm the 3,6-di-alkylation of the carbazole.

*2.2.2 Iodination of **1** to afford 1,8-diiodo-3,6-di-tert-butylcarbazole, **2***

The 1,8-diiodination of **1** is essential for subsequent Ullmann coupling of imidazole to furnish the bimca framework. This functionalisation can be achieved with a variety of iodinating agents, the most efficient of which were found to be (i) ICl and (ii) BTRA·ICl_2 (where BTRA = benzyltrialkyl ammonium and R = methyl or ethyl) (Scheme 2.4). Commercial supplies of BTRA·ICl_2 were found to be prohibitively expensive,[†] thus the dichloroiodate salts were prepared through the known reaction of BTRA·Cl with ICl in a biphasic mixture of DCM and water.[87]

[†]BTMA·ICl_2: AUD 8.8 g^{-1}, BTMA·Cl: AUD 0.44 g^{-1}, ICl: AUD 1.83 g^{-1} from Sigma Aldrich price list as of 2016.

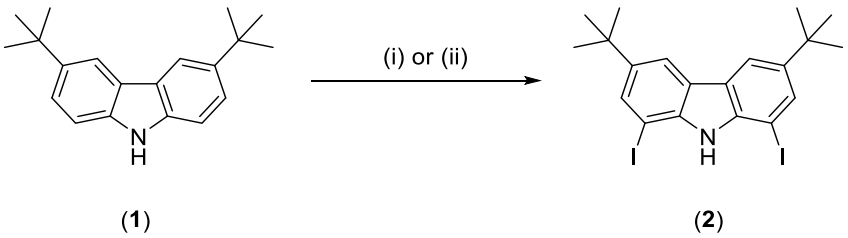

(**1**) (**2**)

Scheme 2.4 different iodination routes of 3,6-di*tert*-butyl carbazole in this work. Reaction conditions for (i): ICl, AcOH, 70 °C, 5 h, (ii): BTRA·ICl_2, AcOH, 60 °C, 18 h.

Route (i) is disadvantaged by an impractically small reaction temperature window, whereby no measurable reaction takes place at temperatures below 65 °C and reaction above 75 °C leads to ICl decomposition and diminished carbazole diiodination (19%), affording copious monoiodinated product or the return of **1**. By contrast, Iodination *via* path (ii) can be conducted under milder reaction conditions (Scheme 2.4), provides a cleaner workup, and gives higher, more reliable yields (80%). Indeed, monitoring of the reaction by TLC (neat hexane) indicates complete consumption of **1** after 30 minutes, and the presence of two products (R_f 0.2, 0.5) that eventually acquiesce to a single reaction product; **2** (R_f 0.5). It was found that the addition of a slight excess of BTMA·ICl_2 greatly increased the rate of the second iodination without the formation of side-products. The reaction profile above is attributable to the formation of monoiodinated di-*tert*-butyl carbazole intermediate, which then undergoes a second iodination to form **2**.

The best yields of **2** are achieved upon dilution of the acetic acid reaction mother liquor with roughly four times the volume of an aqueous solution of 5% (w/v) Na_2SO_3 to precipitate the organic products and quench residual iodinating agent. Subsequent extraction of the crude organic products into hexane (3 x 10 mL g^{-1} of crude **2**) followed by concentration and filtration through a pad of silica affords **2** as a white spectroscopically clean solid (80%).

The ^{1}H NMR (DMSO-d_6) spectrum of **2** is consistent with literature reports for this compound.[56] This includes the disappearance of the 1,8-carbazole proton resonances of **1** at 7.40 ppm and the generation of doublets for the 2,7- and 4,5-carbazole protons at 7.83 ppm and 8.23 ppm, respectively.

*2.2.3 Ullmann coupling of **2** with imidazole to afford **3***

The introduction of imidazole functionalities at the 1,8-carbazole positions was achieved through a modified Ullmann coupling (Scheme 2.5). In our hands, the synthesis originally outlined by Kunz in 2007,[56] which uses a Cu(I) catalyst under air-free conditions, was found to suffer from irreproducible yields and low product purity. These issues were addressed by extending the reaction time to 5 days (from 2-3 days) and a precipitation of the crude product from a methanol-water (3:1) mixture to achieve consistent yields of 79%.

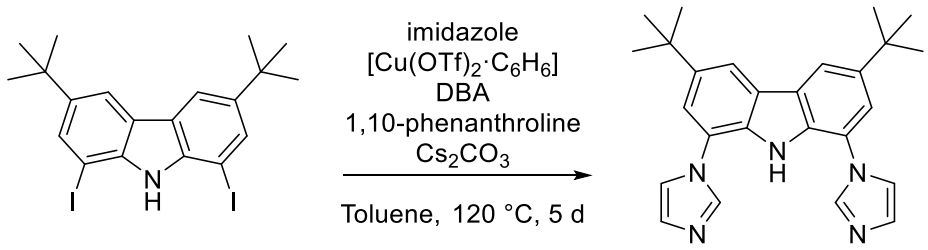

(**2**) (**3**)

Scheme 2.5 Synthesis of **3** *via* modified Ullmann coupling.

It is noteworthy that since this aspect of the project was completed, the Kunz group has reported that this transformation can be achieved with Cu(II) catalysts without the need for air-free techniques and a greatly reduced workup time.[85]

The identity of product **3** was verified by the presence of new imidazole associated signals in its ^{1}H (DMSO-d_6) spectrum. These include resonances for the C2, C4, and C5 protons at 8.20 ppm, 7.71 ppm, and 7.18 ppm respectively, each with signal integrals of 2 relative

to the ^{1}H NMR resonances of the carbazole framework. These resonances are in agreement with those in Kunz's original report and evidence a symmetrical compound in solution with a central, orthogonal mirror plane. [56]

Bis(imidazole)carbazole **3** also provides a versatile platform for *N*-functionalisation at the unsubstituted imidazole nitrogens, potentially enabling the tuning of bimca ligand steric parameters and bis(imidazolium)carbazole solubilities. Indeed collaborative efforts between the Kunz and Cole groups, including those herein (*vide infra* next section), have yielded a wide range of *N*-functionalised bis(imidazolium)carbazoles from a variety of alkylating reagents, each with potential for subsequent use as a bis(NHC)carbazolide (bimca^{R}) chelate ligand.

*2.2.4 The N-Alkylation of **3** to afford bimca^{R} proligands*

The methyl iodide adduct, Hbimca^{Me}(2HI), **4^{Me}**, as previously reported, suffers from poor solubility in the solvents typically used in air-free manipulations, such as long chain and arene hydrocarbons and ethers. In our hands, this has led to greater difficulty in ensuring stoichiometric deprotonation of the bis(imidazolium)carbazole dicationic proligand to the bimca^{R} ligand prior to metallation, occasionally causing irregular deprotonation of the ligand donor sites (*vide infra*). Thus, a more soluble system with similar electronic characteristics was targeted; Hbimca^{iPr}(2HI), **4^{iPr}** (Figure 2.2). We anticipated that the added flexibility of the larger *N*-alkyl substituent would beneficially affect solubility in ethereal solvents such as THF.

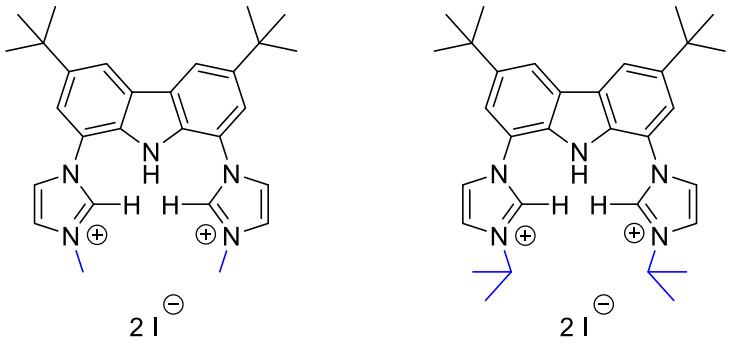

Figure 2.2 *N*-methyl *vs. N*-isopropyl substitution in Hbimca^{Me}(2HI) (**4^{Me}**) and Hbimca^{iPr}(2HI) (**4^{iPr}**)

Following the procedure reported by Kunz for Hbimca^{Me}(2HI), *i.e.* the facile nucleophilic substitution of an alkyl iodide with **3** in acetonitrile at reflux, afforded the analogous Hbimca^{iPr}(2HI), **4^{iPr}**. However, owing to lower thermal stability of isopropyl iodide, this reaction requires the use of a greater excess of the alkylating reagent (from 3 to 3.5 equivalents) than that employed in the original reported preparation of Hbimca^{Me}(2HI).[56] The resulting Hbimca^{iPr}(2HI) salt prepared through this method is devoid of isopropyl iodide decomposition products, such as 2,3-dimethyl butane, despite the excess of alkylating agent used. As expected, isopropyl variant **4^{iPr}** is more soluble in organic solvents than **4^{Me}**.

The ^{1}H NMR (DMSO-d_6) spectrum of **4^{iPr}** confirms symmetrical *N*-alkylation through a shift in key resonances and an integration pattern that is characteristic of a bimca^R species with orthogonal mirror plane symmetry (Figure 2.3; *S1*, *S2*). Particularly, four doublets between 7.77 ppm and 8.63 ppm, comprising the 2,4,5,7-carbazole protons (Figure 2.3; H_A, H_D) and the imidazolium C4 and C5 protons (Figure 2.3; H_B, H_C), each have a signal integration of 2 relative to the septet at 4.74 ppm, attributed to the two methine protons

of the newly introduced isopropyl *N*-substituents. The strong downfield shift of the imidazolyl C2- and carbazole NH resonances from 8.20 ppm and 10.92 ppm in the parent bis(imidazole), **3**, to 9.83 ppm and 11.57 ppm in **4^{iPr}** are typical of imidazolium formation from the parent neutral imidazole. [56]

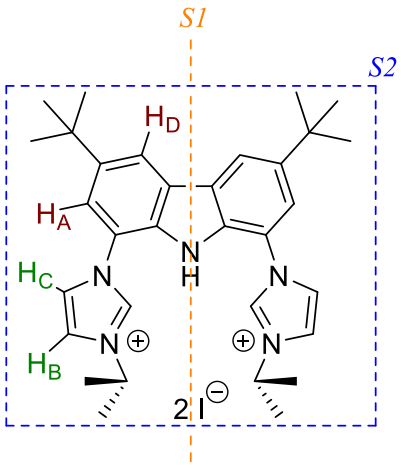

Figure 2.3 Solution state orthogonal mirror plane symmetry (*S1* and *S2*) of **4^{iPr}** as determined by NMR spectroscopy (DMSO-d_6).

Crystals of **4^{iPr}** suitable for single crystal X-ray diffraction structure analysis were grown from a saturated DCM solution diffused with hexane vapour at room temperature. (Figure 2.4)

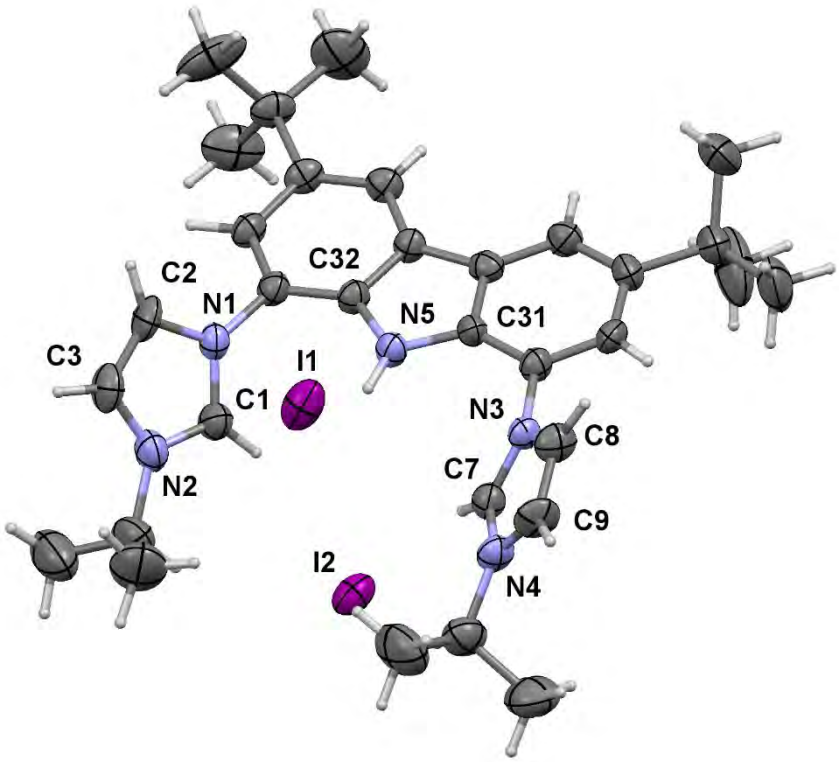

Figure 2.4 Ionic structure of Hbimca^{iPr}(2HI), **4^{iPr}**. Two dications of **4^{iPr}** and their associated iodide counterions are present in the asymmetric unit. Only one **4^{iPr}** is displayed for clarity. Thermal ellipsoids of non-hydrogen atoms are shown at 50% probability, hydrogen atom locations were determined experimentally and refined isotropically. Selected bond lengths and distances (Å): N1-C2: 1.355(8), N2-C3: 1.359(9), N3-C8: 1.393(9), N4-C9: 1.380(9), and angles (°): N1-C1-N2: 108.6(6), N3-C7-N4: 109.3(6), C31-N5-C32: 107.0(5).

The **4^{iPr}** salt crystallises in the triclinic space group $P\bar{1}$ with two ion pairs of **4^{iPr}** in the asymmetric unit and two molecules of heavily disordered partial occupancy hexane in the lattice. The latter were removed using a solvent mask (OLEX 2). All non-hydrogen atoms were refined with anisotropic displacement parameters. The average N-C-N bond angle of the imidazolium moieties is 109.0° which lies in the expected range for imidazolium

species (*e.g.* I*i*Pr·HBr: 108.76(14)°),[88] whilst the carbazole C-N-C bond angle (107.0(5)°) is slightly more acute than those in other related 1,8-disubstituted carbazoles (average of 108.96(13)° in related diimino- and dimesityl carbazoles, Figure 2.5). [54,57]

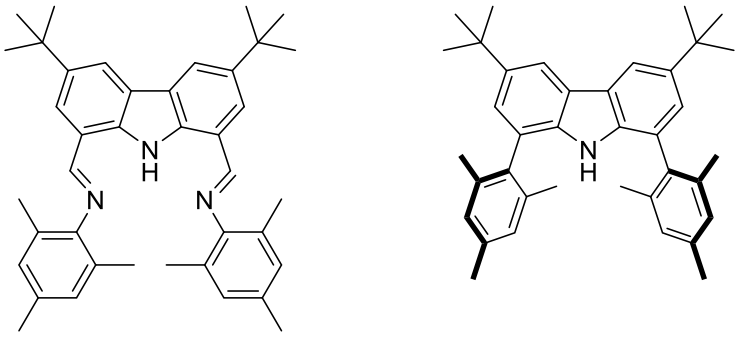

Gibson *et al.* **Kays** *et al.*

Figure 2.5 1,8-disubstituted diimino- and dimesityl carbazoles related to $\mathbf{4^R}$.[54,57]

The packing of $\mathbf{4^{iPr}}$ viewed along the *b* axis shows the location of the ioidide counterions in interstitial voids created between layers of the bimca^{iPr} dications (Figure 2.6), and shows no evidence of either intra- or intermolecular hydrogen bonding interactions, which are otherwise common for imidazolium cations with lighter, more electronegative halide counterions. [89]

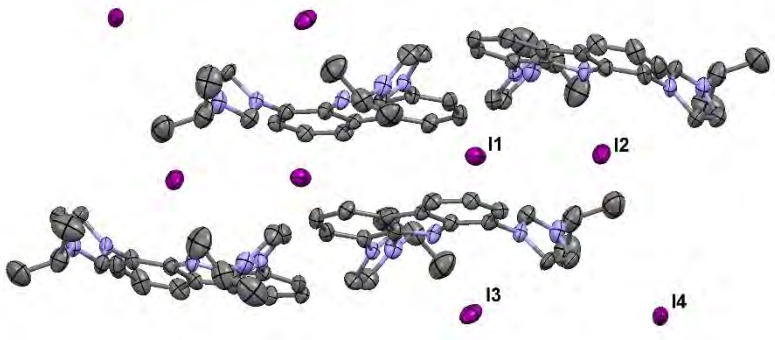

Figure 2.6 Unit cell of $\mathbf{4^{iPr}}$ viewed along the *b* axis. Hydrogen atoms and *tert*-butyl groups are omitted for clarity. Thermal ellipsoids are displayed at 50% probability.

*2.2.5 N-Arylation of **3** to afford bimca^R*

The bimca framework can also be *N*-derivatised using arylating agents. While aryl halide reagents are too deactivated for straightforward nucleophilic substitution reactions, *cf.* alkyl halides, attempts to arylate using highly electrophilic iodonium salts have been shown to work by the Kunz group, who effected *N*-phenylation of **3** with $I(Ph)_2 \cdot BF_4$[90] to afford the diphenyl **4^{Ph}**.[85] For our purposes, attempts were made to adapt the synthesis of **4^{Ph}** to accommodate the bulkier arenes 2,4,6-trimethylphenyl, to access **4^{Mes}**, and 2,4,6-tri-isopropylphenyl (Tripp), to access **4^{Tripp}**. Previous attempts in the Kunz group to synthesise **4^{Mes}** from the unsymmetrical $I(Ph)(Mes)BF_4$ precursor were met with the sole isolation of **4^{Ph}**, which is consistent with the selectivities observed for related C-C bond forming reactions using unsymmetrically substituted $I(Ph)(Ar)BF_4$ systems.[91] Thus a synthetic route was sought that incorporated the known homoaryl reagents $I(Mes)_2 \cdot Tos$[92] (X = pseudo halide or halide), and its unknown Tripp congener, $I(Tripp)_2X$. The reports of Olofsson and co-workers outline the syntheses of a range of symmetrically substituted $I(Ar)_2X$ (Ar = substituted phenyl, including mesityl, and X = pseudo halide)[90,92] salts through (i) the *in situ* oxidation of an aryl iodide to the corresponding periodinane, followed by its reduction to the desired iodonium salt in the presence of an aromatic hydrocarbon (Scheme 2.6 i), (ii) the *in situ* oxidation of aromatic hydrocarbons and elemental iodine, although in lower yields than (i) (Scheme 2.6 ii).

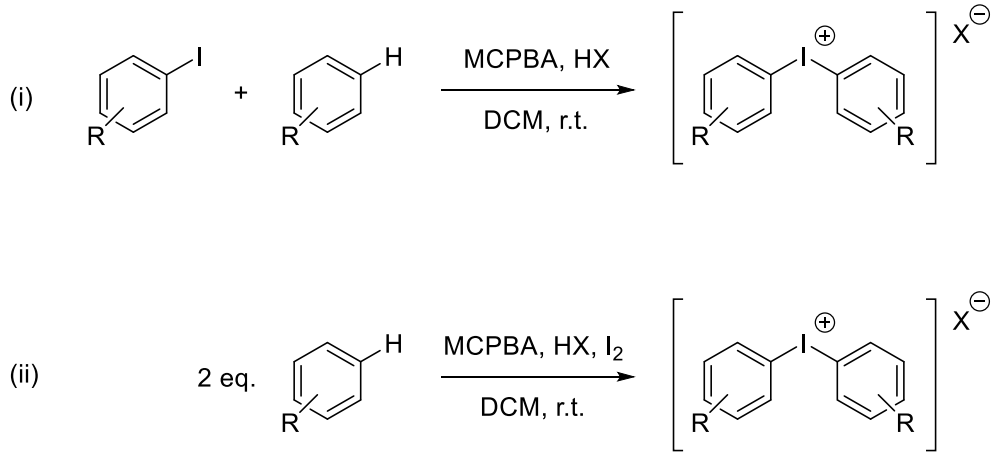

Scheme 2.6 Iodonium salt formation reported by Olofsson *et al.* starting from either (i) an aryl iodide and an aromatic hydrocarbon or (ii) an aromatic hydrocarbon and elemental iodine (R = H or alkyl substituents).

Accordingly, iodomesitylene was oxidised *in situ* in DCM in the presence of MCPBA, mesitylene and toluene sulfonic acid to afford $I(Mes)_2 \cdot Tos$ after 18 hours at room temperature. Concentration of the mother liquor to a viscous oil and recrystallisation through slow addition of diethyl ether afforded white needles from the oil ($DCM:Et_2O$ *ca.* 1:5) that characterise as spectroscopically pure $I(Mes)_2 \cdot Tos$ (47%). The mesityl iodonium salt exhibits a ^1H NMR spectrum (DMSO-d_6) that is in agreement with those of other reports, including a mesityl *meta*-aryl proton singlet at 6.35 ppm with a resonance integral of 4 relative to the tosylate aryl multiplets at 6.77 ppm and 8.08 ppm, each with signal integrals of 2.[92]

In the absence of commercially available TrippI, a synthetic route to the corresponding $I(Tripp)_2 \cdot Tos$ salt was attempted using Olofsson's path (ii) by reacting 1,3,5-triisopropylbenzene with elemental iodine in the presence of a stoichiometric amount of MCPBA and toluene sulfonic acid in DCM. Unfortunately, these reaction conditions failed to afford the target material, instead leading to the isolation of TrippH

and the known TrippI,[93] as evidenced by ^{1}H NMR spectroscopy. Attempts to oxidise this aryl halide to its corresponding iodonium salt using Olofsson's path (i) were also unsuccessful. It is likely that the targeted I(Tripp)$_2^+$ is too extremely hindered and the optimal reaction conditions could not be achieved in our hands.

With I(Mes)$_2$·Tos in-hand, the electrophilic aromatic substitution of **3** was attempted *via* the general methods described by Gao *et al.*,[94] and as adapted by the Kunz group for the generation of **4^{Ph}**,[85] wherein **3** was treated with two equivalents of phenyl iodonium salt in the presence of 10 mol% Cu(OAc)$_2$ in DMF at 100 °C over 18 hours. Use of this procedure with I(Mes)$_2$·Tos, however led to the quantitative recovery of starting materials with no evidence of **4^{Mes}** by ^{1}H NMR spectroscopy. Extension of the reaction time from 18 hours to 3 days was also unfruitful, as evidenced by a ^{1}H NMR spectrum of the vacuum dried reaction mother liquor, which was devoid of resonances attributable to the imidazolium salt C2H resonance. It is conceivable that the high steric demand imposed by the dimesityl iodonium salt hinders its entry into the copper mediated catalytic coupling cycle for this C-N coupling. No further attempts were made to prepare *N*-aryl bimca analogues.

2.3 Sequential deprotonation of 4^R

With attempts to isolate new bimca^{Ar} *N*-aryl derivatives hampered, focus was shifted toward modification of the existing **4^{Me}** and **4^{iPr}** salts to enhance their solubility and synthetic utility by seeking the development of diprotic systems, which were anticipated to be more soluble in organic solvents given their considerably lower molar mass and decreased charge overall. Indeed, previous work in the Cole group had noted the frequent and unintentional isolation of diprotic methyl derivative bimca^{Me}(H$_2$X) (X = Br or Cl)

from THF reaction mixtures containing dibromo indium or dichloro thallium bimca^{Me} complexes,[83] and it was presumed that the formation of these through facile protonation of the bimca^{Me} anion represented a thermodynamic well, likely due to the stable H-bonded nature of the resulting imidazolium carbazolide zwitterion. Therefore, we conjectured that such species may well be isolable and, like **4^{R}** species, potentially air- and moisture stable, but with improved solubility profiles.

2.3.1 Single deprotonation of 4^{Me}

In order to produce appreciable amounts of the diprotic salt bimca(H_2I), **5^{Me}**, the parent diiodide, **4^{Me}**, was reacted with one equivalent of KO*t*Bu in acetonitrile at room temperature for 1 hour without air-free precautions (Scheme 2). Deprotonation generates a bright yellow reaction mixture that emits a characteristic yellow fluorescence under long wave UV light. Removal of volatiles under vacuum followed by removal of the KI by-product by extraction of (**5^{Me}**) into dichloromethane and recrystallisation afforded the product in good yield as a bright yellow DCM solvate. Unsolvated, analytically pure **5^{Me}** was easily accessed by heating the above solid under vacuum at 120 °C for 1 hour. Unlike the parent salt **4^{Me}**, **5^{Me}** enjoys a considerable increase in solubility in ethereal solvents such as THF, which augers well for its application to a wider range of air-sensitive syntheses than the solubility limited **4^{Me}**.

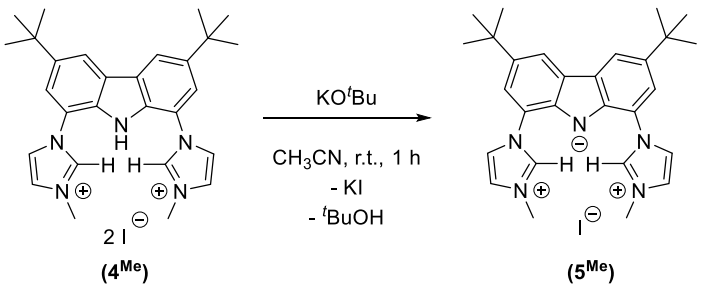

Scheme 2.7 Synthesis of the diprotic proligand **5^{Me}** from **4^{Me}**

The absence of a carbazole NH in the ^{1}H NMR (DMSO-d_6) spectrum of **5^{Me}**, as compared to the spectrum of the parent **4^{Me}**, which displays a singlet at 11.43 ppm,[56] confirms successful deprotonation at this position and thus the generation of **5^{Me}**. This is also consistent with the pK_a values of carbazole (*ca*. 20 in DMSO) and imidazolium C2 protons (*ca*. 24 in DMSO).[95,96] The ^{1}H and ^{13}C NMR spectra of **5^{Me}** also exhibit resonances belonging to chemically equivalent pairs of nuclei across the bimca^{Me} framework, indicating the retention of orthogonal mirror plane symmetry on the spectroscopic timescale (*cf*. Figure 2.3). Two dimensional ^{1}H-^{1}H NOESY, TOCSY, and ^{1}H-^{13}C HSQC experiments were useful in fully assigning the signals of the ^{1}H and ^{13}C NMR spectra of **5^{Me}**. For example, NOE correlations between the *tert*-butyl methyl singlet resonance at 1.48 ppm and the aryl carbazole ^{1}H NMR doublet resonances at 7.68 and 8.22 ppm, originating from protons at the 2,7- and 4,5-positions, respectively, assisted the assignment of these signals, as well as a NOE correlation between the imidazolium C5 proton resonance at 8.74 ppm and the 2,7-carbazole ^{1}H NMR doublet. In combination with the NOESY spectrum, ^{1}H-^{13}C HSQC and HMBC experiments confirmed the position of the C2 bound proton resonance as the most downfield shifted in the ^{1}H NMR spectrum of **5^{Me}** (10.78 ppm). Indeed, relative to the triprotic parent salt **4^{Me}**, the other imidazolium signals of **5^{Me}** are shifted downfield significantly due to the negative charge of the carbazolide. For the C4- and C5 proton resonances, this leads to a shift downfield of $\geq$ 0.67 ppm.

Yellow rectangular plates of **5^{Me}** suitable for single crystal X-ray structure determination were grown from a saturated DCM solution layered with hexane (Figure 2.7). The salt crystallises in the monoclinic space group $P2_1/c$ with a full ion pair (**5^{Me}**) and one molecule of DCM in the asymmetric unit. All non-hydrogen atoms were refined

anisotropically and the positions of hydrogen atoms were derived from difference maps and refined isotropically.

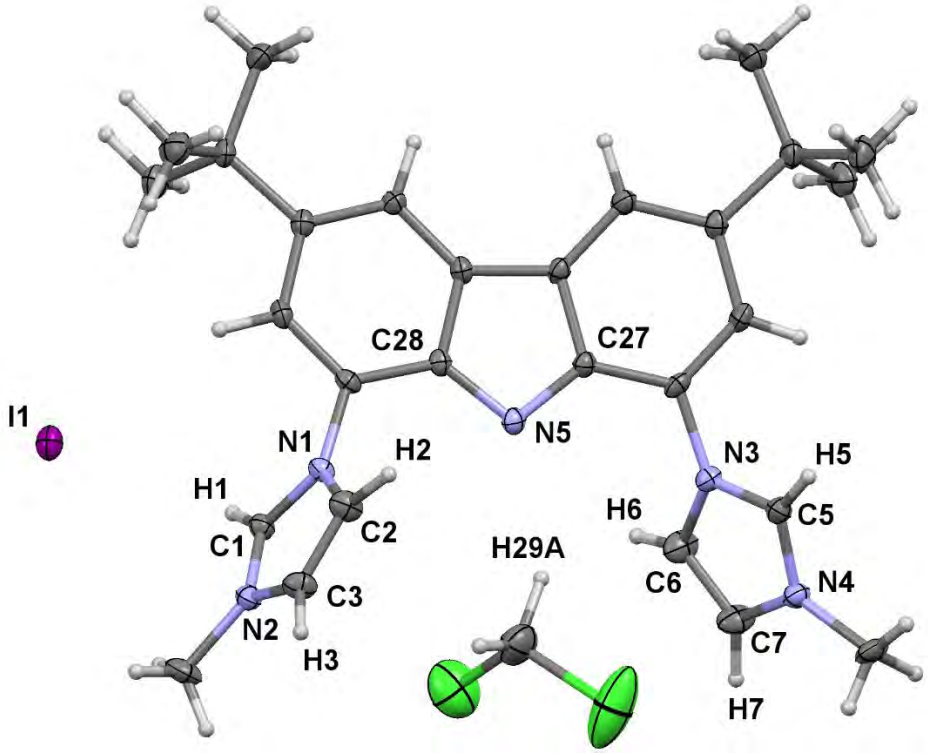

Figure 2.7 Molecular structure of bimca^{Me}(H_2I), **5^{Me}**. Atoms are shown with anisotropic atomic displacement parameters at 50% probability. Selected bond lengths and distances (Å): H1···I1: 3.07(4), N1-C2 1.332(4), N2-C3: 1.375(4), N3-C6: 1.388(4), N4-C7: 1.381(4), N5···H29A: 2.44(9), and angles (°): N1-C1-N2: 108.6(3), N3-C5-N4: 108.8(3), C27-N5-C28: 102.9(2).

The molecular structure of **5^{Me}** exhibits a decreased C-N-C bond angle at the carbazolide (102.9(3)°) relative to the parent carbazole, **4^{Me}**, (107.1(6)°),[56] which is consistent with NH deprotonation.[97] In contrast, the average imidazolium N-C-N bond angle of 108.7° experiences minimal change relative to those of **4^{Me}** (N-C-N 108.7(5)°)[56] and is consistent with the maintenance of protonation at these positions as per its solution phase ^{1}H NMR data.

The packing of $\mathbf{5^{Me}}$ (Figure 2.8) shows the formation of a one-dimensional hydrogen bonded network where the C5 protons of the imidazolium rings act as uncommon C-H donors to form intermolecular hydrogen bonds with the negatively charged carbazolide nitrogen acceptors of other molecules of $\mathbf{5^{Me}}$ with an average H···N distance of 2.56 Å. This is within the sum of the van der Waals' radii of hydrogen and nitrogen (2.75 Å).[98] As a consequence, both imidazolium C2 protons are directed towards lattice voids occupied by the iodide counterions above and below the plane of the carbazole with a C2H···I distance of 3.07(4) Å at an angle of 147(3)°, which is within the sum of the van der Waals' radii of H and I (3.18 Å)[98] and may be considered a weak H-bonding interaction. The formation of the above H···N hydrogen bonded networks is to be expected, since the anionic carbazolide nitrogen presents itself as an excellent H-bond acceptor compared to the parent $\mathbf{4^{Me}}$ (Figure 2.6 above) which does not possess such a functionality.

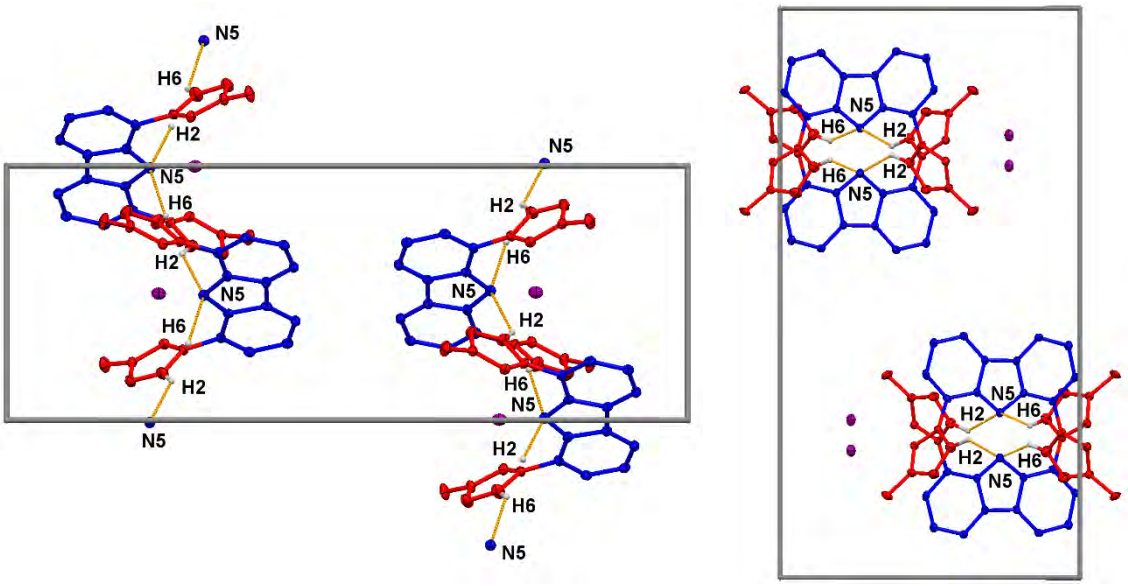

(i) (ii)

Figure 2.8 Unit cell of $\mathbf{5^{Me}}$ viewed along the *a* axis (i) and *c* axis (ii) showing its hydrogen bonding network (cell axes in grey). Non-H-bonded hydrogen atoms, *tert*-butyl groups and solvent molecules have been removed for clarity and the carbazolide- and imidazolium heterocycles have been coloured blue and red, respectively. H-bond contacts are coloured orange. Selected bond lengths (Å): N5···#H2: 2.51(4), N5···#H6: 2.61(4), and angles (°): N5···#H2-#C2: 137(3), N5···#H6-#C6: 137(3). Symmetry operations used to generate equivalent atom positions: *x*, *y*, *z*; 1-*x*, ½+*y*, 1½-*z*; 1-*x*, 1-*y*, 1-*z*; *x*, ½-*y*, -½+*z*.

2.3.2 Single deprotonation of $\boldsymbol{4^{iPr}}$

The formation of the *N*-isopropyl analogue of $\mathbf{5^{Me}}$; $\mathbf{5^{iPr}}$ proceeds in an analogous manner to its methyl relative. The solution state ^{1}H and ^{13}C NMR (DMSO-d_6) spectra of $\mathbf{5^{iPr}}$ provide similar indications regarding bulk mono-deprotonation exclusively at the carbazole NH position, and also exhibit a shift and integration pattern consistent with a symmetrical compound in solution. It is worth noting that $\mathbf{5^{iPr}}$ is considerably more soluble in THF and other organic solvents than $\mathbf{5^{Me}}$.

Like its methyl relative, zwitterion **5^{iPr}** exhibits high crystallinity. Crystals suitable for X-ray diffraction structure determination were grown from a saturated room temperature solution in fluorobenzene. The salt crystallises in the monoclinic space group *C*2/*c* with one ion pair of **5^{iPr}** and one molecule of fluorobenzene in the lattice. All non-hydrogen atoms were refined anisotropically and all hydrogen atoms were located from difference maps and refined isotropically (Figure 2.9).

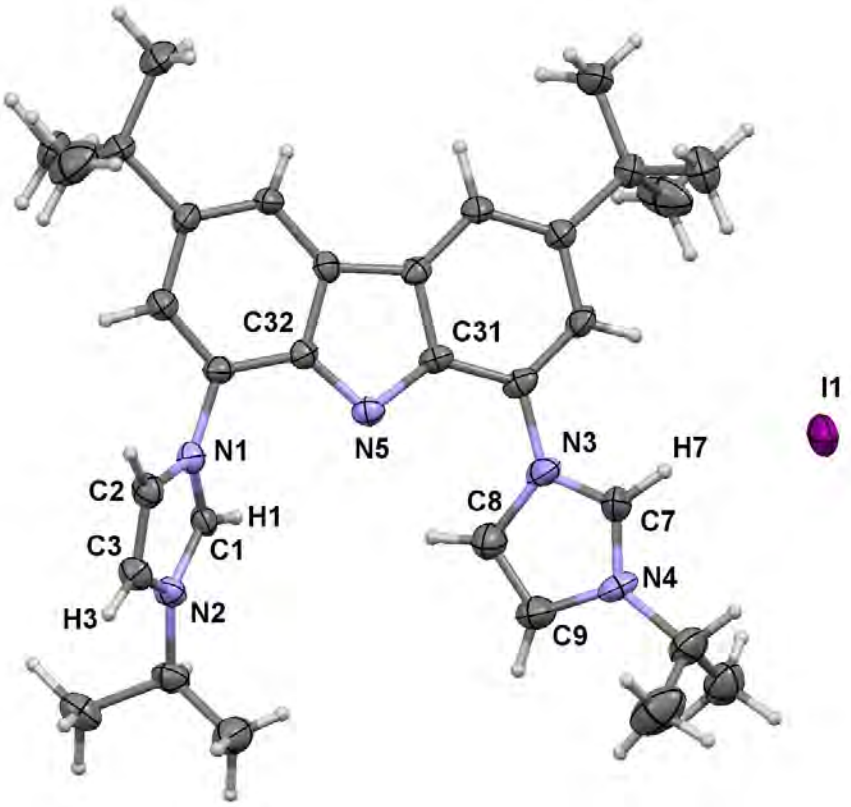

Figure 2.9 Molecular structure of bimca^{iPr}(H_2I), **5^{iPr}**. Atoms are shown with anisotropic atomic displacement parameters at 50% probability. Selected bond lengths and distances (Å): H7···I1: 2.9138(4), N1-C2: 1.380(7), N2-C3: 1.374(7), N3-C8: 1.434(8), N4-C9: 1.429(8), and angles (°): N1-C1-N2: 109.0(5), N3-C7-N4: 113.4(5), C31-N5-C32: 102.5(4).

The salt displays similar metrics to **5^{Me}** and likewise forms intercation imidazolium CH to carbazolide nitrogen H-bonds. A noteworthy distinction to **5^{Me}** with respect to these

solid state interactions is the contact of a single imidazolium C4-H with the anionic carbazolide nitrogen of a second half-eclipsed molecule of **5**^{iPr}, rather than the intracation imidazolium C5···H *cf.* packing of **5**^{Me}, Figure 2.8, *vide supra* (N5···#H3 distance: 2.60(6) Å, sum the of H and N van der Waals' radii = 2.75 Å). Interestingly, the relatively unsymmetrical nature of this hydrogen bonding causes **5**^{iPr} to form discrete hydrogen bonded bimca^{iPr}(2H)$^{+}$ pairs under these conditions, rather than the polymeric networks of the methyl derivative (Figure 2.10). A further consequence of this interaction is the metric disparity of the imidazolium rings, wherein the heterocycle that does not take part in hydrogen bonding exhibits N1-C5 and N3-C4 bond lengths that are noticeably longer (0.05 Å) than those in the H-bonded counterpart, whilst the endocyclic N-C-N angles of these moieties contrast dramatically: 113.5(6)° *versus* 109.0(5)°.

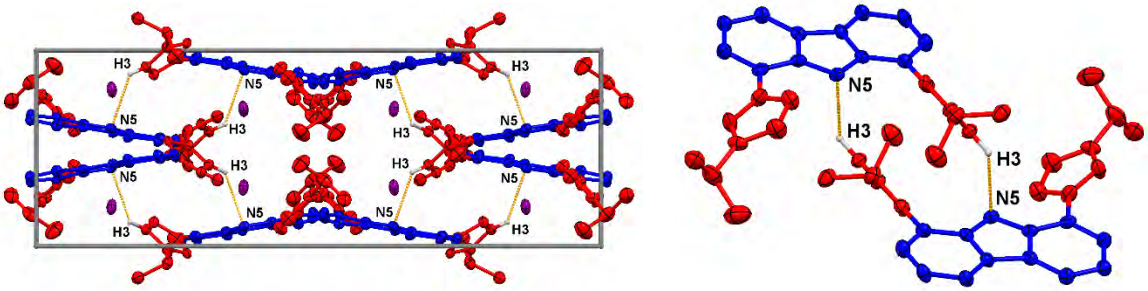

(i) (ii)

Figure 2.10 (i) Unit cell of **5**^{iPr} viewed along the *c* axis (cell axes in grey) and (ii) discrete (bimca^{iPr})$_2^{2+}$ unit showing hydrogen bonded ion pairs. Non-H-bonded hydrogen atoms, *tert*-butyl groups and lattice solvent molecules have been removed for clarity and the carbazolide- and imidazolium heterocycles have been coloured blue and red, respectively. H-bond contacts are coloured orange. Selected distance (Å): N5···#H3: 2.60(6), and angle (°): N5···#H3-#C3: 122(4). Symmetry operations used to generate equivalent atom positions in (ii): *x*, *y*, *z*; ½-*x*, 1½-*y*, 1-*z*.

2.3.3 Attempted double deprotonation of $\mathbf{4^R}$

To further probe the sequential deprotonation of the $\mathbf{4^R}$ triprotic systems, a synthesis for the formally neutral bimca^R(H), $\mathbf{6^R}$, proligand scaffold was sought. Access to such species would in turn lead to simplified metallations, particularly for monovalent metals *e.g.* In(I) and Tl(I). Complexations involving these low valent precursors benefit from streamlined, one-pot reaction conditions due to the relative instability of soluble low valent, non-halide, precursors.[99] Thus, the reaction of either triprotic $\mathbf{4^R}$ or diprotic $\mathbf{5^R}$ with two or one equivalent of base respectively (Scheme 2.8), was pursued as a means of formally accessing neutral $\mathbf{6^R}$ species suitable for downstream reaction with M(I) species with internal base ligands *e.g.* Tl(HMDS).

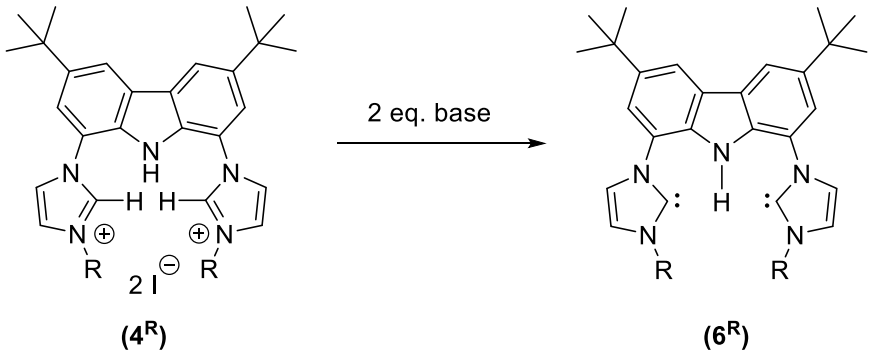

Scheme 2.8 Planned general synthesis of the neutral $\mathbf{6^R}$ proligands from a triprotic $\mathbf{4^R}$ precursor.

Preliminary reactions were carried out using $\mathbf{4^{Me}}$ under an inert atmosphere with two equivalents of either NaH or KHMDS as base. During the initial stage of the reaction, a colour change from colourless to amber to red was observed with the concurrent formation of NaI or KI as a white precipitate over a period of *ca*. 30 minutes. After this time, the reaction mixtures darkened further with the precipitation of large amounts of a bright yellow precipitate. This material behaves similarly to $\mathbf{5^{Me}}$, with a comparable characteristic bright yellow fluorescence under long wave UV light.

Isolation of the reaction supernatants by filtration and removal of volatiles under vacuum afforded red, viscous solid residues that produced ^{1}H NMR (THF-d_8) spectra consistent with a mixture of compounds including imidazolium and protonated carbazole NH moieties, as evidenced by strongly downfield shifted singlet resonances at 10.45 ppm and 11.36 ppm. By contrast the ^{1}H NMR (THF-d_8) spectra of the yellow filtrants are consistent with the chemical shifts and integration patterns of "**5**$^{\mathbf{Me}}$-like" species (*vide supra*). The *in situ* monitoring of this reaction by ^{1}H NMR spectroscopy (THF-d_8) permitted the acquisition of a ^{1}H NMR spectrum of a putative **6**$^{\mathbf{Me}}$ species which is devoid of a NH carbazole resonance and exhibits the expected, although strongly broadened, resonance pattern for a symmetrical **6**$^{\mathbf{Me}}$ species, as distinct from the resonances for the diprotic **5**$^{\mathbf{Me}}$ in THF-d_8. The broadness of these resonances precludes meaningful signal integration, although the resonance at 10.37 ppm is tentatively attributed to the bimca^{Me}(*H*) proton (*cf*. 11.25 for **5**$^{\mathbf{Me}}$ in THF-d_8) whilst the four remaining aryl signals of the aromatic ligand scaffold experience an overall upfield shift compared to **5**$^{\mathbf{Me}}$, consistent with the formation of a formally neutral species. These resonances gradually convolute into a complex mixture of products over a period of *ca*. 30 minutes. This frustrated the acquisition of meaningful ^{13}C NMR data for **6**$^{\mathbf{Me}}$. One interpretation of these outcomes is that **6**$^{\mathbf{Me}}$-type neutral proligands are not stable in solution with respect to proton transfer to afford a bimca^{Me} anion and a bimca^{Me}(2H) dication, and that [bimca^{Me}][bimca^{Me}(2H)] ion pairs (Scheme 2.9) eventuate and equilibrate to afford a complex mixture of species. The insolubility of the yellow, UV active solid (presumably a "**5**$^{\mathbf{Me}}$-like" salt) likely contributes to the dynamic nature of solutions of putative **6**$^{\mathbf{Me}}$.

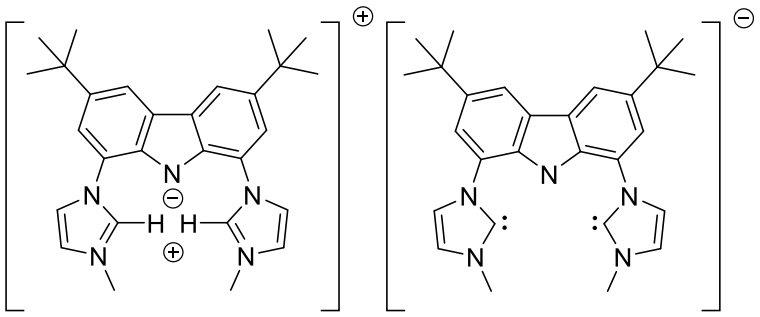

Scheme 2.9 Likely transitional ion pair formation during the attempted synthesis of $\mathbf{6^{Me}}$.

Shifting attention to the bimca^{iPr} system, for which close contact [bimca^{iPr}][bimca^{iPr}(2H)] ion pairs were deemed less likely owing to greater *N*-alkyl steric bulk, afforded a $\mathbf{6^{iPr}}$ derivative with a relatively simple and non-dynamic solution behaviour and presumably therefore a substantially greater stability as a monoprotic neutral species (> 2 weeks), as determined by ^{1}H NMR spectroscopy. Unfortunately, attempts to undertake crystallographic studies on $\mathbf{6^{iPr}}$ were thwarted by its low crystallinity and high solubility (*vis-à-vis* $\mathbf{4^{iPr}}$ and $\mathbf{5^{iPr}}$) when precipitated from a range of non-protic organic solvent systems. As discussed below, while $\mathbf{6^{iPr}}$ is presumably the major product of this reaction (by ^{1}H and ^{13}C NMR spectroscopy), the solutions of $\mathbf{6^{iPr}}$ were persistently blighted by the presence of inseparable impurities, presumably K(bimca^{iPr}) and $\mathbf{5^{iPr}}$. This also frustrated the acquisition of analytically pure samples.

The ^{1}H NMR of $\mathbf{6^{iPr}}$ provides evidence for a neutral bimca^{iPr} scaffold with a high degree of symmetry, as demonstrated by its simple A:B:B:A shift and integration pattern, which is observed for other symmetrical bimca species (*vide supra*), with four sets of aryl proton signals corresponding to the imidazolyl protons (A) and the aryl carbazole protons (B), with signal integrations of 2 relative to the septet at 4.74 ppm which may be attributed to the two isopropyl methine protons. These shifts are also distinct from those of the diprotic $\mathbf{5^{iPr}}$ salt. The signal for the remaining bimca^{iPr}(*H*) proton appears as a broad singlet at

11.12 ppm (*cf.* **6^{Me}** at 10.37 in THF-d_8), presumably due to its likely fluxional behaviour (Scheme 2.10). Similarly, the ^{13}C NMR spectrum of **6^{iPr}** exhibits a simple set of sharp resonances for a major bimca^{iPr} product. This shift pattern is in agreement with an overall symmetrical bimca^{iPr} scaffold. As in the ^{1}H NMR spectrum, the bimca^{iPr}(H) associated imidazolyl C2 carbon is not well resolved and in this case could not be observed directly or through indirect two-dimensional correlation experiments.

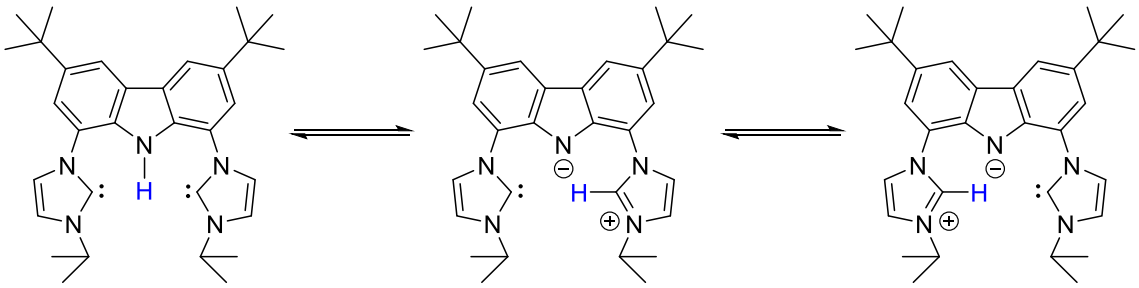

Scheme 2.10 Possible isomeric forms of **6^{iPr}** showing the displacement of the bimca^{iPr}(*H*) proton, presumably the cause of ^{1}H and ^{13}C resonance broadening in the NMR spectra of **6^{iPr}**.

*2.3.4 Three-fold deprotonation of **4^{R}***

The original report of bimca^{Me} by Kunz outlines the triple deprotonation of the salt Hbimca^{Me}(2HI) using three equivalents of LDA to generate the complex Li(bimca^{Me}), Li**7^{Me}**.[56] In collaboration with the Kunz group, we have extended this approach to a wider range of strong, non-nucleophilic group 1 bases *e.g.* *n*BuLi and M(HMDS) (M = Li, Na, K), as well as other **4^{R}** salts, to readily afford the corresponding M(bimca^{R}) species (M**7^{R}**; where M = metal cation, Scheme 2.11). These are useful as salt metathesis ligand transfer agents. The following section focuses on bimca^{R} complexes of lithium and potassium, *i.e.* Li**7^{R}** and K**7^{R}**.

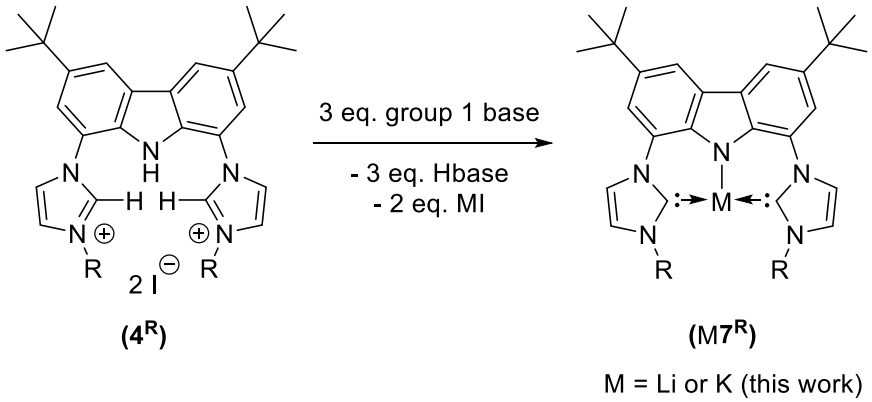

Scheme 2.11 Triple deprotonation of the acidic positions of **4^{R}** to generate the pseudo-meridional bimca^{R} binding cavity starting from **4^{R}**

Addition of three equivalents of a group 1 metal base to THF suspensions of the bis(imidazolium)carbazoles **4^{Me}** or **4^{iPr}** affords an immediate colour change from colourless to bright yellow due to the initial formation of the bimca^{R}(H_2I) salts, **5^{R}** (*vide supra*), which remain as a slurry in THF. In the case of reactions involving lithium bases, such as *n*BuLi, the reaction mixtures gradually darken and become clear over the course of one hour due to the high solubilities of the lithium halide co-products in ethereal solvents, and strong visible blue fluorescence in daylight or under long wave UV light accompanies successful formation of the Li**7^{R}** complex.

In solution, the Li**7^{R}** complexes (R = *i*Pr or Me) adopt symmetrical coordination modes, that produce A:B:A:B proton spin systems by ^{1}H NMR spectroscopy (THF-d_8), that are similar to other symmetrical bimca^{R} compounds (*vide supra*). Deprotonation at the acidic carbazole and imidazolium positions is confirmed by the absence of resonances attributable to these protons in the ^{1}H NMR spectra of Li**7^{R}**. The appearance of a single carbenic resonance in the ^{13}C NMR spectrum (THF-d_8) of Li**7^{iPr}** at 203.66 ppm is consistent with the previously reported value for Li**7^{Me}** (206.1 ppm also THF-d_8),[56] and thusly indicates lithium to NHC coordination in solution, whereby the C2 ^{13}C NMR

chemical shift value is upfield of that for comparable free imidazol-2-ylidenes (IMes: 219.69 ppm, IMe_4: 213.73 ppm THF-d_8).[100] It is noteworthy that these resonances (Li**7^{R}**) are downfield of those reported in mono(NHC) lithium complexes, such as the pendant amido-NHC lithium complex reported by Arnold (198.71 ppm, C_6D_6, *vide infra* Section 2.4, Figure 2.12, i)[101] and lie closer to those in the recently described neutral bis(NHC) lithium complexes of Hofmann and co-workers (205.92 ppm THF-d_8, *vide infra* Section 2.4, Figure 2.12, ii).[102] This supports the supposition that the NHC donors of Li**7^{iPr}** symmetrically coordinate a single lithium atom in THF rather than two distinct lithium cations. However, despite concerted efforts to observe $^{1}J_{CLi}$ coupling, no coupling to spin active $^{6/7}$Li nuclei was deduced in the ^{13}C NMR spectrum of either Li**7^{R}** compound, possibly due to the quadrupolar nature of the $^{6/7}$Li nucleus or rapid exchange processes between the lithium cation of the Li(bimca^{R}) complex and the dissolved LiI co-product (2 eq. relative to Li**7^{R}**). The removal of LiI proved difficult due to the similar solubility profiles of Li**7^{R}** species and LiI in THF. Indeed, the inclusion of LiI in the solid product after drying under vacuum blighted microanalysis data, which consistently returned values that are suggestive of partial $LiI(THF)_n$ inclusion. Thus, the isolation of analytically pure lithium bimca^{R} complexes could not be achieved. It is noteworthy that previous reports of the use of Li**7^{Me}** species have only described their generation and use *in situ*. We also note the extreme air and moisture sensitivity of the Li**7^{R}** species. For example, use of undried "boil-off" nitrogen as an inert gas supply during workup led to facile reprotonation of the Li**7^{R}** species, especially if the workup was not carried out expediently and with minimal manipulation. This furnished copious products akin to **5^{R}** species by ^{1}H NMR spectroscopy despite the otherwise meticulous application of air-sensitive technique.

Further to contamination of solid product, the persistent inclusion of LiI(THF)$_n$ in solutions of Li**7**$^{\mathbf{R}}$ proved problematic for subsequent salt metathesis transmetallations when utilising softer metals with non-iodo halide co-ligands. This manifested as halide scrambling and LiI(THF)$_n$ contamination, which marred the analytical purity of subsequent products (see Chapter 3). To address this, it was hoped that the substitution of lithium for potassium, by employing KHMDS instead of *n*BuLi, would obviate alkali metal iodide inclusion (Scheme 2.12). This is a common strategy when alkali metal halide contamination is undesirable, and capitalises on the decreased solubility of the heavier alkali metal halides, which aids their removal from ethereal reaction mixtures by precipitation.

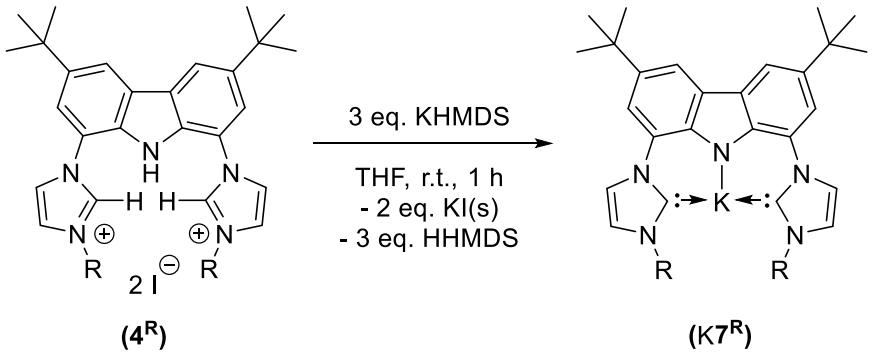

Scheme 2.12 Synthesis of K(bimca^{R}) complexes (K**7**$^{\mathbf{R}}$).

Indeed, the analogous deprotonation reaction of **4**$^{\mathbf{Me}}$ or **4**$^{\mathbf{iPr}}$ with three equivalents of K(HMDS), under the same reaction conditions as those used to generate Li**7**$^{\mathbf{R}}$ species, produced copious solid KI metathesis co-product over the course of one hour that could be removed by filtration. Under these conditions the reaction yields a much darker mother liquor than those of the Li**7**$^{\mathbf{R}}$ species with a similar visible blue fluorescence (*cf.* Li**7**$^{\mathbf{R}}$ complexes in solution). Monitoring the **4**$^{\mathbf{Me}}$ reaction to afford K**7**$^{\mathbf{Me}}$ by ^{1}H NMR spectroscopy (THF-d_8) provides similar evidence for the triple deprotonation of the **4**$^{\mathbf{Me}}$ as for Li**7**$^{\mathbf{Me}}$, as demonstrated by the absence of the NH and imidazolium C2H resonances

of **4^{Me}** (11.43 and 9.75 ppm in DMSO-d_6) and an overall upfield shift of the remaining bimca^{Me} scaffold chemical shifts relative to those of the **5^{Me}** proligand (THF-d_8). Insofar the ^{1}H NMR chemical shift data for K**7^{Me}** are strikingly similar to those of Li**7^{Me}**, displaying minimal differences in the chemical shift values for the imidazolyl protons and carbazolide aryl protons. Key ^{1}H NMR resonance data for K**7^{Me}**, Li**7^{Me}**, **6^{Me}**, and **5^{Me}** are summarised in Table 2.1.

^{1}H NMR Assignment	K**7^{Me}** (ppm)	Li**7^{Me}** (ppm)	**6^{Me}** (ppm)	**5^{Me}** (ppm)
(A) 4-Imidazolyl	7.00	7.16	7.00	7.61
(B) 2,7-Carb.	7.21	7.41	7.41	7.50
(A) 5-Imidazolyl	7.46	7.79	7.85	8.21
(B) 4,5-Carb.	8.02	7.99	8.04	8.12

Table 2.1 Key ^{1}H NMR (THF-d_8) chemical shift data for K**7^{Me}**, Li**7^{Me}**, **6^{Me}**, and **5^{Me}**.

Potassium complexes K**7^{Me}** and K**7^{iPr}** appear to be unstable as solids. Each decomposing readily upon removal of THF/THF-d_8 upon reaction workup. This resulted in intractable mixtures of products by ^{1}H NMR spectroscopy (THF-d_8), and is consistent with the observation that solid state characterisations of mono(NHC) complexes of heavy alkali metal cations are rare and those of bis(NHC) complexes are practically unknown.[102,103] It is also plausible that group 1 cations larger than lithium cannot be accommodated in the bimca^R CNC coordination site, potentially decreasing the stability of these species in the solid state. Despite the outcomes of this aspect of this study, K**7^R** compounds have been used prodigiously as *in situ* metathetical ligand transfer reagents during subsequent studies within the Kunz and Cole groups (*e.g.* Chapters 3 and 4 herein), owing to the

major benefits represented by KI removal upon their formation (*cf.* LiI(THF)$_n$ inclusion in preparations using Li**7**$^{\mathbf{R}}$).

2.4 Isolation and crystallographic studies of Li7^{R} species

In the interest of achieving the solid state characterisation of an alkali metal bimca^{R} species, our focus shifted to the recrystallisation of Li**7**$^{\mathbf{R}}$ salts from ethers such as DME (*cf.* stability of Li**7**$^{\mathbf{R}}$ to drying *in vacuo*) since multiple attempts to do so from THF resulted in crystals of insufficient quality for crystallographic studies. Accordingly, Li**7**$^{\mathbf{iPr}}$ was isolated under strict anaerobic conditions and recrystallised from DME to afford a small number of crystals suitable for characterisation by single crystal X-ray diffraction structure determination (Figure 2.11).

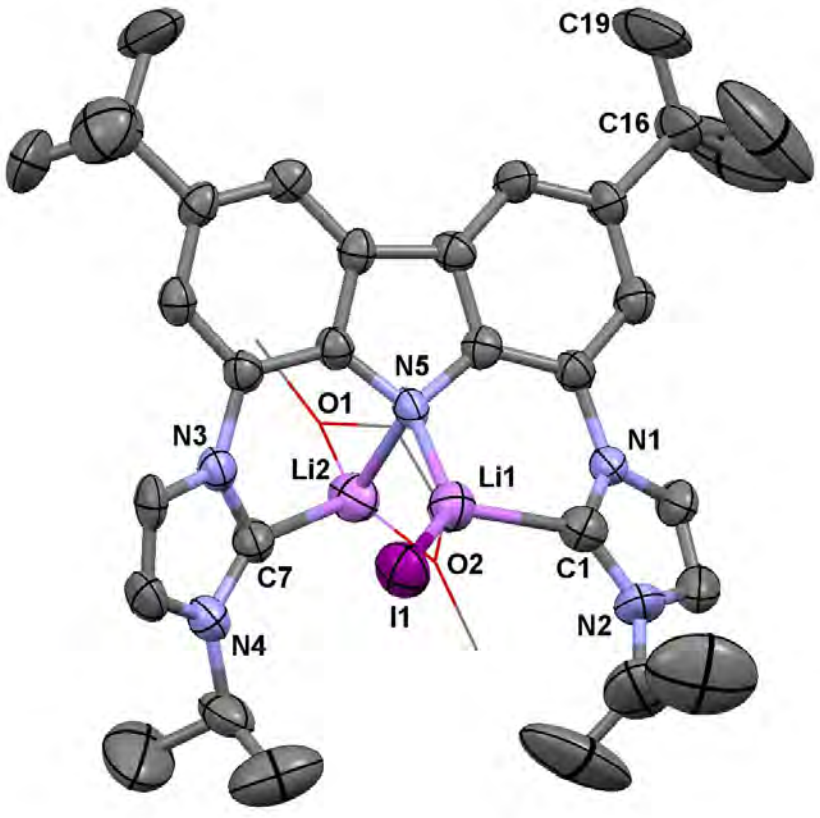

(i)

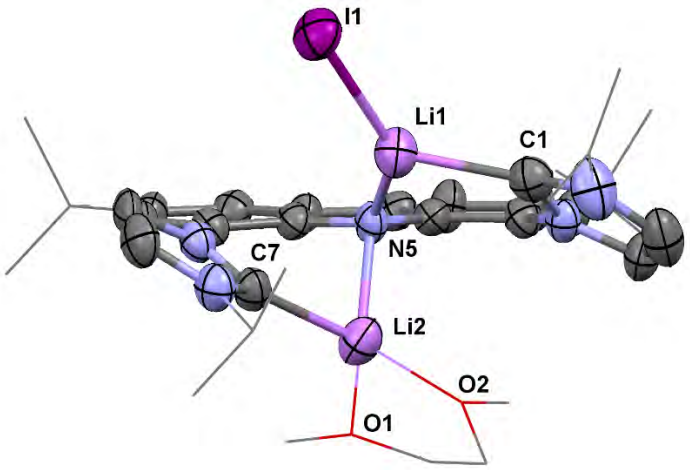

(ii)

Figure 2.11 Molecular structure of Li**7**^{iPr}·LiI(DME) showing the inclusion of one molecule of LiI in the binding cavity. Atoms are shown with anisotropic atomic displacement parameters at 50% probability. In (i) coordinated DME is depicted as wireframes, in (ii) *N*-isopropyl, *tert*-butyl groups, and coordinated DME are depicted as wireframes. Hydrogen atoms are omitted for clarity. Selected bond lengths and distances (Å): C1-Li1: 2.140(11), C7-Li2: 2.131(11), Li1···Li2: 3.041(15), N5-Li1: 1.970(11), N5-Li2: 2.079(11), Li-I1: 2.647(10), O1-Li2: 1.987(12), O2-Li2: 1.908(11), and angles (°): N1-C1-N2: 104.1(5), N3-C7-N4: 103.2(4), C22-N5-C32: 103.5(4), Li1-N5-Li2: 97.3(5).

Complex Li**7**^{iPr}·LiI(DME) crystallises in the monoclinic space group *C*2/*c* with one molecule of Li**7**^{iPr}·LiI(DME) in the asymmetric unit. All non-hydrogen atoms were refined with anisotropic displacement parameters, whilst hydrogen atom positions were constrained to modelled positions with the exception of those on the methyl group C19. The rotational disorder of the *tert*-butyl group centred on C16 could not be modelled adequately and prevents placement of hydrogen atoms at the C19 terminal methyl group. The thermal ellipsoid plot of Li**7**^{iPr}·LiI(DME) (Figure 2.11) represents the first example

of a structurally characterised lithium complex of the bimca^{R} ligand class and a rare example of an alkali metal coordinated NHC.[101,102] The average endocyclic N-C-N angle in the NHC moieties of Li**7**$^{\mathbf{iPr}}$·LiI(DME) is 103.6°, which is consistent with those angles reported for the mono(NHC) lithium complex reported by Arnold and co-workers (average N-C-N: 102.9°, Figure 2.12 i)[101] and characteristically greater than those of free imidazol-2-ylidene carbenes by *ca.* 2° (*e.g.* IMes and IMe$_4$ NCN angles 101.4(2)° and 101.5(1)°, respectively),[100] and wider than those same angles in the mono- and bis(NHC) lithium complexes, comprising tethered alkyl substituted NHC ligands of Hofmann and co-workers (average N-C-N angle: 101.4°, Figure 2.12 ii).[102] The N-C-N angles of Li**7**$^{\mathbf{iPr}}$·LiI(DME) are unlike the previously discussed diprotic zwitterion **5**$^{\mathbf{iPr}}$ (*cf.* H-bonded *versus* non-H-bonded imidazoliums), that is, no significant difference in the N-C-N bond angles between the two NHC moieties could be deduced despite the differing coordination number and co-ligands of their lithium atoms (N-C-N angles in **5**$^{\mathbf{iPr}}$: 109.0(5), 113.4(5)° *vs.* those of Li**7**$^{\mathbf{iPr}}$·LiI(DME): 104.1(5), 103.2(4)°).

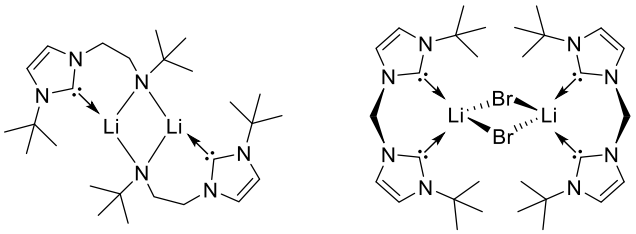

Figure 2.12 (i) NHC-amido lithium complex exhibiting Li-N-Li bifurcation reported by Arnold and co-workers.[101] (ii) bis(NHC) lithium complex reported by Hofmann and co-workers.[102]

The lengths of both NHC carbon to lithium bonds in Li**7**$^{\mathbf{iPr}}$·LiI(DME) are identical within error; 2.140(11) Å (C1-Li1), 2.131(11) Å (C7-Li2), and are in agreement with typical

NHC-Li bond lengths found in the literature, such as the NHC tethered amide supported lithium dimer reported by Arnold and co-workers (Li-C 2.162(4) Å, Figure 2.12 i),[101] which, like the carbazolide nitrogen of Li**7**$^{\mathbf{iPr}}$·LiI(DME), exhibits a bifurcated nitrogen to lithium Li-N-Li moiety. The equivalent bifurcation angle in Li**7**$^{\mathbf{iPr}}$·LiI(DME) is significantly wider (97.3(5)°) than that of the aforementioned amide tethered NHC (average bifurcation angle 73.14°), owing to the relative differences in geometric requirements of the Li_2-N_2 moiety in Arnold's complex and the bimca^{iPr} binding cavity in Li**7**$^{\mathbf{iPr}}$·LiI(DME).

The painstaking handling required to obtaining the solid state structure of Li**7**$^{\mathbf{iPr}}$·LiI(DME) exemplifies the difficulty of crystallising monotopic, let alone ditopic, alkali metal cation NHC complexes. The formation of such species is dependent in part upon the size and "hardness" of the cation involved, whereby alkali metal cations will typically form coordination interactions with hard anions.[103] This preference for relatively hard donors is evident from the inclusion of the DME chelate donor on a single Li centre whilst the relatively "soft" anionic carbazolide nitrogen displays a bifurcated contact to the lithium cations. The strong sigma donation of the *N*-alkyl NHC donors of the bimca^{iPr} ligand in Li**7**$^{\mathbf{iPr}}$·LiI(DME) appears to be attenuated by the inclusion of LiI in preference to meridional bis-NHC coordination of the bimca^{iPr} to a single Li cation. The latter was expected based on the symmetrical nature of Li**7**$^{\mathbf{iPr}}$ in solution, as deduced from ^{1}H and ^{13}C NMR spectra. The unsymmetrical NHC coordination observed in the crystal structure of Li**7**$^{\mathbf{iPr}}$·LiI(DME) was not detected in solution, as deduced by ^{1}H NMR spectroscopy using crystalline samples of Li**7**$^{\mathbf{iPr}}$ from DME reaction mother liquors redissolved in THF-d_8, which gives rise to symmetrical A:B:A:B chemical shift and integration patterns that are in accordance with those observed for Li**7**$^{\mathbf{iPr}}$·LiI produced in THF. Furthermore,

vacuum dried samples of Li**7**$^{\mathbf{iPr}}$·LiI(DME) indicated that the DME co-ligand is labile under these conditions, as evidenced by the absence of ^{1}H NMR signals attributable to DME.

Further to Li-N-Li bond bifurcation in Li**7**$^{\mathbf{iPr}}$·LiI(DME), similar interplays of "soft" carbazolide donors with "hard" lithium cations have been the subject of recent studies. For example, the di- and tetra-*tert*-butyl carbazolide ligands used by Aldridge[104] and Kays[97] display common connectivity to Li**7**$^{\mathbf{iPr}}$, and are worthy of comparison. A particularly pertinent example is the dilithium tetracarbazolide containing dianion of Aldridge (Figure 2.13).[104] The reported bifurcation angles in this complex range from 74.49(13)° to 78.9(3)° and are thus considerably smaller than those of Li**7**$^{\mathbf{iPr}}$·LiI(DME).

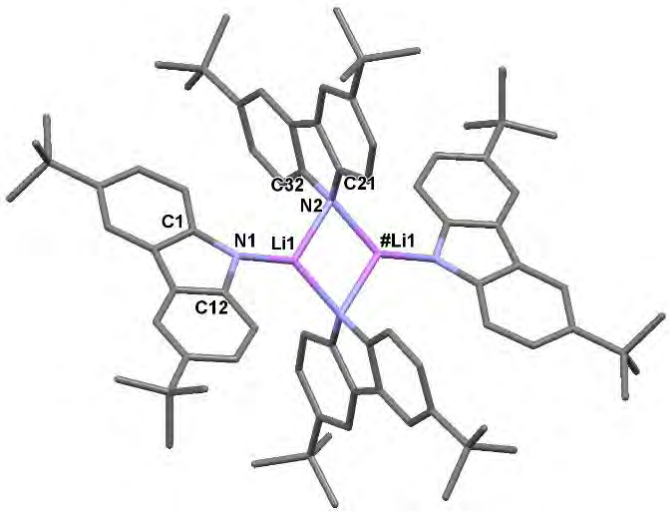

Figure 2.13 Wireframe depiction of the anion of $[Tl(C_7H_8)]_2[Li_2(^tBu_2carb)_4]\cdot 4C_7H_8$ complex reported by Aldridge and co-workers (CSD code: IWAKUN)[104] exhibiting bifurcation of two carbazolide N-donors to two Li cations. Hydrogen atoms, $[Tl(C_7H_8)]$ cations and lattice toluene molecules are omitted for clarity. Selected bond lengths (Å): N1-Li1: 1.938(6), N2-Li: 2.083(9), Li1-Li1A: 2.592(13). Selected bond angles (°): C1-N1-C12: 103.5(3), C21-N2-C32: 104.1(3), Li1-N2-Li1A: 78.9(3). Symmetry operations to generate '#' atoms: -*x*, -*y*, -*z*

2.4.1 Unintentional isolation of a bis("dicarbene")carbazolide

Close control of stoichiometry for any of the aforementioned deprotonation reactions is important as the bimca^{R} scaffold is potentially susceptible to deprotonation at the imidazolyl 4- or 5-positions. Deprotonation at these positions affords carbanionic carbene species, so-called "dicarbenes". Generally, the production of such carbanionic NHCs requires deployment of strong bases,[105-107] as noted, for example, by Robinson and co-workers, who isolated the first structurally characterised "dicarbene" from reactions of IDipp with, *n*BuLi, *n*BuLi·TMEDA, or Li metal in THF (Scheme 2.13).[105]

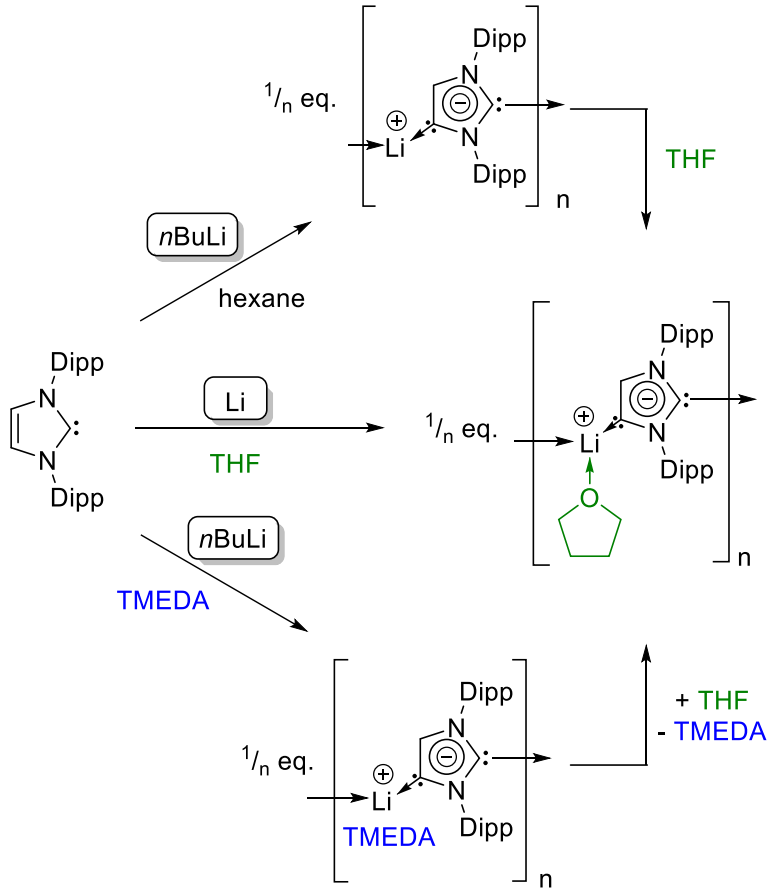

Scheme 2.13 Robinson's synthesis of carbanionic IDipp dicarbene lithium complexes.[105]

Indeed, during a preparation of Li**7**^{Me} from the **5**^{Me} zwitterion and *n*BuLi in THF yielded a very small crop of crystals of a bis("dicarbene")carbazolide, which crystallised from

the THF reaction mother liquor upon addition of hexane and cooling from room temperature to -24° C (Figure 2.14). Crystallographic studies of the resulting air- and moisture sensitive tetra-lithio bimca^{Me} dimer, **8**, or more accurately a doubly deprotonated Li**7**$^{Me"}$ dimer with included LiI, were of suitable quality to establish connectivity, however the poor quality of the crystals, stemming from the heavy disorder of coordinated and lattice THF molecules (omitted from Figure 2.14, see Figure 2.15 for coordinated THF structure), precluded anisotropic refinement of atomic positions and thus the accurate discussion of bonding metrics.

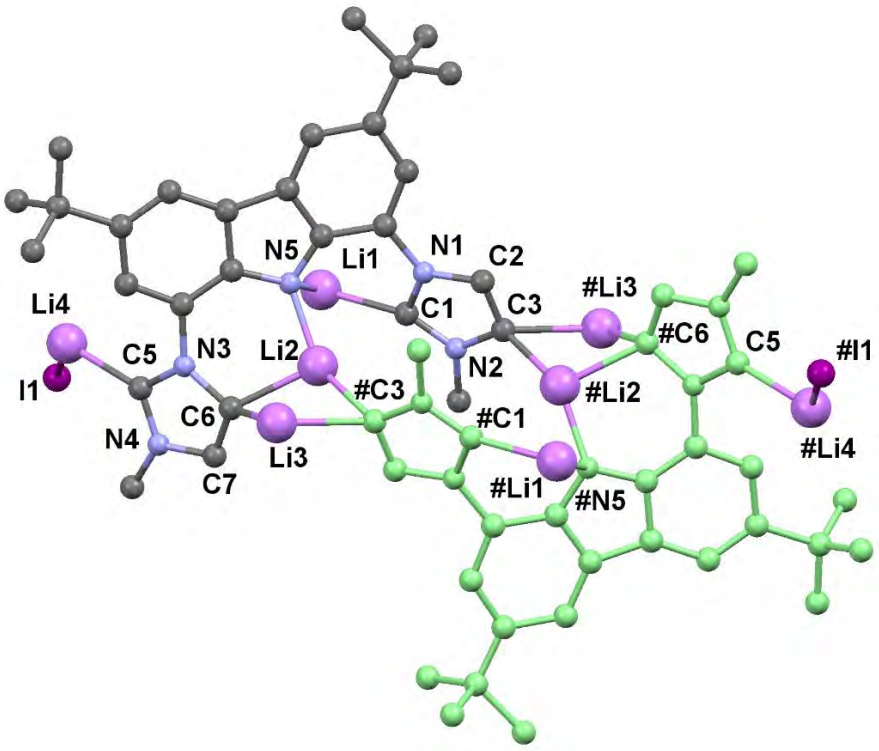

Figure 2.14 van der Waals sphere (arbitrary radius) representation of [{Li_4(bimca$^{Me"}$)I$(THF)_6$}$_2$], **8**. Hydrogen atoms and 12 heavily disordered Li-bound THF co-ligands have been omitted for clarity and the symmetry generated bimca^{Me} trianion is coloured green (symmetry operation used to generate '#' atoms: 1-*x*, 1-*y*, 1-*z*)

Dimer **8** crystallises in the triclinic space group $P\bar{1}$ with half a molecule of **8** and one molecule of heavily disordered partial occupancy THF in the asymmetric unit. The latter was masked from subsequent refinements using the OLEX 2 masking function. Figure 2.14 shows the molecular connectivity of the octalithio bimca^{Me} dimer, **8**, wherein each bimca^{Me} has been deprotonated at the two conventional imidazolium-C2- and C2'H positions, and once each at an imidazole-2-ylidene C4- or C5 position.

The connectivity data for **8** reveals similar chemical behaviour of the imidazolyl moieties to those of other reported carbanionic NHC lithium complexes (Scheme 2.13 above). It is interesting that the so-called "dicarbenes" differ in the position of their second deprotonation; one at the C4 imidazolyl position and one at the C5 imidazolyl position and may suggest enhanced acidity of the C4,C5 protons on bimca^{Me} relative to conventional monodentate NHCs, perhaps due to the Lewis basic carbazolide in **5^{Me}** (see Section 2.3.1), however the formation of **8** was not observed during reactions of **5^{R}**, or **4^{R}** with slight excesses of LiHMDS or LDA. Unfortunately, the small quantity of **8** available from the reaction mother liquor (*NB*: the bulk product being non-crystalline Li**7^{Me}**, as determined by ^{1}H NMR spectroscopy), and its extreme air- and moisture sensitivity precluded further characterisation of **8**.

Additional features of **8** include the preference of the Li cations for "hard" THF oxygen donors (Figure 2.15), as exemplified by the inclusion of twelve THF molecules, as is consistent with the Li**7^{iPr}**·LiI(DME) discussed earlier. It is noteworthy that the relatively "soft" C4/C4' and C5/C5' "carbanion" and carbazolide donors exhibit bifurcated, bridging coordination to two non-iodide coordinated Li cations, the N-donor being analogous to the bifurcated carbazolide anion of Li**7^{iPr}**·LiI(DME). The coordination of the terminal LiI moieties is completed by two THF co-ligands. The clear distinction

between the terminal imidazolyl-C2 coordination (sp^2 donor) and the bridging imidazolyl-C4/C5 coordination (sp^3 donor) is consistent with the assertion that "dicarbenes" are more accurately described as carbanionic NHCs, rather than two-fold 6-valence electron carbon donor systems, that is the term "dicarbene" is a misnomer.

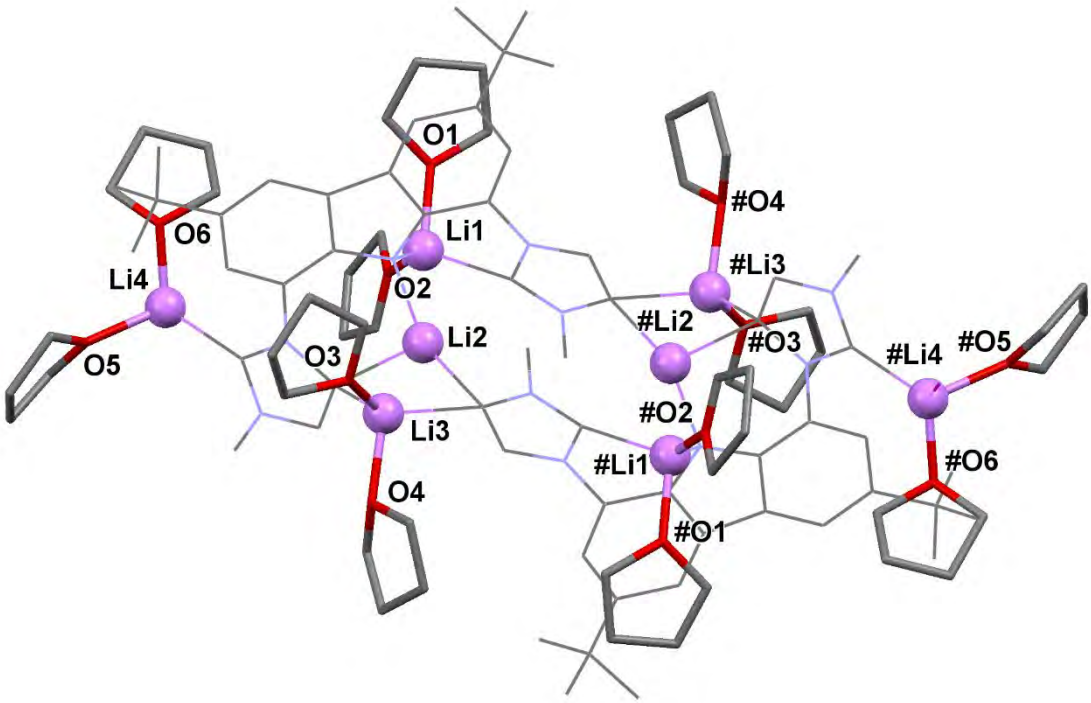

Figure 2.15 "Hard" THF oxygen-lithium donor-acceptor interactions highlighted in the solid state structure of **8**. The hydrogen and disordered atoms have been omitted and the bimca$^{Me"}$ ligand scaffold is pictured as a wireframe for clarity. Symmetry operation used to generate '#' atoms: 1-*x*, 1-*y*, 1-*z*.

2.5 Mg bimca^{Me} complexes and applications

The unexpected instability of the potassium bimca^{R} complexes, K**7**$^{\mathbf{R}}$, prompted the synthesis of an alkaline earth metal alternative, *i.e.* magnesium bimca^{R} "Grignard"

reagent. The higher electrophilicity and smaller ionic radius[108] of Mg^{2+} (72 pm) compared to K^+ (138 pm) was anticipated to aid complexation whilst also producing a synthetically useful ligand transfer agent that could address the problems faced with LiI contamination of previous lithium based salt metathesis reactions. Access to the diprotic zwitterion **5^{Me}** (Section 2.3.1) also promised a facile entry point to the generation of a magnesium bimca^R complex through reaction with [Mg(HMDS)$_2$].

2.5.1 [Mg(bimca^{Me})I(THF)], ***9^{Me}***

The reaction of **5^{Me}** with a stoichiometric amount of [Mg(HMDS)$_2$(Et$_2$O)] in THF was attempted. The low melting, crystalline Mg(HMDS)$_2$ precursor was synthesised from the reaction of two equivalents of KHMDS with one equivalent of MgI_2 through an adapted literature procedure for the preparation of the heavier alkaline metal hexamethyldisilazides; [M(HMDS)$_2$] (M = Ca, Ba),[109,110] and added as a THF solution to a THF suspension of **5^{Me}**. The resulting bright yellow slurry afforded a clear amber solution with a strong blue fluorescence under long wave UV light (*cf.* the blue fluorescence of related Li complexes, whereas **5^{Me}** exhibits a yellow fluorescence under the same conditions) upon stirring for 18 hours at room temperature. Filtration and removal of volatiles from the filtrate *in vacuo* afforded spectroscopically pure [Mg(bimca^{Me})I(THF)], **9^{Me}**, as an off-white air and moisture sensitive microcrystalline solid in near quantitative yield (Scheme 1). The reaction is sluggish at room temperature and may be accelerated by a brief initial period of reflux (15 minutes over a total reaction time of two hours, otherwise at room temperature) without measurable loss of yield.

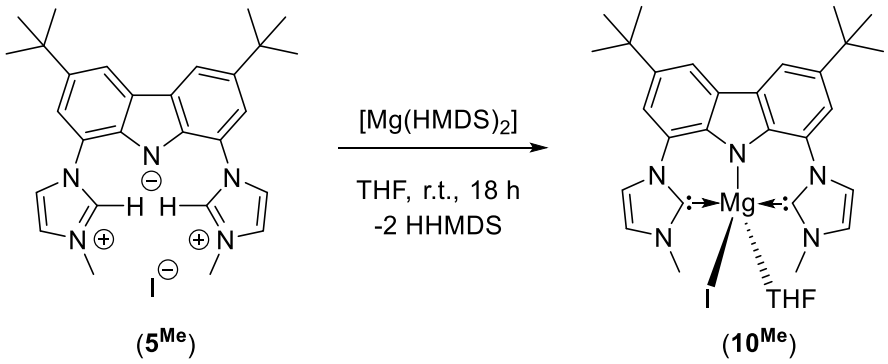

(**5**^{Me}) (**10**^{Me})

Scheme 2.14 Synthesis of **9**^{Me}.

The ^{1}H NMR (THF-d_8) spectrum of **9**^{Me} is devoid of a resonance attributable to the imidazolium C2 protons of **5**^{Me} (11.25 ppm in THF-d_8), as is consistent with the formation of a bis(NHC) species (*cf.* deprotonation of **4**^{Me} with three equivalents of *n*BuLi to afford Li**7**^{Me}). The deprotonation of the imidazolium moieties of **5**^{Me} by [Mg(HMDS)$_2$] to afford **9**^{Me} is further confirmed by the ^{13}C NMR (THF-d_8) spectrum of the reaction mixture, which exhibits a singular carbenic NHC resonance at 190.51 ppm. This chemical shift is in agreement with the previously reported magnesium bis(NHC) complex (185.39 ppm in C_6D_6, Figure 2.16).[101]

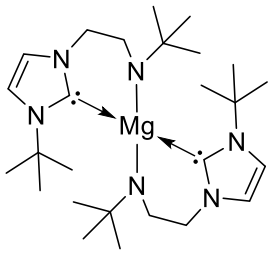

Arnold *et al.*

Figure 2.16 Amido bis(NHC) magnesium complex reported by Arnold *et al.*[101]

Furthermore, the symmetry of the bimca^{Me} ligand remains intact in solution following metallation, as substantiated by the presence of four doublets in the ^{1}H NMR spectrum of **9**^{Me} in the expected A:B:B:A signal integral ratio. These correspond to chemically

equivalent pairs of imidazolyl C4/C5 protons (A) and the aryl carbazole protons (B), each with signal integrations of 2 relative to the singlet at 4.24 ppm, which may be attributed to the six chemically equivalent *N*-methyl protons.

Large hexagonal plates of **9^{Me}** suitable for X-ray diffraction structure determination were grown from THF-d_8 at room temperature (Figure 2.17). The complex crystallises in the orthorhombic space group *Pbca* with a full molecule of **9^{Me}** and one heavily disordered molecule of lattice THF of partial occupancy in the asymmetric unit, the latter was refined isotropically. All of the non-hydrogen atoms of **9^{Me}** were refined with anisotropic displacement parameters and all hydrogen atoms, except those attached to a disordered *tert*-butyl group (centred on C21) and those of the *N*-methyl groups, were located from difference maps and refined isotropically.

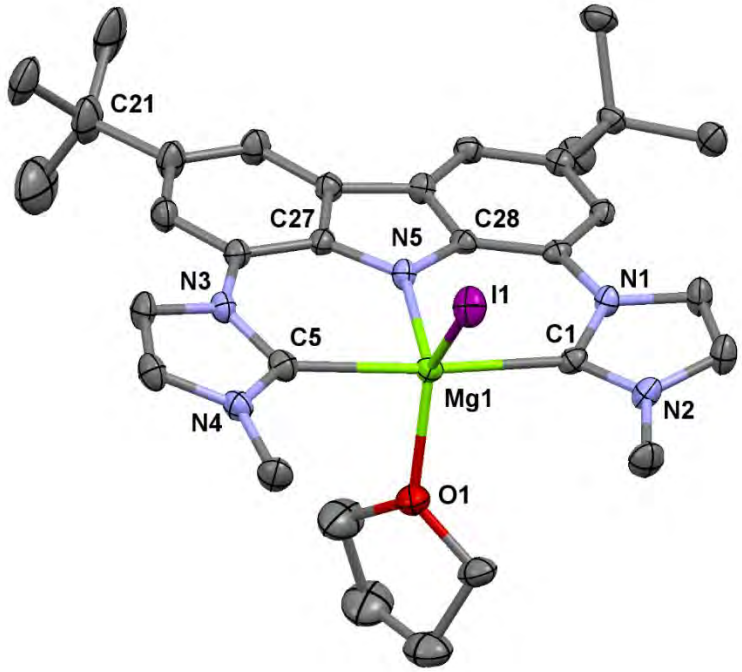

Figure 2.17 Molecular structure of **9^{Me}**. Atoms are shown with anisotropic atomic displacement parameters of 50% probability. Hydrogen atoms and disordered methyl groups of one *tert*-butyl group have been omitted for clarity.

Figure 2.17 (continued) Selected bond lengths and distances (Å): Mg1-N5: 2.035(3), Mg1-C1: 2.226(3), Mg1-C5: 2.252(3), Mg1-O1: 2.093(2), Mg1-I1: 2.8440(10). Selected bond angles (°): N1-C1-N2: 103.5(2), N3-C5-N4: 104.1(2), C27-N5-C28: 104.1(2), N5-Mg1-I1: 116.65(8), O1-Mg1-I1: 128.91(7), average dihedral angle carbazole plane-NHC plane: 14.52.

The solid state structure of **9^{Me}** exhibits a trigonal bipyramidal metal centre supported by the expected planar tridentate pincer binding mode of the bimca^{Me} ligand, with the NHC donors occupying apical positions, and an equatorial iodide ligand, and a coordinated equatorial THF (Figure 2). Complex **9^{Me}** is only the second example of a structurally characterised magnesium bis(NHC) complex, the first example being the bis(amido) tethered NHC complex reported by Arnold *et al.* (Figure 2.16 above),[101] and is the first magnesium iodide supported by an NHC. The Mg-I and Mg-O bond lengths of **9^{Me}** (2.8440(10) Å and 2.093(2) Å respectively) are longer than those of recently reported magnesium metal centres supported by less Lewis basic donors, *e.g.* the tetrahedral tris(1-methyl-3-*tert*-butyl-pyrazolyl)borate, [Mg(Tp^{Me,tBu})I], (Mg-I: 2.6695(9) Å)[111] and Kays' 1,8-dimesityl substituted carbazolide (Mg-I: 2.649(2) Å, Mg-O: 1.966(6) Å, Chapter 1, Figure 1.6),[57] presumably due to steric congestion at the metal centre and strong σ-donation of the NHC moieties in **9^{Me}**. The average imidazolyl-C2-Mg contacts (2.239 Å) are in keeping with those of related mono- and bis(NHC) complexes (*cf.* [Mg(HMDS)$_2$NHC], NHC = IDipp, 2.276(2) Å, or I*t*Bu, 2.241(2) Å respectively),[19,27] as discussed in Chapter 1 Section 1.5.2, and Arnold's amido-tethered NHC (2.2665 Å).[77,81,101]

As with many of the previously reported [M(bimca^{Me})] complexes, the NHC heterocycles of **9^{Me}** buckle out of the carbazolide plane to accommodate the bound metal centre.[56,84]

This distortion effects an average dihedral angle between the plane of the carbazolide phenyl rings and the five-membered NHC rings of 14.52°, but has no appreciable effect on the Mg-N bond length (2.035(3) Å), which is similar to those of the three other reported magnesium carbazolides (Mg-N = 2.101(5),[57] 2.008(5),[57] 2.087(3)[112] Å).

2.5.2 Salt metathesis of $\mathbf{9^{Me}}$ *with* GaI_3

The facile isolation of complex $\mathbf{9^{Me}}$ and literature precedence for the use of poly(NHC)magnesium complexes as metathetical ligand transfer reagents encouraged us to use $\mathbf{9^{Me}}$ for such purposes.[113] Moreover, the well-known precipitation of MgX_2 in the presence of 1,4-dioxane led us to expect that magnesium dihalide metathesis co-products could be more easily removed from subsequent reaction steps than the undesired LiI (*vide supra*, Section 2.4). A highly electrophilic main group halide was sought to test this hypothesis, namely GaI_3 (Scheme 2.15). Additionally, a salt elimination metathesis reaction between $\mathbf{9^{Me}}$ and GaI_3 would also open access to scarcely reported bis(NHC) gallium(III) chemistry (see Chapter 1, Section 1.5.1).[74]

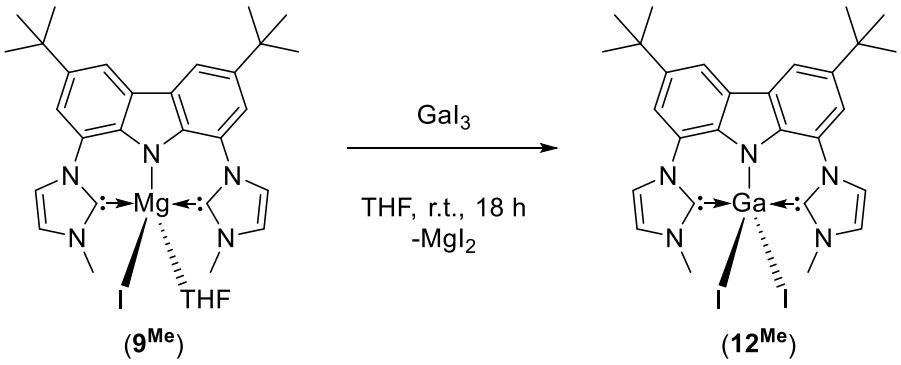

($\mathbf{9^{Me}}$) ($\mathbf{12^{Me}}$)

Scheme 2.15 Salt metathesis of $\mathbf{9^{Me}}$ with GaI_3 to afford [Ga(bimca^{Me})I_2] ($\mathbf{12^{Me}}$).

Thus, a THF solution of $\mathbf{9^{Me}}$ was added to an equimolar THF solution of GaI_3 to afford a slightly cloudy amber reaction mixture. As expected, the MgI_2 co-product precipitated from the reaction mixture when the reaction was carried out at typical preparative

concentrations (*ca.* 1 M in gallium). Alternatively, repeating the reaction at high dilution necessitated drying of the reaction mother liquor to afford a beige solid residue, which was followed by extraction of the product into 1,4-dioxane to remove insoluble [MgI_2(1,4-dioxane)]. Subsequent drying *in vacuo* provided an off-white microcrystalline solid that proved to be remarkably clean by ^{1}H NMR spectroscopy (THF-d_8). Indeed, the ^{1}H NMR spectrum of the crude product is indicative of successful metathesis, displaying the expected A:B:B:A shift and 1:1:1:1 integration pattern of aromatic region doublets (*vide supra*) positioned downfield relative to those of **9^{Me}** (Table 2.2).

Compound	4-NHC-*H* (ppm)	2,7-carb.-*H* (ppm)	4,5-carb.-*H* (ppm)	5-NHC-*H* (ppm)
9^{Me}	7.25	7.64	8.07	8.09
12^{Me}	7.38	7.82	8.19	8.29

Table 2.2 ^{1}H NMR (THF-d_8) aryl region chemical shifts of **9^{Me}** and **12^{Me}**.

These doublets, between 7.38 and 8.29 ppm, each have a signal integral of 2 relative to the six proton *N*-methyl singlet at 4.41 ppm (*cf.* **9^{Me}** 4.24 ppm in THF-d_8). This is consistent with the sole presence of [Ga(bimca^{Me})I_2] (**12^{Me}**) with pseudo mirror-plane symmetry across the bimca^{Me} scaffold, and is discussed in further detail in Chapter 3, Section 3.4.2 of this thesis.

*2.5.3 Substitution of iodide co-ligand of **9^{Me}***

Given the literature precedent for the effective application of NHC stabilised alkaline earth amides to catalyse a variety of hydroamination reactions,[78,81] our focus was drawn to the development of **9^{Me}** as a precatalytic system for similar reactions. Specifically, the THF coordination site of **9^{Me}** encouraged us to pursue the substitution of the iodide co-ligand with HMDS to generate an NHC coordinated bis(amido) system similar to the

mono-NHC supported [Mg(HMDS)$_2$(I*t*Bu)] complex reported as a hydroamination catalyst by Nembenna and co-workers.[81] In this, we rationalised that a simple metathesis with KHMDS would produce a more robust and active catalytic system by virtue of bis(NHC) coordination about the carbazolide anchor ligand whilst also maintaining a binding site for suitably small substrates (Scheme 2.16).

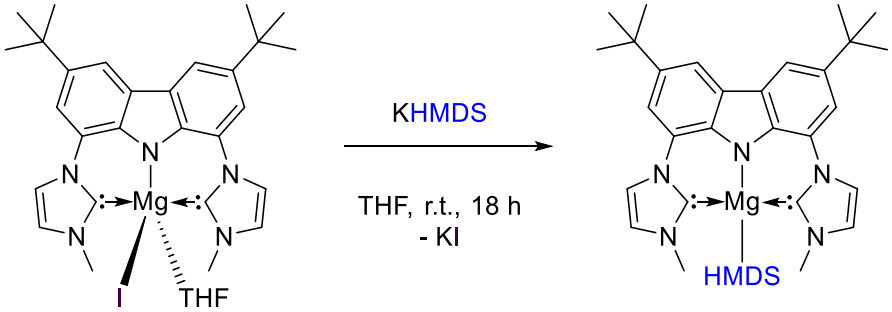

Scheme 2.16 Attempted preparation of [Mg(bimca^{Me})(HMDS)].

The addition of an equimolar quantity of KHMDS to **9^{Me}** afforded a pale red solution with intense blue fluorescence under long wave UV light (*cf.* blue fluorescence of **9^{Me}** under long wave UV light) and the concomitant precipitation of a white solid, presumably KI. Following filtration and removal of volatiles *in vacuo* a pale red solid, **10^{Me}**, was obtained.

The ^{1}H NMR (THF-d_8) spectrum of **10^{Me}** exhibits the same signal and integral pattern as the parent iodide complex **9^{Me}**, with resonance shifts to higher field by varying degrees (Table 2.3). Notably, the signals corresponding to the imidazolyl protons of the NHC moieties are the most shifted, as verified by ^{1}H-^{1}H NOESY and ^{1}H-^{1}H TOCSY experiments. The greatest shift is that of the *N*-methyl singlet resonance from 4.24 ppm in **9^{Me}** to 2.58 ppm in **10^{Me}**. These two-dimensional NMR experiments were also able to confirm that the ligand remains intact after the addition of base, *i.e.* no further deprotonation takes place, which might be the anticipated outcome given the aforementioned "dicarbene" reports of Robinson[105] and our earlier isolation of **8** (Section

2.4.1). Interestingly, the expected HMDS methyl singlet for a coordinated amide ligand (*ca.* 0.3 ppm) was not observed, nor were resonances consistent with its conjugate acid, bis(trimethylsilylamine).

Compound	δ 4-Imidazolyl (^{1}H NMR)	δ 5-Imidazolyl (^{1}H NMR)	δ NC*H*$_3$ (^{1}H NMR)	δ 2-Imidazolyl (^{13}C NMR)
5^{Me}	7.61	8.21	4.32	136.1[a]
9^{Me}	7.25	8.09	4.24	190.51
10^{Me}	6.62	7.59	2.58	199.72

Table 2.3 Summary of salient NMR chemical shifts for **5^{Me}**, **9^{Me}**, and **10^{Me}**, all values are given in ppm from samples dissolved in THF-d_8, [a] in DMSO-d_6.

Pale yellow elongated hexagonal plates of **10^{Me}** suitable for X-ray diffraction structure determination were grown from a room temperature saturated THF solution of **10^{Me}** diffused with hexane, placed at 4 °C. The molecular structure of **10^{Me}** (Figure 2.18) sheds light on the unexpected outcome of this reaction; the six-coordinate, tetra(NHC)magnesium compound [Mg(bimca^{Me})$_2$].

Complex **10^{Me}** crystallises in the monoclinic space group $P2_1/n$ with a full molecule of **10^{Me}** and two heavily disordered THF molecules in the lattice, the latter of which were masked (OLEX 2) from subsequent refinements to achieve improved refinement metrics. The magnesium exhibits an octahedral coordination environment brought about by interlocking of the two bimca^{Me} pincers in a bis(meridianoloid) or "tennis ball" like manner with transoid carbazolide donors (Figure 2.18).

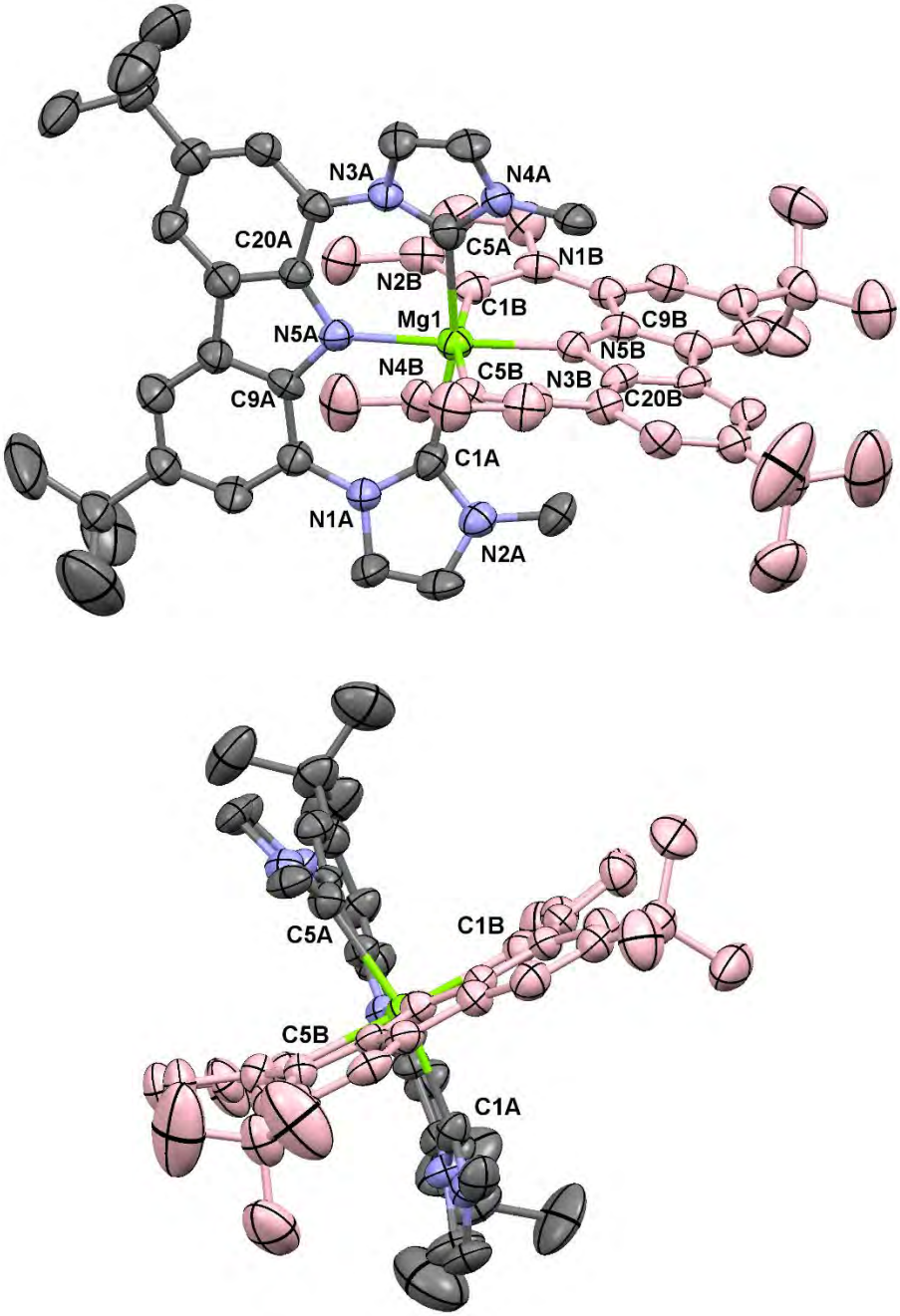

Figure 2.18 Molecular structure of **10**^{Me}. Atoms are shown with anisotropic atomic displacement parameters with 50% probability. Hydrogen atoms have been omitted and one of the two bimca ligands is shown in pink for clarity. Selected bond lengths (Å): Mg1-C1A: 2.345(5), Mg1-C5A: 2.391(4), Mg1-C1B: 2.357(5), Mg1-C5B: 2.366(5), Mg1-N5A: 2.170(4), Mg1-N5B: 2.169(4).

Figure 2.18 (continued) Selected bond angles (°): N1A-C1A-N2A: 102.2(4), N4A-C5A-N3A: 102.0(4), N2B-C1B-N1B: 101.8(4), N4B-C5B-N3B: 102.9(4), C20A-N5A-C9A: 103.9(4), C20B-N5B-C9B: 104.2(4), C1A-Mg1-C5A: 162.10(18), C1B-Mg1-C5B: 166.7(2), C1A-Mg1-C1B: 96.25(15), C1A-Mg1-C5B: 87.96(16), C1B-Mg1-C5A: 96.50(16), C5B-Mg1-C5A: 82.44(16), average carbazolide-NHC dihedral angle: 19.8.

This outcome is consistent with redistribution of the intended [Mg(bimca^{Me})(HMDS)] product to afford the homoleptics [Mg(bimca^{Me})$_2$], **10^{Me}**, and [Mg(HMDS)$_2$], of which the latter is lost during the reaction workup (drying under vacuum).[114] The instability of heteroleptic complexes with respect to such Schlenk-type ligand redistributions is a feature of heavier alkaline earth monoanionic bis(NHC) complexes (*cf*. Chapter 1, Section 1.5.2) but is rare for magnesium.

Monitoring the reaction of **9^{Me}** with KHMDS by ^{1}H NMR spectroscopy (THF-H$_8$, solvent suppression) led to the *in situ* observation of the anticipated but transient [Mg(bimca^{Me})HMDS], **9^{Me}-HMDS** and both homoleptic redistribution products. The heteroleptic **9^{Me}-HMDS** exhibits distinct chemical shifts for the carbazolide aryl proton doublet resonances at 7.59 ppm and 7.96 ppm and the imidazolyl derived C4 and C5 proton derived doublets at 7.26 ppm and 8.02 ppm respectively. Moreover, it was found that the redistribution reaction could be irreversibly skewed towards the homoleptic products by heating the reaction mixture to reflux, suggesting the formation of the homoleptic products is thermodynamically favoured. It is noteworthy that a similar redistribution could not be effected by dissolution of **9^{Me}** in 1,4-dioxane, wherein stirring for 24 hours at room temperature led to a reaction mixture without **10^{Me}** or

[MgI_2(1,4-dioxane)] according to a ^{1}H NMR (THF-d_8) spectrum of the vacuum dried reaction mother liquor.

To evaluate whether the ligand redistribution that generated **10^{Me}** is a consequence of the steric requirements of HMDS, we attempted several metatheses, analogous to the above, with smaller reagents. The chosen metathesis substrates were also selected for their anticipated down-stream synthetic utility (Scheme 2.17). The reaction of **9^{Me}** with one equivalent of LDA, NaOEt, or KH rapidly yield the previously observed redistribution product; **10^{Me}**. Amongst these, only the reaction with LDA generated a transient heteroleptic; [Mg(bimca^{Me})(N*i*Pr$_2$)], **9^{Me}-N*i*Pr$_2$**, that could be clearly identified by *in situ* ^{1}H NMR spectroscopy. **9^{Me}-N*i*Pr$_2$** exhibits a chemical shift and integration pattern that is similar to that of **9^{Me}-HMDS** (*vide supra*), and gives way to the formation of the homoleptic redistribution products **10^{Me}** and [Mg(N*i*Pr$_2$)$_2$] upon heating (Scheme 2.17).

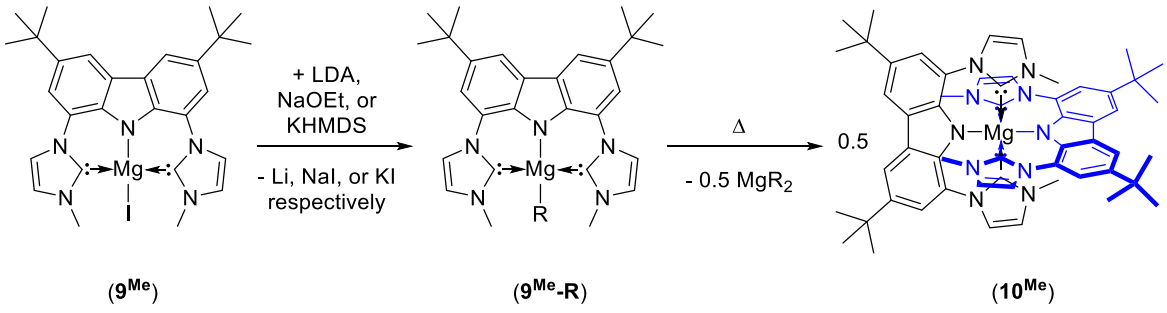

Scheme 2.17 Attempted metathesis reactions carried out with ioidide **9^{Me}** to access **9^{Me}-R** complexes (where R = N*i*Pr$_2$, OEt, or HMDS).

Interestingly, in the case of KH, the formation of dihydrogen gas was also observed (^{1}H NMR spectrum, 4.55 ppm in THF-d_8), during its 1:1 reaction with **9^{Me}**. No further reactivity at the ligand scaffold was observed (*i.e.* no loss of resonance intensity at, for example, the 4,5-imidazolyl positions, *cf.* "dicarbene" formation). We tentatively interpret this as evidence for a competing reductive dehydrogenation decomposition

pathway through a nascent [Mg(bimca^{Me})H] (**9^{Me}-H**) species that delivers a short lived Mg^{I}(bimca^{Me}) species that disproportionates to **10^{Me}** and Mg^{0} (Scheme 2.18).‡ Unfortunately, efforts to isolate the expected but sub-milligram quantity of elemental magnesium co-product during repeat experiments proved fruitless. Likewise, attempts to isolate the proposed Mg(I) intermediate from this reaction before disproportionation to **10^{Me}** and Mg^{0} were unsuccessful. This prompted us to attempt the purposeful chemical reduction of **9^{Me}** to evaluate the stability of a Mg^{I}(bimca^{Me}) intermediate from the above and test the hypothesis that such a species would afford **10^{Me}** and Mg^{0}.

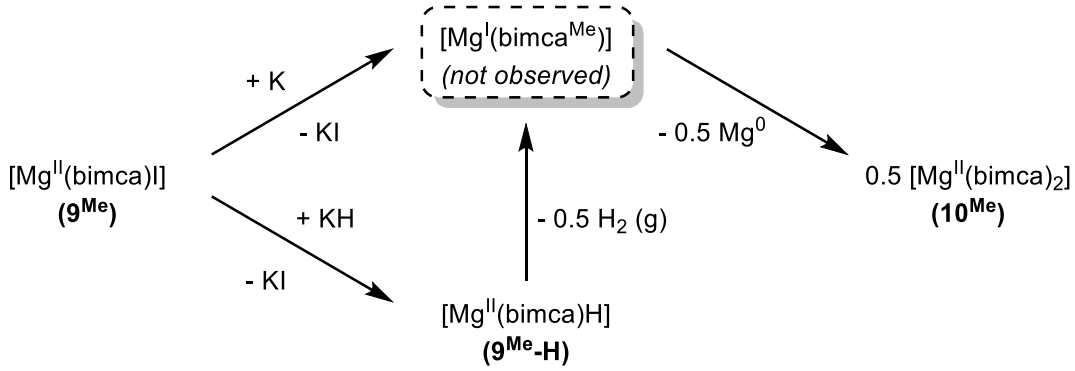

Scheme 2.18 Redox paths from **9^{Me}** to **10^{Me}**.

The stoichiometric addition of a THF solution of **9^{Me}** to a freshly deposited mirror of elemental potassium resulted in an immediate colour change from beige to amber with concomitant production of a white solid, presumably potassium iodide, and a mixture of two or three bimca^{Me} containing products based on *N*-methyl group environments in a ^{1}H NMR spectrum of the vacuum dried mother liquor. Among these, one product exhibits ^{1}H NMR resonances that are consistent with **10^{Me}**. Indeed, when the reaction is monitored *in situ* by ^{1}H NMR spectroscopy (in THF-d_8), the first and major product (t < 15 minutes) is the homoleptic complex **10^{Me}**. This outcome supports the proposal that a reduced

‡ *NB*: no evidence for *β*-hydride elimination, *i.e.* the *in situ* formation of [Mg(bimca^{Me})H], was found in the ^{1}H NMR spectra of the reaction mixtures containing LDA or NaOEt.

$Mg^{I}(bimca^{Me})$ complex is too unstable, with respect to a disproportionation, to be isolated under the conditions used during the reactions shown in Scheme 2.18.

2.6 Conclusions

The synthesis of a new *N*-*i*Pr substituted $bimca^{R}$ bis(imidazolium)carbazole triprotic proligand $\mathbf{4^{iPr}}$ is presented with characterisation. Attempts to synthesise a spatially demanding *N*-mesityl analogue, $\mathbf{4^{Mes}}$, were proved unsuccessful, likely due to the steric requirements of the mesityl substituent. Sequential deprotonation of $\mathbf{4^{iPr}}$ afforded the air- and moisture stable, zwitterionic, $\mathbf{5^{iPr}}$, and the less stable monoprotic, neutral $\mathbf{6^{iPr}}$. The triply deprotonated alkali metal salts $M\mathbf{7^{iPr}}$ (M = Li, K) have been prepared, the lithium congeners of which have been fully characterised. Recrystallisation of $Li\mathbf{7^{iPr}}$ from DME affords a rare example of a structurally authenticated Li-NHC interaction. The method used to produce $\mathbf{5^{iPr}}$ has also been applied to generate the methyl variant; $\mathbf{5^{Me}}$. The crystalline zwitterions $\mathbf{5^{R}}$ (R = Me, *i*Pr) enjoy improved solubility in organic solvents relative to the parent $\mathbf{4^{R}}$ salts and exhibit distinct solid state inter- and intramolecular H-bonding interactions. The importance of stoichiometric control during the deprotonation of $\mathbf{5^{Me}}$ (and therefore $\mathbf{4^{R}}$ and $\mathbf{5^{R}}$) is borne out by the isolation of the lithium bis("dicarbene")carbazolide $bimca^{Me}$"tetralithium iodide dimer **8**.

The new diprotic carbazolide proligand $\mathbf{5^{Me}}$ has proven its utility in generating a divalent magnesium iodide complex $\mathbf{9^{Me}}$, through an efficient protolytic metallation route using $[Mg(HMDS)_2]$. Complex $\mathbf{9^{Me}}$ represents a rare example of a magnesium bis(NHC) complex and exhibits a trigonal bipyramidal geometry around the Mg(II) centre. Its efficacy as a metathetical ligand-transfer agent using a Lewis acidic group 13 metal triiodide has been demonstrated, wherein superior product quality and control eventuates

during reaction workup compared to alkali metal bimca^{Me} reagents in analogous reactions (see Chapter 3 Section 3.4.2). Importantly, workup procedures that include a 1,4-dioxane extraction are shown to completely eliminate MgI_2 contamination post bimca^{Me} ligand transfer (in contrast to LiI contamination during analogous reactions that employ the lithium congener, Li**7**^{Me}, see Chapter 3, Section 3.1).

Attempts to prepare a range of heteroleptic magnesium bimca^{Me} complexes *via* a range of metathesis reactions led to the tetra(NHC) complex, **10**^{Me}, from ligand redistribution processes. Surprisingly, **10**^{Me} is also formed under reducing conditions (K or KH) that likely form a transient Mg^{I}(bimca^{Me}) species. This suggests that the product of chemical reduction of **9**^{Me} is unstable with respect to disproportionation.

2.7 Experimental

General methods

KHMDS,[115] BTRA·ICl_2,[87] DBA,[116] Hbimca^{Me}(2HI),[56] $I(Ph)_2$·BF_4,[90] $I(Mes)_2$·Tos,[92] and MgI_2[117] were synthesised according to literature procedures. Isopropyl iodide was distilled under reduced pressure (200 mbar) prior to its use. All other reagents were used as received from chemical suppliers.

*3,6-di-tert-butylcarbazole, **1**, via Friedel-Crafts alkylation*

Method (i) $AlCl_3$ as Lewis acid:

$AlCl_3$ (17 g, 0.13 mol) was added portionwise to a vigorously stirred DCM (180 mL) suspension of carbazole (20 g, 0.12 mol) to afford a deep red to brown reaction mixture that was cooled to < 0 °C. At this temperature, *tert*-butylchloride (22 g, 0.24 mol) was added dropwise over *ca*. 30 min to give a deep purple slurry that was stirred at < 0 °C for

a further 2 h, whereupon it was allowed to warm to room temperature and stirred for 2 d. Dilution of the reaction mother liquor with DCM (500 mL), and successive washing with aqueous 1 M HCl (500 mL) and brine (500 mL) yielded a pale yellow organic phase, which was separated and dried over anhydrous $MgSO_4$. Filtration and removal of volatiles under reduced pressure gave a white powder, which was dissolved in the minimum amount of hexane (650 mL) at reflux. Slow cooling of the hexane solution to room temperature afforded a crop of microcrystalline **1**, which was isolated by filtration (17 g). A second crop of pure **1** was grown by placing the filtrate at -24 °C (9.3 g, combined yield: 26 g, 79%). The ^{1}H NMR spectroscopic data and melting point of **1** *via* this method are consistent with those of the literature values.[86] ^{1}H NMR (300 MHz, DMSO-d_6): δ 1.41 (s, 18H, *t*Bu-CH_3), 7.39 (m, 4H, 1,2,7,8-carb.-*H*), 8.13 (d, $^4J_{HH}$ = 1.69 Hz, 2H, 4,5-carb.-*H*), 10.90 (br s, 1H, carb.-N*H*). Mp: 225-228 °C melts. (lit.[86] 228-233 °C).

Method (ii), $ZnCl_2$ as Lewis acid:

Di-alkylation of **1** *via* $ZnCl_2$ (9.5 g, 0.070 mol) and carbazole (3.9 g, 0.023 mol) proceeded according to the synthesis outlined by Liu *et al.*[86] and the ^{1}H NMR data and melting point of **1** are consistent with those presented by these researchers (yield: 35 g, 52%). ^{1}H NMR (300 MHz, $CDCl_3$): δ 1.47 (s, 18H, *t*Bu-CH_3), 7.33 (dd, $^3J_{HH}$ = 8.52 Hz, $^5J_{HH}$ = 0.64 Hz, 2H, 1,8-carb.-*H*), 7.48 (dd, $^3J_{HH}$ = 8.52 Hz, $^4J_{HH}$ = 1.96 Hz, 2H, 2,7-carb.-*H*), 7.83 (br s, 1H, carb.-N*H*), 8.10 (dd, $^4J_{HH}$ = 1.96 Hz, $^5J_{HH}$ = 0.64 Hz, 2H, 4,5-carb.-*H*). Mp: 225-228 °C melts. (lit.[86] 228-233 °C).

*Diiodination of **1** to form 1,8-diiodo-3,6-di-tert-butylcarbazole, **2***

Method (i) ICl as iodinating agent:

ICl (0.58 g, 3.6 mmol) was added to a stirred colourless suspension of **1** (0.50 g, 1.8 mmol) in glacial acetic acid (20 mL) at room temperature to afford a brown reaction

mixture that was heated to 65 °C and stirred for 18 hours. During this time the reaction progress was monitored by TLC (neat hexane, $R_f = 0.5$, **2**). It was noted that formation of **2** was sluggish under these conditions as deduced by the persistence of a spot attributed to monoiodinated **1** ($R_f = 0.2$). After 48 hours, the dark brown reaction mixture was poured into an aqueous solution of Na_2SO_3 (60 mL, 5% w/v) to afford a white suspension that was extracted into hexane (3 x 20 mL). The pale yellow combined organic phases were washed with water (3 x 20 mL) and dried over anhydrous $MgSO_4$. Removal of volatiles under reduced pressure afforded a mixture of **2** and monoiodinated **1**, which was separated by filtration through a plug of silica (7 cm, neat hexane eluent). Drying of the colourless filtrate *in vacuo* afforded spectroscopically pure, colourless, microcrystalline **2** (0.18 g, 19%). ^{1}H NMR spectroscopic and melting point data for **2** prepared by this method is in agreement with literature values.[56] ^{1}H NMR (300 MHz, DMSO-d_6): δ 1.39 (s, 18H, *t*Bu-C*H*$_3$), 7.82 (d, $^4J_{HH} = 1.78$ Hz, 2H, 2,7-carb.-*H*), 8.25 (d, $^4J_{HH} = 1.78$ Hz, 2H, 4,5-carb.-*H*), 9.64 (br s, 1H, carb.-N*H*). Mp: 163-165 °C (melts, dec.) (lit.[56] 165-168 °C dec.).

Method (ii) BTRA·ICl_2 as iodinating agent:

BTRA·ICl_2 (54 mmol) was added portionwise over *ca*. 15 min to a stirred grey suspension of **1** (6.0 g, 22 mmol) in acetic acid (120 mL) at room temperature. The reaction mixture was heated to 60 °C and stirred for 18 h, during which it gradually darkened to a brown suspension. After complete formation of the diiodo product, as determined by TLC of aliquots of the reaction mixture (neat hexane, $R_f = 0.5$), the reaction mixture was cooled to room temperature and poured into an aqueous solution of Na_2SO_3 (400 mL, 5% w/v) to give a pale green to white suspension that was extracted into hexane (3 x 75 mL), washed with water (3 x 75 mL), dried over anhydrous $MgSO_4$, and volatiles removed *in*

vacuo to give a treacly amber solid. This solid was dry-loaded (*ca*. 20 mL DCM) onto a pad of silica (7 cm) and eluted with neat hexane. Removal of volatiles from the colourless filtrate *in vacuo* yielded spectroscopically pure colourless, microcrystalline **2** (9.1 g, 80%). ^{1}H NMR and melting point data for **2** prepared by this method is in agreement with literature values.[56] ^{1}H NMR (300 MHz, DMSO-d_6): δ 1.39 (s, 18H, *t*Bu-CH_3), 7.82 (d, $^{4}J_{HH}$ = 1.78 Hz, 2H, 2,7-carb.-*H*), 8.25 (d, $^{4}J_{HH}$ = 1.78 Hz, 2H, 4,5-carb.-*H*), 9.64 (br s, 1H, carb.-N*H*). Mp: 163-165 °C (melts, dec.) (lit.[56] 165-168 °C dec.).

*Ullmann coupling of **2** with two eq. of imidazole to form*

*1,8-Bis(imidazol-1-yl)-3,6-di-tert-butylcarbazole, **3***

A J. Youngs capped ampoule (750 mL) was charged with a stirrer bar, imidazole (94 mmol, 6.4 g), caesium carbonate (13 g, 41 mmol), DBA (0.44 g, 1.9 mmol), 1,10-phenanthroline (6.8 g, 38 mmol), [$(CuOTf)_2 \cdot C_6H_6$] (0.95 g, 1.9 mmol), and **2** (10 g, 19 mmol). Toluene was added to the brown solid mixture at room temperature to yield a brown suspension that was heated to 120 °C, sealed under an atmosphere of N_2, and stirred for 5 days, during which the reaction mixture gradually precipitated a white solid. Subsequent drying of the brown reaction mother liquor *in vacuo* yielded a brown, treacly solid that was extracted into DCM (100 mL) to aid transfer into a round bottomed flask. Removal of volatiles *in vacuo* afforded a brown powdery solid that was washed successively with hexane and water (3 x 100 mL each) aided by sonication, affording crude **3** as a powdery beige solid. Dissolution in methanol (300 mL) followed by precipitation through dropwise addition of water (100 mL) afforded spectroscopically pure **3** as a fine white solid that was isolated by filtration and dried under vacuum overnight (6.1 g, 79%). ^{1}H NMR spectroscopic data for **3** prepared by this adapted method is in agreement with literature values.[56] ^{1}H NMR (300 MHz, DMSO-d_6): δ 1.44 (s, 18H, *t*Bu-CH_3), 7.18 (br s, 2H, 4-imidazole-*H*), 7.43 (d, $^{4}J_{HH}$ = 1.73 Hz, 2H, 2,7-carb.-*H*), 7.71

(br s, 2H, 5-imidazole-*H*), 8.20 (br s, 2H, 2-imidazole-*H*), 8.34 (d, $^4J_{HH}$ = 1.73 Hz, 2H, 4,5-carb.-*H*), 10.92 (s, 1H, carb.-N*H*). Mp: 294-298 °C (dec.) (lit.[56] 296-300 °C dec.).

Synthesis of Hbimca^{iPr}(2HI), ***5^{iPr}***

2-Iodopropane (3.6 g, 21 mmol,) was added to a stirred suspension of **3** (2.5 g, 6.1 mmol) in acetonitrile (50 mL) at room temperature. The reaction mixture was heated to reflux with stirring for 72 h, during which it cleared and darkened to a red solution that, upon concentration under reduced pressure (*ca*. 10 mL), yielded **4^{iPr}** as small prisms upon storage at 4 °C. Isolation of the crystalline product by decantation and washing with cold (0 °C) diethyl ether (3 x 5 mL) afforded analytically pure microcrystalline **4^{iPr}**. Dropwise addition of diethyl ether (20 mL over 30 min) to the acetonitrile supernatant yielded a second crop of **4^{iPr}** as an off-white powder that characterised identically to the first crop by ^{1}H NMR spectroscopy (combined yield 3.9 g, 85%). Rhombohedral colourless plates of **4^{iPr}** suitable for single-crystal X-ray diffraction structure determination were grown from a room temperature saturated solution of **4^{iPr}** in dichloromethane diffused with hexane vapour. ^{1}H NMR (300 MHz, DMSO-d_6): δ 1.47 (s, 18H, *t*Bu-CH_3), 1.61 (d, $^3J_{HH}$ = 6.66 Hz, 12H, N*i*Pr-CH_3), 4.74 (sept, $^3J_{HH}$ = 6.66 Hz, 2H, N*i*Pr-C*H*), 7.77 (d, $^4J_{HH}$ = 1.73 Hz, 2H, 2,7-carb.-*H*), 8.26 (m, 2H, 4-imidazolium-*H*), 8.35 (m, 2H, 5-imidazolium-*H*), 8.63 (d, $^4J_{HH}$ = 1.73 Hz, 2H, 4,5-carb.-*H*), 9.83 (br m, 2H, 2-imidazolium-*H*), 11.57 (br s, 1H, carb.-N*H*). ^{13}C NMR (75 MHz, DMSO-d_6): δ 22.25 (s, N*i*Pr-*C*H$_3$), 31.66 (s, *t*Bu-*C*H$_3$), 34.95 (s, *t*Bu-*C*), 52.97 (s, N*i*Pr-*C*H), 119.17 (s, carb.-*C*), 119.33 (s, 2,7-carb.-*C*), 120.84 (s, 4,5-carb.-*C*), 121.19 (s, 4-imidazolium-*C*), 123.40 (s, 5-imidazolium-*C*), 125.47 (s, carb.-*C*), 132.04 (s, carb.-*C*), 135.79 (s, 2-imidazolium-*C*), 143.78 (s, carb.-*C*). Calcd. for $C_{32}H_{43}N_5I_2$: C, 51.14; H, 5.77; N, 9.32. Found: C, 51.17; H, 5.68; N, 9.20. IR (Nujol on NaCl plates, cm^{-1}): 1736 (*m, sh*), 1596

(*s, sh*), 1561 (*s, sh*), 1318 (*s, sh*), 1263 (*s, sh*), 1144 (*s, sh*), 1114 (*s, sh*), 941 (*m, sh*), 871 (*s, sh*). Mp: 262-264 °C (dec.).

Attempted synthesis of I(Tripp)$_2$·Tos

Toluenesulfonic acid (0.26 g, 1.4 mmol) was added to a dark brown DCM solution (6 mL) of 1,3,5-triisopropylbenzene (0.32 g, 1.6 mmol), iodine (0.10 g, 0.39 mmol), and MCPBA (0.291 g, 1.18 mmol). The colourless reaction mixture was stirred at room temperature for 18 h, during which it cleared and turned yellow. Addition of diethyl ether (*ca*. 30 mL) did not precipitate the anticipated iodonium bis(arene) toluenesulfonate. The reaction mixture was washed with water and the yellow organic phase was dried over anhydrous $MgSO_4$ and concentrated to 0.5 mL under reduced pressure, and dry-loaded (0.5 mL DCM) onto a pad of silica (7 cm). Elution with neat hexane afforded a mixture of products with similar retention times that characterised as mainly 1,3,5-triisopropylbenzene and 1-iodo-2,4,6-triisopropylbenzene by ^{1}H NMR spectroscopy ($CDCl_3$).[93] ^{1}H NMR (400 MHz, $CDCl_3$): δ 1.27 (m, 36H, overlapping *i*Pr-C*H*$_3$), 2.91 (sept, $^3J_{HH}$ = 6.54 Hz, 3H, *i*Pr$_{TrippH}$-C*H*), 3.43 (sept, $^3J_{HH}$ = 6.49 Hz, 1H, *i*Pr$_{TrippI}$-*p*-C*H*), 3.51 (sept, $^3J_{HH}$ = 6.9 Hz, 2H, *i*Pr$_{TrippI}$-*o*-C*H*), 6.95 (s, 2H, aryl$_{TrippI}$-H), 6.99 (s, 3H, aryl$_{TrippH}$-H).

*Hbimca^{Ph}(2HBF$_4$), **4^{Ph}**, from I(Ph)$_2$·BF$_4$*

A stirred, bluish beige DMF (5 mL) suspension of I(Ph)$_2$·BF$_4$ (0.25 g, 0.68 mmol), [Cu(OAc)$_2$] (0.0023 g, 0.011 mmol), and **3** (0.093 g, 0.22 mmol) was heated to 100 °C for 18 h, whereupon water (10 mL) was added to the reaction mother liquor to precipitate beige powdery **4^{Ph}**, which was isolated by filtration, washed with water and dried in a vacuum desiccator (0.090 g, 54%). The ^{1}H NMR spectroscopic data for this compound (chemical shift and integration values) are consistent with those from the report by Kunz

and co-workers on the preparation of **4^{Ph}**.[85] ^{1}H NMR (400 MHz, DMSO-d_6): δ 1.50 (s, 18H, *t*Bu-CH_3), 7.67 (d, $^4J_{HH}$ = 1.22 Hz, 2H, 2,7-carb.-*H*), 7.69 (m, 4H, NPh), 7.91 (m, 2H, 4-imidazolium-*H*), 7.93 (m, 4H, NPh), 8.58 (m, 2H, 5-imidazolium-*H*), 8.70 (m, 4H, 4,5-carb.-*H* and NPh), 10.38 (m, 2H, 2-imidazolium-*H*), 11.77 (br s, 1H, carb.-N*H*). Mp: > 360 °C (dec.).

*Attempted synthesis of Hbimca^{Mes}(2HTos), **4^{Mes}**, from I(Mes)$_2$·Tos and **3***

The syntheses of **4^{Mes}** was attempted analogously to that of **4^{Ph}** described above using I(Mes)$_2$·Tos instead of I(Ph)$_2$·BF_4. ^{1}H NMR data of the vacuum dried reaction mixture exhibit chemical shift and integration values consistent with the starting materials, dimesityl iodonium salt and **3**.

*Bimca^{Me}(H_2I), **5^{Me}**, from deprotonation of **4^{Me}***

Potassium *tert*-butoxide (0.16 g, 1.4 mmol) was added to a stirred, colourless room temperature suspension of **4^{Me}** (1.0 g, 1.4 mmol) in acetonitrile (120 mL) to afford a bright yellow suspension that gradually cleared (*ca*. 15 min). After 1 h, the reaction mixture was filtered and volatiles were removed from the yellow filtrate under reduced pressure to give crude **5^{Me}** as a bright yellow solid, which was dissolved in DCM (100 mL), filtered and dried over anhydrous $MgSO_4$. Isolation of the supernatant by filtration and drying under vacuum yielded the bright yellow DCM solvate of **5^{Me}**. Analytically pure **5^{Me}** was afforded by heating **5^{Me}** under vacuum at 120 °C for 1 h. (0.65 g, 79%). Crystals of the **5^{Me}** DCM solvate suitable for single crystal X-ray diffraction were grown from a room temperature DCM solution of **5^{Me}** layered with hexane. ^{1}H NMR (400 MHz, THF-d_8): δ 1.47 (br s, 18H, *t*Bu-CH_3), 4.32 (br s, 6H, NMe), 7.50 (br s, 2H, 2,7-carb.-*H*), 7.61 (br s, 2H, 4-imidazolium-*H*), 8.12 (br s, 2H, 4,5-carb.-*H*), 8.21 (br s, 2H, 5-imidazolium-*H*), 11.25 (br s, 2H, 2-imidazolium-*H*). ^{1}H NMR (400 MHz, DMSO-d_6): δ 1.48 (s, 18H,

*t*Bu-C*H*$_3$), 4.09 (s, 6H, NMe), 7.68 (d, $^4J_{HH}$ = 1.72 Hz, 2H, 2,7-carb.-*H*), 7.97 (m, 2H, 4-imidazolium-*H*), 8.22 (d, $^4J_{HH}$ = 1.72 Hz, 2H, 4,5-carb.-*H*), 8.74 (m, 2H, 5-imidazolium-*H*), 10.78 (br s, 2H, 2-imidazolium-*H*). ^{13}C NMR (100 MHz, DMSO-*d*$_6$): δ 32.04 (s, *t*Bu-*C*H$_3$), 34.57 (s, *t*Bu-*C*), 36.21 (s, NMe), 112.16 (s, 2,7-carb.-*C*), 116.62 (s, 5-carb.-*C*), 119.56 (s, 4-imidazolium-*C*), 120.17 (s, carb.-*C*), 123.01 (s, 5-imidazolium-*C*), 127.32 (s, carb.-*C*), 136.09 (s, 2-imidazolium-*C*), 137.02, 142.06 (s, carb.-*C*). Calcd. for $C_{28}H_{34}N_5I$: C, 59.26; H, 6.04; N, 12.34. Found: C, 59.22; H, 6.26; N, 12.35. IR (Nujol on NaCl plates, cm^{-1}): 1567 (*m, sh*), 1542 (*m, sh*), 1276 (*m, sh*), 1228 (*s, sh*), 1137 (*m, sh*), 991 (*m, sh*), 843 (*m, sh*), 656 (*m, sh*), 615 (*m, sh*). Mp: 269-270°C (dec.).

*Bimca^{iPr}(H$_2$I), **5^{iPr}**, from deprotonation of **4^{iPr}***

Bis(imidazolium)carbazolide **5^{iPr}** was synthesised analogously to **5^{Me}** from **4^{iPr}** on an equimolar scale (yield: 0.77 g, 86%). Crystals of the **5^{Me}** fluorobenzene solvate suitable for single crystal X-ray diffraction were grown from a saturated room temperature fluorobenzene solution of **5^{Me}** placed at 4 °C. ^{1}H NMR (400 MHz, THF-*d*$_8$): δ 1.50 (s, 18H, *t*Bu-C*H*$_3$), 1.65 (d, $^3J_{HH}$ = 6.69 Hz, 12H, N*i*Pr-C*H*$_3$), 5.58 (sept, $^3J_{HH}$ = 6.69 Hz, 2H, N*i*Pr-C*H*), 7.53 (d, $^4J_{HH}$ = 1.66 Hz, 2H, 2,7-carb.-*H*), 7.97 (m, 2H, 4-imidazolium-*H*), 8.20 (d, $^4J_{HH}$ = 1.66 Hz, 2H, 4,5-carb.-*H*), 8.32 (m, 2H, 5-imidazolium-*H*), 11.28 (m, 2H, 2-imidazolium-*H*). ^{1}H NMR (300 MHz, DMSO-*d*$_6$): δ 1.47 (s, 18H, *t*Bu-C*H*$_3$), 1.64 (d, $^3J_{HH}$ = 6.69 Hz, 12H, N*i*Pr-C*H*$_3$), 4.87 (sept, $^3J_{HH}$ = 6.69 Hz, 2H, N*i*Pr-C*H*), 7.67 (d, $^4J_{HH}$ = 1.67 Hz, 2H, 2,7-carb.-*H*), 8.19 (m, 2H, 4-imidazolium-*H*), 8.22 (d, $^4J_{HH}$ = 1.67 Hz, 2H, 4,5-carb.-*H*), 8.80 (m, 2H, 5-imidazolium-H), 10.65 (br s, 2H, 2-imidazolium-*H*). ^{13}C NMR (75 MHz, DMSO-*d*$_6$): δ 22.36 (s, N*i*Pr-*C*H$_3$), 32.11 (s, *t*Bu-*C*H$_3$), 34.53 (s, *t*Bu-*C*), 52.36 (s, N*i*Pr-*C*H), 112.76 (s, 2,7-carb.-*C*), 116.61 (s, 4,5-carb.-*C*), 119.65 (s,

4-imidazolium-*C*), 120.51 (s, carb.-*C*), 121.39 (s, 5-imidazolium-*C*), 127.19 (s, carb.-*C*), 134.71 (s, 2-imidazolium-*C*), 135.90, 142.26 (s, carb.-*C*). Calcd. for $C_{32}H_{42}N_5I$: C, 61.63; H, 6.79; N, 11.23. Found: C, 61.67; H, 6.78; N, 11.23. IR (Nujol on NaCl plates, cm^{-1}): 1574 (*w, sh*), 1545 (*m, sh*), 1284 (*s, sh*), 1219 (*s, sh*), 1135 (*m, sh*), 1033 *(w, sh*), 991 (*m, sh*), 876 (*m, sh*), 843 (*m, sh*), 666 (*m, sh*), 645 (*m, sh*), 630 (*m, sh*). Mp 268-269 °C (dec.).

*Attempted isolation of Bimca^{Me}(H), **6^{Me}**, from the deprotonation of **4^{Me}***

A THF solution (5 mL) of KHMDS (0.057 g, 0.29 mmol) was added to a THF suspension (15 mL) of **4^{Me}** (0.10 g, 0.14 mmol) to afford an amber suspension that was stirred for 30 min at room temperature. After this time the supernatant gradually darkened to red with the concomitant precipitation of a bright yellow solid (with yellow fluorescence under long wave UV light). Separation of the red supernatant by filtration and removal of volatiles *in vacuo* afforded a red, treacly solid that displayed a ^{1}H NMR spectrum (THF-d_8) consistent with a complex mixture of bimca^{Me} containing products.

*Bimca^{Me}(H), **6^{Me}**(monitored in situ)*

THF-d_8 (0.5 mL) was added to a solid mixture of **4^{Me}** (0.020 g, 0.030 mmol) and KHMDS (0.012 g, 0.060 mmol) to immediately give an amber suspension, of which the ^{1}H NMR spectrum was acquired (t < 15 min). The rapid decomposition of a putative **6^{Me}** compound after this time precluded the acquisition of meaningful ^{13}C NMR data.

^{1}H NMR (400 MHz, THF-d_8): δ 1.46 (br s, 18H, *t*Bu-CH_3), 3.71 (br s, 6H, NMe), 7.00 (br s, 2H, 4-imidazolyl-*H*), 7.41 (br s, 2H, 2,7-carb.-*H*), 7.85 (br s, 2H, 5-imidazolyl-*H*), 8.04 (br s, 2H, 4,5-carb.-*H*), 10.37 (br s, 1H, bimca^{Me}(*H*)). Bimca^{iPr}(H) **6^{iPr}**, from the deprotonation of **4^{iPr}**

A THF solution (5 mL) of KHMDS (0.053 g, 0.27 mmol) was added to a THF suspension (15 mL) of **4^{iPr}** (0.10 g, 0.013 mmol) to immediately afford an amber suspension which

was stirred for 30 min at room temperature. During this time the reaction mixture gradually formed a white precipitate and the reaction mother liquor turned dark amber. Separation of the amber supernatant by filtration and removal of volatiles *in vacuo* afforded dark amber **6**$^{\mathbf{iPr}}$ with the inclusion of unidentifiable and inseparable bimca^{iPr} containing impurities (*ca*. 15% relative to resonances assigned to **6**$^{\mathbf{iPr}}$) by ^{1}H NMR spectroscopy. ^{1}H NMR (400 MHz, THF-d_8): δ 1.46 (br d, $^{3}J_{HH}$ = 6.64 Hz, 12H, N*i*Pr-C*H*$_3$), 1.48 (br s, 18H, *t*Bu-C*H*$_3$), 4.74 (sept, $^{3}J_{HH}$ = 6.64, 2H, N*i*Pr-C*H*), 7.39 (d, $^{4}J_{HH}$ = 1.20 Hz, 2H, 4-imidazolyl-*H*), 7.78 (d, $^{4}J_{HH}$ = 1.43 Hz, 2H, 2,7-carb.-*H*), 8.08 (d, $^{4}J_{HH}$ = 1.43 Hz, 2H, 4,5-carb.-*H*), 8.53 (d, $^{4}J_{HH}$ = 1.20 Hz, 2H, 5-imidazolyl-*H*), 11.12 (br s, 1H, bimca^{iPr}(*H*)). ^{13}C NMR (100 MHz, THF-d_8): δ 23.35 (s, N*i*Pr-*C*H$_3$), 32.78 (s, *t*Bu-*C*H$_3$), 35.15 (s, *t*Bu-*C*), 53.12 (s, N*i*Pr-*C*H), 112.76 (s, 2,7-carb.-*C*), 115.58 (s, 4,5-carb.-*C*), 117.18 (s, 5-imidazolyl-*C*), 121.10 (s, 4-imidazolyl-*C*), 124.26, 128.63, 135.65, 144.16 (s, carb-*C*), 2-imidazolyl-*C* not observed. Microanalysis samples of **6**$^{\mathbf{iPr}}$ persistently returned C, H, N, contents that are lower than the expected values, presumably due to the inclusion of inseparable contaminants such as K**7**$^{\mathbf{iPr}}$ and **5**$^{\mathbf{iPr}}$. A representative analysis is as follows: Calcd. for $C_{32}H_{41}N_5$: C, 77.53; H, 8.34; N, 14.13. Found: C, 74.10; H, 8.24; N, 13.08. IR (Nujol on NaCl plates, cm^{-1}): 1666 (*m*, *sh*), 1593 (*m*, *sh*), 1365 (m, sh), 1261 (*m*, *sh*), 1220 (*m*, *sh*), 1201 (*m*, *sh*), 1171 (*w*, *sh*), 1137 (*w*, *sh*), 1094 (*m*, *br*), 1021 (*m*, *sh*), 934 (*w*, *sh*), 842 (*m*, *sh*), 806 (*m*, *sh*), 755 (*w*, *sh*), 722 (*w*, *sh*), 685 (*w*, *sh*). Mp: 216 - 220 °C (dec.), 238 - 240 °C (melts).

*Isolation of Li(bimca^{Me}), Li**7**$^{\mathbf{Me}}$·LiI*

A hexane stock solution of *n*BuLi (0.518 mmol, 0.26 mL, 1.99 M) was added to a stirred suspension of **4**$^{\mathbf{Me}}$ (0.120 g, 0.173 mmol) in THF (20 mL) *via* syringe at room temperature to afford a yellow suspension that gradually (*ca*. 15 min) cleared and turned amber, with a visible blue fluorescence under ambient light. The reaction mixture was stirred at room

temperature for 1 h, whereupon hexane (60 mL) was added to precipitate beige, extremely moisture sensitive Li**7^{Me}**·LiI. The suspension was allowed to settle and the pale amber, blue fluorescent supernatant was isolated by filtration. The filtrant was dried *in vacuo* at room temperature, yielding Li**7^{Me}**·LiI as a pale amber powder (0.057 g, 56%). Placement of the filtrate at -24 °C yielded a small number of crystals of tetralithium dimer, **8**, suitable for single crystal X-ray crystallographic studies.

^{1}H NMR (400 MHz, THF-d_8): δ 1.50 (s, 18H, *t*Bu-CH_3), 3.96 (s, 6H, NMe), 7.16 (s, 2H, 4-NHC-*H*), 7.41 (d, $^{4}J_{HH}$ = 1.43 Hz, 2H, 2,7-carb.-*H*), 7.79 (s, 2H, 5-NHC-*H*), 7.99 (d, $^{4}J_{HH}$ = 1.43 Hz, 2H, 4,5-carb.-*H*). ^{13}C NMR (100 MHz, THF-d_8): δ 32.76 (s, *t*Bu-*C*H$_3$), 35.08 (s, *t*Bu-*C*), 38.07 (s, NMe), 110.91 (s, 7-carb.-*C*), 114.01 (s, 5-NHC-*C*), 119.49 (s, 5-carb.-*C*), 119.80 (s, 4-NHC-*C*), 127.99, 128.12, 135.19, 143.45 (s, carb.-*C*), 206.14 (s, 2-NHC-*C*). Elemental analyses of Li**7^{Me}**·LiI consistently returned a carbon composition that was higher than expected for Li(bimca^{Me})·LiI. This outcome is likely due to the inclusion of THF in the solid product. Calcd. for $C_{28}H_{32}N_5Li$·(LiI): C, 58.05; H, 5.57; N, 12.09. Calcd. for $C_{28}H_{32}N_5Li$·(LiI)(0.5 THF): C, 58.55; H, 5.90; N, 11.38. Calcd. for $C_{32}H_{40}N_5Li$·(1.5 LiI)(0.5 THF): C, 52.81; H, 5.32; N, 10.26. Calcd. for $C_{32}H_{40}N_5Li$·(LiI)(THF): C, 59.00; H, 6.19; N, 10.75. Found: C, 59.70; H, 5.53; N, 11.46. IR (Nujol on NaCl plates, cm^{-1}) 1664 (*m, sh*), 1574 (*m, sh*), 1547 (w, *sh*), 1226 (*m, sh*), 1169 (*m, sh*), 1154 (*m, sh*), 1079 (*w, sh*), 10718 (*w, sh*), 892 (*w, sh*), 844 (*m, sh*), 723 (*m, sh*). Mp: 213-214°C (dec.).

*Li(bimca^{iPr}), Li**7^{iPr}**·LiI, from the deprotonation of **4^{iPr}***

Li**7^{iPr}**·LiI was prepared analogously to Li**7^{Me}**·LiI on an equimolar scale (0.046 g, 48%). Recrystallisation of the beige Li**7^{iPr}**·LiI from a 50 °C saturated DME solution that was slowly cooled to room temperature and left to stand overnight afforded a small number

of crystals of [Li**7**$^{\mathbf{iPr}}$(DME)·LiI] suitable for single crystal X-ray diffraction structure analysis. NMR samples of Li**7**$^{\mathbf{iPr}}$·LiI were prepared by dissolving vacuum dried Li**7**$^{\mathbf{iPr}}$·LiI in THF-d_8. Crystalline samples of [Li**7**$^{\mathbf{iPr}}$(DME)·LiI] characterised as Li**7**$^{\mathbf{iPr}}$·LiI by ^{1}H NMR spectroscopy upon dissolution in THF-d_8. ^{1}H NMR (400 MHz, THF-d_8): δ 1.49 (s, 18H, *t*Bu-CH_3), 1.63 (d, $^3J_{HH}$ = 6.75 Hz, 12H, N*i*Pr-CH_3), 4.72 (sept, $^3J_{HH}$ = 6.75, 2H, N*i*Pr-C*H*), 7.25 (d, $^3J_{HH}$ = 1.70 Hz, 2H, 4-NHC-*H*), 7.39 (d, $^4J_{HH}$ = 1.67 Hz, 2H, 2,7-carb.-*H*), 7.77 (d, $^3J_{HH}$ = 1.70 Hz, 2H, 5-NHC-*H*), 7.98 (d, $^4J_{HH}$ = 1.67 Hz, 2H, 4,5-carb.-*H*). ^{13}C NMR (100 MHz, THF-d_8): δ 24.25 (s, N*i*Pr-*C*H$_3$), 32.77 (s, *t*Bu-*C*H$_3$), 35.08 (s, *t*Bu-*C*), 53.38 (s, N*i*Pr-*C*H), 111.18 (s, 2,7-carb.-*C*), 113.99 (s, 4,5-carb.-*C*), 116.05 (s, 4-NHC-*C*), 119.44 (s, 5-NHC-*C*), 127.88, 128.26, 135.13, 143.48 (s, carb.-*C*), 203.66 (s, 2-NHC-*C*). Elemental analyses of lithium complex Li**7**$^{\mathbf{iPr}}$·LiI consistently returned a C, H, N composition that was lower than expected for Li(bimca^{iPr})·LiI. This outcome is likely due to adduct formation with the lithium iodide co-product and persistent inclusion of THF in the solid product. Calcd. for $C_{32}H_{40}N_5Li$·(LiI): C, 60.48; H, 6.34; N, 11.02. Calcd. for $C_{32}H_{40}N_5Li$·(LiI)(THF): C, 61.11; H, 6.84; N, 9.90. Calcd. for $C_{32}H_{40}N_5Li$·(1.5 LiI)(0.5 THF): C, 55.30; H, 6.01; N, 9.48. Found: C, 55.29; H, 6.97; N, 10.08. IR (Nujol on NaCl plates, cm^{-1}): 1657 (*m, sh*), 1572 (*m, sh*), 1556 (*m, sh*), 1542 (*m, sh*), 1365 (*s, sh*), 1314 (*m, sh*), 1274 (*m, sh*), 1136 (*m, sh*), 994 (*w, sh*), 843 (*m, sh*). Mp: 210-212°C (dec.).

*K(bimca^{Me}), K**7**$^{\mathbf{Me}}$, from the deprotonation of **4**$^{\mathbf{Me}}$ 1 h*

All K**7**$^{\mathbf{R}}$ compounds were prepared and characterised commensurately; a representative synthesis for K**7**$^{\mathbf{Me}}$ is described below.

A solution of KHMDS (0.086 g, 0.43 mmol) in THF (5 mL) was added to a stirred, colourless suspension of **4**$^{\mathbf{Me}}$ (0.10 g, 0.14 mmol) also in THF (10 mL) at room

temperature to immediately afford a bright yellow suspension that darkened to amber and then dark red with the development of a blue fluorescence under long wave UV light over a period of 1 h. At this point a white precipitate was allowed to settle and the dark red supernatant was filtered to afford a THF solution of K**7**$^{\mathbf{Me}}$ and HHMDS which was used *in situ* for salt metathesis reactions.

Solution phase characterisation of K**7**$^{\mathbf{Me}}$ was carried out by the addition of THF-d_8 (0.5 mL) to a solid mixture of KHMDS (0.0086 g, 0.043 mmol) and **4**$^{\mathbf{Me}}$ (0.010 g, 0.014 mmol) at room temperature. The resulting amber suspension was vigorously agitated and sonicated at room temperature for one hour, after which time ^{1}H and ^{13}C NMR spectra of the dark red, blue fluorescent reaction mixture were acquired. ^{1}H NMR (250 MHz, THF-d_8): δ 1.45 (s, 18H, *t*Bu-CH_3), 3.81 (s, 6H, NMe), 7.00 (s, 2H, 4-NHC-*H*), 7.21 (s, 2H, 2,7-carb.-*H*), 7.46 (s, 2H, 5-NHC-*H*), 8.02 (s, 2H, 4,5-carb.-*H*). ^{13}C NMR (400 MHz, THF-d_8): δ 32.70 (s, *t*Bu-*C*H$_3$), 34.82 (s, *t*Bu-*C*), 56.49 (s, NMe), 114.32 (s, 2,7-carb.-*C*), 116.53 (s, 4,5-carb.-*C*), 119.13 (s, 4-NHC-*C*), 122.64 (s, 5-NHC-*C*), 127.90, 128.45, 129.95, 134.31 (s, carb.-*C*), 2-NHC-*C* not observed.

K(bimca^{iPr}), K7$^{\mathbf{iPr}}$ (NMR scale preparation)

^{1}H NMR (400 MHz, THF-d_8): δ 1.46 (s, 18H, *t*Bu-CH_3), 1.49 (d, $^{3}J_{HH}$ = 7.30 Hz, 12H, N*i*Pr-CH_3), 4.54 (sept, $^{3}J_{HH}$ = 7.30 Hz, 2H, N*i*Pr-C*H*) 6.98 (s, 2H, 4-NHC-*H*), 7.15 (d, $^{4}J_{HH}$ = 1.71 Hz, 2H, 2,7-carb.-*H*), 7.21 (s, 2H, 5-NHC-*H*), 8.02 (d, $^{4}J_{HH}$ = 1.71 Hz, 2H, 4,5-carb.-*H*). ^{13}C NMR (400 MHz, THF-d_8): δ 23.56 (s, N*i*Pr-*C*H$_3$), 32.71 (s, *t*Bu-*C*H$_3$), 35.05 (s, *t*Bu-*C*), 53.00 (s, N*i*Pr-*C*H), 112.76 (s, 2,7-carb.-*C*), 115.00 (s, 4,5-carb.-*C*), 116.88 (s, 4-NHC-*C*), 121.00 (s, 5-NHC-*C*), 128.57, 134.46, 135.21, 144.27 (s, carb.-*C*), 2-NHC-*C* not observed.

K(bimca^{Ph}), K7^{Ph} (NMR scale preparation)

^{1}H NMR (400 MHz, THF-d_8): δ 1.48 (s, 18H, *t*Bu-C*H*$_3$), 7.24 (m, 2H, NPh), 7.33 (d, $^{4}J_{HH}$ = 1.93 Hz, 2H, 4-NHC-*H*), 7.36 (m, 4H, NPh), 7.56 (d, $^{4}J_{HH}$ = 1.68 Hz, 2H, 2,7-carb.-*H*), 7.76 (d, $^{4}J_{HH}$ = 1.68 Hz, 2H 4,5-carb.-*H*), 7.79 (m, 4H, NPh), 8.08 (d, $^{4}J_{HH}$ = 1.93 Hz, 2H, 5-NHC-*H*).

[Mg(HMDS)$_2$(Et$_2$O)] (adapted from literature procedure)[114,118]

A diethyl ether (100 mL) solution of KHMDS (3.7 g, 18 mmol) was added to a stirred, room temperature diethyl ether (100 mL) solution of freshly prepared MgI_2 (2.6 g, 9.2 mmol) to give a cloudy white suspension that was stirred for 18 h. After this time the reaction mixture was allowed to settle and the colourless supernatant was filtered off dried *in vacuo* to give [Mg(HMDS)$_2$(Et$_2$O)] as colourless, low melting, air and moisture sensitive needles (2.2 g, 56%) that give a ^{1}H NMR spectrum and melting point that are consistent with previously reported data:[118] ^{1}H NMR (400 MHz, C_6D_6): δ 0.31 (s, 36H, $SiMe_3$), 0.85 (t, $^{3}J_{HH}$ = 7.13 Hz, 6H, Et$_2$O-C*H*$_3$), 3.37 (q, $^{3}J_{HH}$ = 7.13 Hz, 4H, Et$_2$O-C*H*$_2$). Mp: 40-41 °C (lit.[114] 39 °C).

*[Mg(bimca^{Me})I(THF)], **9**^{Me}, from **5**^{Me}*

A THF solution (5 mL) of [Mg(HMDS)$_2$·Et$_2$O] (0.15 g, 0.35 mmol) was added to a stirred THF (10 mL) suspension of **5**^{Me} (0.20 g, 0.35 mmol). The resulting bright yellow suspension was stirred at room temperature for 18 h, during which it gradually became clear and turned pale amber with visible blue fluorescence in ambient sunlight or under long wave UV light. Filtration and removal of volatiles *in vacuo* gave **9**^{Me} as an extremely air and moisture sensitive pale amber microcrystalline solid (0.19 g, 91 %). Crystals of **9**^{Me} suitable for single crystal X-ray diffraction studies were grown from a saturated THF-d_8 solution upon standing at room temperature. ^{1}H NMR (300 MHz, THF-d_8): δ

1.51 (s, 18H, *t*Bu-C*H*$_3$), 1.77 (m, 4H, THF-C*H*$_2$), 3.62 (m, 4H, THF-OC*H*$_2$), 4.24 (s, 6H, NMe), 7.25 (d, $^3J_{HH}$ = 1.80 Hz, 2H, 4-NHC-*H*), 7.64 (d, $^4J_{HH}$ = 1.64 Hz, 2H, 2,7-carb.-*H*), 8.07 (d, $^4J_{HH}$ = 1.64 Hz, 2H, 4,5-carb.-*H*), 8.09 (d, $^3J_{HH}$ = 1.80 Hz, 2H, 5-NHC-*H*). ^{13}C NMR (75 MHz, THF-d_8): δ 26.19 (s, THF-*C*H$_2$), 32.43 (s, *t*Bu-*C*H$_3$), 35.12 (s, *t*Bu-*C*), 39.94 (s, NMe), 68.04 (s, THF-O*C*H$_2$), 111.95 (s, 2,7-carb.-*C*), 114.24 (s, 4,5-carb.-*C*), 117.90 (s, 5-NHC-*C*), 122.56 (s, 4-NHC-*C*), 126.05, 129.00, 138.29, 140.52 (s, carb.-*C*), 190.51 (s, 2-NHC-*C*). Microanalysis data for **9^{Me}** inexplicably and persistently returned low values for carbon content. Calcd. for $C_{28}H_{32}N_5MgI$(THF): C, 58.07; H, 6.09; N, 10.58. Found: C, 53.74; H, 6.79; N, 10.34. IR (Nujol on NaCl plates, cm^{-1}): 1574 (*w*, *sh*), 1548 (*w*, *sh*), 1276 (*m*, *sh*), 1261 (*m*, sh), 1226 (*m*, *sh*), 1137 (*w*, *sh*), 1093 (*m*, *br*) 1020 (*m*, *br*), 932 (*w*, *sh*), 843 (*m*, *sh*), 802 (*m*, *sh*). Mp: 218-220 °C (dec.), 296 °C (melts).

*[Ga(bimca^{Me})I$_2$] (**13^{Me}**) via salt metathesis with **9^{Me}***

A beige THF (6 mL) solution of **9^{Me}** (0.10 g, 0.18 mmol) was added to a stirred THF (10 mL) solution of GaI_3 (0.079 g, 0.18 mmol) to give a slightly cloudy amber reaction mixture that was stirred for 18 h at room temperature, during which it gradually faded to a pale beige fine suspension. Filtration and removal of volatiles from the filtrate *in vacuo* yielded [Ga(bimca^{Me})I$_2$] as an off-white microcrystalline solid (0.10 g, 74%). ^{1}H NMR (300 MHz, THF-d_8): δ 1.53 (s, 18H, *t*Bu-C*H*$_3$), 4.41 (s, 6H, NMe), 7.38 (d, $^3J_{HH}$ = 2.01 Hz, 2H, 4-NHC-*H*), 7.82 (d, $^4J_{HH}$ = 1.51 Hz, 2H, 2,7-carb.-*H*), 8.19 (d, $^4J_{HH}$ = 1.51 Hz, 2H, 4,5-carb.-*H*), 8.29 (d, $^3J_{HH}$ = 2.01 Hz, 2H, 5-NHC-*H*). ^{13}C NMR (75 MHz, THF-d_8): δ 32.18 (s, *t*Bu-*C*H$_3$), 35.51 (s, *t*Bu-*C*), 38.62 (s, NMe), 112.02 (s, 2,7-carb.-*C*), 114.76 (s, 5-NHC-*C*), 116.16 (s, 4,5-carb.-*C*), 122.72 (s, 4-NHC-*C*), 123.85, 128.26, 135.97, 142.17 (s, carb.-*C*), 167.26 (s, 2-NHC-*C*, resolved with ^{1}H-^{13}C HMBC). Calcd. for $C_{28}H_{32}N_5I_2Ga$: C, 44.13; H, 4.23; N, 9.19. Found: C, 43.44; H, 4.47; N, 9.17. IR (Nujol

on NaCl plates, cm^{-1}): 1765 (*w*, *sh*), 1594 (*w*, *sh*), 1261 (*m*, *sh*), 1230 (w, sh), 1201 (*w*, *sh*), 1096 (*m*, *sh*), 1022 (*m*, *sh*), 866 (*m*, *sh*), 863 (*w*, *sh*), 800 (*m*, *sh*), 700 (*w*, *sh*), 688 (*w*, *sh*), 659 (*w*, *sh*). Mp: 297-298 °C (dec.), 320 °C (melts).

*[Mg(bimca^{Me})$_2$], **10^{Me}**, from KHMDS*

A THF solution (10 mL) of KHMDS (0.034 g, 0.170 mmol,) was added to a stirred beige THF solution (10 mL) of **9^{Me}** (0.100 g, 0.170 mmol) to give a cloudy, pale amber reaction mixture that was stirred at room temperature for 18 h. Over this time its blue fluorescence under long wave UV light intensified and the mixture changed colour to dark amber. The colourless precipitate was allowed to settle and the pale red supernatant isolated by filtration and dried *in vacuo* to give analytically pure **10^{Me}** as a very air and moisture sensitive pale red solid (0.067 g, 34% in Mg). Crystals of **10^{Me}** suitable for single crystal X-ray diffraction studies were grown from a room temperature saturated THF solution diffused with hexane stored at 4 °C. ^{1}H NMR (300 MHz, THF-*d$_8$*): δ 1.51 (s, 36H, *t*Bu-C*H*$_3$), 2.58 (s, 12H, NMe), 6.62 (d, $^3J_{HH}$ = 1.76 Hz, 4H, 4-NHC-*H*), 7.42 (d, $^4J_{HH}$ = 1.80 Hz, 4H, 2,7-carb.-*H*), 7.59 (d, $^3J_{HH}$ = 1.76 Hz, 2H, 5-NHC-*H*), 8.07 (d, $^4J_{HH}$ = 1.80 Hz, 2H, 4,5-carb.-*H*). ^{13}C NMR (75 MHz, THF-*d$_8$*): δ 32.50 (s, *t*Bu-*C*H$_3$), 35.01 (s, *t*Bu-*C*), 35.74 (s, NMe), 113.10 (s, 2,7-carb.-*C*), 113.41 (s, 4,5-carb.-*C*), 117.47 (s, 5-NHC-*C*), 121.91 (s, 4-NHC-*C*), 128.42, 129.42, 137.29, 142.23 (s, carb.-*C*), 199.72 (s, 2-NHC-*C*). Calcd. for $C_{56}H_{64}N_{10}Mg$: C, 74.61; H, 7.16; N, 15.54. Found: C, 74.42; H, 7.21; N, 15.49. IR (Nujol on NaCl plates, cm^{-1}): 1568 (*m*, *sh*), 1548 (*w*, *sh*), 1398 (*m*, *sh*), 1361 (*m*, *sh*), 1292 (*m*, *sh*), 1261 (*s*, sh), 1238 (*m*, *sh*), 1188 (*w*, *sh*), 1097 (*s*, *br*), 1024 (*s*, *br*), 863 (*m*, *sh*), 802 (*s*, *sh*), 708 (*m*, *sh*), 660 (*m*, *sh*). Mp: 235-236 °C (dec.), 294-296 °C (melts).

*[Mg(bimca^{Me})$_2$], **10^{Me}**, from KHMDS (monitored in situ)*

THF (0.5 mL) was added to an equimolar solid mixture of **9^{Me}** (0.010 g, 0.017 mmol) and KHMDS (0.0034 g, 0.017 mmol), sealed in a J. Youngs capped NMR sample tube equipped with a C_6D_6 filled glass capillary. The sample was agitated for *ca*. 5 minutes to give a slightly cloudy, pale amber reaction mixture with a strong blue fluorescence under long wave UV light. A ^{1}H THF solvent-supressed NMR spectrum was acquired (t < 15 min). The redistribution reaction was found to be accelerated to completion by heating (70 °C, 18 h). ^{1}H NMR (400 MHz with THF-H_8 suppression. Resonances of **9^{Me}-HMDS** deduced by omission of those assigned to **10^{Me}** and [Mg(HMDS)$_2$]): δ 0.03 (s, 36H, $SiMe_3$), 1.47 (s, *t*Bu-C*H*$_3$, overlaps with *t*Bu-C*H*$_3$ resonance of **10^{Me}**), 4.08 (s, 6H, NMe), 7.26 (d, $^3J_{HH}$ = 1.66 Hz, 2H, 4-NHC-*H*), 7.59 (d, $^4J_{HH}$ = 1.78 Hz, 2H, 2,7-carb.-*H*), 7.96 (d, $^4J_{HH}$ = 1.78 Hz, 2H, 4,5-carb.-*H*), 8.02 (d, $^3J_{HH}$ = 1.66 Hz, 2H, 5-NHC-*H*). No further data obtained due to transient nature of **9^{Me}-HMDS**.

*[Mg(bimca^{Me})$_2$], **10^{Me}**, from LDA (monitored in situ)*

The formation of **9^{Me}-N*i*Pr$_2$** was monitored analogously to the preparation of **9^{Me}-HMDS** on an equimolar scale in THF-d_8 using LDA instead of KHMDS. ^{1}H NMR (400 MHz, THF-d_8, resonances of **9^{Me}-N*i*Pr$_2$** deduced by omission of those assigned to **10^{Me}** and [Mg(N*i*Pr$_2$)$_2$]: δ 0.96 (d, $^3J_{HH}$ = 6.30 Hz, 12H, N*i*Pr-C*H*$_3$), 1.50 (s, *t*Bu-C*H*$_3$, overlaps with *t*Bu-C*H*$_3$ resonance of **10^{Me}**), 2.85 (sept, $^3J_{HH}$ = 6.30 Hz, 2H, N*i*Pr-C*H*), 4.31 (s, 6H, NMe), 7.25 (d, $^3J_{HH}$ = 1.90 Hz, 2H, 4-NHC-*H*), 7.62 (d, $^4J_{HH}$ = 1.72 Hz, 2H, 2,7-carb.-*H*), 8.03 (d, $^4J_{HH}$ = 1.72 Hz, 2H, 4,5-carb.-*H*), 8.05 (d, $^3J_{HH}$ = 1.90 Hz, 2H, 5-NHC-*H*). No further data obtained due to transient nature of **9^{Me}-N*i*Pr$_2$**.

*[Mg(bimca^{Me})$_2$], **10^{Me}**, from NaOEt (monitored in situ)*

The formation of **9^{Me}-OEt** was monitored analogously to **9^{Me}-N*i*Pr$_2$** on an equimolar scale in THF-d_8 using NaOEt instead of LDA. No heating was required to achieve full conversion to the homoleptic redistribution products. The reaction mixture characterises as **10^{Me}** by ^{1}H NMR (THF-d_8).

*Attempted reduction of **9^{Me}** with K metal*

A beige THF solution (6 mL) of **9^{Me}** (0.15 g, 0.25 mmol) was added to a Schlenk flask containing K metal (0.0099 g, 0.025 mmol) as a mirror. A white solid immediately deposited and the reaction mixture gradually turned pale red. Stirring for a further 18 h, filtration and removal of volatiles *in vacuo* afforded a brown solid that was redissolved in THF-d_8 for identification by ^{1}H NMR spectroscopy. ^{1}H NMR (400 MHz, THF-d_8 with omission of resonances attributed to unidentified bimca^{Me} species): δ 1.51 (s, 36H, *t*Bu-C*H*$_3$), 2.58 (s, 12H, NMe), 6.62 (d, $^3J_{HH}$ = 1.76 Hz, 4H, 4-NHC-*H*), 7.42 (d, $^4J_{HH}$ = 1.80 Hz, 4H, 2,7-carb.-*H*), 7.59 (d, $^3J_{HH}$ = 1.76 Hz, 4H, 5-NHC-*H*), 8.07 (d, $^4J_{HH}$ = 1.80 Hz, 4H, 4,5-carb.-*H*). (Data identical to those for **10^{Me}**).

*Attempted reduction of **9^{Me}** with K metal (monitored in situ)*

THF-d_8 (0.5 mL) was added to a J. Youngs capped NMR tube charged with **9^{Me}** (0.015 g, 0.025 mmol) and potassium metal (0.0099 g, 0.025 mmol) to yield a pale red suspension (with blue fluorescence). The sample was agitated for *ca.* 5 minutes to afford a cloudy red reaction mixture. The resultant off-white precipitate was allowed to settle and a ^{1}H NMR spectrum of the sample was acquired within 15 minutes of mixing which characterised as **10^{Me}** by ^{1}H NMR spectroscopy (THF-d_8). (Data identical to those for **10^{Me}**).

Attempted reduction of $\mathbf{9^{Me}}$ *with KH (monitored in situ)*

THF-d_8 (0.5 mL) was added to a J. Youngs capped NMR tube charged with $\mathbf{9^{Me}}$ (0.015 g, 0.025 mmol) and KH (0.0010 g, 0.025mmol) to give a pale red suspension (with blue fluorescence) which was allowed to react for *ca.* 1 h with continual agitation aided by sonication. After this time an off-white precipitate was allowed to settle and a ^{1}H NMR spectrum was acquired which characterised as $\mathbf{10^{Me}}$ and dissolved H_2 by ^{1}H NMR spectroscopy (THF-d_8). ^{1}H NMR (300 MHz, THF-d_8): δ 1.51 (s, 36H, *t*Bu-CH_3), 2.58 (s, 12H, NMe), 4.55 (s, 0.8H, H_2), 6.62 (d, $^3J_{HH}$ = 1.75 Hz, 4H, 4-NHC-*H*), 7.42 (d, $^4J_{HH}$ = 1.80 Hz, 4H, 2,7-carb.-*H*), 7.59 (d, $^3J_{HH}$ = 1.75 Hz, 4H, 5-NHC-*H*), 8.07 (d, $^4J_{HH}$ = 1.80 Hz, 4H, 4,5-carb.-*H*).

Chapter 3 – Group 13 bimca^{R} complexes

3.1 Introduction

The Lewis acidity inherent to high valent group 13 metals, M(III), where M = Al, Ga, In, Tl is often exploited in studies of their coordination chemistry. Neutral electron pair donors *e.g.* NR_3,[119] PR_3,[120] and NHCs[121,122] have been employed for the purpose of stabilising otherwise transient reaction intermediates or sensitive products; usually resulting in trigonal bipyramidal or tetrahedral coordination geometries (Figure 3.1).[119,123,124] Electronic stabilisation of the M(III) fragment of the resultant Lewis base adduct has allowed for the coordination of "softer" co-ligands to the "hard" metal centre with *e.g.* hydrides or iodides.[123,125] Group 13 metal complexes, particularly hydride complexes, also benefit from steric enshrouding of the metal-hydride moiety through the use of bulky co-ligands. For metal hydrides, these can inhibit access to thermodynamically favourable disproportionation or reductive dehydrogenation pathways (Chapter 1, Section 1.3).[126]

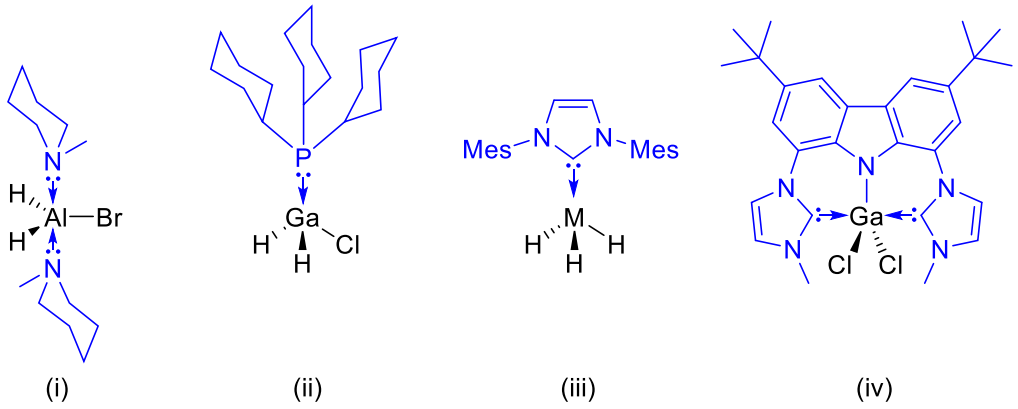

Figure 3.1 Group 13 halide and hydride complexes supported by σ-donor ligands *e.g.* amines,[119] phosphines,[120] NHCs,[121,122] and bimca^{Me} [83]

Little is known about the effect of bis(NHC) coordination on the stability of group 13 elements, due to the scarcity of reports concerning this chemistry (see Chapter 1, Section 1.5). This prompted a previous preliminary study, conducted in the Cole group, on the complexation of the bimca^{Me} ligand to heavy trivalent main group systems.[83] Indeed, only thirteen complexes of trivalent group 13 metals have been structurally characterised,[70] two of which bearing chelating poly(NHC) functionalities (Figure 1.11, Chapter 1 *vide supra*).[75,76] Our previous work has demonstrated that the bimca^{Me} scaffold is capable of stabilising trigonal bipyramidal heavy group 13 bis(NHC) complexes, wherein gallium, indium, and thallium complexes have been structurally authenticated.[83] Complexation was achieved *via* salt metathesis of MX_3 precursors with *in situ* prepared Li(bimca^{Me}), Li**7^{Me}** (Scheme 3.1), analogous to the preparation of [Rh(bimca^{Me})CO] in the original report by Kunz.[56]

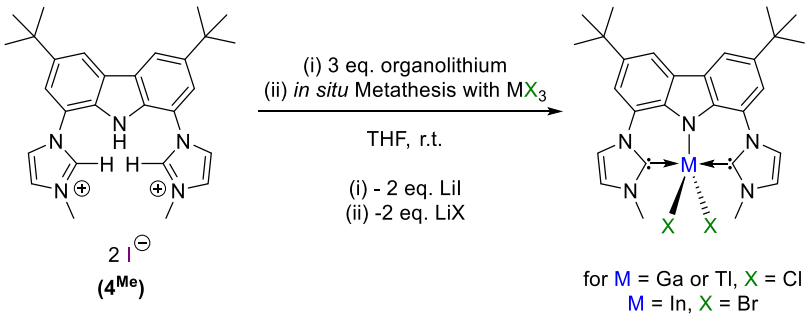

Scheme 3.1 Traditional metallation strategy for generating [M(bimca^{Me})X_2] complexes *via* metathesis reactions

It is noteworthy that this earlier work exposed a number of synthetic hurdles upon transferring this approach to *p*-block halides. Most of these shortcomings hinge on the poor solubility of [M(bimca^{Me})X_2] in solvents other than THF, which marred attempts to remove salt metathesis co-products from the bimca^{Me} complexes. This was evidenced in microanalysis data for these compounds and most strikingly by the structural

characterisation of the mixed chloro/iodo thallium complex [Tl(bimca^{Me})IX] (X = I or Cl), resulting from halide exchange reactions between the nascent [Tl(bimca^{Me})Cl$_2$] and LiI (Figure 3.2).[83]

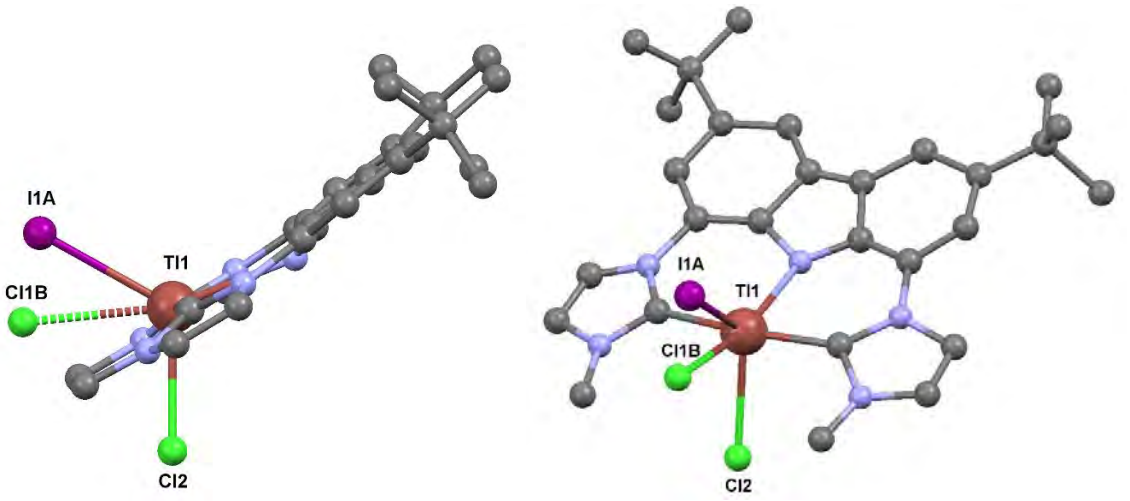

Figure 3.2 Mixed chloro/iodo thallium [Tl(bimca^{Me})ClX] of previous studies, I1A = 66%, Cl1B = 34%.

3.1.1 Purpose of this chapter

This initial investigation provides an opening for the work presented herein, which focuses on the optimisation of paths to clean heavy trivalent group 13 dihalides with a view to the further study of the consequences of bis(NHC) coordination to the M(III) cation by the bimca^{R} scaffold.

This work addresses the shortcomings of the aforementioned strategy, primarily by the development of alternative metallation paths that promise access to a series of M(III) bimca^{R} (R = Me or *i*Pr) diiodides. Additionally, it aims to extend the group 13 bimca^{R} complex series to the lightest metal congener, Al(III). Of this series, the heaviest indium and thallium bimca^{iPr} diiodides will be subjected to iodide-hydride exchange reactions, the latter potentially representing a rare example of a covalently bonded 6th period metal hydride, to study the role of bimca^{Me} coordination under these conditions. Following from

this, preliminary chemical reductions of the high valent group 13 species or complexation with low valent precursors to afford low oxidation state bimca^{R} supported complexes will be investigated.

3.2 Results and Discussion

As seen in the previous study, which used Li**7**^{Me}, an issue experienced with metallations proceeding through Li(bimca^{R}) salt metatheses is contamination of subsequent syntheses with the LiI co-product formed during the *in situ* deprotonation of the proligand iodide salt **4**^{R}, which potentially leads to halide exchange reactions between the nascent [M(bimca^{R})X$_2$] complex and the LiI co-product. Furthermore, the unremoved lithium salts in the reaction mother liquor hamper crystallisation and undermine the analytical purity of the [M(bimca^{R})X$_2$] products. Separation of these salts is impractical since they cannot be selectively precipitated using common, less polar laboratory solvents, owing to the poor solubility of the target group 13 bimca^{R} complexes.

It was thought prudent at the outset of this project to develop strategies that mimicked the original approach but (i) ensured the presence of a single halide counterion to eliminate halide scrambling, and (ii) used heavier *s*-block bimca^{R} reagents (see Chapter 2) to aid the precipitation of the corresponding salt metathesis co-products. An alternate strategy was also conceived that bypassed the formation of *s*-block halide co-products during the metallation reaction of bimca^{R} with the group 13 precursor, *i.e.* (iii) metallation through direct reaction of triprotic bimca^{R} proligands with tris(amido) or trialkyl precursors of the group 13 metals of interest.

In light of the convenient preparation of the known $\mathbf{4^{Me}}$ iodide salt and our studies detailing the isopropyl variant; $\mathbf{4^{iPr}}$ (*vide supra* Chapter 2), a synthetic method (following (i) and (ii) above) that could utilise MI_3 metallic precursors for M = Al and Ga was adapted (Scheme 3.2). The application of a similar approach to heavier group 13 species, *i.e.* In and Tl, was not pursued due to the preference of these metals to exist in the monovalent oxidation state when paired with sufficiently polarisable co-ligands (*cf.* TlI_3 is composed of Tl^+ and I_3^-).[1] Approach (iii) was adopted for these elements, wherein tris(amido)indane and -thallane reagents were reacted with triprotic bimca^R proligand salts (Scheme 3.2).

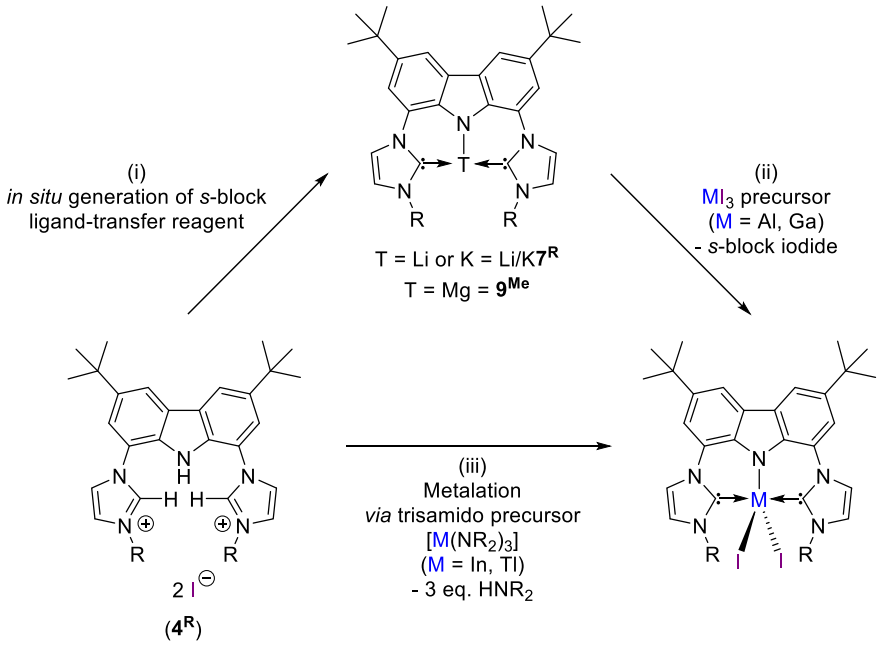

Scheme 3.2 Attempted **s**ynthetic strategies (i and ii) for accessing [M(bimca^{iPr})I_2] complexes (where M = group 13, L = HMDS or CH_3, and T = Li, K, or Mg-I)

*3.3 Synthesis of [Al(bimca^{iPr})I$_2$], **11^{iPr}***

Following strategies (i) and (ii) (Scheme 3.2), commercially obtained AlI_3 was used to generate [Al(bimca^{iPr})I$_2$], **11^{iPr}**, *via* metathesis with *in situ* prepared K(bimca^{iPr}), K**7^{iPr}**, prepared through reaction of **4^{iPr}** with three equivalents of KHMDS (*vide supra,* Chapter 2, Section 2.3.4). It was found that substitution of Li**7^{iPr}** for the potassium congener dramatically improved the separation of the group 1 iodide co-product through its precipitation from the THF mother liquor. However, somewhat counterintuitively, despite enabling rapid removal of solid KI, salt metatheses using K**7^{iPr}** proved less selective than those with their lithium counterpart Li(bimca^{iPr}). For example, it was noted that when using K**7^{iPr}**, the reactions would invariably be incomplete with the cogeneration of partially protonated bimca^{iPr} products (*cf.* **5^{iPr}**, **6^{iPr}** Chapter 2) in *ca*. 20 % relative combined ratio to the major product, [Al(bimca^{iPr})I$_2$], **11^{iPr}**, as determined by ^{1}H NMR spectroscopy on the vacuum dried reaction mother liquor. This is perhaps due to the lower stability of K**7^{iPr}** relative to Li**7^{iPr}** (*vide supra* Chapter 2, Section 2.3.4). Indeed reactions that generated **11^{iPr}** *via* salt metathesis with Li**7^{iPr}** produced far fewer protic impurities (*ca*. 10%, see later). Thus, solution state and bulk solid characterisation of **11^{iPr}** was conducted with samples acquired from reactions of AlI_3 with Li**7^{iPr}**, while crystalline material suitable for single crystal X-ray diffraction structure determination proved most forthcoming from a reaction using K**7^{iPr}** (Figure 3.3).

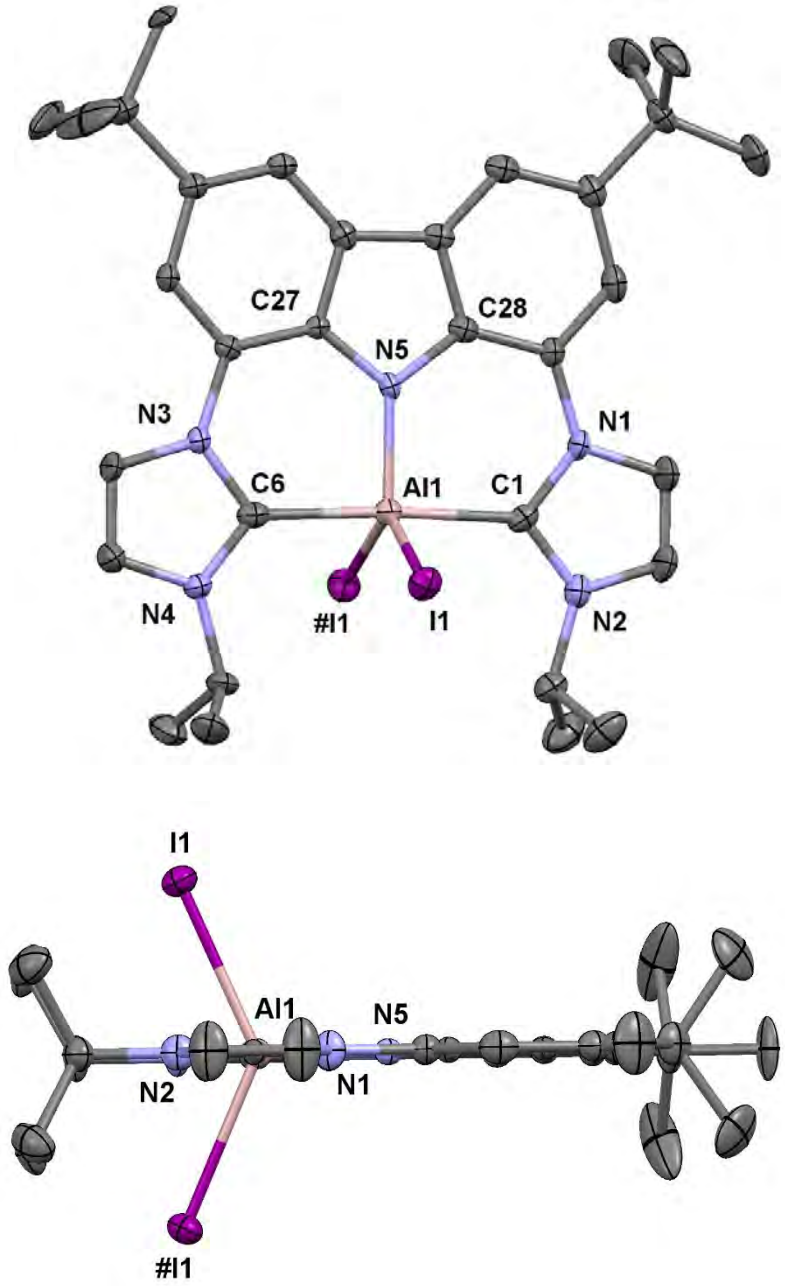

Figure 3.3 Molecular structure of [Al(bimca^{iPr})I$_2$], **11^{iPr}**. Atoms are shown with anisotropic atomic displacement parameters at 50% probability. Hydrogen atoms and disordered *tert*-butyl group omitted for clarity. Selected bond lengths (Å): Al1-C1: 2.053(5); Al1-C6: 2.046(5), Al1-I1: 2.6866(6), Al1-N5: 1.851(4); and angles (°): N1-C1-N2: 104.4(4), N3-C6-N4: 104.3(4), C27-N5-C28: 104.8(4), I1-Al1-N5: 113.48(3), I1-Al1-#I1: 133.00(5), C1-Al1-C6: 176.10(19), average NHC-carbazolide dihedral angle 0.000. Symmetry operations to generate '#' atoms: *x*, ½-*y*, *z*.

Recrystallisation of **11^{iPr}** from a room temperature saturated fluorobenzene solution that was cooled to 4 °C afforded large hexagonal plates of **11^{iPr}**. The complex crystallises in the orthorhombic space group *Pnma* with half a molecule of **11^{iPr}** and half a molecule of fluorobenzene present in the asymmetric unit. All non-symmetry generated atoms were found experimentally and refined with anisotropic- or isotropic displacement parameters (non-hydrogen atoms and hydrogen atoms respectively) except for the methyl hydrogen atoms of a rotationally disordered *tert*-butyl group. Placement of hydrogen atoms on these methyl groups did not yield satisfactory refinement metrics thus they were excluded from the final refinement. Each molecule in the asymmetric unit is bisected by a mirror plane that lies in the carbazolide heterocycle plane and serves to generate the #I1 and half of each *N*-*i*Pr group.

The crystal structure of **11^{iPr}** (Figure 3.3) confirms the successful bimca^{iPr} ligand transfer from the potassium reagent K**7^{iPr}** to give the expected meridional tridentate bound bimca^{iPr} pincer, making it one of few structurally characterised Al(III) poly(NHC) complexes,[75,66,127] The Al-C bond lengths are statistically identical (C1-Al1: 2.053(5) Å; C7-Al1: 2.046(5) Å) and expectedly short compared to those of the aforementioned heavier group 13 bimca^{Me} analogues prepared during our preliminary studies (*vide infra*, Section 3.6, Table 3.2), but are nonetheless consistent with those of other reported bis(NHC) aluminium complexes shown in Figure 3.4 (average C-Al: 2.081 Å[66] and C-Al: 1.999 Å[127]).

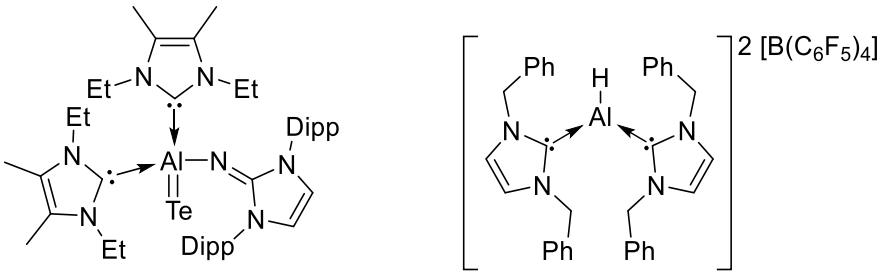

Inoue *et al.* **Stephan** *et al.*

Figure 3.4 Bis(NHC)aluminium complexes reported by Inoue *et al*.[66] and Stephan *et al*.[127]

The Al-I bond lengths in **11^{iPr}** (2.6866(6) Å) are longer than those of the four coordinate AlI_3 adducts with the ubiquitous NHCs IDipp (2.5273(10) Å) and IMes NHC (2.5238(5) Å)[128] but are extended relative to those of comparable pentacoordinate AlI_3 fragments stabilised by two apical Lewis base donors in a trigonal bipyramidal coordination geometry, *e.g.* PEt_3 in $[AlI_3(PEt_3)_2]$ (2.618(3) Å).[71] Unlike the distorted tetrahedral bis(NHC) aluminium complex reported by Inoue and co-workers (Figure 3.4 above),[66] the Al(III) metal centre of **11^{iPr}** is forced to adopt a highly symmetrical pentacoordinate trigonal bipyramidal geometry by virtue of the donor configuration of the bimca^{iPr} ligand. This distortionless geometry about the metal centre is uncharacteristic of other reported bimca^{R} complexes of larger metals, in which a non-zero torsion angle between the planes of the five membered NHC heterocycles and the six membered carbazolide phenyl moieties is observed due to the size mismatch of the tridentate donor site and the metal ionic radius (*vide infra*).[56,83,84] In **11^{iPr}**, the Al(III) metal centre experiences no such buckling out of the binding cavity and the dihedral angle between the respective five- and six-membered NHC heterocycle and carbazolide phenyl planes is 0.000° indicating that the Al(III) metal centre is exactly accommodated by the ligand binding cavity.

The ^{1}H NMR spectrum of the bulk material from the salt metathesis of AlI_3 with Li**7**$^{\mathbf{iPr}}$ verifies that **11**$^{\mathbf{iPr}}$ is the major product, although the presence of unidentified protic bimca^{iPr} co-products in *ca.* 10% combined ratio relative to the signal integrals of **11**$^{\mathbf{iPr}}$ by ^{1}H NMR spectroscopy, is also apparent. To the best of our efforts these co-products could not be reliably separated and proved to be a feature of the facility by which bimca^{R} anions protonate despite efforts to meticulously exclude air and moisture and purify metal precursors for a number of entry paths to compounds like **11**$^{\mathbf{iPr}}$. Consequently, non-conforming microanalysis results for **11**$^{\mathbf{iPr}}$ could not be avoided (see Experimental section of this chapter).

The high symmetry of complex **11**$^{\mathbf{iPr}}$ in the solid state is also apparent in solution, as indicated by the A:B:B:A shift and integration pattern for the aryl region of its ^{1}H NMR (THF-d_8) spectrum, which is typical of the [M(bimca^{R})X$_n$] complexes isolated during our previous study.[83] This signal pattern is deduced from ^{1}H-^{1}H NOESY and TOCSY NMR experiments and thus distinguish the signals produced by **11**$^{\mathbf{iPr}}$ from the observed protic co-products. The NHC C4 and C5 protons (A) and carbazolide aryl protons (B) produce doublets with signal integrals of 2 relative to the methine septet of the *N*-*i*Pr protons at 5.75 ppm. A ^{1}H-^{13}C HMBC (THF-d_8) correlation experiment places the carbenic resonance of the two symmetrical bimca^{iPr} NHC moieties at 173.86 ppm, with correlations to the C4, C5 and *N*-*i*Pr imidazolyl signals at 7.64, 8.63, and 5.75 ppm respectively. The upfield shift of the single carbenic resonance in **11**$^{\mathbf{iPr}}$ relative to that of the Li**7**$^{\mathbf{iPr}}$ starting material (203.66 ppm in THF-d_8) supports symmetrical bis(NHC) coordination and is consistent with the previously reported carbenic resonance shifts of *e.g.* [AlI_3(IMes)][129] and [AlI_3(I*t*Bu)][130] (178.2 and 174.3 ppm in C_6D_6, respectively).

3.3.1 Attempted protolytic metallation paths to access ***11^{iPr}***

In an effort to gain cleaner access to **11^{iPr}**, a synthetic strategy that utilised preinstalled basic ligands (*cf*. Scheme 3.2 path iii) was employed. This comprised use of the basic metallic precursors $Al(CH_3)_3$ and $[Al(HMDS)_3]$. Given our previous success with group 1 and 2 hexamethyldisilazides (HMDS), (*viz*. **4^{R}** and **5^{R}**, Chapter 2, Sections 2.3.1 and 2.3.2), it was conjectured that $[Al(HMDS)_3]$ would present similar reactivity, whilst also being able to yield the desired aluminium diiodide **11^{iPr}** in a single step using **4^{iPr}** without the need for *s*-block bimca^{R} intermediates. However, when the reaction was carried out using one equivalent of $[Al(HMDS)_3]$ no measurable product formation could be determined by ^{1}H NMR spectroscopy, even after prolonged periods at reflux (up to two days). Similarly, when $Al(CH_3)_3$ was used under the same conditions only the Hbimca^{iPr}(2HI) starting material was recovered. We attribute the decrease in reactivity of the aluminium amide compared with lithium or potassium HMDS reagents, to the greater covalency of the Al-N bonds, relative to the more charge-separated and reactive alkali metal HMDS.[103]

3.4 Synthesis of [Ga(bimca^{iPr})I$_2$], ***12^{iPr}***

In a similar fashion to the above, when the preparation of [Ga(bimca^{iPr})I$_2$], **12^{iPr}**, was attempted using $[Ga(HMDS)_3]$, this reagent was found to be insufficiently reactive to deprotonate the carbazole NH and imidazolium C2-H protons of **4^{iPr}**, as verified by ^{1}H NMR spectroscopy, and thereby mirroring the outcomes of previous attempts with AlR_3 (R = CH_3, HMDS) (Scheme 3.3).

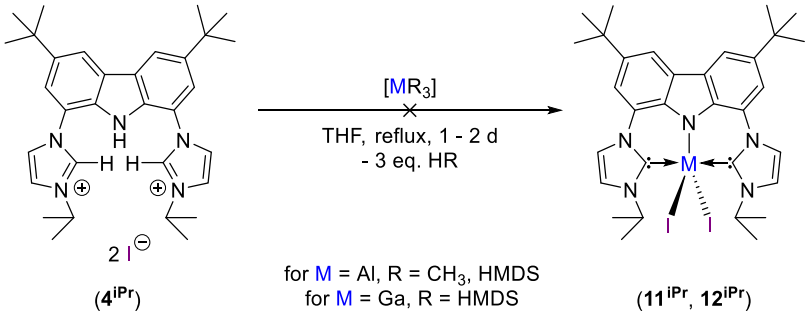

Scheme 3.3 Protolytic metallation route to [M(bimca^{iPr})I$_2$], M = Al or Ga, attempted herein.

3.4.1 Salt metathesis routes to [Ga(bimca^{R})I$_2$] using GaI$_3$

Following from the above, our efforts to isolate the gallium(III) bimca^{iPr} congener turned to the use of GaI$_3$ as a metal precursor for complexation through a salt metathesis strategy. When a THF solution of freshly prepared K**7^{iPr}** was added to a THF solution of one equivalent of GaI$_3$, the reaction returned a mixture of products by ^{1}H NMR spectroscopy (of the filtered and vacuum dried reaction mother liquor), that were comparable to the reaction that generated **11^{iPr}** using K**7^{iPr}** (*vide supra*), albeit with [Ga(bimca^{iPr})I$_2$], **12^{iPr}**, as the major product with a characteristic A:B:B:A ^{1}H NMR aryl region shift and integration pattern (THF-*d*$_8$), and minimal downfield shifting relative to the corresponding ^{1}H NMR signals of the lighter Al(III) congener, **11^{iPr}**. Likewise, the ^{1}H NMR spectrum of crude **12^{iPr}** is also blighted by the presence of protic bimca^{iPr} species in *ca*. 10% yield. These protic impurities proved hard to separate from the desired complex **12^{iPr}** and frustrated its crystallographic characterisation.

*3.4.2 Synthesis of [Ga(bimca^{Me})I$_2$], **12^{Me}**, by salt metathesis*

At a later stage in this PhD project, the magnesium iodide bimca^{Me} transfer agent (see Chapter 2, Section 2.5.2) came forth as an alternative transfer agent for bimca^{Me}. Thus salt metathesis was attempted with **9^{Me}** and GaI$_3$ to address the formation of protic

co-products experienced during the preparations of **11**^{iPr} and **12**^{iPr} using Li- and K**7**^{iPr}. This approach promised to furnish the desired gallium diiodide with fewer impurities, given the previously discussed superior stability of [Mg(bimca^{Me})I(THF)] (**9**^{Me}) compared to its potassium congener 7**K**^{Me}. Thus, the reaction of a beige THF solution of freshly prepared **9**^{Me} was added to a THF solution of GaI_3 at room temperature and stirred for 18 hours, affording a cloudy, colourless suspension. Filtration followed by removal of volatiles *in vacuo* and extraction of the resultant off-white, microcrystalline solid, **12**^{Me}, into 1,4-dioxane and storage of the filtrate at room temperature afforded crystals of **12**^{Me} suitable for single crystal X-ray diffraction structural analysis (Figure 3.5).

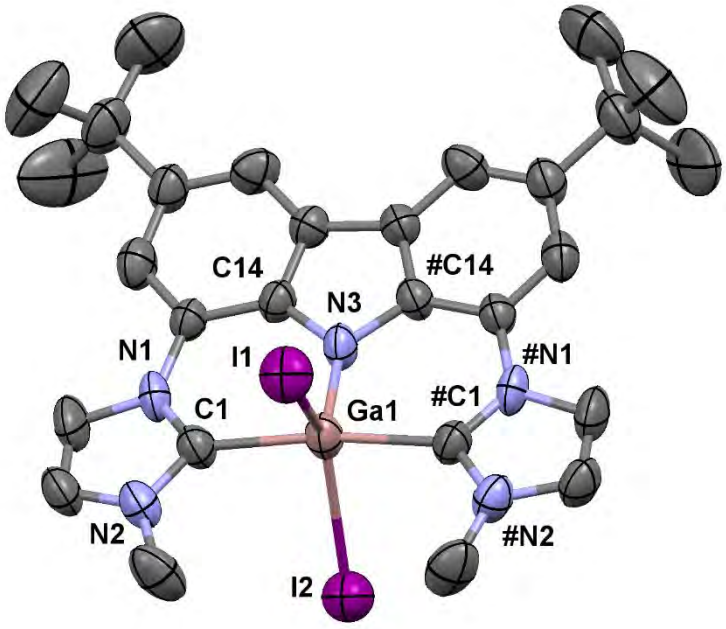

Figure 3.5 Molecular structure of [Ga(bimca^{Me})I_2], **12**^{Me}. Atoms are shown with anisotropic atomic displacement parameters at 50% probability. Selected bond lengths (Å): Ga1-C1: 2.044(5), Ga1-N3: 1.871(5), Ga1-I1: 2.7406(10), Ga1-I2: 2.8988(11), and angles (°) N1-C1-N2: 106.6(4), C14-N3-#C14: 104.7(5), I1-Ga1-I2: 141.09(3), I1-Ga1-N3: 111.43(17), I2-Ga1-N3: 107.48(17), C1-Ga1-#C1: 172.7(3), average NHC-carbazolide dihedral angle: 11.25°.

Complex **12^{Me}** crystallises in the monoclinic space group *C*2/*m* with half a molecule of **12^{Me}** and two and a half heavily disordered 1,4-dioxane molecules present in the asymmetric unit. The complex is bisected by a mirror plane that lies in the I1,Ga1,I2 plane. The heavily disordered lattice 1,4-dioxane molecules proved impossible to model with acceptable thermal parameters and were masked (OLEX 2) from the final refinement. Complex **12^{Me}** is an extremely rare example of an NHC supported pentacoordinate gallium(III), the only other report of such a complex being the related [Ga(bimca^{Me})Cl$_2$] from our previous study[83] (see Table 3.2, Section 3.6, for a structural comparison of the group 13 bimca^{R} complexes of our previous study and those presented herein). The gallium diiodide complex **12^{Me}** is thus the first structurally characterised bis(NHC) supported gallium diiodide and bears structural similarities to other pincer supported GaI$_2$ moieties, *e.g.* the neutral diiminopyridine (dimpy) systems reported by Jones and later by Richeson.[131,132] These complexes also feature distorted trigonal bipyramidal geometries around the gallium centre, enforced by the meridional binding modes of the pincers, which effect smaller I-Ga-I angles of 117.37(4)° [131] and 119.4(1)° [132] in comparison to **12^{Me}** (141.09(3)°) and average Ga-I distances of 2.5267 Å and 2.525 Å, respectively, which are very small relative to those of **12^{Me}** (average Ga-I: 2.8197 Å).

We reason that the distinct coordination geometry at gallium in **12^{Me}** is due to the combination of the steric requirements of the iodide co-ligands and the surrounding bimca^{Me} scaffold, the "soft" donicity of the *N*-donor, and the strong σ-donating NHC moieties. This donor-acceptor relationship abates the electrophilicity of the gallium(III) centre and effects extraordinarily long Ga-I bond lengths (Ga1-I1: 2.7406(10) Å and Ga1-I2: 2.8988(11) Å), which are *ca*. 0.25 Å longer than previously reported bis-Lewis base supported five-coordinate GaI$_2$ fragments (*vide supra*) or those in related

four-coordinate mono(NHC) complexes, *e.g.* [GaI_3(IDipp)] with an average Ga-I bond length of 2.535 Å.[133]

It is worth noting that while the bonding contrasts that observed in earlier pincer complexes, the wide I-Ga-I angle and long Ga-I bonds in **12^{Me}** are consistent with Bent's rule, as evidenced by the comparison of these metrics with those of our previously isolated dichloro gallium species; [Ga(bimca^{Me})Cl_2], with Cl1-Ga1-Cl2: 122.28(3)°, N1-Ga1-Cl1: 121.09(6)°, N1-Ga-Cl2: 116.64(6)°, and average Ga-Cl bond length of 2.3472 Å (Table 3.2, *vide infra*). The gallium dichloride bimca^{Me} species clearly exhibits structural metrics that approach idealised trigonal geometry in the Cl-Ga-Cl plane, owing to the high electronegativity of the chloride co-ligands. These elicit a higher degree of *s*- and *p*-orbital hybridisation and thus trigonal bipyramidal coordination geometry at the gallium(III) metal centre compared with the corresponding iodide co-ligands of **12^{Me}** (Figure 3.6). Similar to **12^{Me}**, the Ga-Cl bond lengths of [Ga(bimca^{Me})Cl_2] are longer than those of previously reported five-coordinate Ga(III) species with two equatorial chloride ligands, as deduced from an examination of the Cambridge Structural Database (average Ga-Cl bond length: 2.19 Å).[70] This supports the above notion that Ga-X bond elongation in [Ga(bimca^{Me})X_2] species may be caused by a combination of steric buttressing of the halide co-ligands with the bimca^{Me} scaffold and electronic saturation of the Ga(III) metal centre by the strong σ-donation of the NHC moieties.

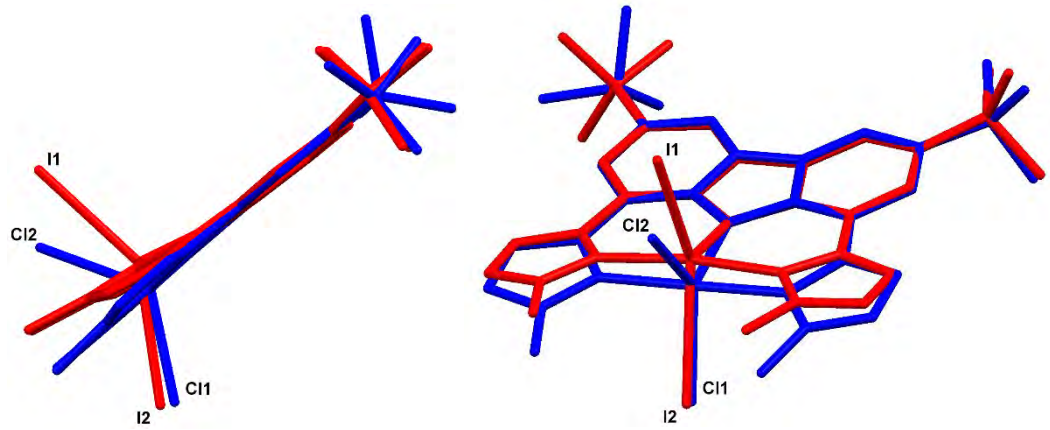

Figure 3.6 Structural overlay of **12^{Me}** (red) and [Ga(bimca^{Me})Cl$_2$] (blue) displaying out-of-plane distortion of imidazolyl moieties and wide I-Ga-I angle in **12^{Me}**

Satisfyingly, salt metathesis of GaI$_3$ with magnesium reagent **9^{Me}** also yielded a much cleaner reaction outcome than the aforementioned metathesis reactions of Li/K**7^{iPr}** with GaI$_3$, the sole bimca^{Me} containing product being **12^{Me}**. The ^{1}H and ^{13}C NMR spectra of the 1,4-dioxane solids are devoid of resonances attributable to protic co-products, as seen in the K**7^{iPr}** / MI$_3$ salt eliminations, and the expected A:B:B:A resonance and integration patterns of aryl ^{1}H NMR doublets evidence bimca^{Me} ligand transfer to the gallium metal centre. Comparison of these signals with those of the dichloro analogue, [Ga(bimca^{Me})Cl$_2$], from our previous studies indicates a slight overall upfield shift of the resonances in **12^{Me}**, consistent with the lower electronegativity of the iodide co-ligands in **12^{Me}** *versus* the chloride co-ligands of [Ga(bimca^{Me})Cl$_2$] (Table 3.1).

Assigment	[Ga(bimca^{Me})I$_2$] (**12^{Me}**) (ppm)	[Ga(bimca^{Me})Cl$_2$] (ppm)
(A) 4-NHC-*H*	7.38	7.47
(B) 2,7-Carbazole-*H*	7.82	7.89
(B) 4,5-Carbazole-*H*	8.19	8.22
(A) 5-NHC-*H*	8.28	8.35

Table 3.1 Comparison of ^{1}H NMR (THF-d_8) aryl region chemical shifts of **12^{Me}** and [Ga(bimca^{Me})Cl$_2$].[83]

Despite the clean production of **12^{Me}** through salt metathesis of **9^{Me}** with GaI$_3$, analogous attempts to generate aluminium complex [Al(bimca^{Me})I$_2$], **11^{Me}** *via* **10^{Me}** and AlI$_3$ did not proceed as cleanly; instead returning large amounts of protic by-products. This is perhaps due to the more highly Lewis acidic AlI$_3$ precursor *vis-à-vis* GaI$_3$. This starting material is known to react with ethers, such as THF, under prolonged reaction conditions.[134] Such increased acidity may also explain the problematic purification of **11^{iPr}** from AlI$_3$ metathesis reaction mixtures (*vide supra*).

3.5 Synthesis of heavy group 13 bimca^R diiodides

The anticipated favourable reactivity of the "softer" heavy group 13 tris(HMDS) precursors (*viz*. [In(HMDS)$_3$] and [Tl(HMDS)$_3$]) encouraged a convergent internal base approach (Scheme 3.2, Section 3.2) for the generation of [M(bimca^R)I$_2$], **13^R**, **14^R** (M = In, Tl; R = Me or *i*Pr).

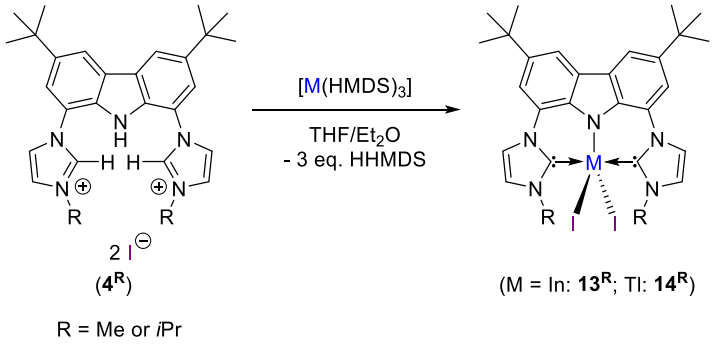

Scheme 3.4 Protolytic metallation route employed for the formation of $\mathbf{13^R}$ and $\mathbf{14^R}$.

*3.5.1 Synthesis of [In(bimca^R)I$_2$], **13^R**, from [In(HMDS)$_3$]*

[In(HMDS)$_3$] was generated *in situ* by addition of three equivalents of KHMDS to InBr$_3$ in diethyl ether at room temperature, resulting in the co-formation of KBr as a cloudy white precipitate. The colourless filtrate of this reaction was added directly to a THF suspension of either $\mathbf{4^{Me}}$ or $\mathbf{4^{iPr}}$, immediately affording a yellow suspension (*cf*. single deprotonation of $\mathbf{4^R}$ to form $\mathbf{5^R}$) that contrasts the observations made for the lighter group 13 congeners when reacting [M(HMDS)$_3$] (M = Al, Ga) reagents with $\mathbf{4^R}$ proligands (*vide supra*) wherein no measurable reaction took place. The reaction mixtures were stirred at room temperature for 18 hours, during which they gradually paled, cleared and lost their yellow fluorescence under long wave UV light. The latter is indicative of proligand consumption and heavy metal coordination. Subsequent filtration and removal of volatiles from the filtrate afforded analytically pure samples of [In(bimca^{iPr})I$_2$], $\mathbf{13^{iPr}}$, and [In(bimca^{Me})I$_2$, $\mathbf{13^{Me}}$ as pale yellow solids (Scheme 3.4).

The ^{1}H and ^{13}C NMR spectra of these complexes are remarkably clean and devoid of protic co-products, *cf*. $\mathbf{11^{iPr}}$ and $\mathbf{12^{iPr}}$, exhibiting characteristic A:B:B:A ^{1}H NMR aryl chemical shift and integration patterns similar to those observed for the lighter congeners of the series ($\mathbf{11^{iPr}}$, $\mathbf{12^{iPr}}$ and $\mathbf{12^{Me}}$), thereby evidencing the symmetrical composition of the $\mathbf{13^R}$ complexes in solution.

Despite our best efforts, crystallographic studies of the *N*-methyl variant **13^{Me}** proved fruitless after multiple attempts to grow crystals from different solvent systems. However, the *N*-isopropyl analogue was found to be more forthcoming and single crystals suitable for X-ray diffraction structure determination, were grown from a room temperature saturated fluorobenzene solution placed at 4 °C (Figure 3.7).

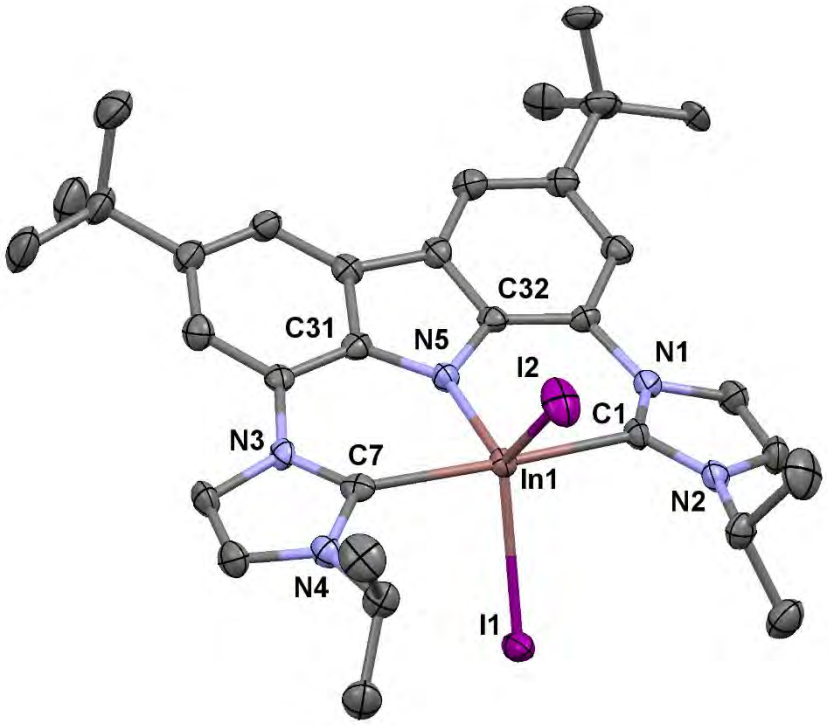

Figure 3.7 Molecular structure of [In(bimca^{iPr})I_2], **13^{iPr}**. Atoms are shown with anisotropic atomic displacement parameters at 50% probability and hydrogen atoms are omitted for clarity. Selected bond lengths (Å): C1-In1: 2.282(5), C7-In1: 2.267(5), N5-In1: 2.143(4), In1-I1: 2.8387(5), In1-I2: 2.7946(5), and angles (°) N1-C1-N2: 105.5(4), N3-C7-N4: 104.6(4), C31-N5-C32: 104.6(4), I1-In1-I2: 121.579(17), I1-In1-N5: 114.01(11), I2-In1-N5: 124.41(11), C1-In1-C7: 168.19(17), average NHC-carbazolide dihedral angle: 20.00°.

Complex **13^{iPr}** crystallises in the monoclinic space group $P2_1/n$ with one molecule of **13^{iPr}** and two molecules of fluorobenzene in the asymmetric unit. All non-hydrogen atoms were refined with anisotropic displacement parameters, whilst all hydrogen atoms, excepting those of the *tert*-butyl groups and the 4,5-imidazolyl protons (riding model), were located from difference maps and refined isotropically.

The solid state structure of **13^{iPr}** expectedly exhibits a rare bis(NHC) supported pentacoordinate trigonal bipyramidal indium(III) that features the bimca^{iPr} ligand in a tridentate meridional binding mode accompanied by two iodide co-ligands. Complex **13^{iPr}** is structurally similar to its Al(III) (**11^{iPr}**) and Ga(III) (**12^{Me}**) congeners, but exhibits increased buckling of the metal cation out of the carbazolide plane due to its increased size *vis-à-vis* Al and Ga, leading to greater distortions of the bimca^{iPr} scaffold away from the coplanar ligand observed in **11^{iPr}**. For example, a slight distortion of the bipyramidal geometry around the metal centre is observed due to an interplay of (i) the longer M-C bonds (average In-C: 2.275 Å *vs.* average Al-C: 2.050 Å in **11^{iPr}** *vs.* Ga-C: 2.044(5) Å in **12^{Me}**), (ii) the steric requirements of the pincer cavity, and (iii) the ionic radius of the In(III) metal centre. In combination, these serve to subtend an average dihedral angle of 20.00° between the five membered NHC rings and the carbazolide phenyl rings (*cf.* **11^{iPr}** dihedral angles: 0.000°; **12^{Me}** dihedral angle: 11.25°). Complex **13^{iPr}** is the first structurally characterised NHC supported indium diiodide and exhibits long In-I contacts (2.8387(5) Å) compared to other Lewis base stabilised In-I fragments, *e.g.* 2.7761(13) Å in [$InI_3(PPh_2Me)_2$]. This continues the trend observed for **11^{iPr}** and **12^{Me}**.[72] Despite this, **13^{iPr}** shows exceptional thermal stability with a decomposition point of 326-327 °C, considerably higher than that of the bis(phosphine) adduct, [$InI_3(PPh_2Me)_2$], (141 °C)[72] and similar to those of the lighter group 13 relatives **11^{iPr}** (331-332 °C) and **12^{iPr}** (306-307 °C). Unlike **12^{Me}**, **13^{iPr}** exhibits a more acute I-In-I angle (121.579(17)°) that is

consistent with the more optimal "soft" donor/acceptor pairing of In(III) with iodide in **13^{iPr}**, *vis-à-vis* Ga(III) with iodide in **12^{Me}**. Additionally, the increased ionic radius of In(III) may be expected to better alleviate likely steric buttressing of the iodide co-ligands with the surrounding bimca^{Me} scaffold compared with Ga(III) in **12^{Me}**.

*3.5.2 Unexpected halide scrambling on **13^{R}***

Noteworthy halide exchange reactions, akin to those observed in [Tl(bimca^{Me})ClI] in our previous study (Section 3.1), were observed by ^{1}H and ^{13}C NMR spectroscopy during preparations of **13^{R}** complexes for which the [In(HMDS)$_3$] precursor was generated *in situ* from three equivalents of KHMDS in THF instead of diethyl ether (*cf.* increased solubility of KBr in THF). Upon reaction of [In(HMDS)$_3$] in THF with either **4^{Me}** or **4^{iPr}** proligands the subsequent formation of the mixed halides [In(bimca^{R})Br$_2$] (**13^{R}**Br$_2$), [In(bimca^{R})BrI] (**13^{R}**BrI**)**, and [In(bimca^{iPr})I$_2$ (**13^{R}**) was observed, as evidenced by the closely separated chemical shift patterns of each complex for both the methyl- and isopropyl analogues. Indeed, the ratio of these species is 1:2:1 by relative ^{1}H NMR resonance signal integrals. The nature of this heterohalide substitution is most evident in the NMR spectra of the *N*-isopropyl species **13^{iPr}**, for which a combination of one-dimensional ^{1}H, and two-dimensional ^{1}H-^{1}H NOESY and COSY NMR experiments was used to distinguish these mixed halides. The isopropyl methyl ^{1}H NMR doublets appear as a series of four overlapping signals between 1.63 ppm and 1.71 ppm in a 1:1:1:1 signal integral ratio, where the two outer sets of doublets correspond to quarter equivalents of both **13^{iPr}**Br$_2$ and **13^{iPr}** and the remaining signals stem from half an equivalent of the mixed halide **13^{iPr}**BrI; the latter of which exhibiting two pairs of chemically inequivalent isopropyl methyl environments resulting from their proximity of these substituents to either a bromide or iodide co-ligand (Figure 3.8).

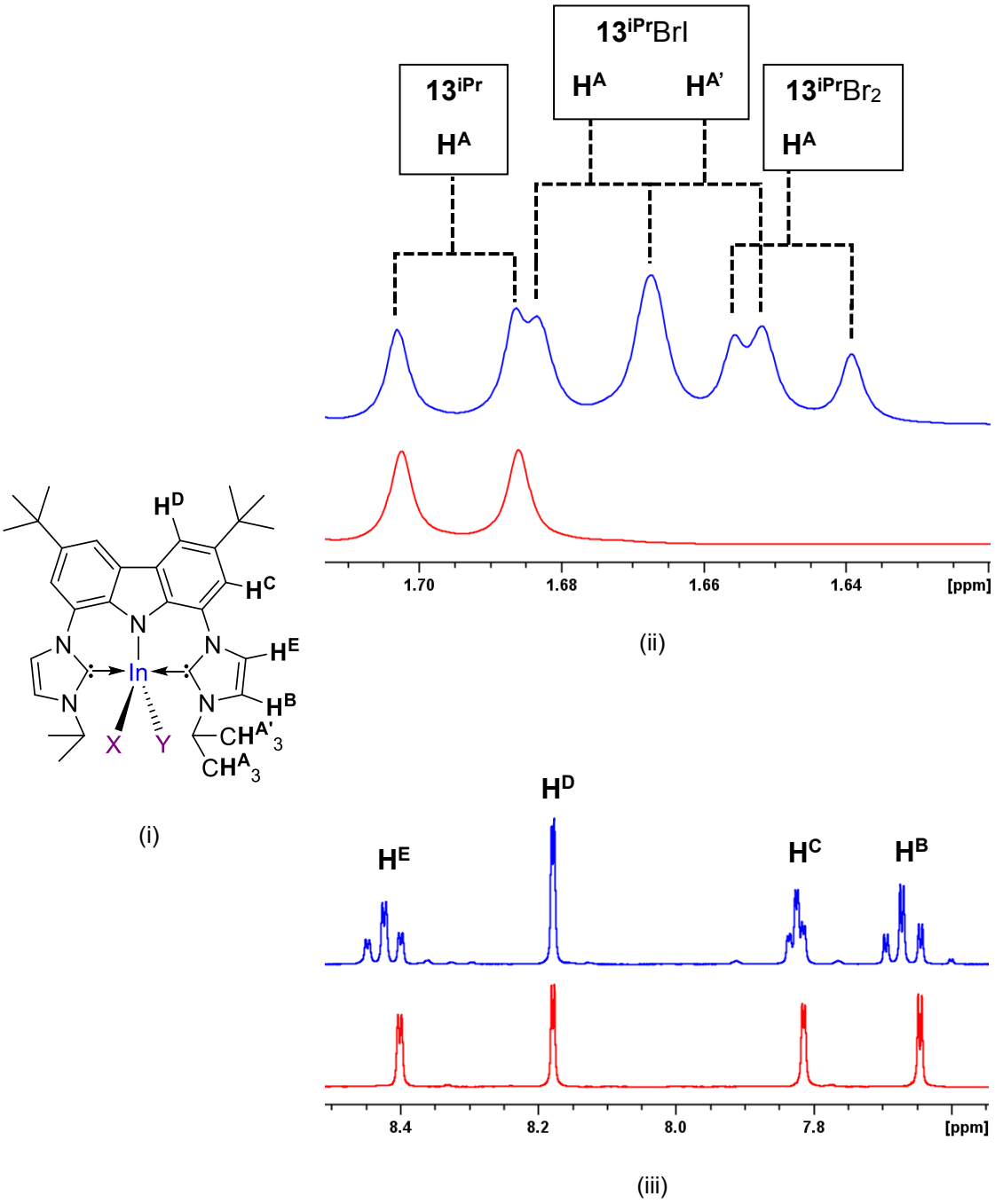

Figure 3.8 (i) Key to proton assignments in figure, and excerpts of the ^{1}H NMR spectra of pure **13^{iPr}** (red) and halide scrambling products **13^{iPr}**XY (X, Y = Br, I) (blue) from (ii) the alkyl chemical shift region, and (iii) the aryl chemical shift region

This outcome is due to contamination of the *in situ* prepared [In(HMDS)$_3$] precursor with at least one equivalent of dissolved KBr from the preceding step, which subsequently undergoes halide exchange reactions with the nascent [In(bimca^{R})I$_2$]. The halide

exchange reaction was easily suppressed by producing the In(III) amide in diethyl ether, in which KBr is sparingly soluble and easily removed by filtration. This modified preparation consistently provided pure samples of each **13^{R}** complex in near quantitative yield.

*3.5.3 Synthesis of [Tl(bimca^{R})I$_2$], **14^{R}**, from [Tl(HMDS)$_3$]*

The synthesis of the heaviest congeners; [Tl(bimca^{R})I$_2$], **14^{R}** was approached in a similar manner to **13^{R}**, *i.e.* through *in situ* protolysis of **4^{R}** with [Tl(HMDS)$_3$]. The tris(amido)thallane was isolated and recrystallised prior to reaction due to the considerable additional difficulties posed by the generation of Tl(III) amide precursors through stoichiometric *in situ* preparations using commercially available TlCl$_3$ sources (see general methods). Indeed, the composition of commercial sources of TlCl$_3$·4H$_2$O are highly unreliable owing to the hygroscopic nature of TlCl$_3$ and the instability of Tl(III) *vis-à-vis* Tl(I) at temperatures close to room temperature.[§] Thus, an excess of [Tl(HMDS)$_3$] was synthesised and isolated prior to its reaction with either **4^{Me}** or **4^{iPr}**.

A pale amber THF solution of freshly recrystallised [Tl(HMDS)$_3$] was added to a colourless THF suspension of either **4^{Me}** or **4^{iPr}** at room temperature, affording yellow reaction mixtures (*cf.* analogous reaction with [In(HMDS)$_3$] *vide supra*). The stirred reaction mixtures gradually cleared and turned bright orange over the course of 18 hours, whereupon filtration and removal of volatiles *in vacuo* afforded analytically pure **14^{Me}** and **14^{iPr}** as bright orange powders. Recrystallisation of **14^{Me}** from a room temperature saturated THF solution placed at 4 °C yielded large orange rectangular plates suitable for single crystal X-ray diffraction structure determination (Figure 3.9), **14^{iPr}** was recrystallised similarly using fluorobenzene instead of THF (Figure 3.10).

[§] TlCl$_3$ typically exists in an equilibrium with TlCl and Cl$_2$ at room temperature

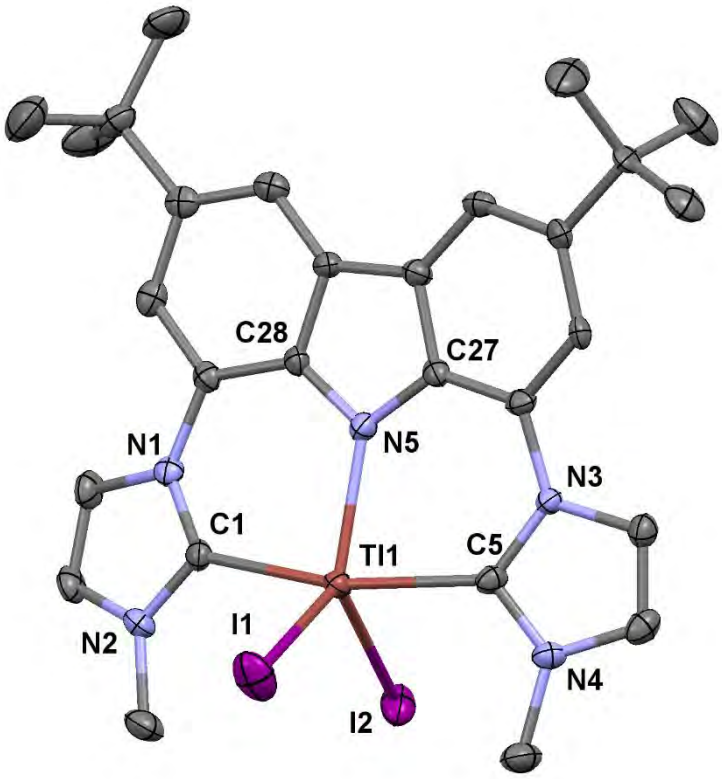

Figure 3.9 Molecular structure of **14^{Me}**. Atoms are shown with anisotropic atomic displacement parameters at 50% probability and hydrogen atoms are omitted for clarity. Selected bond lengths (Å): Tl1-C1: 2.252(4), Tl1-C5: 2.256(5), Tl1-N5: 2.254(4), Tl1-I1: 2.8699(4), Tl1-I2: 2.9554(5), and angles (°) N1-C1-N2: 106.2(4), N3-C5-N4: 105.5(4), C27-N5-C28:105.5(4), I1-Tl1-I2: 118.637(12), I1-Tl1-N5: 129.41(10), I2-Tl1-N5: 111.94(10), C1-Tl1-C5: 164.03(16), average NHC-carbazolide dihedral angle: 18.19°.

Thallium complex **14^{Me}** crystallises in the triclinic space group $P\bar{1}$ with one molecule of **14^{Me}** and two molecules of THF in the asymmetric unit. All non-hydrogen atoms were refined with anisotropic displacement parameters and hydrogen atoms were placed in calculated positions (riding model) and refined isotropically. The geometry of complex **14^{Me}** is similar to its closely related bimca^{iPr} derivative, **14^{iPr}**, (Figure 3.10) and their bonding metrics are discussed in tandem below.

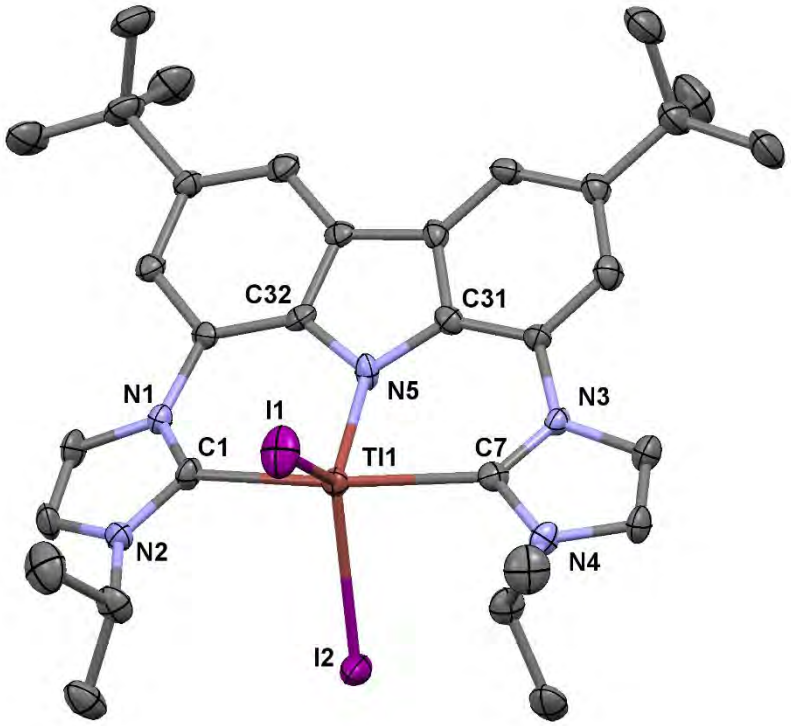

Figure 3.10 Molecular structure of [Tl(bimca^{iPr})I_2], **14^{iPr}**. Atoms are shown with anisotropic atomic displacement parameters at 50% probability and hydrogen atoms are omitted for clarity. Selected bond lengths (Å): Tl1-C1: 2.278(8), Tl1-C7: 2.277(8), Tl1-N5: 2.241(6), Tl1-I1: 2.8620(7), Tl1-I2: 2.9214(6), and angles (°) N1-C1-N2: 105.2(7), N3-C7-N4: 105.1(7), C31-N5-C32: 104.8(6), I1-Tl1-I2: 122.10(2), I1-Tl1-N5: 126.50(18), I2-Tl1-N5: 111.41(18), C1-Tl1-C7: 164.5(3), average NHC-carbazolide dihedral angle: 21.29°.

Complex **14^{iPr}** is isostructural to the indium congener **13^{iPr}** and likewise crystallises in the monoclinic space group $P2_1/n$ with a complete molecule of **14^{iPr}** and two molecules of fluorobenzene in the asymmetric unit. The atomic positions of non-hydrogen atoms were refined with anisotropic displacement parameters whilst all hydrogen atoms were placed in calculated positions (riding model) and refined isotropically.

Thallium diiodide **14^{iPr}** and the aforementioned **14^{Me}** both exhibit meridionaloid coordination of the bimca^{R} ligands to the Tl(III) metal centre with two iodide co-ligands in equatorial sites of a trigonal bipyramidal coordination geometry, as per the lighter structurally characterised group 13 diiodides of the series. Unsurprisingly, **14^{Me}** and **14^{iPr}** display the longest M-I bonds of this series at 2.9554(5) Å (Tl1-I2 in **14^{Me}**) and 2.9214(6) Å (Tl1-I2 in **14^{iPr}**). Despite this, **14^{Me}** and **14^{iPr}** exhibit exceptional thermal stability (*cf.* reductive instability of thallium trihalides with respect to thallium reduction, *vide supra*). The decomposition points of both complexes lie within 227-229 °C, some 70 °C higher than the decomposition temperatures of other reported Lewis base stabilised Tl(III) di- and triiodide species, *e.g.* [$TlI_2Br(OPPh_3)_2$] (dec. 156 °C).[135] We attribute this remarkable stability to the ideal donor-acceptor relationship between the Tl(III) metal centre and the two flanking NHC moieties, which electronically stabilise the iodide co-ligands and subdue the otherwise thermodynamically favourable reductive elimination of I_2 or ionic redistribution (*i.e.* $Tl^{(III)}LI_2 \rightarrow Tl^{(I)}L + I_2$ or $2\ Tl^{(III)}LI_2 \rightarrow [Tl^{(III)}L_2][Tl^{(III)}I_4]$)[1]

Expectedly, the dihedral angle between the NHC five-membered heterocycle and the plane of the attached carbazolide "phenyl" moiety is most pronounced in the *N*-isopropyl species **14^{iPr}** (dihedral angle: 21.29°, with the analogous angle of **14^{Me}** (18.19°) being comparable to that of **13^{iPr}**; 20.00°). This is due to the relatively large Tl(III) ionic radius (88.5 pm, *vs.* In: 80.0 pm).[108]

Both **14^{Me}** and **14^{iPr}** exhibit ^{1}H and ^{13}C NMR (THF-d_8) spectra that evidence a high degree of coordination symmetry in solution, as deduced from the characteristic A:B:B:A chemical shift and signal integral patterns discussed previously for the other solution state symmetrical bimca^{R} complexes. The most striking feature of these spectra, though, is the strong ^{4}J and ^{5}J Tl-H and Tl-C coupling interactions with the 4,5-imidazolyl positions

and the *N*-alkyl substituents; ranging from 93.4 Hz to 29.9 Hz respectively, in the ^{1}H NMR spectra and 175.5 Hz to 109.3 Hz, for the ^{13}C NMR signals corresponding to these same positions. These coupling constants serve to confirm the solution state coordination of the thallium metal centre to the NHC donors in the bimca^{R} binding cavity and are consistent with those previously reported for thallium to ^{1}H and ^{13}C coupling constants in Tl(IIII)-NHC complexes.[83,136]

3.6 Comparison of diiodo group 13 bimca^{R} complexes of this work with our previous studies

The isolation and structural characterisation of the new diiodide complexes, **11^{iPr}**, **12^{Me}**, **13^{iPr}**, **14^{Me}**, and **14^{iPr}** permits their structural comparison with the dihalide bimca^{Me} analogues of our previous studies, [Ga(bimca^{Me}Cl$_2$], [In(bimca^{Me})Br$_2$], and [Tl(bimca^{Me})ClX] (X = I or Cl). [83] The most salient of these metrics are summarised in Table 3.2.

	[Al(L^{iPr})I_2] (11^{iPr})	[Ga(L^{Me})I_2] (12^{Me})	[Ga(L^{Me})Cl_2]	[In(L^{iPr})I_2] (13^{iPr})	[In(L^{Me})Br_2]	[Tl(L^{iPr})I_2] (14^{iPr})	[Tl(L^{Me})I_2] (14^{Me})	[Tl(L^{Me})ClY]
Mp [a] **(°C)**	332	298	> 300	327	> 300	228	228	> 300
Ionic radius (pm) [b]	53.5	62.0	62.0	80.0	80.0	88.5	88.5	88.5
Avg. M-C (Å)	2.050	2.044(5)	2.076	2.275	2.235	2.260	2.254	2.102
M-X (Å)	2.6866(6) [d]	2.7406(10) 2.8988(11)	2.3347(7) 2.3597(7)	2.7946(5) 2.8387(5)	2.5974(15) 2.6105(17)	2.8620(7) 2.9214(6)	2.8699(4) 2.9554(5)	2.8509(17) [e] 2.693(5) [f] 2.826(14) [f]
M-N (Å)	1.851(4)	1.871(5)	1.931(2)	2.143(4)	2.107(8)	2.241(6)	2.254(4)	2.470(11)
Avg. N-C-N (°)	104.3	106.6(4)	104.8	105.1	105.8	105.2	105.9	100.8
X-M-X (°)	133.00(5)	141.09(3)	122.28(3)	121.579(17)	113.91(5)	122.10(2)	118.637(14)	119.06(11) [e] 84.4(3) [f]
C-M-C (°)	176.10(19)	172.7(3)	179.02(10)	168.19(17)	169.1(4)	164.5(3)	164.03(16)	166.5(5)
plane-plane torsion angle (°) [c]	0.0 0.0	11.2 11.2	2.9 4.3	19.1 20.9	2.6 9.9	20.2 22.4	15.0 21.4	10.7 11.0

Table 3.2 Comparison of structural metrics of the bimca^R group 13 dihalides series from this work and our previous study.[83] L = bimca, Y = Cl or I [a] Average value of reported range. [b] Values of effective ionic radius for six-coordinate M(III) metal ions.[108] [c] plane-plane angle of mean carbazolide phenyl (C_6) plane and mean imidazolyl (N,C,N,C,C) plane of the attached hetereocycle. [d] Al1-#I1 is generated by symmetry (*vide supra*). [e] Y = I. [f] Y = Cl.

General trends are observed with increasing atomic number of the bound group 13 metal. For example, the M-N bond lengths and the degree to which the accommodated metal centre buckles out of the plane of the carbazolide backbone, expectedly increase with respect to increasing metal ionic radius. The latter of these measures is indicated by (i) the average plane to plane torsion angle between the five-membered imidazolyl heterocycles and the respective six-membered carbazolide phenyl moieties to which they are bound, and (ii) the C-M-C bond angle. The degree of buckling in the non-iodo complexes is overall less pronounced than that in the diiodide complexes, likely due to the steric demands imposed by the iodide co-ligands.

The lighter diiodide complexes (of aluminium and gallium) show far greater departure from ideal trigonal planar geometry in the I,N,I plane, with I-M-I angles being *ca*. 13° and 21° greater than 120°, respectively, unlike their heavier congeners, which closely approximate this ideal angle despite increasing distortion away from trigonal bipyramidal elsewhere. This further illustrates the spatial imposition of the iodide co-ligands (*vs*. chloride), which frustrates their closer approach to the metal centre, and demonstrates the "hard" donor preference of the lighter metals. This is exemplified by the mitigation of the electrophilicity of the "hard" gallium(III) centre by "hard" chloride ligands (relative to iodide ligands), which results in a large difference in the X-Ga-X angle in [Ga(bimca^{Me})I$_2$] *vs.* [Ga(bimca^{Me})Cl$_2$] (141.09(3)° *vs*. 122.28(3)°). This is also reflected in the M-I bond lengths of the diiodide series, wherein the average Ga-I bond length in **12^{Me}** is comparable to the average In-I in the indium complex **13^{iPr}** (2.820 Å *vs*. 2.817 Å).

From table 3.2, particularly from a comparison of the **14^{R}** species, it may be surmised that the majority of geometrical changes observed in this series result from intrinsic

C_{NHC}-M-X interactions, *i.e.* the increased steric bulk of the *N*-isopropyl substituent seems to have little effect on the overall metrics or thermal stabilities of the complexes.

3.7 Hydride stabilisation and heavy low valent bimca^R complexes

The isolation of the bimca^R supported group 13 metal diiodides, and their exceptional thermal stability, provided encouragement for the substitution of the iodide co-ligands for "softer" hydride co-ligands by means of halide-hydride exchange to potentially access stable metallohydride bimca^R species. Indium and thallium species, **13^{iPr}** and **14^{iPr}**, were of particular interest for these transformations given the absence of reports of bis(NHC) stabilised hydrides of these metals in the literature.[76] The heavy metal hydrides of group 13 are known to undergo reductive dehydrogenation in the absence of suitably bulky or electron donating ligands (*vide supra*).[1] Thus the bimca^{iPr} diiodide scaffolds of **13^{iPr}** and **14^{iPr}** promised to provide a good starting point to pursue the stability of bis(NHC) coordinated indium and thallium hydrides. For the purpose of this preliminary study, we chose $LiHBEt_3$ as a hydride source for its solubility, ease of stoichiometric addition and manipulation, and precedent in the literature for the use of comparable hydroborate reagents used in analogous strategies to access group 13 and 14 hydrides (see Chapter 1, Section 1.3).

*3.7.1 Iodide-hydride exchange of **13^{iPr}** with two equivalents of $LiHBEt_3$*

The reaction of **13^{iPr}** with two equivalents of $LiHBEt_3$ was carried out in a sealed J. Young valved NMR tube, whereby THF-d_8 was condensed onto a solid mixture of the two reagents at -195 °C and allowed to warm to -50 °C with periodic agitation over *ca.* 15 minutes. This formed a pale yellow solution with a slight blue fluorescence under long wave UV light that, upon warming to -30 °C with agitation (over a further 15 minutes),

afforded a ^{1}H NMR spectrum consistent with the complete consumption of the starting materials, *i.e.* resonances belonging to **13^{iPr}** and LiHBEt$_3$ are completely absent with concurrent formation of a new bimca^{iPr} species. The absence of dihydrogen or evidence of a competing reduction pathway, such as NHC reduction (*vide infra*), at this temperature is consistent with successful metathesis to form a stable "In(bimca^{iPr})H$_2$" species.

The initial ^{1}H NMR (THF-d_8) spectrum of the reaction mixture at -30 °C indicates a breakdown of the characteristic symmetry of **13^{iPr}** upon formation of the new complex, most likely resulting from inequivalent chemical environments across the bimca^{iPr} ligand scaffold. This is hallmarked by eight separate resonances in the aryl (imidazolyl and carbazolide) region of the spectrum, *cf.* typical A:B:B:A pattern for equal integration doublets of **13^{iPr}**. This break in symmetry can be rationalised by the formation of an unsymmetrical [InH$_2$(μ-κ^1-κ^2-bimca'^{iPr})BEt$_3$] adduct; **15^{iPr}**·BEt$_3$, where one BEt$_3$ co-product is coordinated by an NHC moiety in the resulting unsymmetrical bimca^{iPr} complex (Scheme 3.5), *cf.* single NHC coordination of InH$_3$ in the previously reported ethylene tethered bis(NHC) dinuclear complex [(InH$_3$)$_2$(μ-κ^1-κ^2-I*t*BuC$_2$H$_4$I*t*Bu)].[76] This supposition is borne out by the ^{1}H NMR resonances, shift patterns, and signal integrals in the aliphatic region of the ^{1}H NMR spectrum, which exhibit signals consistent with free BEt$_3$ and an NHC-coordinated BEt$_3$ in a 1:1 signal integral ratio.

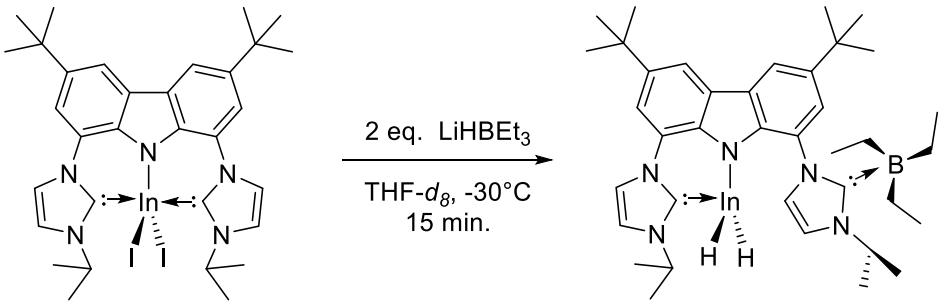

(**13^{iPr}**) (**15^{iPr}**·BEt$_3$)

Scheme 3.5 Proposed product of the halide-hydride exchange process.

Further substantiation of an NHC-borane adduct is provided by an initial ^{13}C NMR (THF-d_8) spectrum of the reaction mixture (also at -30 °C) where the absence of a carbenic NHC resonance for the NHC-borane moiety is consistent with the typically observed quadrupolar broadening caused by spin $^{3}/_{2}$ ^{11}B and spin 3 ^{10}B nuclei. These provide for rapid relaxation of the C2 carbon nucleus coordinated at boron, hindering its resolution under these conditions.[137] The second, putatively indium-bound, NHC C2 resonance is resolved at 170.45 ppm, where NHC-In(III) C2 resonances typically lie.[125] ^{1}H-^{1}H NOESY, COSY and TOCSY NMR experiments provide further insight into this borane adduct, and reveal that one of the pendant alkyl chains is in close proximity to an *N*-iPr substituent while the other two are in range of the 7-carbazolide position of the bimca^{iPr} scaffold, resulting in a NOE correlation between these ethyl groups and the methine proton signal of the *N*-iPr group and the 7-carbazolide-*H* respectively (Figure 3.11). This in turn leads to an inequivalence of the ethyl groups of the coordinated BEt_3 moiety, resulting in a signal integral ratio of 1:2 for the three pendant ethyl chains of the coordinated BEt_3 relative to the methine septet of the NOE associated *N*-*i*Pr substituent at 5.51 ppm. Moreover, the ^{13}C NMR spectrum at -30 °C is also consistent with an unsymmetrical product compared to the axially symmetrical indium diiodide **13^{iPr}** starting material.

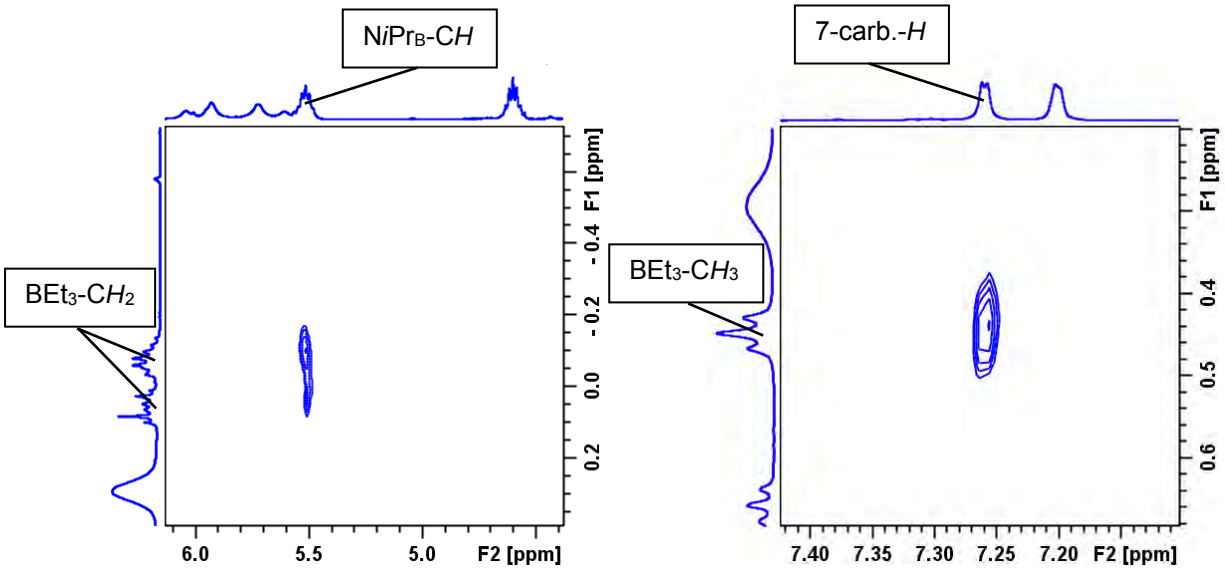

Figure 3.11 Excerpts of ^{1}H-^{1}H NOESY spectrum of **15^{iPr}**·BEt_3 displaying NOE correlations between a BEt_3 group and imidazolyl *N*-*i*Pr and 7-carbazolide-*H* on the bimca^{iPr} scaffold.

The formation of the BEt_3 adduct of **15^{iPr}** (Scheme 3.5) also leads to chemical inequivalence of the indium bound hydrides (*vide infra*), resulting in two broad doublets at 5.66 ppm and 5.99 ppm (fwhm = 16 Hz), where the geminal hydrides couple with a $^{2}J_{HH}$ coupling constant of 47 Hz. These chemical shifts are also consistent with previously reported indium(III) hydrides,[138] as is the quadrupolar broadening of these signals by the spin $^{9}/_{2}$ $^{113/115}$In nuclei, further evidencing hydride coordination to an indium metal centre in **15^{iPr}**·BEt_3.[125,138,139] The close proximity of the hydride co-ligands to each other is also evidenced by NOE correlations between ^{1}H NMR signals for the broad doublets, and the origin of the coupling is clearly substantiated by ^{1}H-^{1}H COSY and TOCSY correlations for these signals (Figure 3.12).

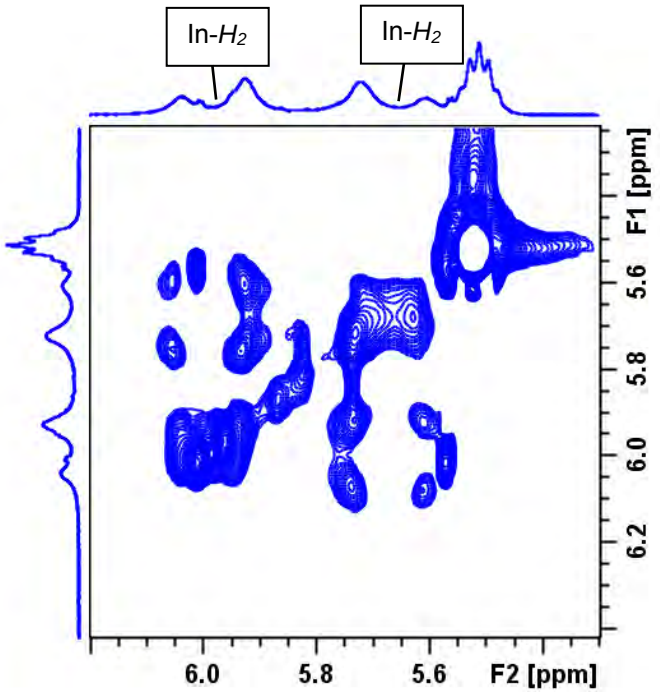

Figure 3.12 Excerpt of ^{1}H-^{1}H TOCSY spectrum of **15^{iPr}**·BEt_3 displaying coupling between signals attributed to the geminal In-H_2.

The combination of the above ^{1}H and ^{13}C NMR spectroscopic evidence allows for the tentative structural assignment of **15^{iPr}**·BEt_3 as a [InH_2(μ-κ^2-κ^1-N/C,C-bimca^{iPr})BEt_3] complex (Scheme 3.5) where the bimca^{iPr} ligand provides $N_{carb.}$,C_{NHC} chelate stabilisation of the indium dihydride moiety and coordinates to a BEt_3 through the remaining pendant NHC donor. The location and placement of the secondary NHC to BEt_3 coordination renders the hydride co-ligands diastereotopic (Figure 3.12 above).

As the reaction mixture that furnished **15^{iPr}**·BEt_3 was slowly warmed to room temperature (*ca*. 10 °C/h) the elimination of dihydrogen gas was observed (singlet at 4.55 ppm) in ^{1}H NMR spectra collected at regular intervals. This is consistent with the decomposition of **15^{iPr}**·BEt_3 *via* reductive dehydrogenation and the potential formation of an In(I) bimca^{iPr} product. ^{1}H NMR resonances for the resulting low valent In(bimca^{iPr}) intermediate could

not be resolved under these conditions, however the signal for H_2(g) was observed to gradually increase with the rise in temperature (Figure 3.13).

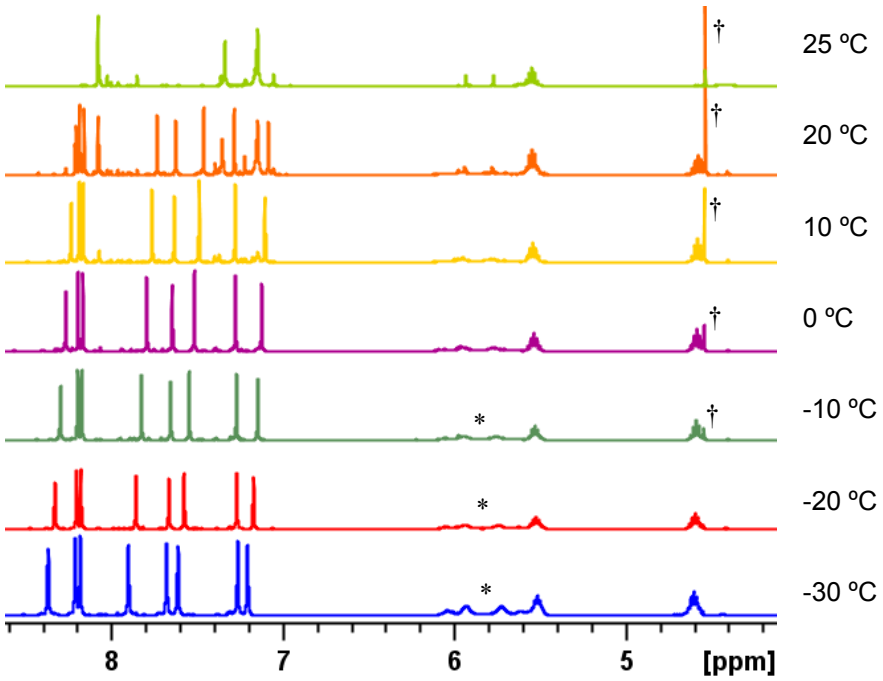

Figure 3.13 Excerpts of the v.t. ^{1}H NMR spectra of the reaction mixture containing **15**^{iPr}·BEt_3 (-30 °C; blue, to ambient temperature; light green) showing decomposition of the InH_2 moiety at 5.66 ppm and 5.99 ppm (*) and the return to a symmetrical product at room temperature with the concurrent evolution of dihydrogen gas at 4.55 ppm (†).

Concurrently, the signal strength of the triplet at 0.73 ppm corresponding to the methyl resonance of free triethyl borane (triplet at 0.73 ppm) decreases with an increase in temperature, whilst the signal integrals of the resonances attributed to the NHC coordinated borane (with a N*i*Pr-C*H* resonance at 5.52 ppm) increase proportionately to the loss of the free borane resonances (triplet at 0.46 ppm) such that the methine signal integral roughly doubles from -30 °C to 25 °C. These changes are accompanied by the gradual appearance of bimca^{iPr} scaffold resonances that are consistent with the formation of a symmetrical bimca^{iPr} decomposition product, showing close to quantitative

conversion in the ^{1}H NMR spectrum of the final room temperature stable product. The ^{1}H NMR spectrum of the final reaction mixture shows no evidence of free borane. The same room temperature THF-d_8 solution also exhibits a strong blue fluorescence under long wave UV light, which is reminiscent of the *s*-block complexes of bimca^{R}, and inconsistent with a heavy metal complex such as **13^{iPr}**, where the metal quenches fluorescence. The formation of a borane-NHC adduct is supported by the disappearance of the NHC-In carbenic resonance at 170.45 ppm in the ^{13}C NMR spectrum with no other carbenic resonance being resolved (Figure 3.14, *cf.* quadrupolar broadening by spin $^{3}/_{2}$ ^{11}B and spin 3 ^{10}B).

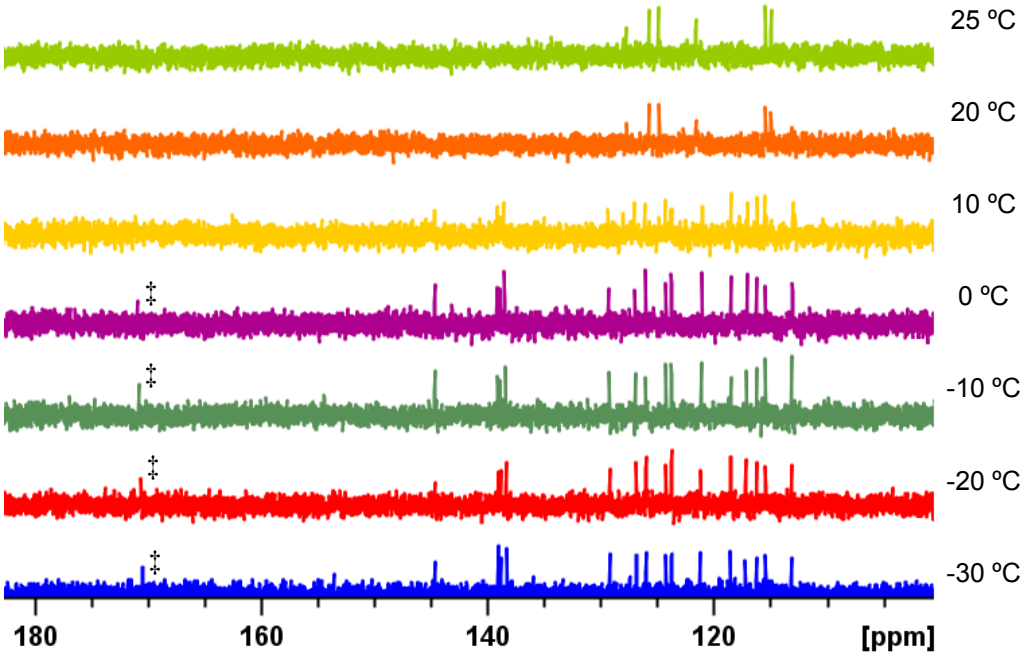

Figure 3.14 Excerpts of the v.t. ^{13}C NMR spectra of the reaction mixture containing **15^{iPr}**·BEt_3 showing the return to a symmetrical decomposition product at room temperature with the concurrent disappearance of the carbenic carbon resonance at 170.45 ppm (‡).

This resting state for the reaction mixture is indefinitely stable at room temperature, despite the presence of the remaining reaction decomposition products. These data,

especially the fluorescent nature of the decomposition product, led us to postulate that the LiI co-product from the conversion of **13^{iPr}** to **15^{iPr}**·BEt_3 reacts with a transient In(I) species (bottom right, Scheme 3.6) to form InI(s) and [Li(bimca^{iPr})·$(BEt_3)_2$], **16^{iPr}** (Scheme 3.6). Metatheses between lithium halides and low oxidation state indium species, such as the putative In(bimca^{iPr})·BEt_3 intermediate proposed above, have featured in reports of low oxidation state indium chemistry. For example, in 2005 Jones and co-workers reported an analogous salt elimination of InBr from the reaction of LiBr and a nascent indium(I) hydride to afford LiH. The poor solubility of the latter in organic solvents was suggested to be one driving force for this decomposition pathway.[140] Herein, the poor solubility of InI(s) may act similarly.

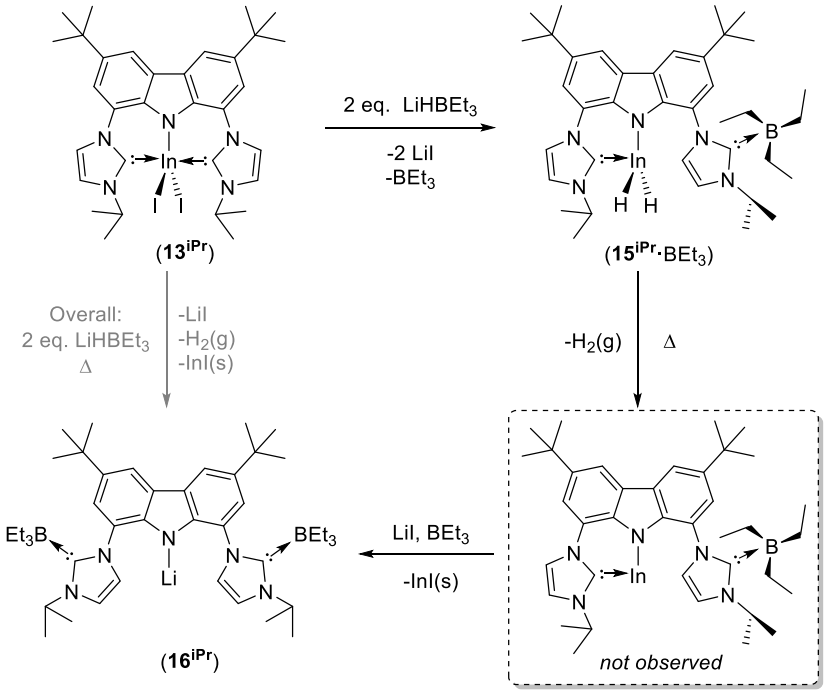

Scheme 3.6 Proposed preparation and decomposition pathway of **15^{iPr}**·BEt_3 to **16^{iPr}** following warming from -30 °C to room temperature.

It is worth noting that the deliberate synthesis of **16^{iPr}** was attempted, by the stoichiometric reaction of two equivalents of $LiHBEt_3$ with one equivalent of the diprotic

salt **5^{iPr}** at room temperature. This reaction proved to be uncontrollable under these conditions and did not yield the intended **16^{iPr}** complex, instead producing an intractable mixture of unidentifiable bimca^{iPr} related compounds, perhaps due to competing non-stoichiometric reaction pathways.

3.7.2 Attempted isolation of an indium(III) bimca^{R} supported dihydride

Encouraged by the variable temperature ^{1}H NMR spectroscopic study of the conversion of **13^{iPr}** to **15^{iPr}**·BEt_3, an attempt was made to repeat the reaction on a larger scale, such that the putative indium dihydride could be isolated at low temperature. Indium hydrides are known to be more stable in the solid state than in solution,[126] thus in this preparation **13^{iPr}** was replaced with its lower solubility relative; [In(bimca^{Me})I_2], **13^{Me}**. This, it was hoped, would expedite the isolation of the targeted dihydride by precipitation either directly from the reaction mixture or through the addition of a non-polar solvent to the reaction mixture. Despite the lower THF solubility of the methyl variant, **13^{Me}**, no precipitation was observed during the course of an iodide-hydride exchange reaction of **13^{Me}** with two equivalents of $LiHBEt_3$ at -78 °C in THF. Accordingly, hexane (*ca*. two volume equivalents) was added to the THF reaction mixture, leading to the gradual precipitation of an off-white solid, presumably containing **15^{Me}** or **15^{Me}**·BEt_3, which was isolated by filtration.

The THF/hexane reaction supernatant was found to contain [$LiI(THF)_3$], as confirmed by single crystal X-ray diffraction studies conducted on crystalline solids forthcoming from the removal of reaction volatiles. This indicates that a reaction between the $LiHBEt_3$ reagent with **13^{Me}** takes place.

The precipitated reaction solids were extracted into THF below -30 °C, and the resulting solution was recrystallised at -24 °C, but proved to be unproductive after several days of

standing at this temperature. Placement of the solution at room temperature afforded the deposition of a black solid and colour change of the supernatant from colourless to pale amber. It is noteworthy that the supernatant did not fluoresce strongly under long wave UV light, unlike the resting point reaction mixture containing **16^{iPr}** from the above *in situ* NMR spectroscopic study.

The ^{1}H NMR (THF-d_8) spectrum of a vacuum dried aliquot of the room temperature supernatant indicates a complicated mixture of bimca^{Me} containing products. This contrasts observations made during the NMR scale study that produced **15^{iPr}**·BEt_3 and likely results from the BEt_3 deficient reaction conditions upon warming to room temperature (*cf*. precipitation of the **15^{Me}** hydride product with hexane). Amongst the complicated mixture of bimca^{Me} containing products a major symmetrical bimca^{Me} species is present (*ca*. 50% by ^{1}H NMR aryl signal integrals) with an A:A:B:B (A = 4,5-NHC, B = 2,4,5,7-carbazolide) chemical shift and integration pattern that is consistent with a [Li(bimca^{Me})·$(BEt_3)_2$] species; **16^{Me}**, with ^{1}H-^{1}H NOE correlations between a *N*-methyl proton resonance at 3.95 ppm and a resonance for a pendent B-Et moiety located at 0.42 ppm (CH_3) and 0.51 ppm (CH_2), comparable to those signal correlations observed for **16^{iPr}**. The remaining complicated mixture of minor products could not be reliably identified.

The THF extract, warmed to room temperature, yielded a significant amount of dark brown to black amorphous solid upon standing with a small number of crystals that appeared stable at room temperature. Repeated attempts at crystallographic analyses of this small amount of crystalline material failed to obtain data of suitable quality for anisotropic refinement of non-hydrogen atoms, however the full isotropically refined data was used to deduce atomic connectivity (Figure 3.15). These single crystal X-ray

diffraction structure determination data indicate the modification of one bimca^{Me} NHC moiety to an "H_2 reduced" NCH_2N aminal (bimca'^{Me}HH) and reveal the formation of an indium(II) dimer, **17**, with an In···In contact. The coordination of each indium(II) metal centre is completed by the carbazolide and one NHC donor of a bimca'^{Me}HH ligand and an iodide co-ligand**.**

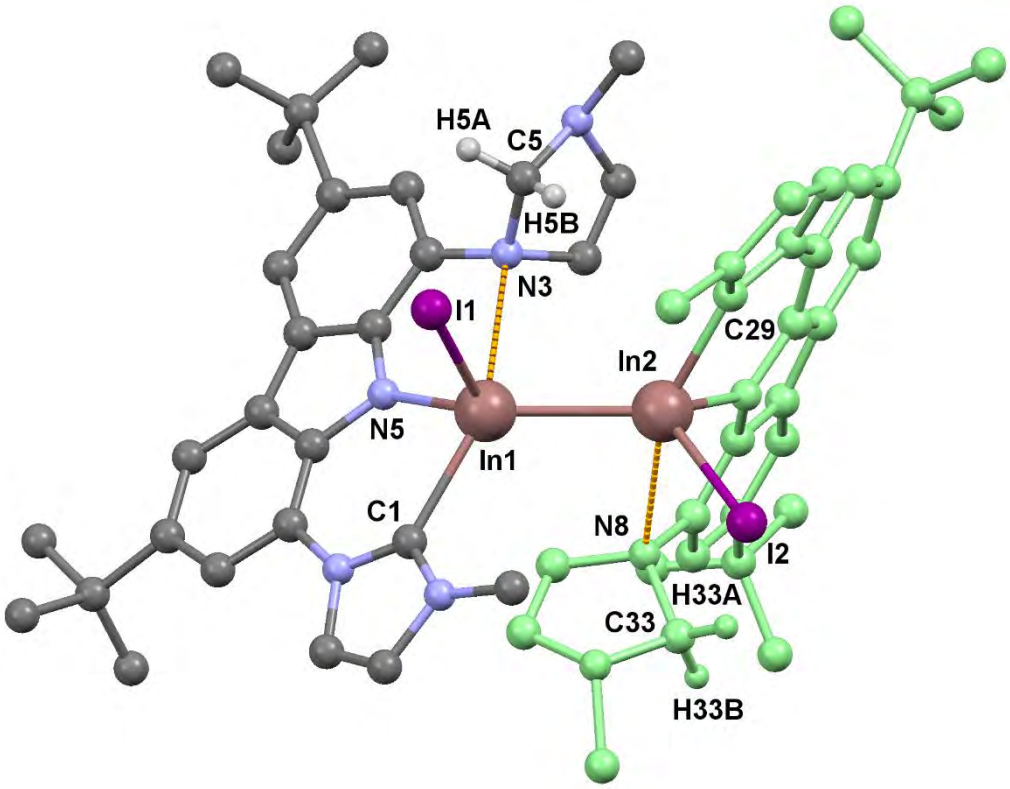

Figure 3.15 Van der Waals' sphere representation (arbitrary radius) of the bimca'^{Me}HH ligand containing In(II) dimer, **17**. All hydrogen atoms excepting aminal protons are omitted for clarity. One bimca'^{Me}HH unit is coloured green, and suspected N···In contacts are coloured orange for emphasis.

Aside from the reduced nature of the indium atoms in **17**, the most striking feature of the atomic connectivity of this In(II) dimer is the departure from planarity of the two N3 and

N8 imidazolyl rings (one per bimca'^{Me}HH moiety). These envelope-shaped imidazolyl rings strongly suggest full reduction at the C2 position to form the corresponding aminal with concomitant pyramidalisation at the nitrogens. This demonstrates a departure from the NCN delocalisation of an imidazolium or imidazol-2-ylidene, and seemingly permits coordination of the nitrogen to the indium metal centre (N3···In1: 2.930 Å, N8···In2: 2.951 Å). The formation of such aminals during the decomposition of indium hydride NHC adducts, has precedent in the decomposition path observed for the ring expanded NHC supported indium trihydride complex [InH_3(7Dipp)] (7Dipp = 1,3-bis(2,6-diisopropylphenyl)-1,3-diazepan-2-ylidene), recently reported by our group,[138] which affords the 7Dipp derived aminal (7DippHH), indium metal and dihydrogen gas from the reductive dehydrogenation of [InH_3(7Dipp)] at -25 °C (Scheme 3.7).

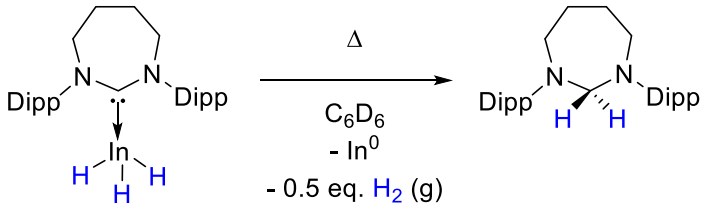

Scheme 3.7 Reductive decomposition of [InH_3(7Dipp)] to yield the corresponding 7Dipp aminal.[138]

In the case of [InH_3(7Dipp)] dihydrogen elimination leads to an unstable In(I) hydride coproduct that, in the absence of a suitably stabilising co-ligand, loses H_2 rapidly to deposit indium metal.[1] For **15^{Me}**/**15^{Me}**·BEt_3, this second reductive pathway is obviated by the presence of further stabilising donors leading to the formation of **17**, whereby reductive dehydrogenation of **15^{Me}** affords a more stable In(I) bimca'^{Me}HH intermediate (Scheme 3.8) *via* a reductive proton/hydride transfer to a coordinated NHC moiety to

afford the corresponding aminal (co-product A, Scheme 3.8). In the presence of InI (co-product B), which we propose is a co-product of the formation of [Li(bimca^{Me})·(BEt$_3$)$_2$], **16^{Me}**; we reason that the In(I) bimca'^{Me}HH aminal undergoes a disproportionation to yield In^0 and the In(II) iodide, "In(bimca'^{Me}HH)I" that exists as the observed dimer [{In(bimca'^{Me}HH)I}$_2$], **17** (Scheme 3.8).

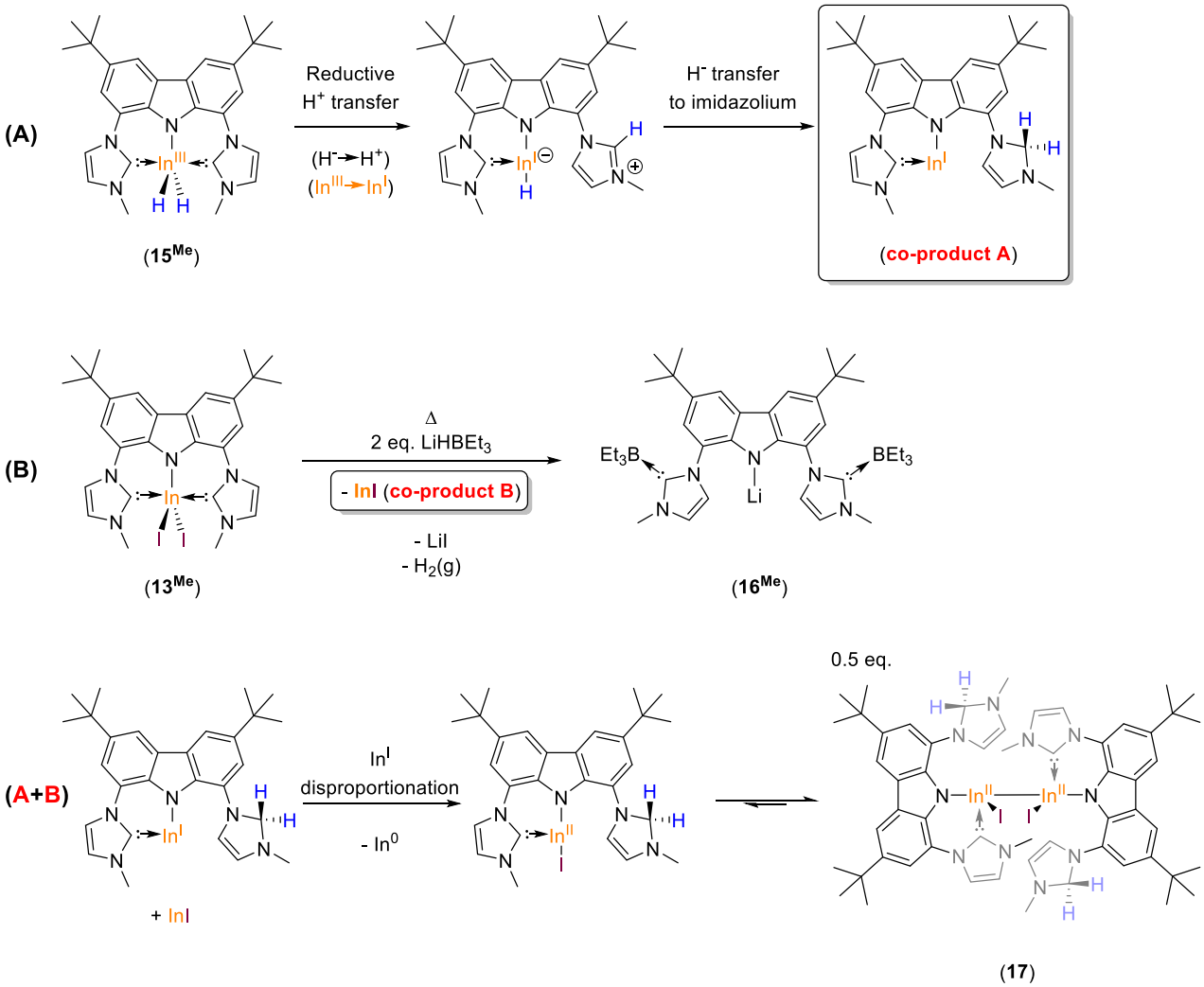

Scheme 3.8 Proposed mechanism for the formation of **17**.

3.7.3 Attempts to directly access low oxidation state In(bimca^R) complexes

The isolation of small amounts of the In(II) dimer **17**, from the reductive dehydrogenation of its parent dihydride, indicates that the bimca^{Me} ligand is capable of supporting low oxidation state indium centres. Thus, efforts were undertaken to access such low valent

species through (i) the chemical reduction of the parent diiodide, **13^{R}** (Scheme 3.9), or (ii) salt metathesis of an *s*-block bimca^{R} complex with an indium(I) precursor, *e.g.* InBr (Scheme 3.9). Access to an In(bimca^{R}) species through a protolytic pathway, *e.g.* using In(HMDS), analogous to that used to access the In(III) complexes **13^{R}**, was dismissed due to the inherent instability of this and other In(I) amides due to facile disproportionation [99] and the established difficulty of handling of bimca^{R}(H) proligands (*cf.* ion pairing and decomposition of bimca^{Me}(H) Chapter 2, Section 2.3.3).

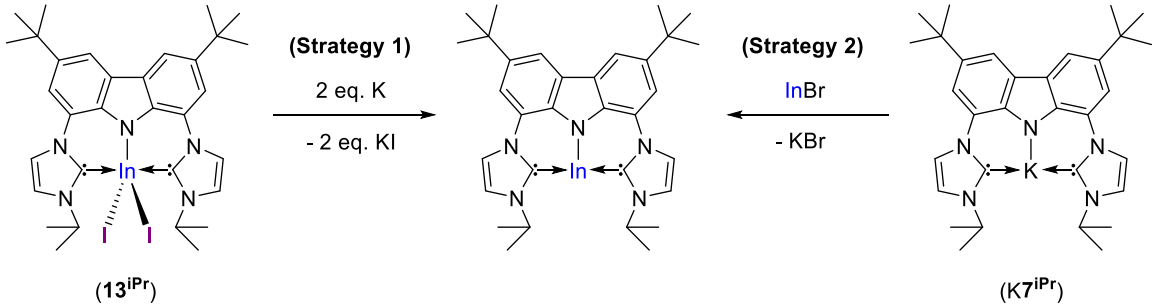

Scheme 3.9 Strategies for accessing low valent In(bimca^{R}) complexes.

Chemical reduction of **13^{Me}** with two equivalents of elemental potassium (as per strategy 1, Scheme 3.9 above) proved very hard to control, affording an indistinguishable mixture of inseparable bimca^{Me} containing compounds and the precipitation of a large amount of grey solid, presumably In^{0} (mp. 153 °C, lit.[1] 156.6 °C). Thus, focus was shifted to salt metathesis strategy 2 (Scheme 3.9) to determine if an In(I) metal centre could be directly supported by the bimca^{iPr} ligand, wherein *in situ* generated K**7^{iPr}** was added to a THF suspension of InBr at room temperature. Over the course of 18 hours the reaction mixture gradually turned from amber to crimson and lost its blue fluorescence under UV light, which is consistent with the consumption of the K**7^{iPr}** ligand transfer agent. This coincided with the gradual precipitation of a lustrous grey solid that later identified as indium metal by its melting point (153 °C) and indigo combustion flame. Filtration of the reaction mixture to isolate the supernatant, followed by removal of volatiles *in vacuo*

yielded a dark red solid, **18**, that was recrystallised from a room temperature saturated THF solution stored at -24 °C to afford small, red-amber, parallelepipeds. Unfortunately, these were of insufficient size and quality for crystallographic studies. The ^{1}H and ^{13}C NMR (THF-*d*$_8$) spectra of the vacuum dried mother liquor are surprisingly clean and exhibit chemical shift and ^{1}H NMR signal integral patterns that are consistent with the formation of a symmetrical bimca^{iPr} species. Interestingly, the ^{1}H NMR resonances (fully assigned from the ^{1}H-^{1}H NOESY spectrum of **18**) of the NHC-associated protons (A) are shifted upfield considerably, relative to those of the trivalent diiodo congener **13^{iPr}**, while the 2,7- and 4,5-carbazole signals (B) remain relatively unchanged. This results in a distinct A:B:A:B resonance pattern rather than the A:B:B:A ^{1}H NMR resonance pattern observed for **13^{iPr}** and A:A:B:B pattern observed for **16^{iPr}**. The upfield shift of the 4,5-imidazolyl and *N*-*i*Pr resonances for **18** relative to those of **13^{iPr}** is akin to the upfield shift of the *N*-methyl ^{1}H resonance observed in the bis(bimca^{Me}) magnesium complex, **10^{Me}**, relative to its mono(bimca^{Me}) iodide precursor, [Mg(bimca^{Me})I(THF)], **9^{Me}** (Chapter 2, Section 2.5.3) as summarised in Table 3.3.

Assignment	**13^{iPr}** δ (ppm)	**18** δ (ppm)	**9^{Me}** δ (ppm)	**10^{Me}** δ (ppm)
N^{iPr}-C*H*$_3$	1.70	0.35	-	-
N^{iPr}-C*H*/NMe	5.78	4.07	4.24	2.58
4-NHC-*H* (A)	7.65	7.21	7.25	6.62
2,7-carb.-*H* (B)	7.82	7.62	7.64	7.42
5-NHC-*H* (A)	8.40	8.00	8.09	7.59
4,5-carb.-*H* (B)	8.18	8.23	8.07	8.07

Table 3.3 Comparison of ^{1}H NMR chemical shift data of **13^{iPr}**, **18**, **9^{Me}**, and **10^{Me}**.

In addition to the NMR spectroscopic data for **18**, the reaction outcomes, *i.e.* indium metal deposition and no evidence for other bimca^{iPr} containing reaction products, are consistent with the formation of a bis(bimca^{iPr}) complex through disproportionation of an In(I) bimca^{iPr} intermediate to afford an In(II) analogue, *e.g.* [In(bimca^{iPr})$_2$] (Scheme 3.10). However, in the absence of further data, no conclusive structural assignment is possible.

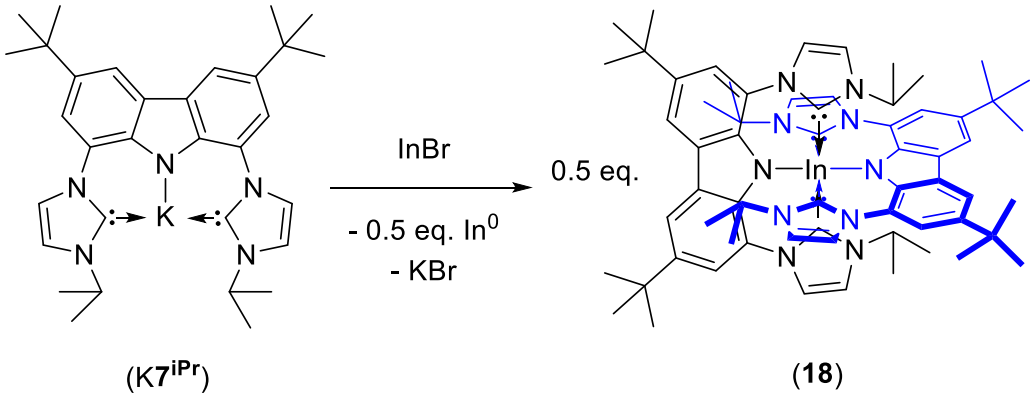

(K**7**^{iPr}) (**18**)

Scheme 3.10 Possible formation of **18** through disproportionation of "In(bimca^{iPr})".

*3.7.4 Iodide-hydride exchange of **14**^{iPr} with two equivalents of LiHBEt$_3$*

The promising results of our indium bimca^{iPr} iodide-hydride exchange reactions using **13**^{iPr} led us to extend this approach to the heavier thallium congener, **14**^{iPr}. Thus, analogous to the reaction that formed indium dihydride **15**^{iPr}·BEt$_3$, a NMR experiment scale reaction with the thallium diiodide **14**^{iPr} and two equivalents of LiHBEt$_3$ was carried out at low temperature in THF-d_8. However, the anticipated [Tl(bimca^{iPr})H$_2$], **19**^{iPr}, or its BEt$_3$ adduct (*cf.* **15**^{iPr}·BEt$_3$), proved to be substantially less stable than its indium congener. For example, unlike **15**^{iPr}·BEt$_3$, where dihydrogen gas evolution began at > -30 °C, the evolution of H$_2$ (4.55 ppm in THF-d_8) was observed immediately in a ^{1}H NMR spectrum of the reaction mixture at -30 °C. This was accompanied by the development of blue fluorescence for the pale yellow reaction mixture when exposed to

long wave UV light (*cf.* fluorescence for **16^{iPr}**), as well as the deposition of a grey-amber solid upon warming to room temperature. Interestingly, ^{1}H NMR resonances corresponding to the symmetrical bimca^{iPr} bis(borane) adduct **16^{iPr}** (*cf.* thermal decomposition of **15^{iPr}**·BEt_3 in the presence of free BEt_3) were clearly present in the final reaction mixture, providing support for a similar reaction pathway to that observed for **13^{iPr}** with two equivalents of $LiHBEt_3$ (Figure 3.16). Thus, we propose that this reaction proceeds through a transient bimca^{iPr} thallium dihydride intermediate **19^{iPr}** that undergoes reductive elimination of dihydrogen and TlI, the latter from salt metathesis with LiI in the reaction mixture, to form **16^{iPr}** (*cf.* Scheme 3.6, Section 3.7.1). Unfortunately, unlike **15^{iPr}**·BEt_3, very little evidence for the short lived intermediate **19^{iPr}** could be gathered due to increased temperature sensitivity *vis-à-vis* **15^{iPr}**·BEt_3 and substantial J_{TlH} coupling, which results in broader more complex resonance patters than those observed in the ^{1}H NMR spectrum of **15^{iPr}**·BEt_3.

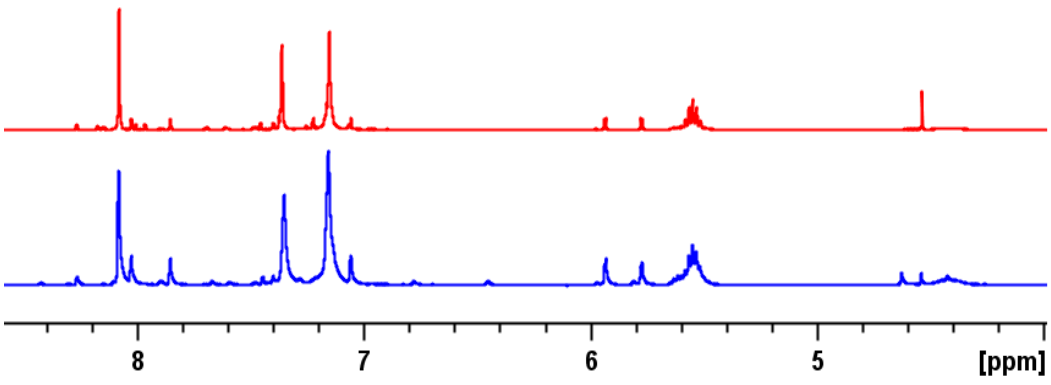

Figure 3.16 Excerpts of the ^{1}H NMR (THF-d_8) spectra of the resting state reaction mixtures of **13^{iPr}** with 2 eq. $LiHBEt_3$ (red) and **14^{iPr}** with 2 eq. $LiHBEt_3$ (blue).

*3.7.5 Iodide-hydride exchange of **14^{iPr}** with one equivalent of $LiHBEt_3$*

The mixed halide-hydride species of lighter group 13 metals are known to possess greater thermal stability than the corresponding trihydrides.[120] Furthermore, the isolation of In(II)

dimer **17** indicates that retention of iodide ligands can increase product isolability post metal hydride decomposition. Thus, attempts to furnish the mixed thallium hydride-iodide bimca^{Me} complex; [Tl(bimca^{Me})HI], **20^{Me}**, were made.

The reaction of **14^{Me}** and LiHBEt$_3$ was carried out on a preparative scale and afforded a mixture of products. A low temperature (-78 °C) THF solution of LiHBEt$_3$ was added to an orange -78 °C THF solution of [Tl(bimca^{Me})I$_2$] (**14^{Me}**) resulting in a suspension that was stirred at -78 °C for one hour before removal of volatiles under vacuum at -78 °C. At this temperature the powdery orange solid product exhibited a blue fluorescence under long wave UV light, akin to **16^{iPr}** (*vide supra*) and inconsistent with thallium-bimca^{Me} coordination (*cf.* quenching of luminescence). A room temperature ^{1}H NMR spectrum of this solid shows the presence of residual **14^{Me}** (*cf.* ^4J and $^5J_{TlH}$ coupling of bimca^{Me} resonances) and a second set of defined, bimca^{Me} and BEt$_3$ containing product resonances that overlap with those identified for [Li(bimca^{Me})·(BEt$_3$)$_2$], **16^{Me}**, during the preparative scale decomposition of **15^{Me}**. This latter product is inconsistent with thallium coordination due to the absence of J_{TlH} coupling. From this we infer that the intended [Tl(bimca^{Me})HI] species, **20^{Me}**, undergoes ligand redistribution to afford **14^{Me}** and **19^{Me}**, the latter of which undergoing rapid decomposition to yield **16^{Me}** (*cf.* 2:1 reaction of LiHBEt$_3$ with **14^{iPr}**) (Scheme 3.11).

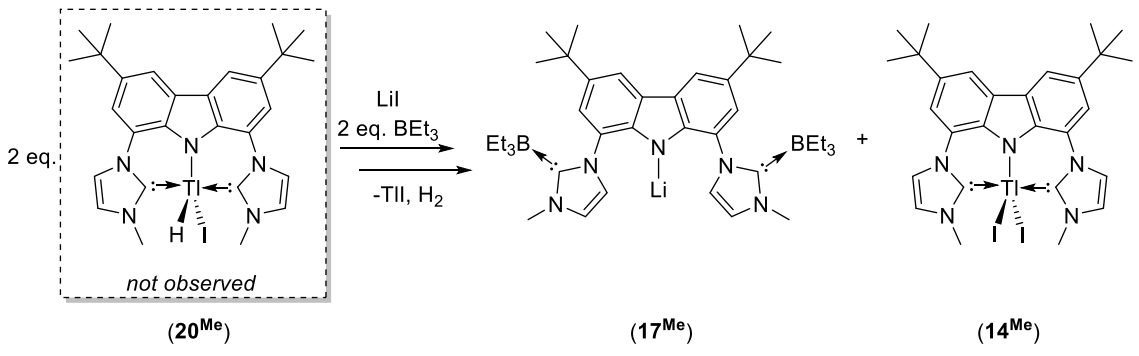

Scheme 3.11 Likely decomposition path of the putative thallium iodohydride **20^{Me}**.

3.8 Conclusions

An extensive series of group 13 diiodide complexes supported by the bimca^{R} ligand has been synthesised.

Synthetic strategies that attempted bimca^{R} complexation through protolysis have exposed the relative difficulty of deprotonating the triprotic Hbimca^{R}(2HI) precursors, **4^{R}**, with the tris(hexamethyldisilazides) of aluminium and gallium, and trimethylaluminium, making these paths unsuitable for accessing [M(bimca^{R})I$_2$] complexes (M = Al, Ga). Consequently, the diiodo aluminium and gallium bimca^{R} complexes; **11^{iPr}**, **12^{iPr}** and **12^{Me}** have been accessed by salt metathesis using *s*-block bimca^{R} reagents and the respective metal triiodides. This approach is particularly noteworthy for the preparation of the first five coordinate aluminium bis(NHC) pincer complex; **11^{iPr}**.

The heavier group 13 analogues, **13^{R}** and **14^{R}**, could not be accessed from MI$_3$ precursors (*cf.* reductive processes to afford M(I) species), and earlier studies have shown us that lighter trihalide precursors suffer from halide scrambling on the "softer" metal centre to furnish mixed chloride- (M = Tl) and bromide- (M = In) iodide products (*cf.* iodide counterions in **4^{R}** and **5^{R}**). Thus a convergent methodology using [M(HMDS)$_3$] reagents (M = In and Tl) was developed to provide superior control of product purity and led to the isolation of two rare thermally stable thallium(III) diiodide complexes; **14^{Me}** and **14^{iPr}**.

Preliminary iodide-hydride exchange reactions have been carried out using complexes **13^{iPr}** and **14^{iPr}** and monitored *in situ* by NMR spectroscopy, resulting in the synthesis of a putative indium dihydride borane adduct; **15^{iPr}**·BEt$_3$, which decomposes in the presence of free BEt$_3$ to the bis(borane)bimca^{iPr} complex **16^{iPr}** at temperatures above -30 °C. The analogous thallane could not be identified under identical conditions but was shown to

likewise form **16^{iPr}** under similar reaction conditions. This indicates **19^{iPr}** may decompose by a similar path to its indium congener.

3.9 Experimental

General methods

[M(HMDS)$_3$] (M = Al, Ga, In, Tl) compounds were synthesised *via* adapted literature methods.[141,142] The Al to In tris(amides) were generated in diethyl ether and used *in situ*. [Tl(HMDS)$_3$] was prepared and isolated prior to use by the following procedure:

A pressure vessel was charged with commercially obtained $TlCl_3 \cdot 4H_2O$ (2.2 g, 7.0 mmol) and cooled to -196 °C. Under a flow of nitrogen, excess thionyl chloride (5 mL, 68 mmol) was added slowly and allowed to freeze, upon which the flask was sealed under vacuum and warmed to room temperature with stirring over 18 hours. After this time volatiles were removed *in vacuo* at room temperature and the resultant off-white residue was extracted into cold (0 °C) THF (200 mL). Volatiles were removed *in vacuo* and the solid resuspended in toluene (50 mL) at room temperature. Addition of a solution of KHMDS (4.2 g, 21 mmol) in toluene (100 mL) afforded an amber suspension with small amounts of thallium metal deposited as a mirror. The reaction mixture was stirred at room temperature for 18 h in the absence of light and filtered twice to remove precipitated KCl and thallium metal. Concentration of the toluene mother liquor yielded [Tl(HMDS)$_3$] as large pale amber rectangular blocks upon storage at room temperature. These were isolated by filtration, crushed by action of a stirrer bar, dried under vacuum, and stored in the absence of light under an argon atmosphere (2.6 g, 54%).

*[Al(bimca^{iPr})I$_2$], **11^{iPr}**, from metathesis with AlI$_3$*

A solution of LiHMDS (0.10 g, 0.60 mmol) in THF (5 mL) was added to a colourless suspension of **4^{iPr}** (0.15 g, 0.20 mmol) in THF (20 mL) to immediately afford a yellow suspension that gradually turned beige, cleared, and developed a blue fluorescence in daylight or under long wave UV light. The reaction mixture was stirred for 1 h, after which it was added to a colourless solution of AlI$_3$ (0.081 g, 0.20 mmol) in THF (20 mL) and stirred at room temperature for 18 h. Over this time the reaction mixture darkened to amber and became cloudy whilst its blue fluorescence subsided under long wave UV light. Filtration and removal of volatiles *in vacuo* afforded a pale yellow treacly solid that was triturated with hexane, aided by sonication, to give **11^{iPr}** as a powdery pale yellow solid that exhibits weak pale blue fluorescence under long wave UV light (0.11 g, 69%). Microanalysis results repeatedly returned results consistent with "LiI(THF)$_n$" contamination (see below for example). **11^{iPr}** was also formed *via* salt metathesis with K**7^{iPr}** and AlI$_3$ in an analogous manner to the above procedure. A saturated solution of the vacuum dried reaction mother liquor from this reaction placed at room temperature yielded large beige rectangular plates suitable for single crystal X-ray diffraction structure determination. Spectroscopic data of the dried mother liquor indicated formation of **11^{iPr}** with a higher proportion of protonated bimca^{iPr} by-products relative to the *in situ* Li**7^{iPr}** preparation. ^{1}H NMR (400 MHz, THF-d_8): δ 1.51 (s, 18H, *t*Bu-CH_3), 1.73 (d, $^3J_{HH}$ = 6.62 Hz, 12H, N*i*Pr-CH_3), 5.75 (sept, $^3J_{HH}$ = 6.62 Hz, 2H, N*i*Pr-C*H*), 7.64 (d, $^3J_{HH}$ = 2.16 Hz, 2H, 4-NHC-*H*), 7.80 (d, $^4J_{HH}$ = 1.60 Hz, 2H, 2,7-carb.-*H*), 8.11 (d, $^4J_{HH}$ = 1.60 Hz, 2H, 4,5-carb.-*H*), 8.36 (d, $^3J_{HH}$ = 2.16 Hz, 2H, 5-NHC-*H*). ^{13}C NMR (100 MHz, THF-d_8): δ 22.53 (s, N*i*Pr-*C*H$_3$), 32.14 (s, *t*Bu-*C*H$_3$), 35.40 (s, *t*Bu-*C*), 52.78 (s, N*i*Pr-*C*H), 111.80 (s, 2,7-carb.-*C*), 115.17 (s, 4,5-carb.-*C*), 115.84 (s, 5-NHC-*C*), 118.70 (s, carb.-*C*), 123.62 (4-NHC-*C*), 128.61, 135.97, 142.44 (s, carb.-*C*), 173.86 (s, 2-NHC-*C*, resolved with

^{1}H-^{13}C HMBC). Calcd. for **11^{iPr}**, $C_{32}H_{40}N_5I_2Al$: C, 49.56; H, 5.20; N, 9.03. Calcd. for **11^{iPr}**·LiI(THF), $C_{36}H_{48}N_5I_3AlO$: C, 44.06; H, 4.93; N, 7.14. Found: C, 44.36; H, 5.80; N, 7.71. IR (Nujol on NaCl plates, cm^{-1}): 1597 (*w*, *sh*), 1548 (*w sh*), 1261 (*m*, *sh*), 1138 (*m*, sh), 1097 (*m*, *br*), 1023 (*m*, *br*), 881 (*m*, *sh*), 849 (*m*, *sh*), 803 (*w*, *sh*), 600 (*w*, *sh*). Mp: 331-332 °C (dec.).

*[Ga(bimca^{iPr})I$_2$], **12^{iPr}**, from metathesis with GaI$_3$*

A solution of KHMDS (0.080 g, 0.40 mmol) in THF (5 mL) was added to a colourless suspension of **4^{iPr}** (0.10 g, 0.13 mmol) in THF (20 mL) to immediately afford a yellow suspension that gradually turned brown, precipitated KI as a white solid, and developed a blue fluorescence under long wave UV light. The reaction mixture was stirred for 1 h, after which the brown supernatant was isolated by filtration to remove the KI by-product, and added to a colourless solution of GaI_3 (0.060 g, 0.13 mmol) in THF (20 mL) and stirred at room temperature for 18 h. Over this time the reaction mixture paled to amber and became cloudy whilst the blue fluorescence of K**7^{iPr}** subsided. Filtration and removal of volatiles *in vacuo* afforded **12^{iPr}** as a powdery pale yellow solid that exhibits a weak blue fluorescence under long wave UV light (0.064 g, 59%). ^{1}H NMR (300 MHz, THF-d_8): δ 1.52 (s, 18H, *t*Bu-CH_3), 1.77 (d, $^{3}J_{HH}$ = 6.65 Hz, 12H, N*i*Pr-CH_3), 5.78 (sept, $^{3}J_{HH}$ = 6.65 Hz, 2H, N*i*Pr-C*H*), 7.61 (d, $^{3}J_{HH}$ = 2.10 Hz, 2H, 4-NHC-*H*), 7.81 (d, $^{4}J_{HH}$ = 1.51 Hz, 2H, 2,7-carb.-*H*), 8.16 (d, $^{4}J_{HH}$ = 1.51 Hz, 2H, 4,5-carb.-*H*), 8.35 (d, $^{3}J_{HH}$ = 2.10 Hz, 2H, 5-NHC-*H*). ^{13}C NMR (75 MHz, THF-d_8): δ 22.65 (s, N*i*Pr-*C*H$_3$), 32.20 (s, *t*Bu-*C*H$_3$), 35.52 (s, *t*Bu-*C*), 52.46 (s, N*i*Pr-*C*H), 112.01 (s, 2,7-carb.-*C*), 115.95 (s, 4,5-carb.-*C*), 116.06 (s, 5-NHC-*C*), 122.73 (s, 4-NHC-*C*), 123.62, 128.13, 135.90, 142.04 (s, carb.-*C*), 2-NHC-*C* not resolved. Calcd. for $C_{32}H_{40}N_5I_2Ga$: C, 46.97; H, 4.93; N, 8.56. Found: C, 46.35; H, 5.31; N, 8.18. IR (Nujol mull on NaCl plates, cm^{-1}): 1727 (*w*, *sh*),

1580 (*m*, *sh*), 1564 (*m*, *sh*), 1095 (*m*, *sh*), 1020 (*w*, *sh*), 8.69 (*m*, *sh*), 896 (*m*, *sh*), 804 (*w*, *sh*), 742 (*m*, *sh*), 686 (*m*, *sh*), 665 (*w*, *sh*). Mp: 306-307 °C (dec.).

*[Ga(bimca^{Me})I$_2$], **12^{Me}**, from metathesis with GaI$_3$*

See Chapter 2.1 experimental section.

*[In(bimca^{R})I$_2$], **13^{R}**, from [In(HMDS)$_3$]*

Complexes **13^{iPr}** and **13^{Me}** were prepared commensurately; a representative synthesis of **13^{iPr}** is given below.

A solution of KHMDS (0.20 g, 1.0 mmol) in diethyl ether (6 mL) was added to a suspension of $InBr_3$ (0.12 g, 0.33 mmol), also in diethyl (20 mL), and stirred for 1 h at room temperature. After this time the resulting colourless suspension was allowed to settle and the supernatant was added directly to a colourless THF (50 mL) suspension of **4^{iPr}** (0.25 g, 0.33 mmol) to give a bright yellow suspension that was stirred at room temperature for 18 h resulting in a slightly cloudy, pale yellow solution that had no visible fluorescence under long wave UV light. Filtration and removal of volatiles *in vacuo* afforded **13^{iPr}** as an off-white powdery solid (0.22 g, 86%). Large off-white rectangular blocks suitable for X-ray diffraction structure determination were grown from a saturated room temperature fluorobenzene solution of **13^{iPr}** cooled to 4 °C. ^{1}H NMR (400 MHz, THF-*d*$_8$): δ 1.52 (s, 18H, *t*Bu-C*H*$_3$), 4.39 (s, 6H, NMe), 7.46 (d, $^{3}J_{HH}$ = 1.99 Hz, 2H, 4-NHC-*H*), 7.83 (d, $^{4}J_{HH}$ = 1.56 Hz, 2H, 2,7-carb.-*H*), 8.20 (d, $^{4}J_{HH}$ = 1.56 Hz, 4,5-carb.-*H*), 8.37 (d, $^{3}J_{HH}$ = 1.99 Hz, 2H, 5-NHC-*H*). ^{13}C NMR (100 MHz, THF-*d*$_8$): δ 23.46 (s, N*i*Pr-*C*H$_3$), 32.13 (s, *t*Bu-*C*H$_3$), 35.29 (s, *t*Bu-*C*), 52.68 (s, N*i*Pr-*C*H), 113.28 (s, 4,5-carb.-*C*), 115.42 (s, 2,7-carb.-*C*), 117.96 (s, 5-NHC-*C*), 118.64 (s, carb.-*C*), 123.61 (s, 4-NHC-*C*), 129.08, 137.97, 141.07 (s, carb.-*C*), 175.84 (s, 2-NHC-*C*, resolved with ^{1}H-^{13}C HMBC). Calcd. for $C_{32}H_{40}N_5I_2In$: C, 44.52; H, 4.67; N, 8.11; Found: C, 44.50, H,

4.94; N, 7.89. IR (Nujol on NaCl plates, cm^{-1}): 1580 (*m*, *sh*), 1403 (*s*, *sh*), 1330 (*m*, *sh*), 1309 (*m*, sh), 1288 (*m*, *sh*), 1262 (*m*, *sh*), 1241 (*m*, *sh*), 1173 (*w*, *sh*), 1134 (w, *sh*), 1101 (*m*, *br*), 1020 (*m*, *br*), 868 (*m*, *sh*), 840 (*m*, *sh*), 661 (*m*, *sh*). Mp: 326-327 °C (dec.), 339-340 °C (melts).

[In(bimca^{Me})I$_2$], ***13^{Me}***

^{1}H NMR (400 MHz, THF-d_8): δ 1.52 (s, 18H, *t*Bu-CH_3), 1.70 (d, $^3J_{HH}$ = 6.54 Hz, 12H, N*i*Pr-CH_3), 5.78 (sept, $^3J_{HH}$ = 6.54 Hz, 2H, CH-N*i*Pr), 7.65 (d, $^3J_{HH}$ = 2.18 Hz, 2H, 4-NHC-*H*), 7.82 (d, $^4J_{HH}$ = 1.60 Hz, 2H, 2,7-carb.-*H*), 8.18 (d, $^4J_{HH}$ = 1.60 Hz, 4,5-carb.-*H*), 8.40 (d, $^3J_{HH}$ = 2.18 Hz, 2H, 5-NHC-*H*). ^{13}C NMR (100 MHz, THF-d_8): δ 32.13 (s, *t*Bu-*C*H$_3$), 35.29 (s, *t*Bu-*C*), 38.54 (s, NMe), 113.19 (s, 4,5-carb.-*C*), 115.62 (s, 2,7-carb.-*C*), 116.90 (s, 5-NHC-*C*), 118.64 (s, carb.-*C*), 123.61 (s, 4-NHC-*C*), 129.08, 137.97, 141.07 (s, carb.-*C*), 175.84 (s, 2-NHC-*C*, resolved with ^{1}H-^{13}C HMBC). Calcd. for $C_{28}H_{32}N_5I_2In$: C, 41.66; H, 4.00; N, 8.68; Found: C, 41.94, H, 4.35; N, 8.16. IR (Nujol on NaCl plates, cm^{-1}): 1580 (*m*, *sh*), 1403 (*s*, *sh*), 1173 (*w*, *sh*), 1134 (w, *sh*), 1101 (*m*, *br*), 1020 (*m*, *br*), 868 (*m*, *sh*), 841 (*m*, *sh*), 742 (w, sh), 693 (*m*, *sh*), 661 (*m*, *sh*). Mp: 326-327 °C (dec.), 354-356 °C (melts).

[Tl(bimca^{R})I$_2$], ***14^{R}****, from [Tl(HMDS)$_3$]*

Complexes **14^{iPr}** and **14^{Me}** were prepared commensurately; a representative synthesis of **14^{iPr}** is given below.

A pale amber solution of [Tl(HMDS)$_3$] (0.23 g, 0.33 mmol) in THF (10 mL) was added to a colourless suspension of **4^{iPr}** (0.25 g, 0.33 mmol) in THF (40 mL) to immediately afford a bright yellow suspension that was stirred at room temperature for 18 h resulting in a slightly cloudy amber solution with no visible fluorescence under long wave UV light. Filtration and removal of volatiles *in vacuo* afforded **14^{iPr}** as a bright orange

powdery solid (0.28 g, 90%). Crystals of **14^{iPr}** suitable for X-ray diffraction analysis were grown from a room temperature saturated fluorobenzene solution placed at 4 °C. ^{1}H NMR (400 MHz, THF-d_8): δ 1.52 (s, 18H, *t*Bu-CH_3), 1.73 (d, $^{3}J_{HH}$ = 6.63 Hz, 12H, N*i*Pr-CH_3), 5.83 (dd, $^{4}J_{TlH}$ = 29.3 Hz, 2H, N*i*Pr-C*H*), 7.71 (dd, $^{4}J_{TlH}$ = 87.0 Hz, 2H, 4-NHC-*H*), 7.78 (s, 2H, 2,7-carb.-*H*) , 8.20 (s, 2H, 4,5-carb.-*H*), 8.43 (dd, $^{4}J_{TlH}$ = 93.0 Hz, 2H, 5-NHC-*H*). Imidazolyl and carbazolide J_{HH} values could not be calculated due to signal broadening. ^{13}C NMR (100 MHz, THF-d_8): δ 23.72 (s, N*i*Pr-*C*H$_3$), 32.21 (s, *t*Bu-*C*H$_3$), 35.25 (s, *t*Bu-*C*), 53.14 (d, $^{3}J_{TlC}$ = 109.5 Hz, N*i*Pr-*C*H), 113.54 (s, 4,5-carb.-*C*), 115.95 (s, 2,7-carb.-*C*), 117.96 (d, $^{3}J_{TlC}$ = 218.8 Hz, 4-NHC-*C*), 118.37 (d, $^{3}J_{TlC}$ = 188.4 Hz, 5-NHC-*C*), 125.04 (s, resolved with ^{1}H-^{13}C HMBC, carb.-*C*), 128.81, 139.22, 140.36 (s, carb.-*C*), 2-NHC-*C* not resolved. Calcd. for $C_{32}H_{40}N_5I_2Tl$: C, 40.34; H, 4.23; N, 7.35; Found: C, 40.20; H, 4.26; N, 7.29. IR (Nujol on NaCl plates, cm^{-1}): 1584 (*w*, *sh*), 1285 (*m*, *sh*), 1261 (*m*, *sh*), 1234 (*m*, *sh*), 1167 (*w*, *sh*), 1113 (*m*, *sh*), 986 (*w*, *sh*), 877 (*m*, *sh*), 856 (*m*, *sh*), 837 (*m*, *sh*), 744 (*m*, *sh*), 736 (*m*, *sh*), 663 (*w*, *sh*). Mp: 228-229 °C (dec.), 268-269 °C (melts).

*[Tl(bimca^{Me})I$_2$], **14^{Me}**, from [Tl(HMDS)$_3$]*

Orange rectangular blocks of **14^{Me}** suitable for X-ray diffraction structure determination were grown from a saturated room temperature THF solution of **14^{Me}** placed at 4 °C. ^{1}H NMR (300 MHz, THF-d_8): δ 1.52 (s, 18H, *t*Bu-CH_3), 4.46 (dd, $^{4}J_{TlH}$ = 13.0 Hz, 6H, NMe), 7.54 (dd, $^{4}J_{TlH}$ = 86.5 Hz, 2H, 4-NHC-*H*), 7.79 (s, 2H, 2,7-carb.-*H*), 8.24 (s, 2H, 4,5-carb.-*H*), 8.38 (d, $^{4}J_{TlH}$ = 94.03 Hz, 2H, 5-NHC-*H*). Imidazolyl and carbazolide J_{HH} values could not be calculated due to signal broadening. ^{13}C NMR (150 MHz, THF-d_8): δ 32.24 (s, *t*Bu-*C*H$_3$), 35.36 (s, *t*Bu-*C*), 38.59 (d, $^{3}J_{TlC}$ = 113.10 Hz, NMe), 113.40 (s, 4,5-carb.-*C*), 116.21 (s, 2,7-carb.-*C*), 117.03 (d, $^{3}J_{TlC}$ = 205.0 Hz, 4-NHC-*C*), 123.14 (s, carb.-*C*), 124.23 (d, $^{3}J_{TlC}$ = 205.0 Hz, 5-NHC-*C*), 128.94, 139.08, 140.31 (s, carb.-*C*),

2-NHC-*C* not resolved. Calcd. for $C_{28}H_{32}N_5I_2Tl$: C, 37.50; H, 3.60; N, 7.81. Found: C, 37.48; H, 3.51; N, 7.86. IR (Nujol mull on NaCl plates, cm^{-1}): 1580 (*m, sh*), 1285 (*m*, *sh*), 1261 (*m*, *sh*), 1234 (*m*, *sh*), 1167 (*w*, *sh*), 1114 (*m*, *sh*), 986 (*w*, *sh*), 877 (*m*, *sh*), 856 (*m*, *sh*), 837 (*m*, *sh*), 743 (*m*, *sh*), 736 (*m*, *sh*). Mp: 227-229°C (dec.).

*[In(bimca^{iPr})H$_2$·BEt$_3$], **15^{iPr}**, monitored in situ by NMR spectroscopy*

THF-d_8 (0.5 mL) was condensed onto a solid mixture of **13^{iPr}** (0.012 g, 0.014 mmol) and $LiHBEt_3$ (0.0029 g, 0.028 mmol) at -196 °C. The solid reaction mixture was warmed to -50 °C to dissolve the reactants, aided by intermittent agitation by inversion over 15 minutes to give a clear beige reaction mixture with weak blue fluorescence under long wave UV light. ^{1}H and ^{13}C NMR Spectra were acquired at *ca*. 2 h intervals in 10 °C increments from -30 °C to room temperature. At room temperature the reaction mixture formed a grey precipitate and pale yellow supernatant with visible blue fluorescence under ambient and long wave UV light. ^{1}H NMR (400 MHz, THF-d_8, -30 °C): δ -0.06 (q, $^3J_{HH}$ = 7.48 Hz, 4H, BEt_3-CH_2), 0.06 (q, $^3J_{HH}$ = 7.45 Hz, 2H, BEt_3-CH_2), 0.30 (br s, 6H, free BEt_3-CH_2), 0.46 (t, $^3J_{HH}$ = 7.48 Hz, 6H, BEt_3-CH_3), 0.66 (t, $^3J_{HH}$ = 7.45 Hz, 3H, BEt_3-CH_3), 0.73 (t, $^3J_{HH}$ = 7.67 Hz, 9H, free BEt_3-CH_3), 1.44 (s, 9H, *t*Bu$_B$-CH_3), 1.51 (s, 9H, *t*Bu$_{In}$-CH_3), 1.52 (d, $^3J_{HH}$ = 6.29 Hz, 3H, N*i*Pr$_B$-CH_3), 1.55 (d, $^3J_{HH}$ = 6.69 Hz, 6H, N*i*Pr$_{In}$-CH_3), 1.60 (d, $^3J_{HH}$ = 6.29 Hz, 3H, N*i*Pr$_B$-CH_3), 4.61 (sept, $^3J_{HH}$ = 6.69 Hz, 1H, N*i*Pr$_{In}$-C*H*), 5.52 (sept, $^3J_{HH}$ = 6.29 Hz, 1H, N*i*Pr$_B$-C*H*), 5.66 (br d, $^2J_{HH}$ = 46.7 Hz, 1H, In-*H*), 5.99 (br d, $^2J_{HH}$ = 46.7 Hz, 1H, In-*H*), 7.21 (d, $^3J_{HH}$ = 1.52 Hz, 1H, 5-NHC$_B$-*H*), 7.27 (d, $^4J_{HH}$ = 1.71 Hz, 1H, 7-carb.-*H*), 7.62 (d, $^3J_{HH}$ = 1.52 Hz, 1H, 4-NHC$_B$-*H*), 7.68 (d, $^4J_{HH}$ = 1.26 Hz, 1H, 2-carb.-*H*), 7.90 (d, $^3J_{HH}$ = 1.52 Hz, 1H, 4-NHC$_{In}$-*H*), 8.19 (d, $^4J_{HH}$ = 1.26 Hz, 1H, 4-carb.-*H*), 8.22 (d, $^4J_{HH}$ = 1.71 Hz, 1H, 5-carb.-*H*), 8.37 (d, $^3J_{HH}$ = 1.52 Hz, 1H, 5-NHC$_{In}$-*H*). ^{13}C NMR (100 MHz, THF-d_8, -30 °C): δ BEt_3-*C*H$_2$ signals not observed for any BEt_3 moiety, 11.56 (br s, free BEt_3-*C*H$_3$), 13.96 (br s, BEt_3-*C*H$_3$), 22.12

(s, N*i*Pr-*C*H$_3$), 22.72 (s, N*i*Pr-*C*H$_3$), 23.24 (s, N*i*Pr-*C*H$_3$), 31.44 (s, *t*Bu$_B$-*C*H$_3$), 31.46 (s, *t*Bu$_{In}$-*C*H$_3$), 34.27 (s, *t*Bu$_B$-*C*), 34.53 (s, *t*Bu$_{In}$-*C*), 48.94 (s, N*i*Pr$_B$-*C*H), 53.44 (s, N*i*Pr$_{In}$-*C*H), 113.20, 115.47, 116.28, 117.28, 118.56, 121.28, 123.71, 123.78, 124.25, 125.98 (s, NHC- or carb.-*C*), 126.82, 129.14, 138.28, 138.79, 139.01, 144.64 (s, carb.-*C*), 170.45 (s, 2-NHC$_{In}$-*C*), 2-NHC$_B$-*C* not observed.

^{1}H NMR (400 MHz, THF-d_8, 25 °C): δ -0.02 (m, 8H, BEt$_3$-C*H*$_2$), 0.16 (m, 4H, BEt$_3$-C*H*$_2$), 0.56 (t, $^3J_{HH}$ = 6.65 Hz, 12H, BEt$_3$-C*H*$_3$), 0.69 (t, $^3J_{HH}$ = 7.63 Hz, 6H, BEt$_3$-C*H*$_3$), 1.44 (s, 18H, *t*Bu-C*H*$_3$), 1.54 (d, $^3J_{HH}$ = 6.65 Hz, 12H, N*i*Pr-C*H*$_3$), 5.55 (sept, $^3J_{HH}$ = 6.65 Hz, 2H, N*i*Pr-C*H*), 7.15 (d, $^3J_{HH}$ = 1.52 Hz, 2H, 2,7-carb.-*H*), 7.17 (d, $^4J_{HH}$ = 1.71 Hz, 2H, 4-NHC-*H*), 7.34 (d, $^3J_{HH}$ = 1.71 Hz, 2H, 5-NHC-*H*), 8.08 (d, 1.52 Hz, 2H, 4,5-carb.-*H*). ^{13}C NMR (100 MHz, THF-d_8, 25 °C): δ BEt$_3$-*C*H$_2$ signals not observed, 14.80 (br s, BEt$_3$-*C*H$_3$), 18.43 (br s, BEt$_3$-*C*H$_3$), 24.92 (s, N*i*Pr-*C*H$_3$), 32.50 (s, *t*Bu-*C*H$_3$), 34.81 (s, *t*Bu-*C*), 49.55 (s, N*i*Pr-*C*H), 115.59 (s, 5-NHC-*C*), 116.14 (s, 4,5-carb.-*C*), 122.27 (s, 2,7-carb.-*C*), 125.58 (s, 4-NHC-*C*), 126.42, 127.60, 128.40, 146.42 (s, carb.-*C*), 2-NHC-*C* not observed.

Preparative scale halide hydride exchange reaction of ***13^{Me}*** *with 2 eq. of LiHBEt$_3$*

A solution of LiHBEt$_3$ (0.049 g, 0.46 mmol) in THF (10 mL) at -78 °C was added to a colourless solution of **13^{Me}** (0.20 g, 0.23 mmol) in THF (20 mL) at -78 °C to afford a clear, colourless reaction mixture with a weak blue fluorescence under long wave UV light. The reaction mixture was stirred for *ca*. 2 h at -78 °C, at which point hexane (*ca*. 70 mL at -78 °C) was added to precipitate an off-white solid. The colourless supernatant was isolated by filtration and placed at -24 °C and the filtrant was dried *in vacuo* at -78 °C, redissolved in THF (20 mL), concentrated under vacuum (*ca*. 8 mL), and placed at -24 °C. After standing at this temperature for 5 days the mother liquor proved to be

unproductive and was warmed to room temperature over a period of *ca*. 1 h. During this time it changed colour from colourless to amber, deposited a grey to black solid, and its blue fluorescence under long wave UV light subsided. Small brown triangular prisms were grown at room temperature from the THF mother liquor. These were found to be suitable for X-ray diffraction structure determination and characterised as **18**. A vacuum dried aliquot of the room temperature stored mother liquor characterised as a complicated mixture of bimca^{Me} containing products by ^{1}H and ^{13}C NMR spectroscopy, including **16^{Me}** as the major product (*ca*. 50% by ^{1}H NMR). ^{1}H NMR (400 MHz, THF-d_8 with omission of unidentified minor components): δ -0.08 (m, 8H, BEt_3-CH_2), 0.11 (m, 4H, BEt_3-CH_2), 0.42 (t, $^{3}J_{HH}$ = 7.69 Hz, 12H, BEt_3-CH_3), 0.51 (t, $^{3}J_{HH}$ = 7.89, 6H, BEt_3-CH_3), 3.95 (s, 6H, NMe), 7.10 (d, $^{3}J_{HH}$ = 1.90 Hz, 2H, 5-NHC-*H*), 7.28 (d, $^{3}J_{HH}$ = 1.90 Hz, 2H, 4-NHC-*H*), 7.40 (d, $^{4}J_{HH}$ = 1.72 Hz, 2H, 2,7-carb.-*H*), 8.29 (d, $^{4}J_{HH}$ = 1.72 Hz, 2H, 4,5-carb.-*H*). ^{13}C NMR (100 MHz, THF-d_8, with omission of unidentified minor components): δ BEt_3-*C*H_2 signals not observed, 11.03 (s, BEt_3-*C*H_3), 11.78 (s, BEt_3-*C*H_3), 31.91 (s, *t*Bu-*C*H_3), 35.18 (s, *t*Bu-*C*), 37.35 (s, NMe), 117.38 (s, 4,5-carb.-*C*), 118.07 (s, carb.-*C*), 123.34 (s, 4-NHC-*C*), 123.59 (5-NHC-*C*), 124.44 (s, 2,7-carb.-*C*), 135.37, 139.20, 143.26 (s, carb.-*C*).

*Metathesis of K7^{iPr} with InBr to afford **19***

A solution of KHMDS (0.060 g, 0.30 mmol) in THF (5 mL) was added to a colourless suspension of **4^{iPr}** (0.075 g, 0.10 mmol) in THF (10 mL) to afford a yellow suspension that gradually turned brown with precipitated KI as a white solid, and developed a blue fluorescence under long wave UV light. The reaction mixture was stirred for 1 h, after which the brown supernatant was isolated by filtration and added to a stirred colourless solution of InBr (0.019 g, 0.10 mmol) in THF (20 mL). During 18 h of stirring the reaction mixture changed from brown to crimson, lost its blue fluorescence under long wave UV

light, and formed indium metal as a lustrous grey solid. Isolation of the red supernatant by filtration and removal of volatiles afforded a treacly dark amber solid that was triturated with hexane. Filtration and drying under vacuum yielded In(II) dimer complex **19** as small dark amber rectangular plates that were unsuitable for X-ray crystallographic studies (0.021 g, 19% in In). Microanalysis was not carried out on compound **19** due to its low yield and contamination of the crystalline material. ^{1}H NMR (300 MHz, THF-d_8): δ 0.35 (d, $^{3}J_{HH}$ = 6.91 Hz, 24H, N*i*Pr-C*H*$_3$), 1.51 (s, 36H, *t*Bu-C*H*$_3$), 4.07 (sept, $^{3}J_{HH}$ = 6.91 Hz, 4H, N*i*Pr-C*H*), 7.21 (s, 4H, 4-NHC-*H*), 7.62 (s, 4H, 2,7-carb.-*H*), 8.00 (s, 4H, 5-NHC-*H*), 8.23 (s, 4H, 4,5-carb.-*H*). ^{13}C NMR (100 MHz, THF-d_8): δ 22.39 (s, N*i*Pr-*C*H$_3$), 31.72 (s, *t*Bu-*C*H$_3$), 34.80 (*t*Bu-*C*), 49.48 (s, N*i*Pr-*C*H), 114.59 (s, 2,4,5,7-carb.-*C*), 118.24 (s, 4-NHC-*C*), 120.06 (s, 5-NHC-*C*), 125.09, 129.18, 138.28, 141.11 (s, carb.-*C*). IR (Nujol mull on NaCl plates, cm^{-1}): 1674 (*m*, *sh*), 1573 (*m*, *sh*), 1178 (*w*, *sh*), 1096 (*m*, *sh*), 1020 (*m*, *sh*), 932 (*m*, *sh*), 842 (*w*, *sh*), 802 (*m*, *sh*), 723 (*m*, *sh*). Mp: 192-196 °C (dec.).

*Halide hydride exchange reaction of [Tl(bimca^{iPr})I$_2$], **14^{iPr}**, with 2 eq. LiHBEt$_3$ monitored in situ by NMR spectroscopy*

THF-d_8 (0.5 mL) was condensed onto a solid mixture of **14^{iPr}** (0.021 g, 0.023 mmol) and LiHBEt$_3$ (0.0050 g, 0.047 mmol) at -196 °C. The solid reaction mixture was warmed to -50 °C to dissolve the reactants, aided by intermittent agitation by inversion over 15 minutes to give a clear beige reaction mixture with weak blue fluorescence under long wave UV light. Spectra were acquired at *ca*. 30 min intervals in 10 °C increments from -30 °C to room temperature. At room temperature the reaction mixture formed an amber precipitate and pale yellow supernatant with visible blue fluorescence under ambient and long wave UV light. ^{1}H NMR spectra of the reaction mixture below room temperature exhibited a multitude of intractable signals due to the highly transient and

reactive nature of the targeted [Tl(bimca^{iPr})H$_2$], **19^{iPr}**, which precluded the assignment of these resonances. ^{1}H NMR (400 MHz, THF-*d*$_8$, 25 °C): δ 0.02 (m, 8H, BEt$_3$-C*H*$_2$), 0.17 (m, 4H, BEt$_3$-CH$_2$), 0.56 (t, $^3J_{HH}$ = 7.48 Hz, 12H, BEt$_3$-C*H*$_3$), 0.75 (t, $^3J_{HH}$ = 7.63 Hz, 6H, BEt$_3$-C*H*$_3$), 1.43 (s, 18H, *t*Bu-C*H*$_3$), 1.48 (br d, 12H, N*i*Pr-C*H*$_3$), 5.55 (br sept, 2H, N*i*Pr-C*H*), 7.16 (br d, 4H, overlapping 4-NHC-*H* & 2,7-carb.-*H*), 7.35 (br d, 5-NHC-*H*), 8.08 (br d, 2H, 4,5-carb.-*H*). Note that signal broadening, likely due to high sample concentration, precluded calculation of coupling constants of some ^{1}H NMR signals.

*Preparative scale halide hydride exchange reaction of **14^{Me}** with 2 eq. of LiHBEt$_3$*

A solution of LiHBEt$_3$ (0.0089 g, 0.084 mmol) in THF (10 mL) at -78 °C was added to an orange solution of **14^{Me}** (0.075 g, 0.084 mmol) in THF (20 mL) at -78 °C to afford a clear, bright orange reaction mixture with a blue-yellow fluorescence under long wave UV light. The reaction mixture was stirred for *ca*. 2 h at -78 °C, whereupon volatiles were removed *in vacuo* at -78 °C to afford a bright orange powder with a yellow fluorescence under long wave UV light. A room temperature ^{1}H NMR (THF-*d*$_8$) spectrum of the solid product characterised as a *ca*. 1:1 mixture of **14^{Me}** and **16^{Me}**.

Chapter 4 – Group 14 bimca^R complexes

4.1 Introduction

Based on previous reports, bis(NHC) complexes of heavy divalent group 14 metals are rare and exceedingly difficult to isolate due to the reactivity of the electron rich metal centre.[143-145] The bis(IDipp) complexes reported by Turbervill and co-workers are particularly noteworthy as they represent the first examples of an "abnormal" neutral NHC (*a*NHC) binding mode on Sn(II), where one NHC is invariably forced into a C4-NHC binding mode following a 1,3-proton migration (Scheme 4.1).

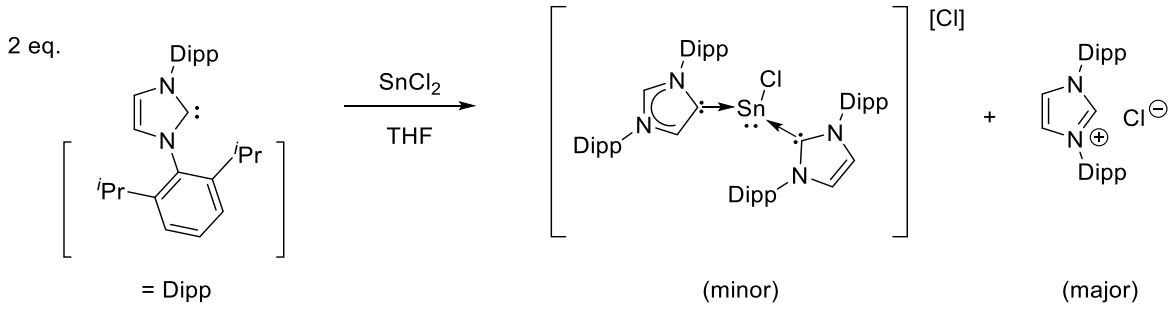

Scheme 4.1 Attempts to isolate bis(NHC) Sn(II) complexes resulting in the [Sn(*a*IDipp)(IDipp)Cl][Cl] complex as a minor co-product.[143]

The authors posit that the abnormally coordinated IDipp is a consequence of the steric demand of the *N*-2,6-diisopropylphenyl substituents, and that the resulting congestion around the Sn(II) metal centre forces abnormal binding of one NHC ligand to alleviate the steric pressure within the resulting cationic complex [Sn(*a*IDipp)(IDipp)Cl][Cl].[143] This behaviour has been reported before for sterically encumbered NHC ligands, albeit more commonly in combination with transition metal centres,[146,147] making [Sn(*a*IDipp)(IDipp)Cl][Cl] a rare example of an "abnormally" bound NHC (*a*NHC) complex with a main group element.[148-150] Turbervill and co-workers detail that the preparation of these complexes using a tin(II) precursor, either $SnCl_2$ or $Sn(OTf)_2$, with

two equivalents of free IDipp NHC invariably led to the production of large amounts of the corresponding IDipp·HX imidazolium salt, even under strictly anaerobic conditions.

The authors were unable to elucidate the exact mechanism of this facile protonation, but speculate that the complex is able to deprotonate the THF solvent. This they substantiated by monitoring the persistent and gradual decomposition of the tin(II) product in solution to imidazolium by-products by ^{1}H NMR spectroscopy.[143] The speculated instability of tin(II) bis-NHC complexes may lie in the redox flexibility of divalent tin, which is anticipated to be enhanced by strong electron donors, such as NHCs, allowing for oxidative addition of suitable substrates.[75]

Building on the *s*-block studies of Hill and co-workers, who prepared ionic bis(IDipp) complexes of the form [M'(IDipp)$_2$][M''(HMDS)$_3$] (M' = Li, Na, K and M'' = Mg, Ca, Sr, Ba) by reaction of two equivalents of IDipp with one equivalent of each M'HMDS and [M''(HMDS)$_2$],[103] Goicoechea and co-workers presented several carbanionic ("dicarbene") *a*NHC' complexes of Ge(II) and Pb(II),[144] generated from the addition of a potassium dicarbene, [K(*a*NHC')], to [M(HMDS)$_2$] (M = Ge, Pb) to form [K][M(*a*NHC')(HMDS)$_2$] in solution. Such compounds were observed to undergo irreversible ligand redistributions to form the crystalline [M(*a*IDipp')$_2$(HMDS)]$^-$ complexes and the homoleptic [M(HMDS)$_3$]$^-$ compounds (Scheme 4.2).[144] Interestingly, Goicoechea *et al*. note that an analogous ligand rearrangement is not observed for [Sn(*a*IDipp')(HMDS)$_2$]$^-$.[144]

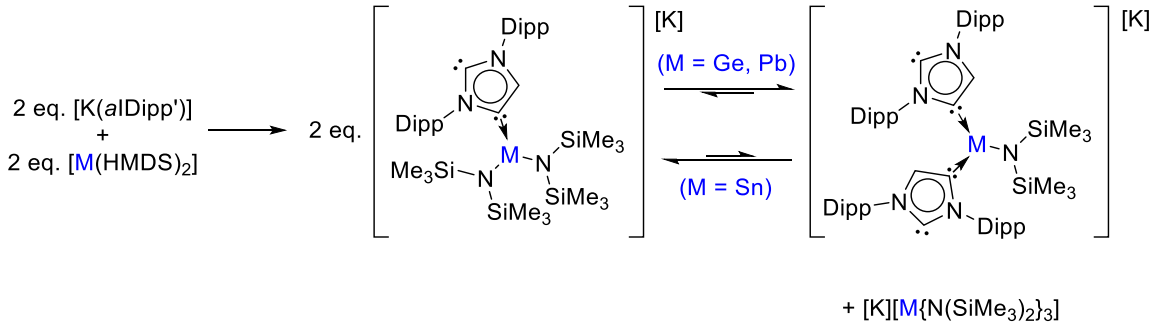

Scheme 4.2 The preparation of divalent group 14 complexes of the anionic NHC *a*IDipp' reported by Goicoechea.[144]

4.1.1 Purpose of this chapter

The aim of this chapter is to assess the coordination chemistry of heavy group 14 metals, particularly in the divalent oxidation state, with the bimca^{R} pincer ligand. For our purposes, the added entropic stabilisation of the bimca^{R} pincer framework makes this ligand a good candidate for probing the outcomes of such bis(NHC) coordination. Additionally, the isolation of the In(II) dimer **17** in Chapter 3 evidences that the bimca^{R} scaffold can support low valent main group metal centres. At the outset of this chapter, low valent group 14 hydride complexes are also a focus, for their fundamental study and their potential downstream synthetic utility.

4.2 Results and discussion[4]

As discussed in Chapter 3, Section 3.2, bimca^{R} metallation strategies may be grouped into two categories. In the specific context of divalent group 14 species these are (i) 1:1 stoichiometric salt metatheses employing *s*-block bimca^{R} reagents (Chapter 2, Sections 2.3.4 and 2.5.1) with a MX_2 precursor (M = Sn, Pb; X = halide or pseudo-halide) to afford

[4]The majority of the synthetic work presented in this Chapter was conducted at the University of Tübingen in the group of Prof. Doris Kunz.

the [M(bimca^{R})X] complex and an *s*-block halide co-product, or (ii) a protic bimca^{R} precursor is reacted with a divalent group 14 species equipped with suitably basic co-ligands, *e.g.* [M(HMDS)$_2$], with protolysis leading to [M(bimca^{R})X] and HHMDS (Scheme 4.3).

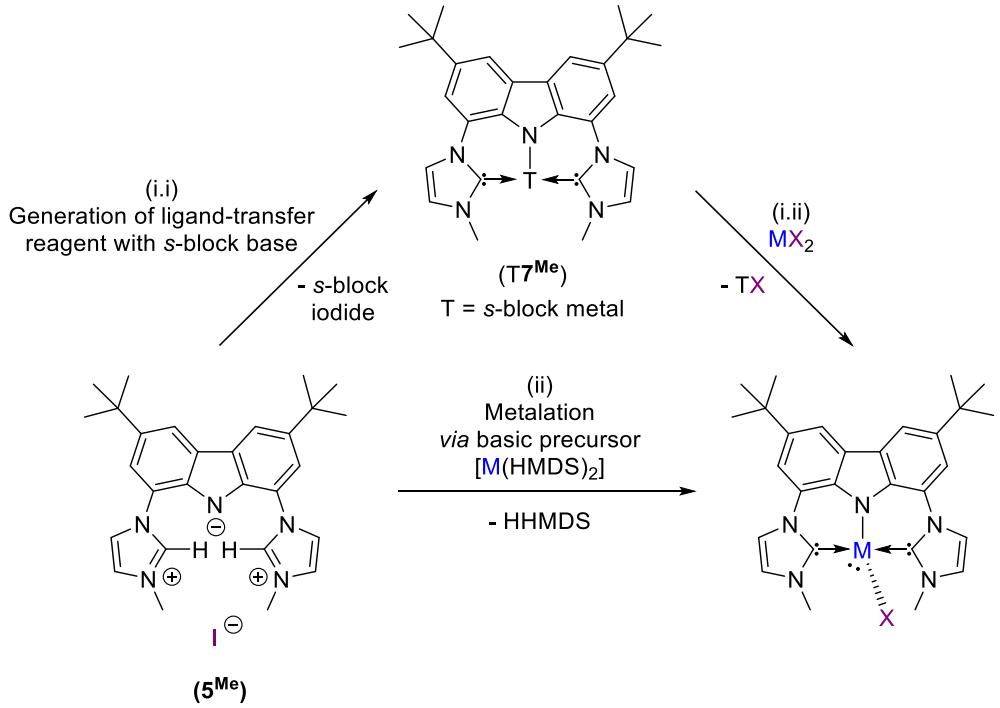

Scheme 4.3 Synthetic strategies (i and ii) for accessing [M(bimca^{Me}I] complexes where R = HMDS, M = Sn(II), Pb(II), and T = *s*-block metal.

Metalation path (ii) is particularly attractive for Pb(II) chemistry, where metathesis reactions proceeding *via* (i) are anticipated to be sluggish if not prohibited by the low solubility of Pb(II) halides. By contrast, [Pb(HMDS)$_2$] is soluble in all common laboratory solvents used for main group organometallic synthesis. Thus, with straightforward access to the diprotic bimca^{Me}(H$_2$I) proligand, **5^{Me}** (*cf.* Chapter 2, Section 2.3.1) the preparation of [M(bimca^{Me})X] complexes was attempted using the protolysis strategy (ii in Scheme 4.3) as the primary route. This has analogies to the magnesium studies detailed in Chapter 2 using [Mg(HMDS)$_2$].

4.2.1 Synthesis of [M(HMDS)$_2$] precursors

The hexamethyldisilazides of Sn(II) and Pb(II) are easily synthesised from metatheses with the respective M(II) chlorides and LiHMDS in diethyl ether.[24] Interestingly, in our hands, use of sodium and potassium HMDS salts did not achieve metathesis when using $PbCl_2$ (the original report makes no mention of the use of heavier alkali metal HMDS compounds). By contrast, PbI_2 reacts with NaHMDS and KHMDS to give [Pb(HMDS)$_2$], perthaps because the electropositvity of the alkali metal cation and ionic composition of the halide salt co-product are determinant in achieving metathesis, where compatible "hard" and "soft" donor/acceptor pairs in the resulting products dictate reactivity, *viz*. LiCl *vs*. Na/KCl (Scheme 4.4). It is worth noting that the bis(HMDS) complexes of Sn(II) and Pb(II) are both dense liquids at room temperature, thus these reagents were generated and used *in situ* or as hexane stock solutions to aid subsequent manipulations.

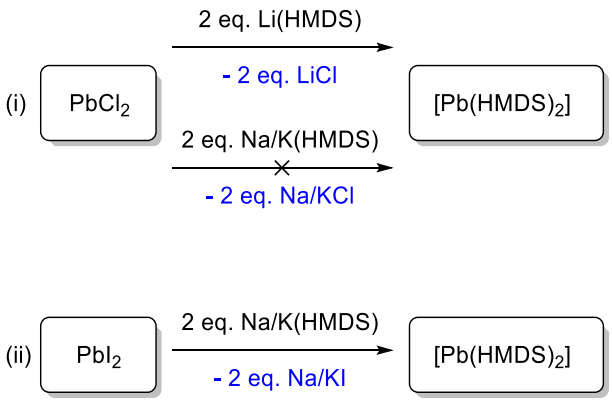

Scheme 4.4 Reactivity profile of Pb(II) halides with alkali metal hexamethyldisilazides.

*4.2.2 Protolysis of bimca^{Me}(H$_2$I), **5^{Me}**, with [Sn(HMDS)$_2$]*

With access to both [M(HMDS)$_2$] and bimca^{Me}(H$_2$I), **5^{Me}**, reagents, metallation *via* path (ii) (Scheme 4.3 above) was carried out by the addition of a diethyl ether solution of [Sn(HMDS)$_2$] to an equimolar yellow THF suspension of the bimca^{Me}(H$_2$I) salt. The reaction mixture did not change colour or appearance after extended stirring at room

temperature but paled in colour after a period of reflux under an inert atmosphere. Filtration of the resultant suspension yielded a pale yellow poorly soluble solid upon work up, **21^{Me}**, which was found to be of the same composition as the filtrant by ^{1}H NMR spectroscopy (THF-*d*$_8$). The ^{1}H NMR spectrum of **21^{Me}** exhibits a shift and signal integral profile indicative of either a 1:1 solution of two symmetrical bimca^{Me} products (deduced from their signal integrals) or a single unsymmetrical bimca^{Me} product, as deduced from the duplication of resonances for the *N*-methyl protons at 2.60 ppm and 4.46 ppm, and similarly for the *tert*-butyl methyl resonances at 1.52 ppm and 1.54 ppm. There are also nine distinct imidazolyl and carbazolide proton resonances between 6.70 ppm and 10.59 ppm, the low field resonance being consistent with an imidazolium moiety. Attempts to verify the presence of either one or two products by two-dimensional NMR experiments were unsuccessful but a single unsymmetrical product with an imidazolium moiety was deemed more likely in view of a structurally characterised unsymmetrical and monoprotic [W(bimca^{Me}H)CO$_4$] complex from the Kunz group that exhibits a strikingly similar chemical shift profile to **21^{Me}** (*vide infra*, Table 4.1), (Scheme 4.5).[151]

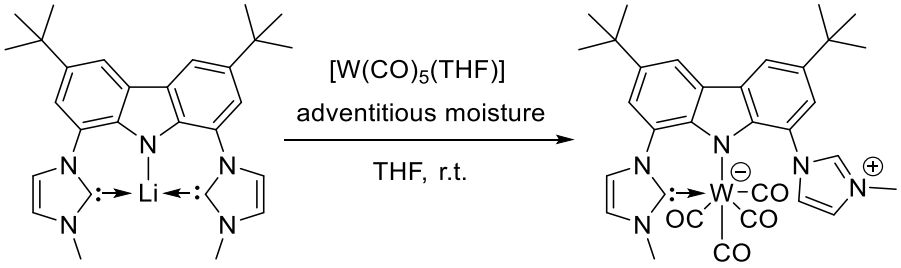

Scheme 4.5 Generation of a monoprotic, unsymmetrical [W(bimca^{Me}H)CO$_4$] complex from [Li(bimca^{Me})] and [W(CO)$_5$(THF)].[151]

Indeed, a similar unsymmetrical bimca^{R} species was isolated during our initial attempts to prepare [Ga(bimca^{Me})I$_2$], **12^{Me}**, in Chapters 2 and 3 due to partial hydrolysis of the

intended product. This resulted in the isolation of the monoprotic Ga(III) complex [Ga(bimca'^{Me}H)I_2][I] (**22^{Me}**), which is discussed here due to its clear similarity to **21^{Me}**.

The poorly soluble protic bimca^{Me} complex **22^{Me}** was isolated as several small crystals from the THF reaction mother liquor for [Ga(bimca^{Me})I_2], **13^{Me}** from the reaction of [Mg(bimca^{Me})I(THF)] (**9^{Me}**) with GaI_3. We reason that **22^{Me}** results from partial hydrolysis of the **9^{Me}** reagent as freshly prepared **9^{Me}** led to clean **12^{Me}**. The crystallinity of **22^{Me}** permitted its structure determination by single crystal X-ray diffraction. Unfortunately, the size and quality of crystals grown (fluorobenzene solution placed at 4 °C) were insufficient for full anisotropic refinement, but the atomic connectivity and composition of **22^{Me}** have been firmly established by partial anisotropic refinement of the data (Figure 4.1).

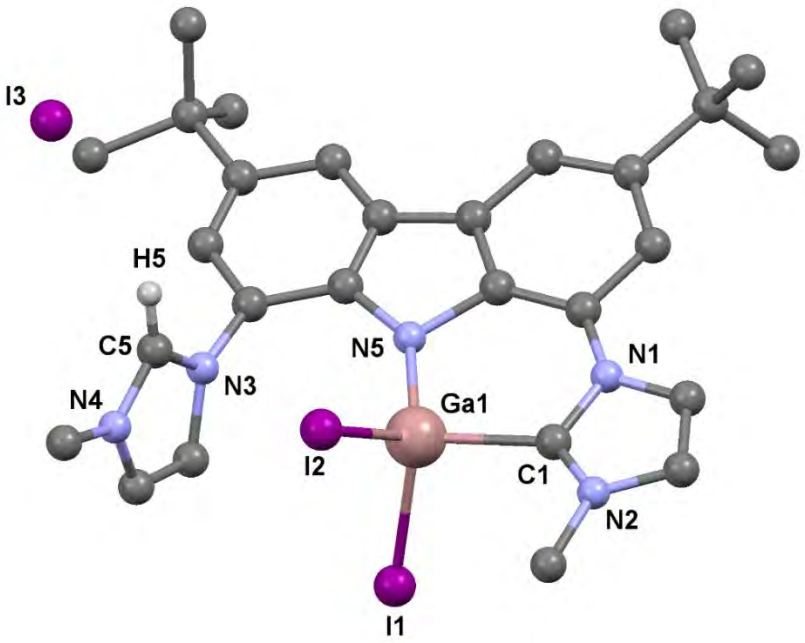

Figure 4.1 van der Waals' sphere (arbitrary radius) representation of the monoprotic, unsymmetrical [Ga(bimca'^{Me}H)I_2][I], **22^{Me}**. H-atoms are omitted for clarity, excepting imidazolium proton H5.

Complex **22^{Me}** crystallises in the triclinic space group $P\bar{1}$ with one unique ion pair and a heavily disordered fluorobenzene molecule of low chemical occupancy in the asymmetric unit. The latter was removed using a solvent mask (OLEX 2). All atoms were refined isotropically excepting the gallium and iodine atoms, which were refined with anisotropic displacement parameters, and all hydrogen atoms were placed in calculated positions (riding model). The molecular structure of **22^{Me}** clearly exhibits inequivalent imidazolyl environments, wherein one moiety coordinates the gallium(III) metal centre as the NHC and the second is present as an imidazolium cation. Coordination of carbenic C1 to Ga1 elicits a distorted tetrahedral geometry around the metal centre, which is consistent with other mono(NHC) adducts of gallium(III) halides.[123] The near orthogonal orientation of the imidazolium ring and the projection of the NCN group toward the iodide counterion (I3) are consistent with the protonation of C5 and thus imidazolium formation. Owing to the poor quality of the data, bonding parameters are not discussed further.

The inequivalent imidazolyl environments of **22^{Me}** are also reflected in its ^{1}H and ^{13}C NMR spectra (THF-d_8), wherein a ^{1}H singlet at 9.79 ppm and its ^{1}H-^{13}C HSQC correlation to the ^{13}C singlet at 139.35 ppm is consistent with imidazolium formation. ^{1}H-^{1}H NOESY and TOCSY correlations of the imidazolium C2-H resonance to the *N*-methyl singlet at 4.11 ppm distinguish this resonance from the *N*-methyl singlet of the NHC moiety at 4.16 ppm, each with relative resonance integrals of 3. The latter also exhibits a ^{1}H-^{13}C HMBC correlation to a carbenic resonance at 154.41 ppm in the ^{13}C NMR spectrum of **22^{Me}**, which is shifted upfield relative to the analogous carbenic ^{13}C resonance in the intended bis(NHC) gallium complex; [Ga(bimca^{Me})I$_2$], **12^{Me}**, at 167.26 ppm (Chapter 3, Section 3.4.2).

*4.2.3 Unsymmetrical monoprotic Sn(II) complex **21^{Me}***

In light of the tungsten carbazolide imidazolium species isolated during Kunz's studies and the preceding gallium complex **22^{Me}**, it seemed plausible that the **21^{Me}** isolated from the reaction of **5^{Me}** and [Sn(HMDS)$_2$] may be an unsymmetrical monoprotic Sn(II) complex. For example, the imidazolium C2 proton of **21^{Me}** was identified as a second order triplet at 10.59 ppm in its ^{1}H NMR spectrum and is substantiated by its ^{1}H-^{1}H NOESY and COSY correlations to the *N*-methyl resonance at 4.46 ppm (Figure 4.2). Interestingly, a singlet at 0.04 ppm is also observed for **21^{Me}** with a relative signal integral of 18. This is consistent with the presence of a non-volatile HMDS containing group in **21^{Me}** and is in agreement with the chemical shift value reported by Goicoechea (*vide supra*) for the HMDS group of K[Sn(HMDS)$_2$(*a*IDipp')] (0.04 ppm in THF-*d*$_8$).[144] As the amine HHMDS is a volatile species, as is the tin(II) precursor [Sn(HMDS)$_2$], (*cf*. work up conditions include drying the reaction products under vacuum at 100 °C), the observation of a HMDS resonance leads us to suspect that either (i) [Sn(HMDS)$_2$] is insufficiently basic to achieve two-fold deprotonation of **5^{Me}**, and thus retains a Sn-HMDS fragment and one imidazolium moiety in the product, or (ii) the anticipated [Sn(bimca^{Me})I] product activates HHMDS under the reaction conditions (*vide infra*) with both pathways leading to a product of the composition [Sn(bimca'^{Me}H)(HMDS)][I].

Further signal correlations for the *N*-methyl environment at 4.46 ppm with C4 and C5 proton signals at 8.78 ppm and 8.37 ppm support its connection to an imidazolium fragment. Combined with the aforementioned C2 proton resonance, these signals and their multiplicity are similar to those of the imidazolium precursor **5^{Me}**, the aforementioned imidazolium containing gallium(III) complex **22^{Me}**, and the tungsten species from Kunz (Table 4.1).

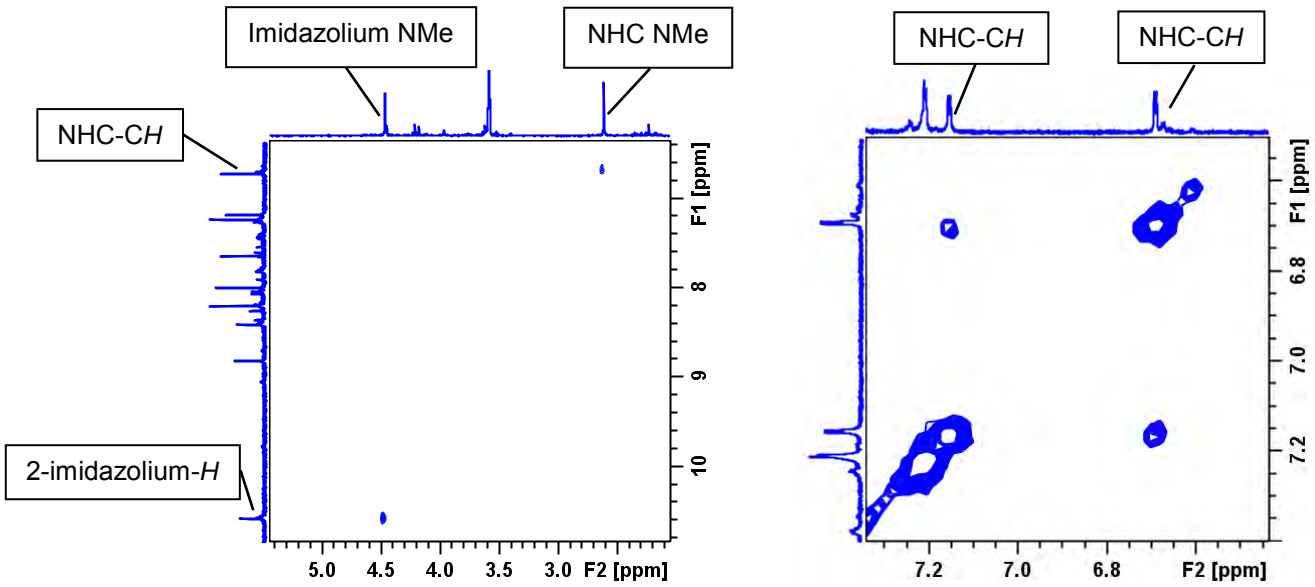

Figure 4.2 Excerpts from the ^{1}H NMR ^{1}H-^{1}H NOESY (left) and COSY (right) spectra of **21^{Me}** showing NOE correlations of the two methyl proton singlets with the imidazolyl proton resonances, and coupling of the imidazolyl proton resonances, respectively.

Proton environment	**21^{Me}** (ppm)	**22^{Me}** (ppm)	**5^{Me}** (ppm)	**[W(LH)CO$_4$]** (ppm)
Imidazolium *N*-methyl	4.45	4.11	4.32	4.00
Imidazolium C4	8.78	7.75	7.61	7.64
Imidazolium C5	8.37	7.96	8.21	8.05
Imidazolium C2	10.59	9.79	11.25	9.10

Table 4.1 Tabulated resonance chemical shifts (THF-d_8) for the imidazolium moieties of Sn(II) complex **21^{Me}**, monoprotic Ga(III) complex **22^{Me}**, the diprotic proligand **5^{Me}**, and the [W(bimca^{Me}H)CO$_4$] complex studied by the Kunz group.[151]

The strongly upfield shifted resonance at 2.60 ppm in the ^{1}H NMR (THF-d_8) spectrum of **21^{Me}**, which is attributable to an *N*-methyl environment, is noteworthy since these are

normally observed at 4.0 ppm (± 0.5 ppm) in the previously discussed bimca^{Me} complexes (Chapters 2 and 3). Correlations for this resonance using ^{1}H-^{1}H COSY and NOESY experiments determined that this *N*-methyl environment is part of a NHC, associated with imidazolyl signals at 6.70 ppm and 7.17 ppm (Figure 4.2 above).

The unsymmetrical nature of **21^{Me}** is also displayed in the remaining chemically distinct carbazolide aryl proton resonances at 7.22 ppm, 7.63 ppm, 7.99 ppm, and 8.19 ppm, each with a relative signal integral of 1. Thus, while the exact coordination environment of this complex cannot be determined solely by NMR spectroscopic experiments, we tentatively suggest that the coordinated NHC in **21^{Me}** (*cf.* *N*-methyl resonance at 2.60 ppm) is consistent with an "abnormal" C5 bound carbene, *cf.* *a*IDipp coordination to Sn(II) (*vide supra*, Scheme 4.6).[143] This is further borne out by the absence of a NOE correlation between the doublets of the NHC bound protons, which is typically observed for the C4-C5 protons in bimca^{Me} complexes containing C2 bound NHC donors (Scheme 4.6).

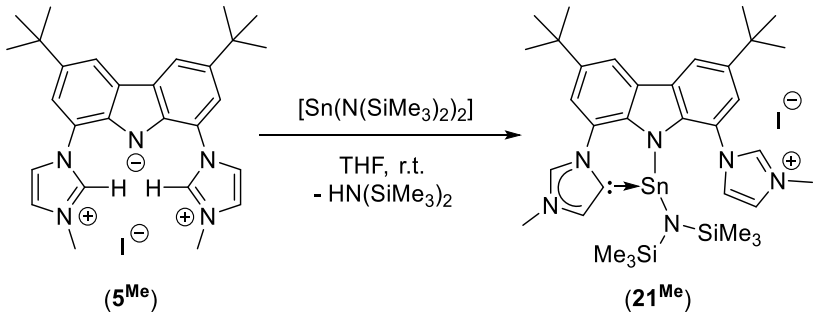

(**5^{Me}**) (**21^{Me}**)

Scheme 4.6 Possible outcome of 1:1 reaction of [Sn(HMDS)$_2$] with bimca^{Me}(H$_2$I) (**5^{Me}**).

Unfortunately, quaternary ^{13}C resonances, including the carbenic NHC resonance of **21^{Me}**, could not be identified in its ^{13}C NMR or two-dimensional ^{1}H-^{13}C NMR spectra due to its low solubility or instability in common deuterated solvents. For example, NMR experiments in dichloromethane-d_2 resulted in decomposition of **21^{Me}** to a mixture of unidentifiable protic bimca^{Me} species as evidenced by numerous sets of multiplets in the

aryl shift region of its ^{1}H NMR spectrum. Moreover, attempts to grow crystals of **21^{Me}** to assess its connectivity in the solid state were unsuccessful due to its poor solubility or instability in the available recrystallisation solvents.

4.2.4 Salt metathesis of K(bimca^{Me}) with $SnCl_2$

To rule out the possibility of stymied reactivity of the [Sn(HMDS)$_2$] as the origin of single NHC coordination, the preparation of a [Sn(bimca^{Me})X] species was attempted *via* metathesis path (i) (Scheme 4.3) using K(bimca^{Me}), K**7^{Me}**, and $SnCl_2$, rather than the protolysis of **5^{Me}** with [Sn(HMDS)$_2$]. The K(bimca^{Me}) reagent was generated *in situ* from the reaction of two or three equivalents of KHMDS with either bimca^{Me}(H$_2$I) (**5^{Me}**) or Hbimca^{Me}(2HI) (**4^{Me}**) respectively as per the methods outlined in Chapter 2, Section 2.3.4. The resulting brown, blue fluorescent K**7^{Me}** containing reaction mixture was separated from its precipitated KI co-product by filtration and added directly to a THF solution of $SnCl_2$ resulting in a colour change from brown to crimson and a loss of blue fluorescence under long wave UV light. Filtration followed by removal of volatiles *in vacuo* with heating afforded a red solid that exhibits similar ^{1}H NMR spectroscopic characteristics to **21^{Me}**, *i.e.* the formation of an unsymmetrically coordinated, metal complex of monoprotic bimca^{Me}. For example, the ^{1}H NMR (THF-d_8) spectrum of **23^{Me}** indicates the presence of NHC- and imidazolium resonances with equal signal integrals. However, unlike **21^{Me}**, the NHC *N*-methyl resonance of **23^{Me}** is placed at 4.01 ppm, which is consistent with a "normally" bound *N*-methyl NHC. The imidazolium moiety resonances are at similar chemical shifts to those of **21^{Me}** (*vide infra*, Table 4.2).

Perhaps the most noteworthy aspect of the ^{1}H NMR spectrum of **23^{Me}** is a singlet resonance at 0.04 ppm with a signal integral of 18 relative to the resonances of the bimca^{Me} scaffold (*cf.* ^{1}H NMR singlet at 0.04 ppm in **21^{Me}**). The chemical shift and

integration of this signal are consistent with the inclusion of coordinated HMDS and its integration value does not change when the solid sample is warmed to 100 °C under vacuum for *ca*. 3 hours, *cf*. workup of **21^{Me}**. It should be emphasised that this ^{1}H NMR resonance (as well as the HMDS resonance observed for **21^{Me}**) are distinguishable from those of silicon grease at 0.11 ppm and free [Sn(HMDS)$_2$] at 0.28 ppm in THF-d_8. Furthermore, despite the meticulous air sensitive methods used during the syntheses of **21^{Me}** and **23^{Me}**, the monoprotic NHC/imidazolium HMDS inclusion products were observed persistently as the sole isolable reaction product across multiple syntheses.

The remaining signals of the ^{1}H NMR spectrum for **23^{Me}** (THF-d_8) are consistent with the proposed monoprotic bimca^{Me} product depicted in Figure 4.3, which is similar to the gallium bimca^{Me} complex **22^{Me}**.

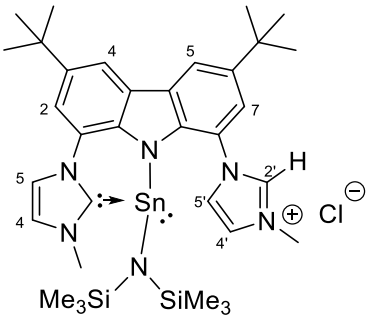

Figure 4.3 Proposed composition of Sn(II) bimca^{Me}H complex **23^{Me}**.

The singlet attributable to the *N*-methyl protons of the NHC moiety at 4.09 ppm displays NOE correlation to the doublet at 7.61 ppm, which is placed at a typical chemical shift for C4 bound protons on coordinated bimca^{Me} species. The ^{1}H-^{1}H COSY correlation between the doublets at 7.61 ppm and 8.37 ppm is consistent with that of imidazolyl C4/C5 protons on related NHCs and bimca^{Me} complexes presented herein. Furthermore, the doublet attributable to the NHC C5 proton resonance (8.37 ppm) exhibits a NOE

correlation to the carbazolide 2-position doublet (7.83 ppm), while a comparable suite of ^{1}H-^{1}H NOE and COSY correlations are observed for the imidazolium fragment of the bimca^{Me}H molecule. The connectivity of these two halves and the single product outcome of this reaction is supported by the resonances of the remaining magnetically inequivalent carbazolide 4,5-position aryl protons, which were identified by their ^{1}H-^{1}H COSY interactions to the carbazolide 2- and 7-position protons, consequently allowing for the assignment of the ^{1}H NMR singlets of the inequivalent *tert*-butyl groups. The most upfield of these (1.48 ppm) exhibits NOE correlations to the doublets of the 5,7-carbazolide protons, whilst the singlet at 1.52 ppm may be assigned to the second *tert*-butyl group through similar NOE correlations to the 2,4-carbazolide protons (Figure 4.4). It is worth noting that the signals of the 4,5-carbazolide protons do not exhibit NOE correlations to one another, presumably due to their spatial separation. This is unsurprising since the analogous signals of the structurally authenticated monoprotic gallium complex, **22^{Me}**, and the preceding tin complex, **21^{Me}**, likewise do not exhibit such correlations.

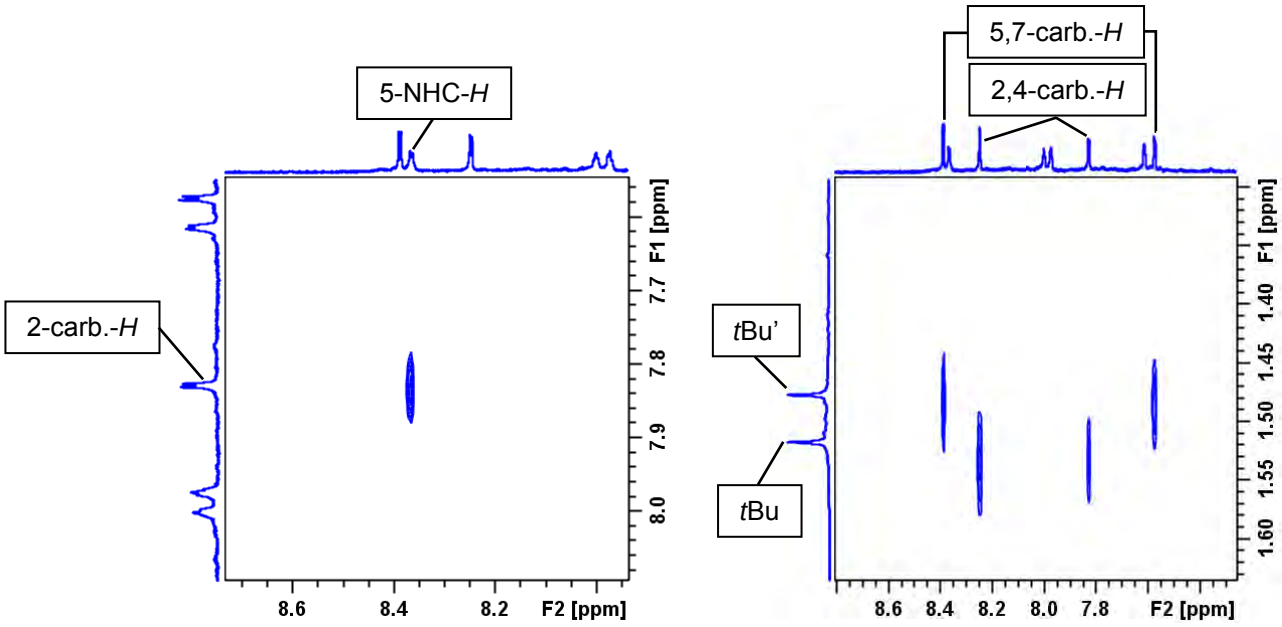

Figure 4.4 Excerpts of the ^{1}H-^{1}H NOESY spectrum of **23^{Me}** showing NOE correlations between the 5-NHC proton doublet and the 2-carbazole proton doublet (left) and NOE correlations between the two *tert*-butyl groups and carbazolide aryl resonances.

In view of the genesis of the method for accessing **23^{Me}**, *i.e.* the suspected incomplete deprotonation of **5^{Me}** by [Sn(HMDS)$_2$], this outcome strongly suggests that a nascent [Sn(bimca^{Me})X] (X most likely Cl) species activates the N-H bond of residual HHMDS (*cf.* preparation of K**7^{Me}**) amine in the reaction medium to afford a species that represents an imidazolium chloride analogue of **21^{Me}** with the same inclusion of an HMDS co-ligand (Scheme 4.7).

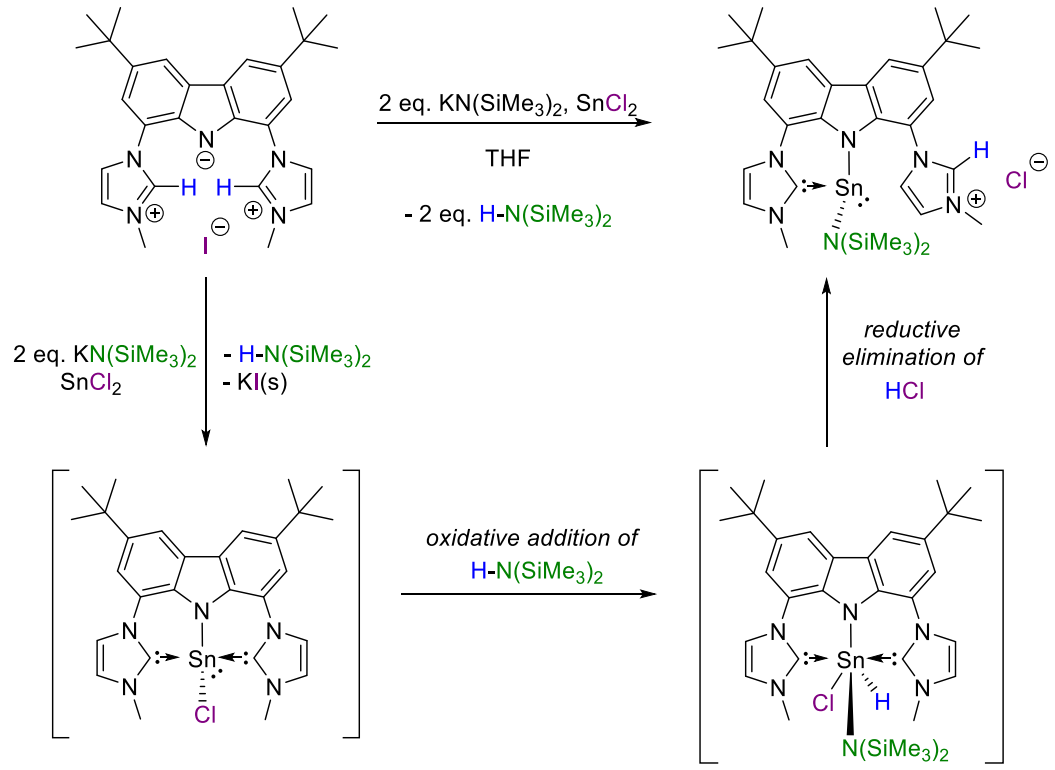

Scheme 4.7 Proposed mechanism for the generation of the monoprotic unsymmetrical bimca^{Me}H complex **23^{Me}**.

The activation of N-H bonds by Sn(II) systems has been reported by Power *et al.* who exemplified this kind of behaviour on sterically activated Sn(II) bis(2,6-terphenyls), which are able to react with ammonia under mild conditions to give amido bridged Sn(II) dimers, (*cf.* Chapter 1, Section 1.2).[13] A feature of this reaction is the elimination of one equivalent of protonated ligand from what is presumed to be a Sn(IV) hydride intermediate that is reached through oxidative addition of ammonia to the Sn(II) metal centre. We hypothesise that the expected bis(NHC) species; [Sn(bimca^{Me})Cl] enters a similar redox pathway whereby the residual HHMDS (*cf.* preparation of K**7^{Me}** from KHMDS) oxidatively adds to the Sn(II) metal centre to form a sterically congested [Sn(bimca^{Me})(Cl)(H)(HMDS)] Sn(IV) intermediate, which reductively eliminates HCl through formation of an imidazolium function on the bimca^{Me} pincer. This proposed

mechanism is also consistent with, but not conclusive evidence for, the formation of **21^{Me}**, whereby a [Sn(bimca^{Me})I] intermediate could also activate HHMDS in a similar manner as both reaction mixtures contain free HHMDS amine. Taking this into consideration, it is possible that the steric demand of the iodide co-ligand in [Sn(bimca^{Me})I] may cause the NHC to adopt an "abnormal" binding mode *vis-à-vis* the normal binding mode postulated in **23^{Me}**.

Upon storage of **23^{Me}** at -24 °C in THF solution, degradation was observed by ^{1}H NMR spectroscopy over 24 hours with full decomposition after *ca*. 3 days. This resulted in broad indistinguishable signals in the ^{1}H NMR spectrum of the decomposed **23^{Me}**. This unexpected instability is possibly caused by the latent reactivity of the HMDS co-ligand, which may act as a source of base that initiates further deprotonation of the bimca^{Me} scaffold, causing slow decomposition. This instability frustrated crystallographic studies of **23^{Me}**, wherein all attempts at recrystallisation resulted in decomposition before samples of suitable quality could be isolated. Furthermore, two-dimensional NMR correlation experiments on **23^{Me}** could only provide information on the connectivity of the bimca^{Me} ligand and failed to give further information on the chemical environment of the HMDS co-ligand, perhaps due to a combination of its distal position relative to other protons on the ligand scaffold, and a sufficiently different relaxation rate, which would serve to hinder the detection of correlated signals as per typical ^{1}H-^{1}H NOESY experiments.

Attempts to further characterise **23^{Me}** by high resolution mass spectrometry were made difficult by its air- and moisture sensitivity, as evidenced by the overwhelming presence of a fragment of *m/z* 136.11, which may be attributed to the molecular ion $[SnO + H]^{+}$, likely produced during sample preparation.

In order to leverage more information on the redox decomposition pathway and subsequent formation of **23^{Me}**, a method for the purposeful synthesis of a monoprotic, unsymmetrical derivative was devised, thereby probing the general stability and likelihood of forming such compounds under the previous reaction conditions. Replacement of the HMDS co-ligand for a less reactive chloride substituent was also deemed crucial in order to produce a more stable complex that could be characterised.

4.2.5 Direct synthesis of a monoprotic, unsymmetrical Sn(II) bimca^{Me}(H) complex

To this end, [Sn(bimca^{Me}H)(Cl)][Cl], **24^{Me}**, was targeted from the reaction of bimca^{Me}(H), **6^{Me}** with $SnCl_2$, Scheme 4.8 (see Chapter 2, Section 2.3.3 for the preparation of **6^{R}** compounds).

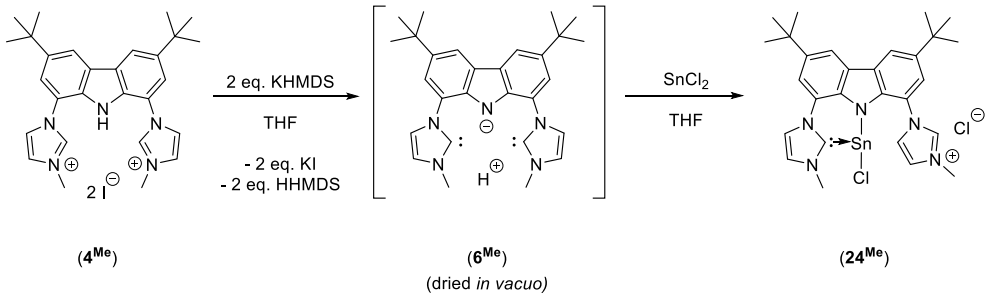

Scheme 4.8 Direct strategy for obtaining [Sn(bimca^{Me}H)(Cl)][Cl], **24^{Me}** from **4^{Me}** *via* reaction of **6^{Me}** with $SnCl_2$.

The monoprotic proligand **6^{Me}** was synthesised by the addition of one equivalent of KHMDS to bimca^{Me}(H_2I) (**5^{Me}**) to give an amber suspension. A ^{1}H NMR (THF-d_8) spectrum of the reaction mixture *in situ* (t < 10 min) confirmed the expected A:B:B:A chemical shift pattern for **6^{Me}**, including a broad singlet at 10.39 ppm. This is attributable to the single "fluxional environment" bimca^{Me}(*H*) proton of **6^{Me}** (Chapter 2, Section 2.3.3). To ensure the absence of HHMDS amine, which was expected to cause complications in the subsequent step, volatiles were removed under vacuum. The

resulting amber solid was then resuspended in THF-d_8 and reacted with a stoichiometric quantity of solid $SnCl_2$. This afforded an immediate colour change from amber to a slightly opaque orange, and a subsequent ^{1}H NMR spectrum of the reaction mixture indicated the clean formation of a monoprotic, unsymmetrical bimca^{Me}·HCl complex consistent with the composition [Sn(bimca^{Me}H)(Cl)][Cl], **24^{Me}**.

Unlike **21^{Me}** and **23^{Me}**, **24^{Me}** proved to be indefinitely stable in solution at room temperature, presumably due to replacement of the HMDS group with a more inert chloride co-ligand (*cf*. HMDS in **21^{Me}** and **23^{Me}**). This increased stability, relative to **21^{Me}** and **23^{Me}**, also allowed for the acquisition of ^{13}C NMR data for **24^{Me}**, although acquisition experiments and sample concentrations that would allow for the resolution of a likely Sn-C coupling could not be achieved.

A singlet at 174.98 ppm in the ^{13}C NMR spectrum of **24^{Me}**, is assigned to the carbenic carbon of the NHC moiety Two-dimensional ^{1}H-^{13}C HSQC experiments were able to verify the presence of an imidazolium C2 carbon with a resonance at 140.05 ppm, which correlates to the imidazolium proton resonance at 9.65 ppm in the ^{1}H NMR spectrum.

The ^{1}H NMR chemical shift pattern of **24^{Me}** is strikingly similar to that of bimca^{Me} HMDS complex **23^{Me}**, with clearly distinguishable NHC and imidazolium environments that produce two *N*-methyl singlets at 3.99 ppm and 4.20 ppm, respectively. A comparison of the aryl regions of the three unsymmetrical Sn(II) complexes **21^{Me}**, **23^{Me}** and **24^{Me}** is shown in Figure 4.5, with salient chemical shift data in Table 4.2 (gallium(III) complex **22^{Me}** is included for comparison).

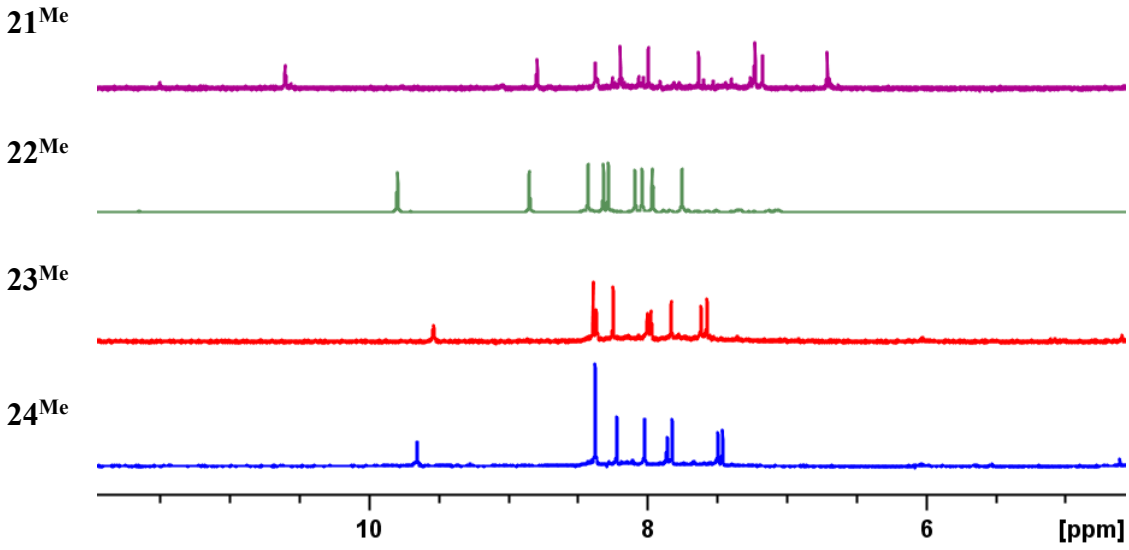

Figure 4.5 Comparison of an excerpt of the aryl region of the ^{1}H NMR spectra of **21^{Me}**, **22^{Me}**, **23^{Me}**, and **24^{Me}**.

Proton environment	21^{Me} (ppm)	22^{Me} (ppm)	23^{Me} (ppm)	24^{Me} (ppm)
NHC *N*-methyl	2.60	4.16	4.09	3.99
NHC C4	6.70	8.09	7.61	7.49
NHC C5 or C2 for 21^{Me}	7.17	8.85	8.37	8.37
Imidazolium *N*-methyl	4.46	4.11	4.20	4.20
Imidazolium C4	8.78	7.75	7.98	7.86
Imidazolium C5	8.37	7.96	8.00	8.02
Imidazolium C2	10.59	9.79	9.54	9.65
Carbazolide 2	7.22	8.04	7.83	7.82
Carbazolide 4	7.99	8.32	8.25	8.22
Carbazolide 5	8.19	8.43	8.39	8.37
Carbazolide 7	7.63	8.28	7.57	7.46

Table 4.2 Comparison of salient ^{1}H NMR (THF-d_8) chemical shift data for **21^{Me}**, **22^{Me}**, **23^{Me}**, and **24^{Me}**.

From the distinct entry paths to **21^{Me}**, **23^{Me}**, and **24^{Me}** it may be concluded that, in the case of **23^{Me}** and possibly **21^{Me}**, the latent reactivity of the Sn(II) electron lone pair facilitates

the oxidative addition of HHMDS in the reaction milieu with reductive elimination of HX as the pendant imidazolium moiety. These unexpected products hampered progress towards an analogous Sn(II) hydride complex through halide-hydride exchange approaches (*cf.* Chapter 3 Section 3.7), which appear to be inappropriate for such ionic complexes especially in view of the likely HMDS (and not halide) coordination at **21^{Me}** and **23^{Me}**. To evaluate this the attempted chloride-hydride exchange of **24^{Me}** with one and two equivalents of KHB*sec*Bu$_3$ was attempted (*cf.* use of LiHBEt$_3$ in Chapter 3, Section 3.7.1). It should be noted that the basicity of borohydride reagents, like LiHBEt$_3$, has been shown to generate NHC complexes when reacted with imidazolium salts to give borane-NHC adducts.[152] Thus, in light of the studies of Rivard a further benefit of a reaction between **24^{Me}** and a hydride source would be to probe whether a borane Lewis acid stabilised Sn(II) halide or hydride complex is accessible through **24^{Me}** (Scheme 4.9).

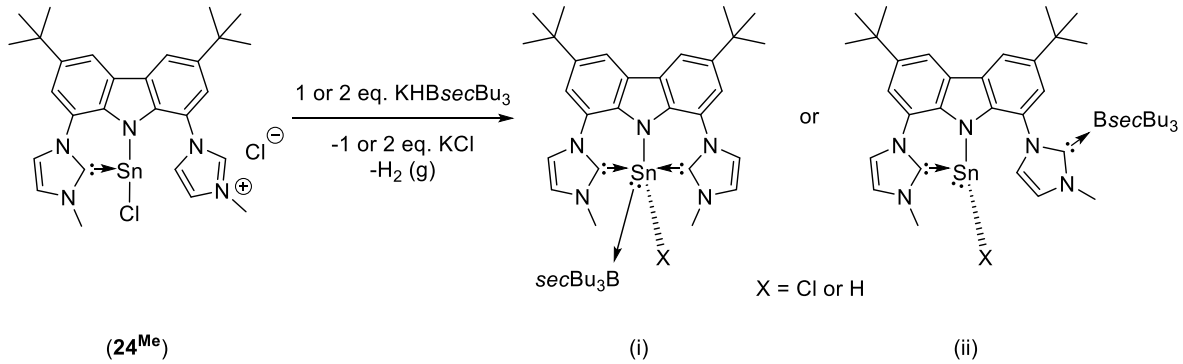

Scheme 4.9 Possible reaction outcomes of **24^{Me}** reacting with 1 or 2 equivalents of KHB*sec*Bu$_3$: (i) a Lewis acid stabilised tridentate bimca^{Me} complex, or (ii) a borane NHC adduct as per reference [152].

As referred to above, this kind of approach to heavy group 14 methylene stabilisation has been pioneered by Rivard and co-workers, wherein the Lewis acid passivates the basicity of the divalent group 14 metal in tandem with strong donation by an NHC (*vide infra*).[153]

Unfortunately, the addition of one or two equivalents of KHB*sec*Bu$_3$ to a THF-d_8 solution of **24^{Me}** resulted in the deposition of tin metal and complex ^{1}H NMR spectra that were inconsistent with bimca^{Me} species observed previously, aside from the presence of a signal at 9.75 ppm that suggests retention of an imidazolium function (*cf.* C2 proton). The rate of metal deposition is greatly enhanced in the 2:1 reaction of KH*sec*Bu$_3$ with **24^{Me}**. These observations are consistent with halide-hydride exchange at the metal centre followed by reductive elimination of tin (*cf.* formation of **17** Chapter 3 Section 3.7.2).[153]

4.2.6 Further study of the Sn(II) oxidative addition decomposition pathway

Driven by a curiosity to understand and further evidence the putative activation of the HHMDS amine by the tin(II) metal centre during the preparation of **23^{Me}**, an analogous metathesis to the one that formed **23^{Me}** was carried out in the presence of H*N*iPr_2 from LDA instead of HHMDS derived from KHMDS. We anticipated that the isopropyl moieties on the putative amide co-ligand of complexes such as **21^{Me}**·N*i*Pr_2 and **23^{Me}**·N*i*Pr_2 would provide a superior ^{1}H NMR spectroscopic handle compared to the $SiMe_3$ groups of the HMDS amide (Scheme 4.10). Specifically, the methine protons of HN*i*Pr_2 were viewed as useful probes for their chemical environment, potentially aiding the elucidation of any H*N*R_2 activation pathway.

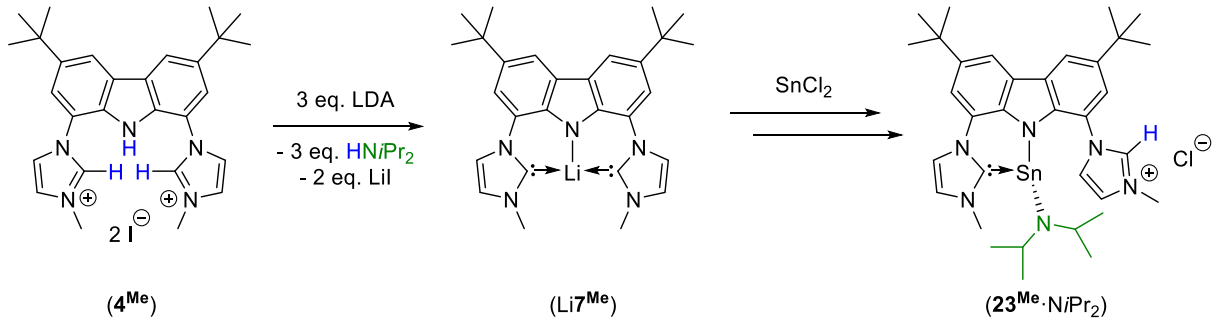

Scheme 4.10 Attempted preparation of a diisopropylamide derivative of **23^{Me}** (**23^{Me}**·N*i*Pr_2) assuming H-N activation and imidazolium elimination.

Accordingly, THF-d_8 was added to a solid mixture of three equivalents of LDA and Hbimca^{Me}(2HI) (**4^{Me}**) to form Li(bimca^{Me}) (Li**7^{Me}**) and three equivalents of H*Ni*Pr$_2$ in a characteristically clear beige (blue fluorescent under long wave UV light) reaction mixture. Monitoring of this reaction by *in situ* ^{1}H NMR spectroscopy was employed to ensure full deprotonation of **4^{Me}** and to directly observe the formation of the diisopropylamine before addition of one equivalent $SnCl_2$, as a solid, to the reaction mixture. Upon addition of $SnCl_2$, the vigorously agitated reaction mixture immediately changed colour from beige to orange and formed a brick red coloured sol that settled as a precipitate over a period of 24 hours. The ^{1}H NMR spectrum of the reaction mixture 15 minutes after reaction exhibits very weak, broad signals in the aryl proton region, indicating the marked insolubility of the bimca^{Me} containing product, alongside strong, sharp resonances attributable to free diisopropylamine, inclusive of a clear NH singlet at 0.63 ppm. Indeed, precipitation of the bimca^{Me} containing species frustrated further efforts to characterise the bimca^{Me} product of this reaction, as the brick red precipitate was also found to be insoluble in all of the inert deuterated NMR solvents at our disposal. However, it was noted that the signal integral ratio of the diisopropylamine resonances to residual ^{1}H THF signal at 3.58 ppm (OC*H*D), decreased from 3:1 to 2:1 (*H*N*i*Pr$_2$: OC*H*D) upon addition of the $SnCl_2$. While inconclusive, this is consistent with the consumption of one equivalent of diisopropylamine into the insoluble bimca^{Me} species.

4.2.7 Salt metathesis in the absence of amines to target [Sn(bimca^{Me})X]

In an effort to bypass the suspected amine activation pathway (*cf.* formation of **21^{Me}**, **23^{Me}**) and to generate a complex of the form [Sn(bimca^{Me})Cl], the preparation of this species was pursued in the strict absence of amines or proton sources. This could be achieved by either (i) removal of HHMDS from the reaction mixture prior to tin(II)

coordination, or (ii) the preparation of bimca^{Me} using KH and not a metal amide reagents to deprotonate **4^{Me}**.

The removal of residual HHMDS amine under vacuum prior to Sn(II) metallation seemed a sensible avenue (i, above), however previous efforts to isolate solid K**7^{Me}** (see Chapter 2) resulted in decomposition affording intractable mixtures of bimca^{Me} containing species. Thus, an attempt to remove most of the interfering amine co-product was made by concentrating a preparation of K(bimca^{Me}) (K**7^{Me}**) containing three equivalents of HHMDS co-product to the point of incipient crystallisation in THF, followed by the precipitation of K**7^{Me}** by addition of approximately ten volume equivalents of hexane (*NB:* K**7^{Me}** exhibits very poor solubility in hexane) to leave the HHMDS in solution. Decantation of the near colourless supernatant followed by dissolution of the brown solid in THF provided a solution that maintained its characteristic blue fluorescence under UV light. Addition of this solution to $SnCl_2$ in THF led to immediate quenching of fluorescence, precipitation of KI, and paling of the reaction mixture. Filtration and removal of volatiles *in vacuo* yielded a brown solid.

The ^{1}H NMR spectrum (THF-d_8) of the dried reaction supernatant suggests a complex mixture of products that is inconsistent with **21^{Me}**, **23^{Me}**, and a solubility profile that is distinct to that of the LDA reaction outcome. The ^{1}H NMR spectrum of the reaction solubles exhibits a noteworthy sharp second order multiplet at 2.34 ppm coupled to a second order triplet at 4.21 ppm and a second order multiplet at 5.63 ppm, and two further second order multiplets at 5.87 ppm and 5.98 ppm, with a relative integral ratio of 2:2:1:1:1. These resonances are consistent with the products of ring-opening THF, *e.g.* metal but-3-en-1-olates (Scheme 4.11).[154] (*NB:* The formation of such enolates from THF in the presence of alkyllithiums is reported in the literature).[154]

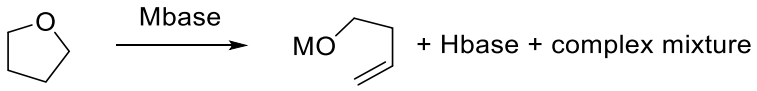

Scheme 4.11 Metal but-3-en-1-olate from the decomposition of THF solvent in the presence of strong bases.[154]

Such solvent activation may stem from either the concentration of K**7**$^{\mathbf{Me}}$ prior to its reaction with $SnCl_2$ or due to activation of THF by a [Sn(bimca^{Me})X] complex. To rule out the former, a more efficient synthesis of K**7**$^{\mathbf{Me}}$ was devised that could bypass its isolation as a solid, and avoid amine co-production using KH, which presents itself as an ideal reagent (*cf.* H_2(g) co-product). Thus, THF-d_8 was added to a solid mixture of KH and **4**$^{\mathbf{Me}}$ to produce a brown, blue fluorescent (under long wave UV light) reaction mixture with the concomitant precipitation of KI. The dissolution of KH and degassing of the reaction mixture was aided by sonication over a reaction time of two hours. Addition of a THF-d_8 solution of one equivalent of $SnCl_2$ led to a reaction mixture of lighter colouration and the precipitation of KI as a colourless solid.

The ^{1}H NMR spectrum of the reaction supernatant exhibits broad signals that partially overlap with those of the complexes **23**$^{\mathbf{Me}}$ and **24**$^{\mathbf{Me}}$ (Section 4.2.5), marked by a broad, weak resonance at 9.76 ppm that possibly emanates from an imidazolium environment (**23**$^{\mathbf{Me}}$; 9.54 ppm, **24**$^{\mathbf{Me}}$; 9.65 ppm) however no further identification of the reaction products was possible due to the complexity of the remaining chemical shift pattern.

These data suggest that, in the absence of an accessible amine N-H substrate, the tin(II) activates solvent molecules, *e.g.* THF/THF-d_8. This is consistent with the report of Turbervill for [Sn(IDipp)(*a*IDipp)Cl_2] (*cf.* major product IDipp·HCl). Unfortunately in both instances the remaining bimca^{Me} reaction products could not be identified due to a lack of reaction specificity.

4.3 Targeting [Sn(bimca^{Me})X] by blocking the reactive Sn(II) site

Thus far, the major synthetic hurdle faced in attempts to prepare bis(NHC) coordinated [Sn(bimca^{Me})X] complexes appears to lie with the inherent nucleophilicity of Sn(II) and its suspected ability to activate solvent or amine species. As such, quenching this reactivity either by (i) the use of a Lewis acid protecting group or (ii) deployment of sterically demanding *N*-substituents at the NHC donors was targeted as a logical means for the trapping of stable Sn(II) "unprotonated" bimca^{R} complexes (Scheme 4.12).

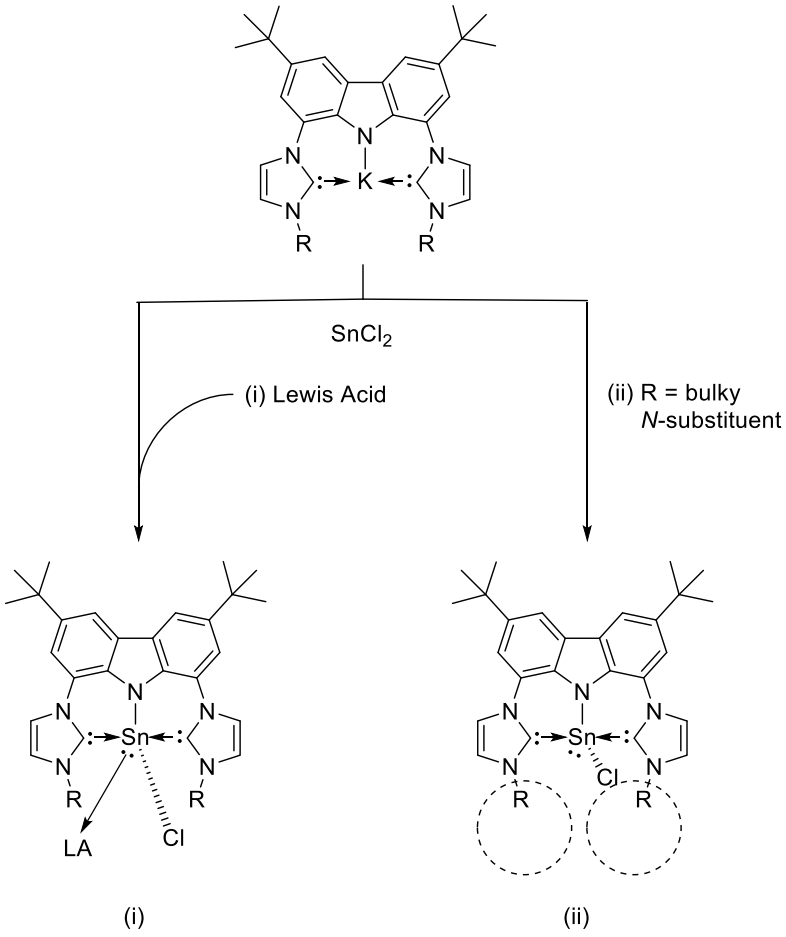

Scheme 4.12 Strategies for protecting the nucleophilic Sn(II) centre of [Sn(bimca^{R})Cl] by (i) Lewis adduct formation (R = Me) or (ii) steric shielding of the Sn(II) (R = Ph).

4.3.1 Employment of a Lewis acid protecting group

Strongly Lewis acidic group 6 pentacarbonyls are known to form stable adducts of tin(II).[155,156] Indeed, mono(NHC) and *N*-heterocyclic olefin (NHO) complexes of tin(II) halides and hydrides have been stabilised with these and related transition metal fragments.[157,158] Notably, Rivard and co-workers have shown that the tungsten adduct $[SnH_2(IDipp)\{W(CO)_5\}]$ is exceptionally stable by virtue of the highly Lewis acidic $W(CO)_5$ fragment, providing an electron acceptor for the tin(II) centre while maintaining divalency and Lewis acidity at tin. This has been substantiated by Mössbauer spectroscopy.[159] In the absence of tungsten pentacarbonyl the tin(II) dihydride complex is highly unstable and reductively eliminates the hydride co-ligands to furnish the IDipp derived aminal (*cf*. Chapter 3, complex **17**) and elemental tin.[153]

Having established the inherent instability of $[Sn(bimca^{Me})X]$ species (*cf*. $\mathbf{21^{Me}}$, $\mathbf{23^{Me}}$, $\mathbf{24^{Me}}$), the use of a $W(CO)_5$ protecting group post $bimca^{Me}$ complex formation represents a flawed strategy. Thus a "pre-protected" tin-tungsten adduct was used for the metathetical preparation of $[Sn(bimca^{Me})X]$ despite the possibility that a competing $bimca^{Me}$ coordination to the tungsten moiety could result (*cf*. $[W(bimca^{Me}H)(CO)_4$, Section 4.2.2, *vide supra*).

$[SnCl_2\{W(CO)_5\}]$ was chosen as a suitable precursor for this metathesis in view of its facile synthesis[155] and precedent use as a tin-tungsten source by Rivard and co-workers.[157] Coordination of the $bimca^{Me}$ ligand was effected by metathesis of *in situ* formed $[SnCl_2\{W(CO)_5\}]$ with $\mathbf{K7^{Me}}$ also prepared *in situ* from $\mathbf{4^{Me}}$ and three equivalents of KH. The resulting crimson solution was filtered to remove precipitated colourless KI and dried under vacuum to afford the crimson solid $\mathbf{25^{Me}}$. The ^{1}H NMR (THF-d_8) spectrum of this material exhibits an A:B:B:A chemical shift pattern in the aryl region of the spectrum

which is typical of axially symmetrical bimca^{R} complexes (*cf*. Chapters 2 and 3). This was further substantiated by two-dimensional ^{1}H-^{1}H NMR correlation experiments. Interestingly, **25^{Me}** may also be prepared in the presence of HHMDS (*cf*. preparation of K**7^{Me}** using KHMDS), suggesting that the redox protonation pathway is supressed by formation of the Sn-W adduct. The W(CO)$_5$ fragment is evidenced in the ^{13}C NMR spectrum of **25^{Me}** through carbonyl ^{13}C resonances at 198.18 ppm and 200.60 ppm. These resonances lie in the range of those previously reported for NHC-Sn-W(CO)$_5$ fragments such as those in [SnCl$_2$(IDipp){W(CO)$_5$}] and [SnH$_2$(IDipp){W(CO)$_5$}] (197.3 and 199.8 ppm; 200.8 and 203.1 ppm, respectively).[157] The IR spectrum of **25^{Me}** exhibits strong absorbances at 1978 and 1922 cm^{-1}, which may be assigned to the CO ligands at tungsten. Overall, these are red shifted with respect to those frequencies reported by Rivard and co-workers for the related mono(NHC) [SnCl$_2$(IDipp){W(CO)$_5$}] complex (2067 and 1922 cm^{-1}),[157] which suggests that coordination of the bimca^{Me} ligand enhances the donicity of the tin(II) to the tungsten metal centre, resulting in a decreased stretching frequency for the CO co-ligands. These frequencies are also distinct from those of the CO containing starting materials (W(CO)$_6$: 1972 cm^{-1},[160] and [SnCl$_2$W(CO)$_5$]: 2000, 1951 cm^{-1}).[155]

Unfortunately, repeated attempts to grow crystals of **25^{Me}** for single crystal X-ray diffraction structure determination from a variety of solvent systems proved fruitless.

*Chloride-hydride exchange reactions of [Sn(bimca^{Me})ClW(CO)$_5$], **25^{Me}** with KHBsecBu$_3$*

With the "unprotonated" bis(NHC) tin(II) halide complex **25^{Me}** in-hand, its potential for stabilising a tin(II) hydride was investigated through chloride-hydride exchange. This method has proven effective for the installation of hydrides at the aforementioned

$W(CO)_5$ stabilised adducts of $SnCl_2$(NHC/NHO) complexes. These include the so-called "push-pull" complexes in Figure 4.6.[157,158]

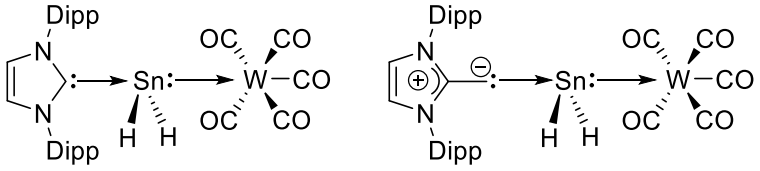

Figure 4.6 Lewis adduct stabilised tin(II) hydrides reported by Rivard (i),[157] (ii).[158]

For our purposes KHB*sec*Bu_3 and $NaBH_4$ represented good candidates for investigating the chloride-hydride exchange capability of **25^{Me}**, based on their ease of manipulation and their literature precedent for effecting such transformations.[43] The addition of one equivalent of either borohydride reagent (KHB*sec*Bu_3 as a THF-d_8 solution or $NaBH_4$ as a solid) to an agitated THF-d_8 solution of **25^{Me}** resulted in a colour change from crimson to dark brown with the precipitation of the corresponding potassium or sodum chloride as a fine white solid. The reaction mixture was maintained in a sealed NMR tube in both cases to assess for the formation of H_2 as an indicator of reductive dehydrogenation. A ^{1}H NMR spectrum of the reaction mixture for KHB*sec*Bu_3 with **25^{Me}** exhibits very broad overlapping signals where resonances for the bimca^{Me} scaffold would normally lie. Amongst these, no signals for a protic imidazolium or carbazole, nor the presence of H_2 could be identified. The intractable set of broad resonances suggest comprehensive decomposition of the starting material or the expected hydride product.

Moving to the milder $NaBH_4$ hydride source, reaction with **25^{Me}** in THF-d_8 afforded a ^{1}H NMR spectrum of similar appearance to that of KHB*sec*Bu_3, indicating a competing side reaction or decomposition pathway that does not yield the targeted tin(II) bimca^{Me} monohydride as the final product. However, unlike the KH*sec*Bu_3 reaction, the resulting

^{1}H NMR spectrum exhibits sharper resonances. These are reminiscent of the aforementioned THF decomposition products observed during our initial attempts to isolate [Sn(bimca^{Me})X] in the absence of protic co-products (see Section 4.2.4). From the evidence gathered for both of the above halide-hydride exchange reactions it seems that the stabilisation of the nucleophilic Sn(II) metal centre by the $W(CO)_5$ Lewis acid is insufficient for the bimca^{Me} ligand to coordinate a stable Sn(II)-H fragment. Thus, our attention was shifted to increased steric protection of the pincer binding cavity. Isolation of a tin(II) pincer complex with an accessible metal lone electron pair was deemed a worthwhile pursuit since this avenue of reactivity is anticipated to be useful for subsequent synthetic applications. This was targeted by tuning the steric parameters of the bimca^{R} ligand scaffold by means of imidazolyl *N*-substituents.

4.3.2 Kinetically stabilised [Sn(bimca^{R})X] targets

Accordingly, complexation was attempted with the *N*-phenyl bimca variant, bimca^{Ph}, generated from the reaction of bis(imidazole)carbazole **3** with two equivalents of diphenyliodonium tetrafluoroborate (see Chapter 2, Section 2.2.5). An added benefit of the use of the bimca^{Ph} framework is the likely electron withdrawing effect of the *N*-phenyl substituents on the NHC donors, which is expected to reduce the overall bimca NHC σ-donor strength.[85] This, it was reasoned, may reduce the redox susceptibility of the ensuing [Sn(bimca^{Ph})X] species. Unfortunately, a ^{1}H NMR spectrum of the product returned from the one-pot reaction of K(bimca^{Ph}) (K**7^{Ph}**) with $SnCl_2$ in THF exhibits signals that are consistent with multiple protonated unsymmetrical bimca^{Ph} products, as demonstrated by resonances at 10.02 ppm and 11.06 ppm, which likely arise from imidazolium C2 protons and carbazole N-H resonances. Furthermore, two pronounced second order multiplets at 2.17 ppm and 4.21 ppm are suggestive of THF decomposition, with other likely alkenyl resonances overlapping with bimca^{Ph} resonances (see Section

4.2.7). Therefore, we reason that while the HHMDS amine (*cf*. use of KHMDS to generate K**7**$^{\mathbf{Ph}}$) may be spatially excluded from the Sn(II) reactive site, the THF solvent is activated by the nascent [Sn(bimca^{Ph})Cl] product, in a similar manner and results in an outcome comparable to that hypothesised for the preparation of [Sn(bimca^{Me})Cl] in the absence of HHMDS (see Section 4.2.7).

4.4 Lead(II) bimca^{R} coordination

In light of the unforthcoming reactivity of the tin(II) bimca^{R} complexes, synthesis of the heaviest group 14 congener, *i.e*. lead(II), was expected to provide a simple modification that would markedly supress the Lewis basicity of a divalent group 14 bimca^{R} species and render it more amendable to further study. The overall stability of the +II oxidation state of lead results from a relative contraction of the 6*s* valence orbital and is in keeping with the trend in redox potentials of other low valent 6th period elements.[3] Consequently, Lewis basic Pb(II) species are scarce in the literature,[34] in contrast to the well-established Lewis basic behaviours of Ge(II) and Sn(II).[156] In view of the pronounced difficulties encountered with [Sn(bimca^{Me})X] preparations, this boded well for the study of [Pb(bimca^{R})X] complexes and suggested protection using a Lewis acid was unnecessary (*cf*. W(CO)$_5$ adduct formation for the Sn(II) congener).

*4.4.1 Protolysis of bimca^{iPr}(H$_2$I), **5**$^{\mathbf{iPr}}$, with one equivalent of [Pb(HMDS)$_2$]*

One downside of divalent lead chemistry is the poor solubility of most precursors in common organic solvents. For this reason, [Pb(HMDS)$_2$] was identified as an ideal precursor for bimca^{R} complex preparation, despite the unwanted side reactions when using its Sn(II) analogue; **21**$^{\mathbf{Me}}$, which we propose emanate chiefly from HHMDS activation by the Sn(II) metal centre. Thus, the isolation of the desired Pb(II) bimca^{Me}

complex was attempted using a near identical procedure to that used during the formation of **21^{Me}** (Scheme 4.13).

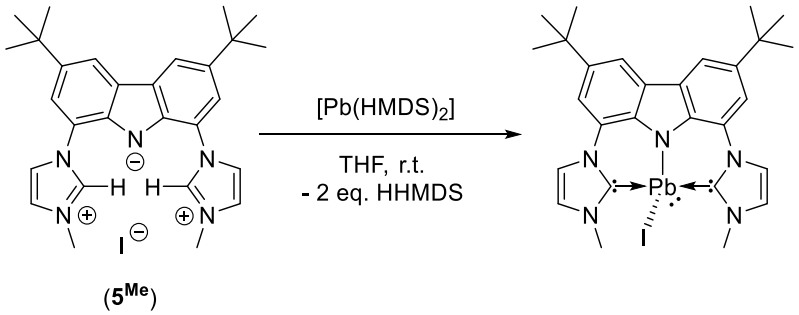

Scheme 4.13 Attempted 1:1 reaction of [Pb(HMDS)$_2$] with bimca^{Me}(H$_2$I) (**5^{Me}**) to form [Pb(bimca^{Me})I].

The reaction of [Pb(HMDS)$_2$] with one equivalent of bimca^{Me}(H$_2$I) (**5^{Me}**) in THF returned a poorly soluble pale yellow product, **26^{Me}**, upon filtration and vacuum drying of the reaction supernatant. This compound exhibits a similar, albeit broader, ^{1}H NMR (THF-d_8) resonance and chemical shift profile to its lighter Sn(II) congener; **21^{Me}**, (Figure 4.7), which is consistent with an analogous monoprotic composition, *i.e.* [Pb(bimca'^{Me}H)(HMDS)][I]. For example, the presence of a broad singlet at 10.55 ppm is consistent with imidazolium formation (10.59 ppm in **21^{Me}**) and the broad singlet at 0.04 ppm, with a relative signal integral of 18, is attributable to a HMDS moiety and suggests its incorporation into **26^{Me}** (*cf.* HMDS inclusion in **21^{Me}**, 0.04 ppm in THF-d_8).[144] The resonances in the aryl region, although not well defined, overlap with those observed for the unsymmetrical product **21^{Me}** (Figure 4.7). In the present instance, it is not clear whether the resonance broadening is a consequence of poor solubility or the presence of a significantly heavier atom.[5]

[5] Heating the THF-d_8 NMR sample to reflux for 18 h failed to initiate a second deprotonation *via* the HMDS co-ligand on the metal centre, and this treatment did not elicit a change in its ^{1}H NMR spectrum.

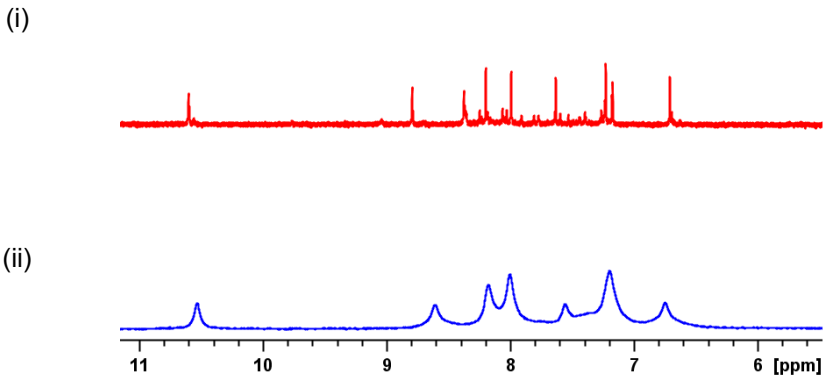

Figure 4.7 Comparison of excerpts of the ^{1}H NMR spectra of [M(HMDS)$_2$] + bimca^{Me}(H$_2$I) (**5^{Me}**) where (i) **21^{Me}** M = Sn, and (ii) **26^{Me}** M = Pb.

Similar to the ^{1}H NMR spectrum of **21^{Me}**, the ^{1}H NMR spectrum of **26^{Me}** displays signals attributable to two distinct *N*-methyl environments at 2.38 ppm and 4.42 ppm with equal relative signal integrals. This is consistent with the *N*-substituents of an *a*NHC and an imidazolium moiety, respectively (as observed for **21^{Me}**). From these data it is not clear if the distinct *a*NHC and imidazolium environments in **26^{Me}** are produced as a result of an underlying redox process, *i.e.* reductive elimination of an imidazolium, as per the tin(II) species **23^{Me}**, poor solubiliy of **26^{Me}** that impairs further reaction, or innate stability of **26^{Me}** that prohibits complete imidazolium deprotonation of the **5^{Me}** starting material. The poor solubility of **26^{Me}** frustrated characterisation by ^{13}C NMR spectroscopy and attainment of samples suitable for single crystal X-ray crystallographic studies.

4.4.2 Attempted salt metathesis of K7^{Me} with PbCl$_2$ to target [Pb(bimca^{Me})X]

To bypass the possibility of partially inert [Pb(HMDS)$_2$] with respect to bis(imidazolium) deprotonation of **5^{Me}**, and to assess the possibility of a redox decomposition pathway, analogous to that proposed for the formation of **23^{Me}**, a direct metathetical reaction of K(bimca^{Me}) (K**7^{Me}**, formed *in situ* from KHMDS) with PbCl$_2$ in the presence of HHMDS was attempted in THF-d_8 and ^{1}H NMR spectroscopy was employed to monitor the

reaction *in situ* by ^{1}H NMR. The sluggish reactivity of $PbCl_2$ is exemplified by the ^{1}H NMR spectrum of the reaction mixture, which identifies a significant amount of K**7^{Me}** starting material after 24 hours of continuous agitation by inversion. However, as the reaction slowly progressed over a period of four days, ^{1}H NMR signals for up to three distinct products form, deduced from singlets at 4.85, 5.01, and 5.05 ppm tentatively assigned to *N*-methyl environments. Unfortunately, signals near 0.04 ppm (where M-HMDS signals typically lie)[144] are crowded out by the HHMDS methyl singlet, which does not permit the direct monitoring of HMDS inclusion in the Pb(II) bimca^{Me} product. However, the signal integral of the HHMDS NH singlet at 0.95 ppm decreases gradually with reaction progression relative to the ^{1}H THF multiplet at 3.58 ppm (OC*H*D), possibly due to consumption of the amine. These data coincide with the growth of a singlet at 11.49 ppm that is consistent with imidazolium formation, however the identity of the products of this reaction could not be determined.

*4.4.3 Protolysis of bimca^{iPr}(H$_2$I), **5^{iPr}**, with excess [Pb(HMDS)$_2$]*

The slow and unproductive nature of the metathetical approach due to $PbCl_2$ insolubility precluded the purposeful synthesis of an unsymmetrical monoprotic Pb(II) analogue of **24^{Me}** through bimca^{Me}(H) (as per the reaction of $SnCl_2$ with **6^{Me}**) to purposely prepare a mixed NHC/imidazolium species. This prompted us to revisit use of the more soluble lead(II) precursor, [Pb(HMDS)$_2$] with application of two key modifications: (i) use of a 2:1 reaction stoichiometry to ensure complete deprotonation of the **5^{R}** proligand, and (ii) application of the more soluble *N*-isopropyl bimca^{iPr} proligand, **5^{iPr}** (Scheme 4.14).

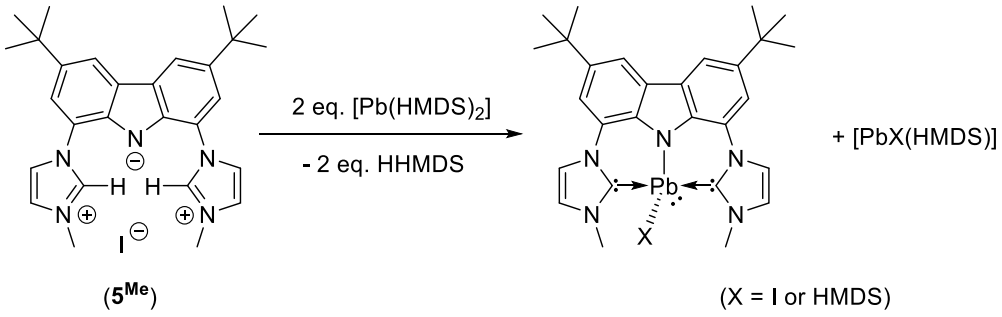

Scheme 4.14 Attempted synthesis of a [Pb(bimca^{iPr})X] complex in the presence of excess base.

This approach was anticipated to furnish a mononuclear [Pb(bimca^{iPr})X] complex (Scheme 4.14) where X represents either I or HMDS, of which the latter (X = HMDS) was expected to be more soluble than its iodide counterpart and would arise from a potential ligand redistribution reaction between [Pb(bimca^{iPr})I] and [Pb(HMDS)$_2$] to yield [Pb(bimca^{iPr})(HMDS)] and [Pb(HMDS)I]. Further deprotonation of the bimca^{iPr} scaffold by excess [Pb(HMDS)$_2$], *e.g.* at the C4/C5-imidazolyl positions was deemed unlikely considering the stability of the bimca^{R} scaffold under comparable conditions *cf.* inertness of the C4/C5-imidazolyl positions of [Mg(bimca^{Me})I] (**9^{Me}**) in the presence of KHMDS, or [Mg(bimca^{Me})$_2$] (**10^{Me}**) in the presence of [Mg(HMDS)$_2$], and based on the supposition that such "dicarbene" formation requires deployment of stronger bases, *e.g.* alkyllithiums (see Chapter 2, Section 2.4.1).[105-107]

The above strategy also presented the distinct possibility of generating a dinuclear Pb(II) bimca^{iPr} due to the two-fold excess of lead(II), however this alternative outcome was thought to be beneficial since it may alleviate the strong σ-donation of the two NHC donors on a single central lead(II) atom. Based on our observations of what we suspected to be [Pb(bimca'^{Me}H)(HMDS)][I] as **26^{Me}**, it seemed possible that the reaction of two equivalents of [Pb(HMDS)$_2$] could first afford the isopropyl variant, **26^{iPr}**, by incomplete

initial deprotonation, in which case the second equivalent of [Pb(HMDS)$_2$] would be available to deprotonate the remaining imidazolium moiety whilst maintaining one HMDS co-ligand and generating a "PbI(HMDS)" containing dinuclear bimca^{iPr} species (Scheme 4.15).

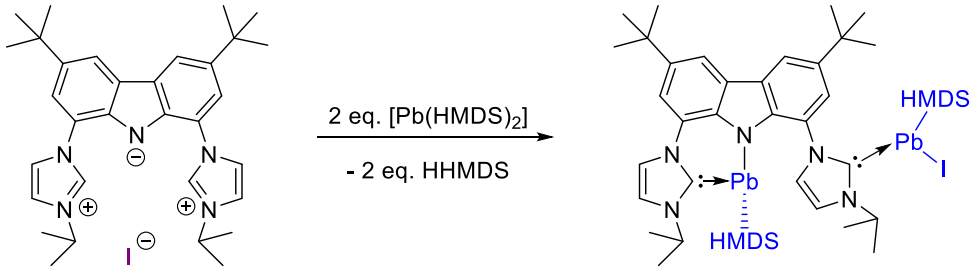

(**5^{Me}**)

Scheme 4.15 Possible formation of a dinuclear lead bimca^{iPr} complex in the presence of excess base.

Thus, two equivalents of [Pb(HMDS)$_2$] in hexane were added to a yellow slurry of bimca^{iPr}(H$_2$I) (**5^{iPr}**) in THF. As the reaction proceeded the mother liquor changed appearance from a bright yellow suspension to a clear amber solution within two hours of mixing. Filtration and removal of volatiles *in vacuo* yielded a beige powder; **27^{iPr}**, which immediately changed colour to bright yellow upon exposure to air. This air-sensitivity is reminiscent of observations made in Chapter 2, wherein *s*-block bimca^{R} complexes, such as Li/K**7^{R}** and **9^{Me}**, would rapidly form diprotic bimca^{R}(H$_2$X) upon exposure to air. Beige **27^{iPr}** was redissolved in the minimum volume of THF at room temperature, diffused with hexane, and placed at 4 °C to yield small pale amber rhombohedral plates that were found to be suitable for single crystal X-ray crystallographic studies, leading to the identification of **27^{iPr}** as [Pb$_2$(bimca"^{iPr})(HMDS)I] (Figure 4.8).

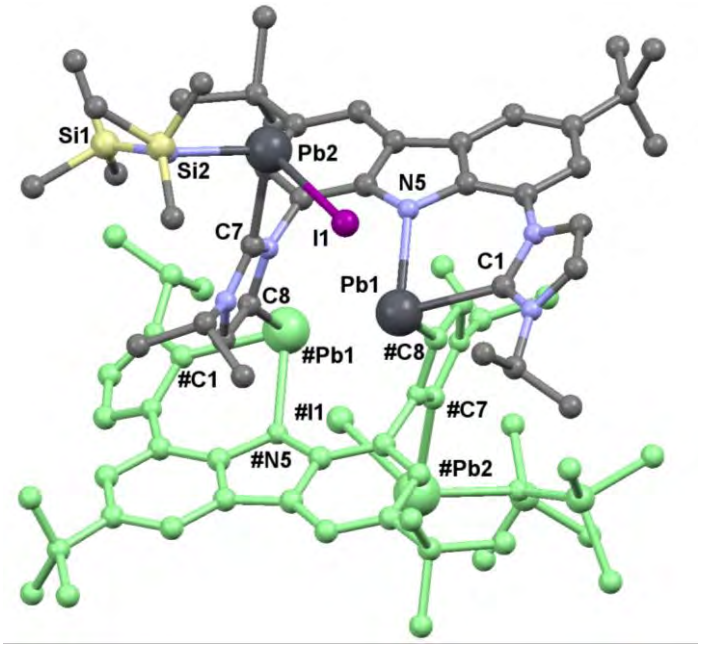

(i)

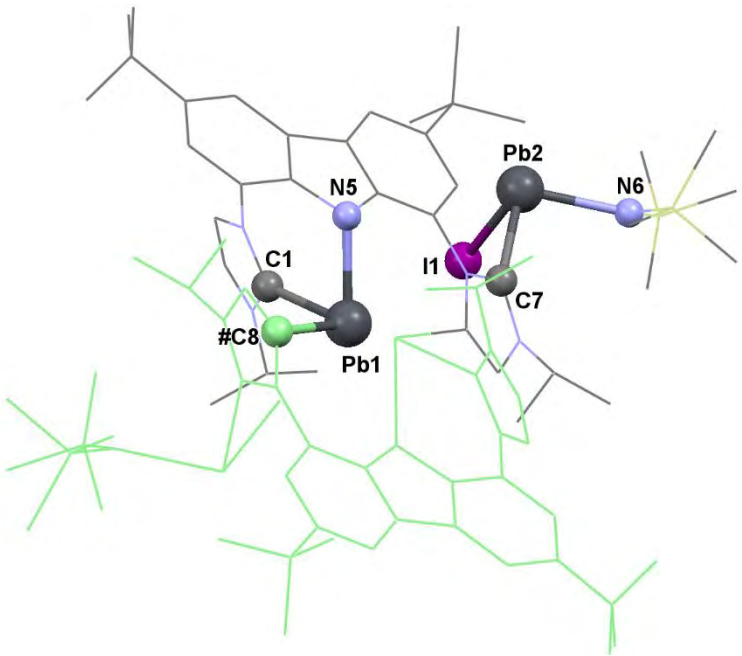

(ii)

Figure 4.8 Van der Waals' sphere representation (arbitrary radius) of the tetranuclear Pb(II) bimca^{iPr} dimer **27^{iPr}**, symmetry generated atoms are shown in green (i), selected distance (Å): Pb1···#Pb1: 4.555. Symmetry operations to generate '#' atoms: $^{3}/_{2}$-*x*, $^{7}/_{2}$-*y*, 2-*z*. Highlighted core Pb1 and Pb2 geometries (ii).

Complex **27^{iPr}** crystallises in the monoclinic space group *C*2/*c* with one monomer of the dimer and two molecules of heavily disordered hexane solvent in the asymmetric unit. The disorder of the latter could not be modelled with satisfactory occupancies and were thus masked (OLEX 2) to aid refinement. The insufficient quality of the data for **27^{iPr}** could not be improved for this highly sensitive compound, allowing only an isotropic refinement and preventing a broader discussion of its metric parameters. However, the connectivity of **27^{iPr}** is reliable and shows the incorporation of two Pb(II) atoms per bimca"^{iPr} ligand, one in the carbazolide/NHC meridional binding site and one external to the bimca"^{iPr} pocket, coordinated by an NHC and iodide. The latter, Pb2, maintains one HMDS co-ligand. However, the carbazolide bound lead (Pb1), that occupies the bimca"^{iPr} binding cavity through bidentate coordination to the carbazolide and the second NHC, is no longer coordinated by an HMDS co-ligand, as may be expected from the composition of **26^{Me}** and Goicoechea's [Pb(*a*IDipp')$_2$(HMDS)]$^-$. Instead, the lead coordination is completed by the deprotonation of the NHC that coordinates Pb2 at the imidazolyl C5 position (C8) to generate a carbanionic *a*NHC' or "dicarbene" (Figre 4.9, *cf*. octalithium species **8** in Chapter 2). It is noteworthy that **27^{iPr}** exhibits no bifurcated bonding between the carbazolide nitrogen or the C5 carbanions of the imidazolyl donors on the bimca"^{iPr} scaffold to either of the Pb(II) cations and thereby contrasts the analogous interactions observed in **8** (Chapter 2, Section 2.4.1).

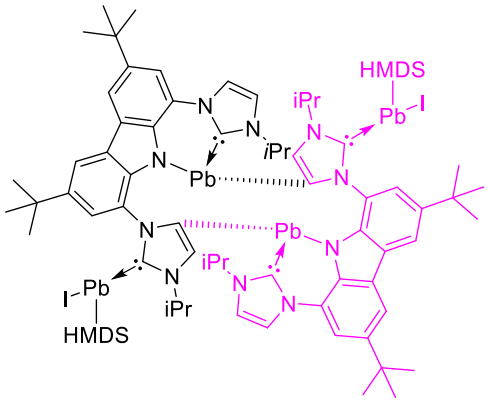

Figure 4.9 Illustration of tetranuclear **27^{iPr}** showing different lead(II) coordination environments.

As with **26^{Me}**, broadening of the bimca"^{iPr} resonances in the ^{1}H NMR spectrum of **27^{iPr}** is observed. This, coupled with the extreme moisture sensitivity of **27^{iPr}**, frustrated the acquisition of ^{13}C NMR and two-dimensional NMR spectroscopy data. Further to the ^{1}H NMR spectrum of **27^{iPr}**, two distinct imidazolyl environments, consistent with the molecular structure of **27^{iPr}**, are readily apparent in the ^{1}H NMR spectrum (THF-d_8) of **27^{iPr}**, marked by two separate *N*-isopropyl methine septets at 4.49 ppm and 5.12 ppm. Furthermore, one *N*-isopropyl substituent is rotationally locked or diastereotopic, resulting in two closely separated *Ni*Pr-CH_3 doublets at 1.00 and 1.03 ppm, each with relative signal integrals of 12. The resultant break in symmetry is marked by four inequivalent 2,4,5,7-carbazolide aryl proton resonances while the absence of a ^{1}H resonance attributable to a 5-position proton for the carbanionic *a*NHC'.

4.5 Conclusions

The redox flexibility of M(II) group 14 metals appears to be a major hurdle for bis(NHC) coordination of these metals. Based on **21^{Me}** and **23^{Me}**, the strong donation of the NHC moieties of the bimca^{R} ligand class may exacerbate this susceptibility by inviting

oxidative addition. Such activation has been evidenced herein by the facile thermodynamic decomposition of [M(bimca^{R})X] intermediates to monoprotic **21^{Me}** and **23^{Me}** and cannot be ruled out for Pb(II), *cf*. isolation of **26^{Me}**. Such redox mechanisms serve to alleviate the strong electron donation of the bimca^{R} ligand at Sn(II) and may be passivated in future projects by protection of the Sn(II) metal centre with strong Lewis acids, *cf*. synthesis of the Sn-W(CO)$_5$ adduct, **25^{Me}**, herein. For Sn(II) we have observed that these decomposition pathways result in the protonation of an NHC donor by multiple avenues, *e.g*. activation of solvent or protic co-products, eventuating in unsymmetrical monoprotic bimca^{R} reaction products.

4.6 Experimental

General methods

[M(HMDS)$_2$] (M = Sn, Pb) compounds were synthesised according to literature methods[24] and used *in situ* or as hexane stock solutions. The concentration of stock solutions was determined by ^{1}H NMR spectroscopy (C_6D_6) with a toluene-H$_8$ internal standard.

*Reaction of [Sn(HMDS)$_2$] with bimca^{Me}(H$_2$I), **5^{Me}**, to form [Sn(bimca$^{\prime Me}$H)(HMDS)] [I], **21^{Me}***

A solution of LiHMDS (0.099 g, 0.59 mmol) in diethyl ether (5 mL) was added to a suspension of $SnCl_2$ (0.056 g, 0.30 mmol) in diethyl ether (10 mL) to give pale red reaction mixture that was stirred at room temperature for 2 h. The resultant colourless precipitate was allowed to settle and the red supernatant was transferred to a yellow, fluorescent, suspension of bimca^{Me}(H$_2$I) (**5^{Me}**) (0.17 g, 0.30 mmol) in THF (10 mL) to afford a yellow reaction mixture that was stirred at room temperature for 18 h, during

which time no colour change, or change in fluorescence under long wave UV light, was observed. The reaction was heated to reflux under an inert atmosphere for 18 h resulting in a colour change to straw yellow suspension. The straw yellow supernatant was isolated by filtration and dried *in vacuo* with heating to 100 °C to give **21^{Me}** as a pale yellow solid (0.16 g, 64%). The pale yellow filtrant was found to be of the same composition as the vacuum dried filtrate product by ^{1}H NMR spectroscopy. ^{1}H NMR (400 MHz, THF-d_8): δ 0.04 (s, 18H, $SiMe_3$), 1.52 (s, 9H, *t*Bu'-CH_3)[#], 1.54 (s, 9H, *t*Bu-CH_3), 2.60 (s, 3H, *a*NHC NMe), 4.46 (s, 3H, imidazolium NMe), 6.70 (d, $^{3}J_{HH}$ = 1.80 Hz, 1H, 4-*a*NHC-*H*), 7.17 (d, $^{3}J_{HH}$ = 1.80 Hz, 1H, 2-*a*NHC-*H*), 7.22 (d, $^{4}J_{HH}$ = 1.72 Hz, 1H, 2-carb.-*H*), 7.63 (d, $^{4}J_{HH}$ = 1.77 Hz, 1H, 7-carb.-*H*), 7.99 (d, $^{4}J_{HH}$ = 1.72 Hz, 1H, 4-carb.-*H*), 8.19 (d, $^{4}J_{HH}$ = 1.77 Hz, 1H, 5-carb.-*H*), 8.37 (m, 1H, 5-imidazolium-*H*), 8.78 (m, 1H, 4-imidazolium-*H*), 10.59 (m, 1H, 2-imidazolium-*H*). ^{13}C NMR (100 MHz, THF-d_8, quaternary aryl ^{13}C resonances could not be resolved due to low sample solubility, aryl *C*-H resonances were identified by ^{1}H-^{13}C HSQC experiments): δ 0.82 (s, $SiMe_3$), 32.35 (s, *t*Bu'-*C*H_3), 32.57 (s, *t*Bu-*C*H_3), 35.25 (s, *t*Bu'-*C*), 35.36 (s, *t*Bu-*C*), 37.53 (s, *a*NHC NMe), 38.67 (s, imidazolium NMe), 112.4 (s, 2-carb.-*C*), 115.60 (s, 4-carb.-*C*), 117.58 (s, 7-carb.-*C*), 117.67 (s, 5-carb.-*C*), 118.7 (s, 5-imidazolium-*C*), 119.12 (s, 2-*a*NHC-*C*), 123.27 (s, 4-*a*NHC-*C*), 125.39 (s, 4-imidazolium-*C*), 137.58 (s, 2-imidazolium-*C*). Calcd. for $[C_{34}H_{51}N_6Si_2Sn]^+$, : *m/z* 719.27. MS (FAB, acetonitrile matrix, + ion mode): *m/z* 719.31 [Sn(bimca'^{Me}H)(HMDS)]$^+$. IR (Nujol mull on NaCl plates) 1673 (*m*, *sh*), 1594 (*w*, *sh*), 1094 (*m*, *br*), 1020 (*m*, *br*), 846 (*w*, *sh*), 801 (*m*, *sh*), 722 (*w*, *sh*), 665 (*m*, *sh*). Mp: 226-228 °C (dec.).

[#] *t*Bu denotes the *tert*-butyl group attached to the carbazole 3-position, *t*Bu' denotes the *tert*-butyl group attached to the carbazole 6-position.

*Isolation of [Ga(bimca$^{'Me}$H)I$_2$][I], **22^{Me}***

A sample of **9^{Me}** (0.100 g, 0.17 mmol) that had been stored in a glove box for *ca*. one month was dissolved in THF (5 mL) to afford an amber solution that was added to a colourless solution of GaI_3 (0.77 g, 0.17 mmol) in THF (15 mL). The reaction mixture gradually paled to a colourless fine suspension over a period of 18 h, whereupon it was filtered and volatiles were removed *in vacuo* to afford a colourless microcrystalline solid. Recrystallisation of this solid from a saturated room temperature THF solution placed at -24 °C afforded small rectangular plates of **22^{Me}** suitable for single crystal X-ray diffraction structure determination. Subsequent characterisation was carried out on this crop of crystals. The yield of crystalline material was insufficient for carrying out microanalysis for **22^{Me}**. ^{1}H NMR (400 MHz, THF-*d*$_8$): δ 1.50 (s, 9H, *t*Bu'-C*H*$_3$), 1.53 (s, 9H, *t*Bu-CH$_3$), 4.11 (s, 3H, imidazolium NMe), 4.16 (s, 3H, NHC NMe), 7.75 (m, 1H, 4-imidazolium-*H*), 7.96 (m, 1H, 5-imidazolium-*H*), 8.04 (d, $^4J_{HH}$ = 1.53 Hz, 1H, 2-carb.-*H*) 8.09 (d, $^3J_{HH}$ = 1.92 Hz, 1H, 4-NHC-*H*), 8.28 (d, $^4J_{HH}$ = 1.88 Hz, 1H, 7-carb.-*H*), 8.32 (d, $^4J_{HH}$ = 1.53 Hz, 1H, 4-carb.-*H*), 8.43 (d, $^4J_{HH}$ = 1.88 Hz, 1H, 5-carb.-*H*), 8.85 (d, $^3J_{HH}$ = 1.92 Hz, 1H, 5-NHC-*H*), 9.79 (br m, 1H, 2-imidazolium-*H*). ^{13}C NMR (100 MHz, THF-*d*$_8$): δ 31.97 (s, *t*Bu-*C*H$_3$), 32.12 (s, *t*Bu'-*C*H$_3$), 35.55 (s, *t*Bu-*C*), 35.67 (s, *t*Bu'-*C*), 37.25 (s, NHC NMe), 37.32 (s, imidazolium NMe), 114.28 (s, 2-carb.-*C*), 116.83 (s, 4-carb.-*C*), 118.66 (s, 5-carb.-*C*), 119.30, 121.20, 122.24 (s, carb.-*C*), 124.29 (s, 5-imidazolium-*C*), 126.85 (s, 4-NHC-*C*), 127.76 (s, 7-carb.-*C*), 128.55, 128.82 (s, carb.-*C*), 128.98 (4-imidazolium-*C*), 134.11 (s, carb.-*C*), 139.35 (s, 5-NHC-*C*), 142.29 (s, 2-imidazolium-*C*), 143.90, 144.42 (s, carb.-*C*), 154.41 (s, 2-NHC-*C*). IR (Nujol on NaCl plates, cm^{-1}): 1618 (*m*, *sh*), 1539 (*m*, *sh*), 1294 (*m*, *sh*), 1261 (*m*, *sh*), 1094 (*m*, *br*), 1027 (*m*, *br*), 965 (*w*, *sh*), 924 (*w*, *sh*), 876 (*m*, *sh*), 800 (*s*, *sh*). Mp: 338-340 °C (dec.).

*Reaction of [K(bimca^{Me})] from KHMDS with $SnCl_2$ to form **23^{Me}***

A solution of KHMDS (0.091 g, 0.46 mmol) in THF (5 mL) was added to a yellow suspension of **5^{Me}** (0.13 g, 0.23 mmol) in THF (10 mL) and stirred at room temperature for *ca*. 1 h to give a brown, blue fluorescent (under long wave UV light) reaction mixture with an off-white suspended solid that settled upon standing. The brown, blue fluorescent supernatant was added to a solution of $SnCl_2$ (0.043 g, 0.23 mmol) in THF (10 mL) to immediately give a crimson, non-fluorescent reaction mixture with precipitation of an off-white solid. The reaction mixture was stirred at room temperature for 18 h after which the white precipitate was allowed to settle. Filtration and removal of volatiles from the filtrate *in vacuo* afforded **23^{Me}** as a highly air- and moisture sensitive crimson solid (0.071 g, 41%) that proved to be unstable in solution over a short timeframe. ^{1}H NMR (400 MHz, THF-*d*$_8$): δ 0.04 (s, 18H, $SiMe_3$), 1.48 (s, 9H, *t*Bu'-C*H*$_3$), 1.52 (s, 9H, *t*Bu-C*H*$_3$), 4.09 (s, 3H, NHC NMe), 4.20 (s, 3H, imidazolium NMe), 7.57 (d, $^4J_{HH}$ = 1.87 Hz, 1H, 7-carb.-*H*), 7.61 (d, $^3J_{HH}$ = 1.77 Hz, 1H, 4-NHC-*H*), 7.83 (d, $^4J_{HH}$ = 1.66 Hz, 1H, 2-carb.-*H*), 7.98 (m, 1H, 4-imidazolium-*H*), 8.00 (m, 1H, 5-imidazolium-*H*), 8.25 (d, $^4J_{HH}$ = 1.66 Hz, 1H, 4-carb.-*H*), 8.37 (d, $^3J_{HH}$ = 1.77 Hz, 1H, 5-NHC-*H*), 8.39 (d, $^4J_{HH}$ = 1.87 Hz, 1H, 5-carb.-*H*), 9.54 (m, 1H, 2-imidazolium-*H*). ^{13}C NMR (100 MHz, THF-*d*$_8$, quaternary aryl ^{13}C resonances could not be resolved due to product instability in solution, aryl *C*-H resonances were identified by ^{1}H-^{13}C HSQC experiments): δ 0.79 (s, $SiMe_3$), 31.68 (s, *t*Bu'-*C*H$_3$), 31.71 (s, *t*Bu-*C*H$_3$), 34.85 (s, *t*Bu-*C*), 35.00 (s, *t*Bu-*C*), 36.86 (s, NHC NMe), 37.12 (s, imidazolium NMe), 113.63 (s, 2-carb.-*C*), 116.00 (s, 4-carb.-*C*), 118.49 (s, 5-carb.-*C*), 119.01 (s, 5-NHC-*C*), 121.85 (s, 7-carb.-*C*), 124.47 (s, 4-imidazolium-*C*), 124.60 (s, 5-imidazolium-*C*), 125.59 (s, 4-NHC-*C*), 141.88 (s, 2-imidazolium-*C*). Calcd. for $[C_{34}H_{51}N_6Si_2Sn]^+$, : *m/z* 719.27. MS (FAB, acetonitrile matrix, + ion mode): *m/z* 719.32 [Sn(bimca'^{Me}H)(HMDS)]$^+$. Mp: 221-224 °C (dec.).

*Reaction of bimca^{Me}(H) with $SnCl_2$ to form **24^{Me}** (monitored by NMR spectroscopy)*

THF-d_8 (0.5 mL) was added to a solid mixture of Hbimca^{Me}(2HI) (**4^{Me}**) (0.021 g, 0.030 mmol) and KHMDS (0.012 g, 0.059 mmol) to immediately give an amber suspension with weak blue fluorescence under long wave UV light. The reaction mixture was sonicated at room temperature for 1 h, over this time it darkened slightly, ^{1}H NMR spectroscopy confirmed the formation of bimca^{Me}(H). Volatiles were removed *in vacuo* and the resulting amber solid was dried under vacuum for a further 1 h. Resuspension in THF-d_8 (0.5 mL) and addition of solid $SnCl_2$ (0.0056 g, 0.030 mmol,) gave an orange, slightly cloudy reaction mixture that was agitated by inversion further for *ca*. 1 h. The ^{1}H NMR spectrum of the reaction mixture indicates quantitative conversion to **24^{Me}**. ^{1}H NMR (400 MHz, THF-d_8): δ 1.47 (s, 9H, *t*Bu'-CH_3), 1.52 (s, 9H, *t*Bu-CH_3), 3.99 (s, 3H, NHC NMe), 4.20 (s, 3H, imidazolium NMe), 7.46 (d, $^4J_{HH}$ = 1.52 Hz, 1H, 7-carb.-*H*), 7.49 (d, $^3J_{HH}$ = 1.72 Hz, 1H, 4-NHC-*H*), 7.82 (d, $^4J_{HH}$ = 1.68 Hz, 1H, 2-carb.-*H*), 7.86 (m, 1H, 4-imidazolium-*H*), 8.02 (m, 1H, 5-imidazolium-*H*), 8.22 (d, $^4J_{HH}$ = 1.68 Hz, 1H, carb.-4), 8.37 (overlapping multiplets, 2H, 5-NHC-*H* & 5-carb.-*H*), 9.65 (m, 1H, 2-imidazolium-*H*). ^{13}C NMR (100 MHz, THF-d_8): δ 32.08 (s, *t*Bu'-*C*H_3), 32.14 (s, *t*Bu-*C*H_3), 35.14 (s, *t*Bu'-*C*), 35.35 (s, *t*Bu-*C*), 36.30 (s, NHC NMe), 37.41 (s, imidazolium NMe), 113.78 (s, carb.-2), 116.12 (s, 4-carb.-*C*), 118.62 (s, 5-carb.-*C*), 119.16 (s, 5-NHC-*C*), 120.63 (s, carb.), 121.66 (s, 7-carb.-*C*), 122.67 (s, carb.), 124.36 (s, 4-NHC-*C*), 125.05 (4-imidazolium-*C*), 125.27 (s, carb.), 125.66 (s, 5-imidazolium-*C*), 128.95, 129.61, 136.94 (s, carb.), 140.05 (s, 2-imidazolium-*C*), 141.26, 141.67, 141.72 (s, carb.), 175.02 (s, 2-NHC-*C*).

Reaction of [Li(bimca^{Me})] from LDA with $SnCl_2$ (monitored by NMR spectroscopy)

THF-d_8 (0.5 mL) was added to a solid mixture of LDA (0.011 g, 0.098 mmol) and **4^{Me}** (0.023 g, 0.033 mmol) to give a yellow suspension that was agitated by inversion for 15

minutes to give a pale beige, slightly cloudy reaction mixture with strong blue fluorescence. Addition of the supernatant to solid $SnCl_2$ (0.0062 g, 0.033 mmol) gave an amber coloured reaction mixture that was agitated by inversion for 15 min. After 5 minutes the reaction had formed a brick coloured sol that settled on standing for 18 h to give a pale amber supernatant.

^{1}H NMR (400 MHz, THF-d_8, before addition of $SnCl_2$, t = 0): δ 0.63 (br s, 3H, *H*N*i*Pr$_2$), 0.96 (d, $^3J_{HH}$ = 5.85 Hz, 36H, HN*i*Pr$_2$-C*H*$_3$), 1.49 (s, 18H, *t*Bu-C*H*$_3$), 2.86 (sept, $^3J_{HH}$ = 5.85 Hz, 6H, HN*i*Pr$_2$-C*H*), 3.94 (s, 6H, NMe), 7.16 (d, $^3J_{HH}$ = 1.70 Hz, 2H, 4-NHC-*H*), 7.39 (d, $^4J_{HH}$ = 1.60 Hz, 2H, 2,7-carb.-*H*), 7.72 (d, $^4J_{HH}$ = 1.60 Hz, 2H, 4,5-carbazole-*H*), 7.99 (d, $^3J_{HH}$ = 1.70 Hz, 2H, 5-NHC-*H*).

^{1}H NMR (400 MHz, THF-d_8, after addition of $SnCl_2$, t = 15 min. bimca^{Me} associated resonances are very broad and poorly resolved due product insolubility. Full width at half maximum (fwhm) values are given for the most prominent signals): δ 0.63 (br s, 2H, *H*N*i*Pr$_2$), 0.96 (d, $^3J_{HH}$ = 5.85 Hz, 24H, HN*i*Pr$_2$-C*H*$_3$), 1.49 (br s, fwhm = 49 Hz, *t*Bu-C*H*$_3$), 2.86 (sept, $^3J_{HH}$ = 5.85 Hz, 4H, HN*i*Pr$_2$-C*H*), 7.08 (br s, fwhm = 159 Hz), 7.92 (br s, fwhm = 82 Hz).

^{1}H NMR (400 MHz, THF-d_8, after addition of $SnCl_2$, t = 24 h. The resonances of the poorly soluble bimca^{Me} product could not be identified): δ 0.63 (br s, 2H, *H*N*i*Pr$_2$), 0.96 (d, $^3J_{HH}$ = 5.85 Hz, 24H, HN*i*Pr$_2$-C*H*$_3$), 2.86 (sept, $^3J_{HH}$ = 5.85 Hz, 4H, N*i*Pr$_2$-C*H*).

Reaction of vacuum dried [K(bimca^{Me})] with $SnCl_2$

A solution of KHMDS (0.12 g, 0.60 mmol) in THF (5 mL) was added to a yellow suspension of **5^{Me}** (0.17 g, 0.30 mmol) in THF (10 mL) to give a brown, blue fluorescent (under long wave UV light) reaction mixture with an off-white precipitate. The reaction mixture was stirred for 1 h and the solid settled upon standing. The brown, blue

fluorescent supernatant was filtered off and the filtrate was concentrated to incipient crystallisation. Hexane (100 mL) was added to the filtrate to speed up the precipitation of K**7**$^{\mathbf{Me}}$. The supernatant was filtered off rapidly (< 5 min) and the solid K**7**$^{\mathbf{Me}}$ residue was dried briefly under vacuum (5 min). Dissolution in THF (10 mL) and addition to a solution of $SnCl_2$ (0.057 g, 0.30 mmol) in THF (10 mL) afforded a dark amber non-fluorescent reaction mixture and precipitation of an off-white solid. After stirring for 18 h at room temperature, the suspended white solid was allowed to settle and the dark amber supernatant was isolated by filtration. Removal of volatiles *in vacuo* afforded a treacly brown solid that produced a complicated ^{1}H NMR spectrum that evidenced THF decomposition. ^{1}H NMR (400 MHz, THF-d_8, resonances of likely THF decomposition products listed by omission of bimca^{Me} associated resonances): δ 2.34 (m, 2H, OCH_2CH_2), 4.21 (m, 2H, OCH_2CH_2), 5.63 (m, 1H, CH_2CH), 5.87 (m, 1H, $CHCH_2$), 5.98 (m, 1H, $CHCH_2$).

Reaction of [K(bimca^{Me})] from KH with $SnCl_2$

THF-d_8 (0.5 mL) was added to a solid mixture of **4**$^{\mathbf{Me}}$ (0.017 g, 0.024 mmol) and KH (0.0029 g, 0.073 mmol) to give a yellow suspension with formation of a white precipitate and H_2 gas evolution. The reaction mixture was sonicated for 1 h at room temperature. Solid $SnCl_2$ (0.0046 g, 0.024 mmol) was added to the resulting brown, blue fluorescent reaction mixture and agitated to immediately give a slightly paler reaction mixture with no fluorescence under visible or long wave UV light. Removal of volatiles *in vacuo* yielded a treacly brown solid. ^{1}H NMR (THF-d_8): δ 1.49 (br s, fwhm = 37 Hz), 4.07 (br s, fwhm = 85 Hz), 7.92 (br m, fwhm = 386 Hz).

Reaction of [K(bimca^{Me})] with [SnCl$_2$W(CO)$_5$] to form ***25^{Me}***

A white suspension of $SnCl_2$ (0.0504 g, 0.266 mmol) and $W(CO)_6$ (0.0936 g, 0.266 mmol) in THF (15 mL) was irradiated with a 120 W mercury discharge lamp (at a distance of 10 cm from the walls of the vessel) in a quartz Schlenk flask for 3 d at room temperature to give a yellow solution. In a separate flask a solution of KHMDS (0.11 g, 0.53 mmol) in THF (5 mL) was added to a suspension of **5^{Me}** (0.15 g, 0.27 mmol) in THF (15 mL) to give an amber reaction mixture that was stirred for 1 h. After this time the reaction mixture turned brown, blue fluorescent and solid KI settled out on standing. The supernatant was added to the yellow solution of [$SnCl_2W(CO)_5$] leading to a colour change to a dark amber solution no fluorescence. The reaction mixture was stirred at room temperature for 18 h, allowed to settle and filtered to remove precipitated KCl. Removal of volatiles from the filtrate *in vacuo* afforded crude **25^{Me}**. Recrystallisation from the minimum amount of toluene (*ca*. 20 mL) yielded spectroscopically pure **25^{Me}** as a crimson microcrystalline solid (0.071 g, 29%). ^{1}H NMR (400 MHz, THF-d_8): δ 1.51 (s, 18H, *t*Bu-CH_3), 4.25 (s, 6H, NMe), 7.41 (d, $^3J_{HH}$ = 1.95 Hz, 2H, 4-NHC-*H*), 7.77 (d, $^4J_{HH}$ = 1.72 Hz, 2H, 2,7-carbazole-*H*), 8.17 (d, $^4J_{HH}$ = 1.72 Hz, 2H, 4,5-carb.-*H*), 8.23 (d, $^3J_{HH}$ = 1.95 Hz, 2H, 5-NHC-*H*). ^{13}C NMR (63 MHz, THF-d_8): δ 32.08 (s, *t*Bu-*C*H$_3$), 35.26 (s, *t*Bu-*C*), 37.78 (s, NMe), 112.77 (s, 2,7-carb.-*C*), 115.40 (s, 4,5-carb.-*C*), 115.53 (s, 5-NHC-*C*), 123.74 (s, 4-NHC-*C*), 129.45, 136.66, 137.33, 142.32 (s, carb.-*C*), 181.01 (s, 2-NHC-*C*), 198.18 (s, *C*O), 200.60 (s, *C*O). Calcd. for [$C_{38}H_{43}N_6O_5SnW$]$^+$: *m/z* 967.18, [$C_{32}H_{35}N_6O_2SnW$]$^+$: *m/z* 839.14, [$C_{28}H_{32}N_5Sn$]$^+$: *m/z* 558.17 MS (FAB, acetonitrile matrix, + ion mode): *m/z* 967.51 [Sn(bimca^{Me})W(CO)$_4$(THF)][CH$_3$CN]$^+$, *m/z* 839.63 [Sn(bimca^{Me})W(CO)$_2$(CH$_3$-CN)]$^+$, *m/z* 558.25 [Sn(bimca^{Me})]$^+$. IR (KBr disc): 2963 (*m, sh*), 2064 (*w, sh*), 1978 (*w, sh, CO*), 1922 (*m, br, CO*), 1792 (*w, sh*), 1262 (*s, sh*), 1097 (*s, br*), 1020 (*s, br*), 799 (*s, sh*). Mp: 160-162 °C (dec.).

*Attempted chloride-hydride exchange reaction of **25**^{Me} with KHBsecBu$_3$*

A solution of KHB*sec*Bu$_3$ (0.0084 g, 0.038 mmol) in THF-d_8 (0.3 mL) was added to a crimson solution of **25**^{Me} (0.035 g, 0.038 mmol) in THF-d_8 (0.2 mL) to give a slightly cloudy brown reaction mixture that was agitated for 15 minutes at room temperature. The resulting off-white precipitate was allowed to settle and the supernatant analysed by ^{1}H NMR spectroscopy. The complex nature of the ^{1}H NMR spectra for this reaction precluded full assignment, see Section 4.3.1 for discussion.

*Attempted chloride-hydride exchange reaction of **25**^{Me} with NaBH$_4$*

THF-d_8 (0.5 mL) was added to a solid mixture of **25**^{Me} (0.032 g, 0.035 mmol) and NaBH$_4$ (0.0013 g, 0.035 mmol) to give a slightly cloudy dark red reaction mixture which was agitated at room temperature over 18 h and monitored intermittently by ^{1}H NMR spectroscopy over this time. Over this time the NaBH$_4$ was gradually consumed resulting in a brown, slightly cloudy reaction mixture. The complex nature of the ^{1}H NMR spectra for this reaction precluded full assignment, see Section 4.3.1 for discussion.

Reaction of [K(bimca^{Ph})] with SnCl$_2$

A solution of KHMDS (0.041 g, 0.21 mmol) in THF (5 mL) was added to a white suspension of Hbimca^{Ph}(2HBF$_4$) (**4**^{Ph}) (0.051 g, 0.069 mmol) to immediately give an amber suspension that became clearer and darker after 1 h of stirring at room temperature. The resulting fine precipitate was filtered off and the brown, blue fluorescent supernatant was added to a solution of SnCl$_2$ (0.013 g, 0.069 mmol) in THF (10 mL) to give a dark amber reaction mixture which gradually lost its blue fluorescence with the concomitant precipitation of a white solid. The reaction mixture was stirred for 18 h after which the precipitate was allowed to settle and the dark amber supernatant was filtered off *via* filter cannula and dried *in vacuo* to give a treacly dark amber solid that had a complicated

^{1}H NMR spectrum and included resonances consistent with THF decomposition. ^{1}H NMR (400 MHz, THF-d_8, resonances of likely THF decomposition products listed by omission of bimca^{Ph} associated resonances): δ 2.17 (m, 2H, OCH_2CH_2), 4.21 (m, 2H, OCH_2CH_2), 5.01 (m, 1H, CH_2CH) 5.33 (m, 1H, $CHCH_2$) 5.98 (m, 1H, $CHCH_2$).

Reaction of [Pb(HMDS)$_2$] with bimca^{Me}(H$_2$I) to form ***26^{Me}***

A solution of LiHMDS (0.089 g, 0.53 mmol) in diethyl ether (5 mL) was added to a suspension of $PbCl_2$ (0.074 g, 0.26 mmol) in diethyl ether (10 mL) to give a pale orange reaction mixture that was stirred at room temperature for 2 h. The precipitated LiCl was allowed to settle and the red supernatant was added to a yellow THF (15 mL) suspension of **5^{Me}** (0.15 g, 0.26 mmol). The resulting yellow reaction mixture was stirred at room temperature for 18 h. After this time the reaction mixture turned from bright yellow to straw yellow and the suspended solids were allowed to settle. The pale yellow supernatant was filtered off and volatiles were removed from the filtrate *in vacuo* aided by heating to 100 °C to give **26^{Me}** as a pale yellow solid. The filtrant and filtrate were found to be of the same composition by ^{1}H NMR spectroscopy (combined yield: 0.14 g, 58%). ^{1}H NMR (400 MHz, THF-d_8): δ 0.04 (s, 18H, $SiMe_3$), 1.50 (overlapping br s, 18H, *t*Bu-CH_3 x 4, 2.57 (br s, 3H, *a*NHC NMe), 4.42 (br s, 3H, imidazolium NMe), 6.75 (br s, 1H, 4-*a*NHC-*H*), 7.20 (br s, 2H, overlapping 5-*a*NHC-*H* & 2-carb.-*H*), 7.56 (br s, 1H, 7-carb.-*H*), 8.00 (br s, 1H, 4-carb.-*H*), 8.18 (br s, 2H, overlapping 5-imidazolium-*H* & 5-carb.-*H*), 8.61 (m, 1H, 4-imidazolium-*H*), 10.55 (br s, 1H, 2-imidazolium-*H*). Microanalyses of **26^{Me}** persistently returned values low in C, H, and N, consistent with incomplete sample combustion. Example analysis as follows: Calcd. for $C_{34}H_{51}N_6PbISi_2$: C, 43.72; H, 5.50; N, 9.00; Found: C, 41.53; H, 5.25; N, 7.68. IR (Nujol on NaCl plates, cm^{-1}): 1726 (*w*, *sh*), 1665 (*w*, *sh*), 1580 (*m*, *sh*), 1266 (*s*, *sh*), 1220 (*m*, *sh*), 1169 (*m*, *sh*), 932 (*w*, *sh*), 842 (*m*, *sh*). Mp: 208-209 °C (dec.).

Reaction of [K(bimca^{Me})] from KHMDS with $PbCl_2$

THF-d_8 (0.5 mL) was added to a solid mixture of **5^{Me}** (0.013 g, 0.022 mmol) and KHMDS (0.0088 g, 0.044 mmol) to give an amber suspension. The reaction mixture was agitated by inversion for 1 h and turned brown (with blue fluorescence under long wave UV light) and produced an off-white precipitate over this time. Solid $PbCl_2$ (0.0061 g, 0.022 mmol) was added directly to the reaction mixture, which was agitated by inversion for 3 d whilst being monitored by ^{1}H NMR spectroscopy. Over this time the blue fluorescence of K**7^{Me}** gradually disappeared to give a brown reaction mixture that indicated the presence of multiple byproducts which were not purified further. The complex nature of the ^{1}H NMR spectra for this reaction precluded full assignment, see Section 4.4.2 for discussion.

*2:1 Reaction of [Pb(HMDS)$_2$] with bimca(H$_2$I) to form **27^{iPr}***

A hexane stock solution of [Pb(HMDS)$_2$] (5.7 mL, 0.80 mmol, 0.14 M) was added to a yellow suspension of **5^{iPr}** (0.25 g, 0.4 mmol) in THF (20 mL) and stirred at room temperature for 18 h. Over this time the reaction mixture gradually became clearer and turned from yellow to amber. The reaction mixture was filtered and volatiles were removed *in vacuo* to afford **27^{iPr}** as a beige-amber air sensitive solid. Recrystallisation from a saturated room temperature THF solution diffused with hexane and placed at -24 °C formed hexagonal plates of **27^{iPr}** suitable for single crystal X-ray diffraction structure determination (0.38 g, 40%). Microanalyses of **27^{iPr}** persistently returned values low in C, H, and N, potentially due to the inclusion of six equivalents of water, likely incurred during sample handling of this highly moisture sensitive compound. ^{1}H NMR (400 MHz, THF-d_8): δ -0.14 (s, 36H, SiMe$_3$), 1.00 (d, $^3J_{HH}$ = 6.92 Hz, 12H, *a*NHC' N*i*Pr-C*H*$_3$), 1.03 (d, $^3J_{HH}$ = 6.92 Hz, 12H, *a*NHC' N*i*Pr-C*H*$_3$), 1.48 (br s, 18H, *t*Bu-C*H*$_3$), 1.59 (br s, 18H, *t*Bu-C*H*$_3$), 1.63 (d, $^3J_{HH}$ = 6.72 Hz, 24H, NHC N*i*Pr-C*H*$_3$), 4.49 (sept, $^3J_{HH}$ = 6.92 Hz, 2H, *a*NHC' N*i*Pr-C*H*), 5.12 (sept, $^3J_{HH}$ = 6.72 Hz, 2H, NHC N*i*Pr-C*H*), 5.20 (br s, 2H,

5-*a*NHC'-*H*), 7.13 (d, $^{3}J_{HH}$ = 1.48 Hz, 2H, 4-NHC-*H*), 7.72 (d, $^{4}J_{HH}$ = 1.55 Hz, 2H, 7-carb.-*H*), 7.86 (d, $^{4}J_{HH}$ = 1.72, 2H, 2-carb.-*H*), 8.27 (d, $^{4}J_{HH}$ = 1.55, 2H, 5-carb.-*H*), 8.43 (d, $^{4}J_{HH}$ = 1.72 Hz, 2H, 4-carb.-*H*), 8.45 (d, $^{3}J_{HH}$ = 1.48 Hz, 2H, 5-NHC-*H*). Acquisition of ^{13}C NMR data for **27^{iPr}** was frustrated by high sample sensitivity and dilution due to the low reaction yield. Calcd. for $C_{76}H_{114}I_2N_{12}Pb_4Si_4$, **27^{iPr}**: C, 38.18; H, 4.81; N, 7.03. Calcd. for **27^{iPr}**·6 H_2O: C, 36.53; H, 5.07; N, 6.73. Found: C, 35.18; H, 4.67; N, 6.49. IR (Nujol mull on NaCl plates, cm^{-1}): 2358 (*w, sh*), 1660 (*w, sh*), 1538 (*w, sh*), 1260 (*m, sh*), 1169 (*w, sh*), 1094 (*m, sh*), 1019 (*m, sh*), 931 (*w, sh*), 840 (*m, sh*). Mp: 150-153°C (dec.).

Chapter 5 – Main group triazenides: moving from bulky to superbulky supports

5.1 Introduction

Amidinates and guanidinates (Figure 5.1 a - c) have been employed ubiquitously as strong *N*,*N'*-chelates for a range of coordination complexes.[161,162] Careful tuning of the electronic and steric characters of individual ligands can be achieved through judicious selection of substituents at the N and C atoms of the diazaallyl moiety. The chemistry involved for achieving these substitutions is well understood and has generated a comprehensive library of ligands for a variety of niches.[161,162]

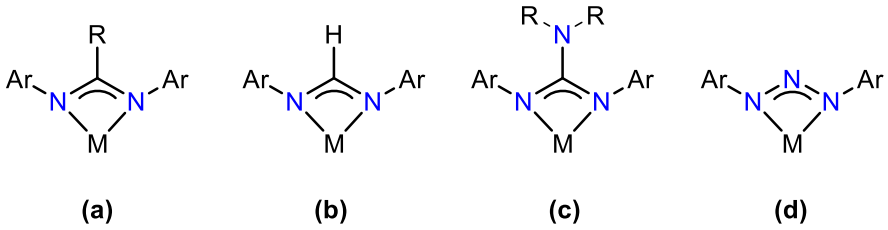

Figure 5.1 General structure of *N*,*N*'-bis(aryl) (a) amidinates, (b) formamidinates, (c) guanidinates, and (d) triazenides (R = cyclic- or acyclic alkyl substituent; Ar = 2,6-di- or 2,4,6-trialkyl substituted phenyl).

Related triazenides (Figure 5.1 d) have similarly found applications in coordination chemistry, albeit with less attention, particularly in main group systems.[163,164] Their steric profile is practically identical to that of the formamidinates (Figure 5.1 b), in turn allowing for close study of the electronic influence of the bridgehead atom (C for formamidinates and N for triazenides) on the resulting coordination complex. Additionally, triazenide ligands have been shown to support metal-metal bonded species through κ^1,κ^1-bridging binding motifs (*vide infra*).

The facile tuning of the steric parameters of the aforementioned ligand systems has been applied to achieve the stabilisation of coordinatively unsaturated metal centres, often using metal-aryl interactions to the flanking *N*,*N'*-aryl substituents (Figure 5.2).[165]

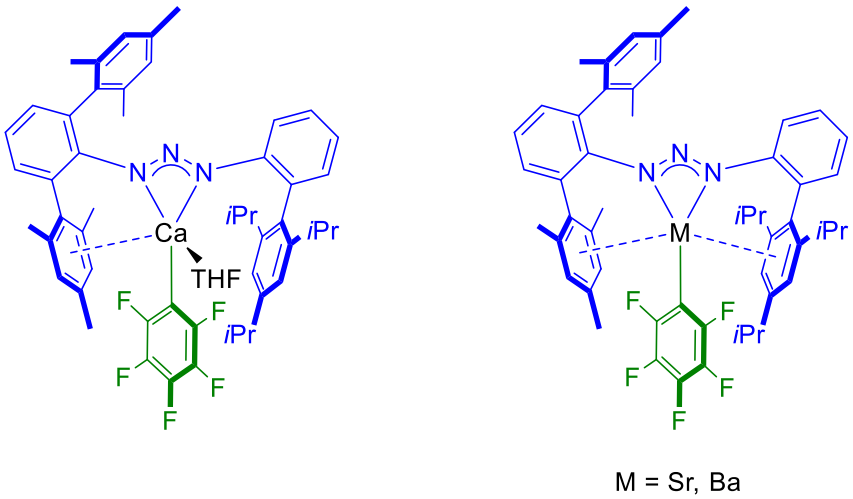

Figure 5.2 Some coordinatively unsaturated *s*-block complexes with bulky triazenide ligands reported by Niemeyer and co-workers supporting rare C_6F_5 ligands.[165]

In general, two methods are used for the synthesis of *N*,*N*'-bis(aryl)triazenides, either (i) proceeding *via* the addition of an aniline to an *in situ* generated diazonium salt,[166] or (ii) from the addition of an aryl carbanion to an electrophilic aryl azide. The latter of these strategies is often employed for "superbulky" *N*-2,6- and 3,5-terphenyl substituents owing to their poor solubility in the aqueous reaction conditions, otherwise necessary for diazotisation (Scheme 5.1), and higher yielding reactions.[165,167] Note that path (ii) is generally followed by hydrolysis to afford the free triazene proligand, which may be stored before deprotonation and complexation.

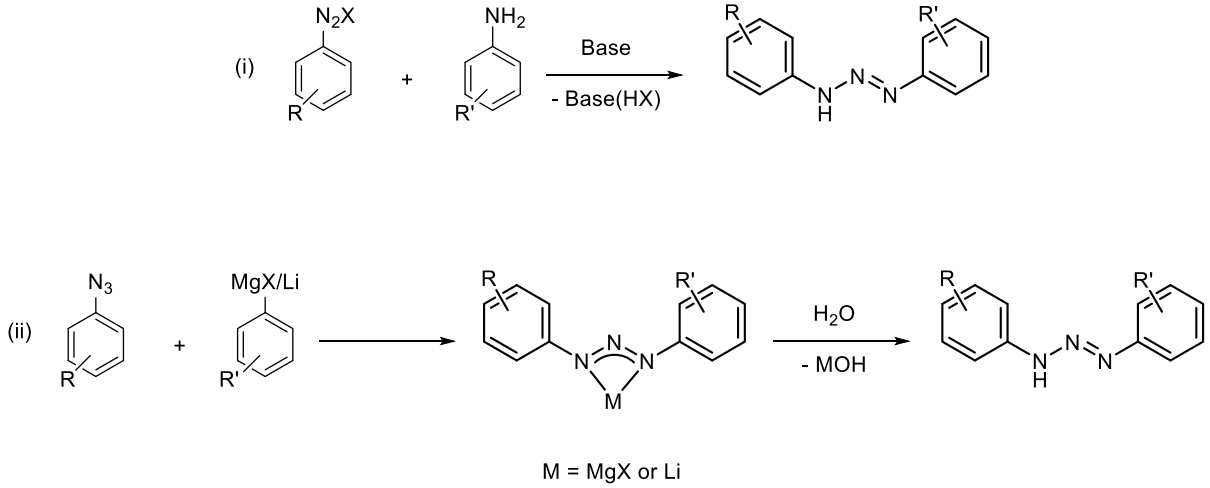

Scheme 5.1 Two general synthetic methods for accessing triazenes.

Additionally, path (ii) benefits from the ability to more easily generate unsymmetrically *N*,*N*'-disubstituted ligand systems through the addition of aryl carbanions to differently substituted aryl azides (Figure 5.3), whereas the typical *in situ* generation of unstable diazonium salts mandates *N,N'*-symmetrical substitution.[165,167]

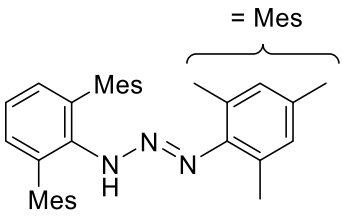

Figure 5.3 Representative example of an unsymmetrical *N*,*N*'-disubstituted triazene.[167]

Surprisingly, only a few reports of triazenide supported main group elements exist,[163,165,167-169] providing an opening for this work. It is generally accepted that triazenides are less σ-donating than their formamidinate counterparts, owing to the electronegativity of the bridgehead nitrogen (Figure 5.1 above) leading to lower overall donation with retention of kinetically stabilising *N*,*N*'-chelation. For this reason triazenides offer themselves as ideal candidates for stabilising low oxidation state main

group elements, which are generally stabilised by electron withdrawing substituents that induce hybridisation of the metal *s*- and *p*-atomic orbitals, according to Bent's rule.[170,171]

Furthermore, the bridgehead nitrogen possesses latent, albeit rarely demonstrated, donor functionality, unlike its formamidinate counterparts. To this end, relatively small *N*-substituents (*e.g.* alkyl, silylalkyl, or unsubstituted aryls) can occasionally enable unusual triazenide binding modes (Figure 5.4 **D**, **E**)[172,173] that deviate from the common κ^2-N1,N3 chelation, κ^1,κ^1-N1,N3 bridging dinuclear, and κ^1-N1 monodentate motifs (Figure 5.4, **A**-**C**).

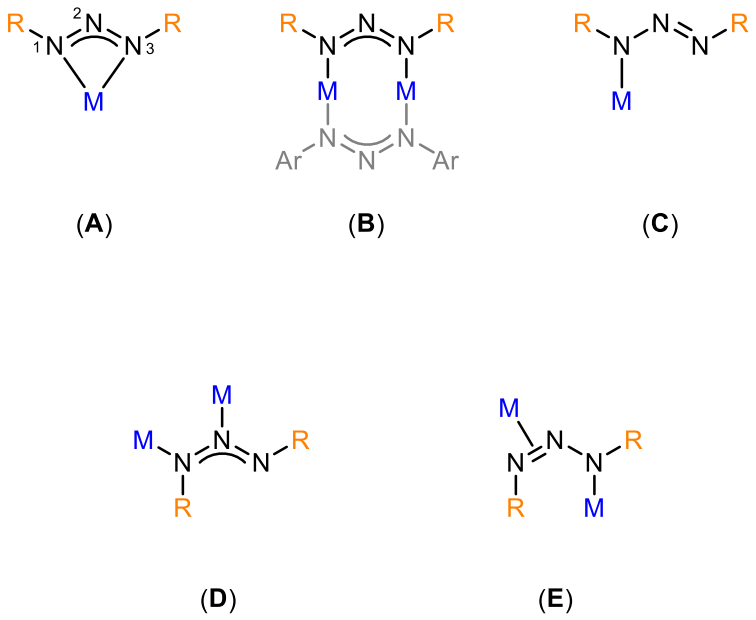

Figure 5.4 κ^2-N1,N3 chelation (**A**), κ^1,κ^1-N1,N3 bridging (**B**), and κ^1-N1 monodentate (**C**) binding modes of triazenides, and the less common κ^1,κ^1-N1,N2 bridging (**D**) and κ^2-N1,N2-κ^1-N3 (**E**).

Coordination modes **A** and **B** above are by far the most commonly reported binding motifs in the literature,[174] where the latter is often observed for metals with a high affinity for metal-metal bonding *e.g.* group 6 and group 11 elements,[175,176] whilst **C** is reported

less frequently, for example in systems with bulky or pendent donor *N*-substituents.[169] Likewise, the rare **D** binding mode is observed only in three examples of nickel and copper bearing an *N*-pyridyl ancillary donor.[172,177] In lanthanide[173] and heavy *s*-block[174] systems the uncommon κ^2-N1,N2-κ^1-N3 motif (**E**) is occasionally observed.

5.1.1 Purpose of this chapter

This chapter seeks to further develop the low valent group 14 coordination chemistry initiated in Chapter 4 to address the shortcomings of the bimca^R ligand system by employment of bulky amide and NHC donors. To this end, focus will be shifted to lead(II), with the anticipation that its redox inflexibility and larger ionic radius, relative to tin(II), will be beneficial for studying its behaviour in tetra-donor coordination environments of the general composition [Pb(Ar_2N_3)(X)(NHC)] (Ar = bulky aryl, X = amide or halide, NHC = IMes) which, to some extent, mimic those of the bimca^R scaffold (*i.e*. anionic *N*-donor with NHC donors), albeit with mono(NHC) coordination.

In view of the benefits of employing a soluble lead(II) bis(amide) complex precursor *vs*. a dihalide (see Chapter 4, Section 4.2), protolytic metallations employing the [Pb($HMDS)_2$] reagent will be used in a pilot study employing the triazene, $Dipp_2N_3H$, the aim being to introduce an NHC donor in a second step, thereby emulating the tridentate coordination of bimca^R in a stepwise fashion and without the rigid pincer framework. This pilot study will also provide entry into the as yet unexplored field of lead triazenide coordination chemistry, which in turn can be developed to include superbulky *N*-substituents, such as the new *N,N'*-unsymmetrical triazenide ligand, 1-(2,6-dimesitylphenyl)-3-(2,6-dibenzhydryl-4-methylphenyl)triazenide (Rock*N_3) which will be targeted herein in a related study.

5.2 Results and Discussion

5.2.1 Pilot studies with $Dipp_2N_3H$

The synthetic hurdles encountered during attempts to coordinate bimca^R at low valent group 14 metals and possible ensuing redox activity, in the case of Sn(II), (Chapter 4, Section 4.2.4) prompted the deployment of a more stepwise approach to this goal. We reasoned that initial coordination by an *N,N'*-bis(aryl) triazenide organoamide, which co-aligns with the application of a carbazolide (*cf.* bimca^{Me}, Chapter 4), would impart beneficial solubilising properties to the resulting complex and likely provide steric protection of the metal centre from potential deleterious side reactions before introduction of a separate NHC ligand. Thus, we sought the development of a sterically encumbered triazenide based ligand system with the option of introducing an NHC co-ligand at a later stage in the synthesis to mimic the donor qualities of the bimca^R framework (Scheme 5.2 i). Alternatively, this approach may be reversed, whereby NHC coordination is carried out first, followed by triazenide coordination (Scheme 5.2 ii). The high solubility of $[Pb(HMDS)_2]$, relative to Pb(II) halide precursors, was noted during studies outlined in Chapter 4, thus inclusion of this organolead amide in our synthetic strategy was deemed crucial.

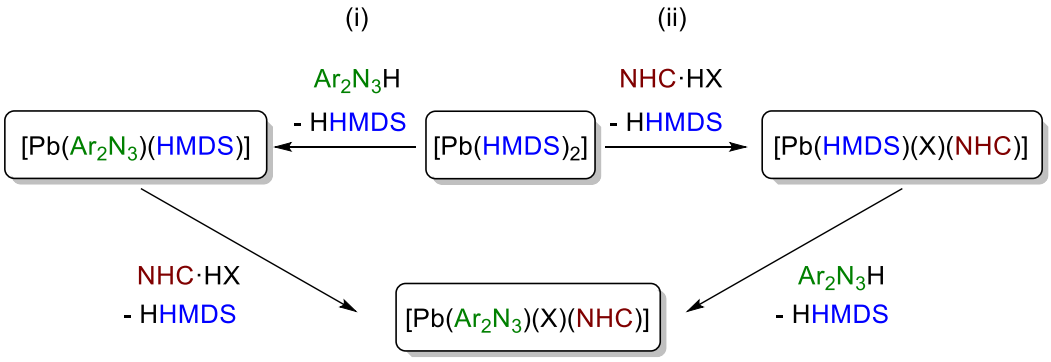

Scheme 5.2 Synthetic strategies for accessing $[Pb(Ar_2N_3)(X)(NHC)]$ *via* protolysis using a $[Pb(HMDS)_2]$ precursor.

The $Dipp_2N_3$ (Dipp = 2,6-diisopropylphenyl) triazenide was chosen for a pilot study given its ease of synthesis and anticipated ability to sterically allow for the coordination of an NHC co-ligand and a monodentate anionic donor, *e.g.* halide, hydride, or amide. Although this approach was unlikely to produce a complex that could spatially accommodate two NHC ligands, as was the goal of the preceding bimca^R study, the possibility of synthesising an enshrouded Pb-X moiety (X = halide, hydride) was attractive.

5.2.2 $Dipp_2N_3H$ triazene Synthesis

This study began with the synthesis of the $Dipp_2N_3H$ triazene proligand in one step by an adapted literature method[166,174] from commercially available starting materials. Freshly distilled $DippNH_2$ was oxidised to the corresponding triazene with two equivalents of freshly prepared isoamyl nitrite. The resulting crude triazene was recrystallised five times from pentane at -24 °C until residual 2,6-diisopropylaniline was less than 10% relative to the major triazene product, as determined by the relative ^1H signal integral ratio of the methine proton septets of these individual species in the ^1H NMR spectrum (C_6D_6) of the recrystallised product ($Dipp_2N_3H$; 3.34 ppm, $DippNH_2$; 2.65 ppm). It is worth noting that the $Dipp_2N_3H$ triazene exhibits low thermal stability and decomposes slowly when stored at room temperature, thus the samples used in this study were stored at -24 °C without noticeable decomposition over extended periods of storage.

The presence of the intractable aniline residue is a common problem faced in this synthetic route and has been discussed in the literature.[174] The difficult removal of all traces of residual aniline starting material is attributed to a strong hydrogen-bonded triazene···aniline pair. Fortunately, the presence of residual aniline did not unduly hamper the subsequent reactivity studies of the desired triazene.

5.2.3 Reaction of $Dipp_2N_3H$ with $[Pb(HMDS)_2]$ in 2:1 stoichiometry

With $Dipp_2N_3H$ in-hand, its reactivity with $[Pb(HMDS)_2]$ and subsequent triazenide coordination was assessed. Coordination through a metathetical ligand transfer reaction (*i.e.* reaction of an alkali metal triazenide salt with a Pb(II) dihalide) was avoided in light of the unforthcoming outcomes obtained *via* this approach during the $bimca^{Me}$ studies presented in Chapter 4, Section 4.4.2, wherein the marked insolubility of the $PbCl_2$ precursor was deemed problematic. By contrast, a protolytic pathway using $[Pb(HMDS)_2]$ promised greater product control. Similar to the $bimca^{R}(H_2I)$ (**5^{R}**) systems, protolysis of the triazene by the HMDS amide was expected to produce the corresponding $[Pb(Dipp_2N_3)_2]$ bis(triazenide) complex, **28**, in a simple one-pot synthesis (Scheme 5.3).

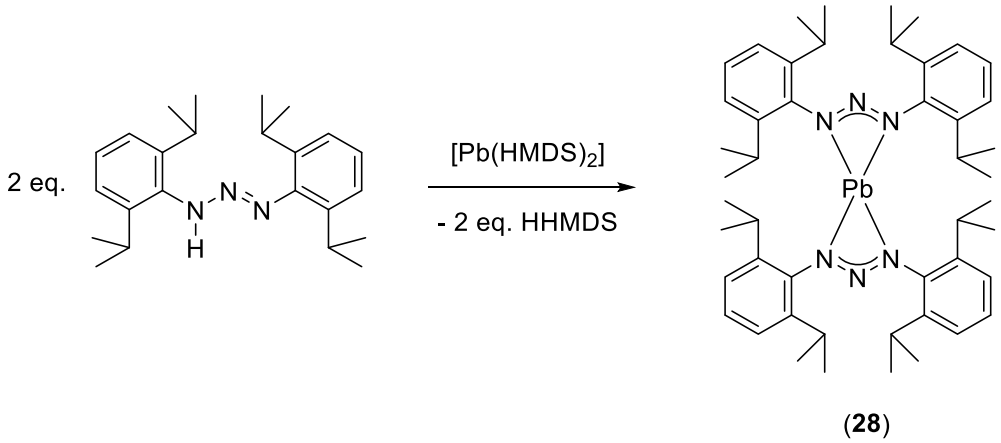

Scheme 5.3 Synthetic strategy for bis(triazenide) complex **28**.

The addition of two equivalents of $DippN_3H$ to one equivalent of $[Pb(HMDS)_2]$ in toluene produced an immediate colour change from amber to bright orange. After 18 hours of stirring at room temperature, removal of the volatiles from the reaction mixture yielded a bright orange microcrystalline solid, **28**. The ^{1}H NMR (C_6D_6) spectrum of the crude product exhibits resonances consistent with a triazenide complex, as indicated by the near disappearance (*ca*. 90%) of the triazene NH singlet resonance at 9.00 ppm in the parent

triazene proligand and an overall downfield shift in the Dipp derived resonances. For example, the methine septet is located at 3.41 ppm with that of the parent triazene at 3.34 ppm.

The ^{1}H NMR spectrum of complex **28** shows no evidence of rotationally locked *N*-2,6-diisopropylphenyl groups, which may be expected around a congested Pb(II) metal centre.[178] Herein, the isopropyl derived resonances of **28**, *i.e.* a single methyl doublet (1.19 ppm) and a methine septet (3.41 ppm) are single sharp resonances at room temperature on the NMR time scale, suggesting that **28** is highly symmetrical and the isopropyl groups are rotationally mobile in solution under these conditions.

The solid state structure of **28** provides further information on the bonding arrangement of the two triazenide ligands about its Pb(II) metal centre (Figure 5.5). Large, orange rectangular prisms of **28** were grown from a saturated room temperature hexane solution placed at 4 °C and subsequently analysed by single crystal X-ray diffraction structure determination.

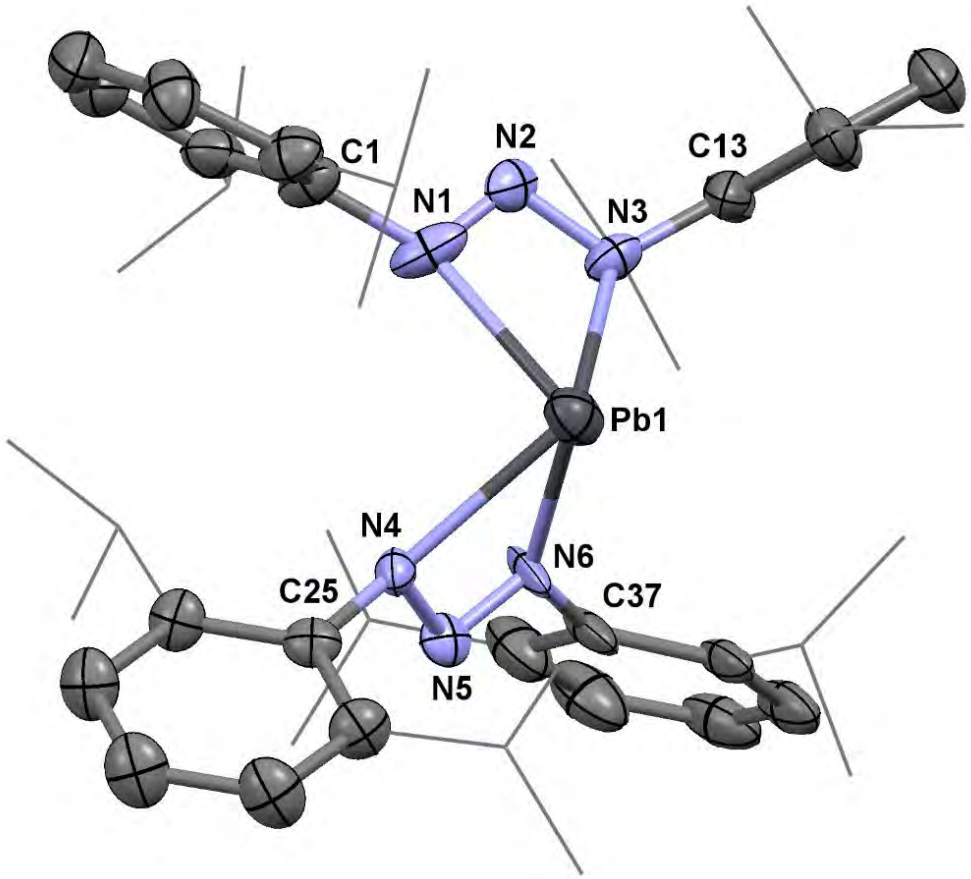

Figure 5.5 Molecular structure of [Pb(Dipp$_2$N$_3$)$_2$], **28**, shown with thermal ellipsoids of 50% probability. Hydrogen atoms, lattice solvent, and disordered atoms are omitted and isopropyl groups are displayed as wireframes for clarity. Selected bond lengths (Å): Pb1-N1: 2.358(7), Pb1-N3: 2.363(7), Pb1-N4: 2.402(6), Pb1-N6: 2.401(6), N1-C1: 1.439(11), N3-C13: 1.503(9), N1-N2: 1.250(11), N2-N3: 1.301(9), N4-C25: 1.452(10), N6-C37: 1.450(10), N4-N5: 1.290(9), N5-N6: 1.269(9), and angles (°): N1-N2-N3: 110.7(7), N4-N5-N6: 110.6(6), N3-Pb1-N6: 87.5(2), N1-Pb1-N4: 88.9(3), N1,N3,Pb1-N1,N2,N3: 24.5, N4,N6,Pb1-N4,N5,N6: 21.6.

Complex **28** crystallises in the monoclinic space group $P2_1/c$ with one molecule of **28** and one heavily disordered hexane molecule in the asymmetric unit. Two *N*-Dipp rings are considerably disordered, presumably due to the interaction of their isopropyl methyl substituents with the Pb(II) metal centre (*vide infra*). All non-hydrogen atoms were

located experimentally and refined using anisotropic displacement parameters. Hydrogen atoms were placed in calculated positions (riding model).

The molecular structure of **28** (Figure 5.5) clearly shows the coordination of two $Dipp_2N_3$ ligands at a four coordinate Pb(II) metal centre that may be described as a heavily distorted "seesaw" (AX_4E) valence geometry, with each triazenide nitrogen donor viewed as a two-electron point donor, and where the vacant coordination site on Pb1 is presumably occupied by the metal non-bonding electron pair, *vide infra*. Complex **28** is the first structurally authenticated Pb(II) triazenide and its AX_4E coordination geometry, although highly strained, is consistent with other more flexible four-coordinate divalent tetra-*N*-donor lead species;[179-181] for example, the *N*-trimethylsilyl NacNac complex, $[Pb\{(SiMe_3)_2NacNac\}_2]$, reported by Lappert and co-workers (Figure 5.6), which exhibits N-Pb-N angles of 166.21(10)° and 92.86(10)° between the axial and equatorial nitrogen donors respectively.[179] The analogous measures in **28** deviate from ideal geometry considerably; N3-Pb1-N4: 122.0(2)° and N1-Pb1-N6: 97.0(3)°, which is indicative of the smaller bite angle of the $Dipp_2N_3$ ligand and the steric buttressing of the *N*-Dipp substituents.

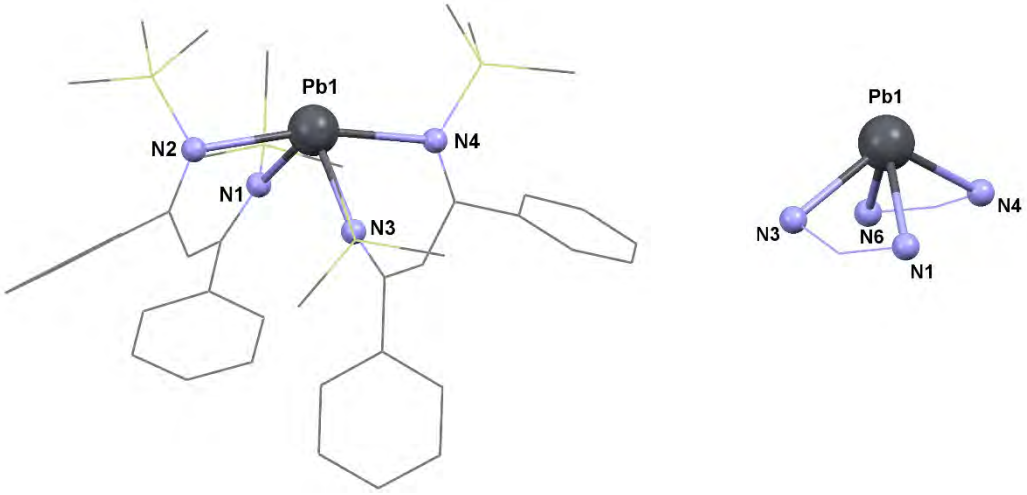

Lappert *et al.* (**28**)

Figure 5.6 Molecular structure of [Pb{(SiMe$_3$)$_2$NacNac}$_2$] reported by Lappert and co-workers exhibiting distorted AX$_4$E geometry about the lead(II) metal centre (left) (CSD code: FOCPET).[179] Pb-N core of complex **28** (right). Non-participating *N*-substituents are depicted as wireframes (left) or omitted (right) for clarity.

The unusually strained core of **28** exhibits similar metrics to the previously reported and similarly strained bis(formamidinate); [Pb(Fiso)$_2$] (Fiso = *N,N′*-bis(2,6-diisopropylphenyl)formamidinate), [178] which provides a further useful literature comparison.

Both **28** and [Pb(Fiso)$_2$] exhibit near identical core structures, including an out-of-plane distortion in the N,E,N,Pb metallacycles (E = N in **28**; CH in [Pb(Fiso)$_2$]), wherein the bridgehead atom projects outward from the N,N,Pb plane by an average of 23.1° in **28** and 14.4° in [Pb(Fiso)$_2$]. Figure 5.7 provides an overlay of the metallacyclic cores of both **28** and [Pb(Fiso)$_2$].

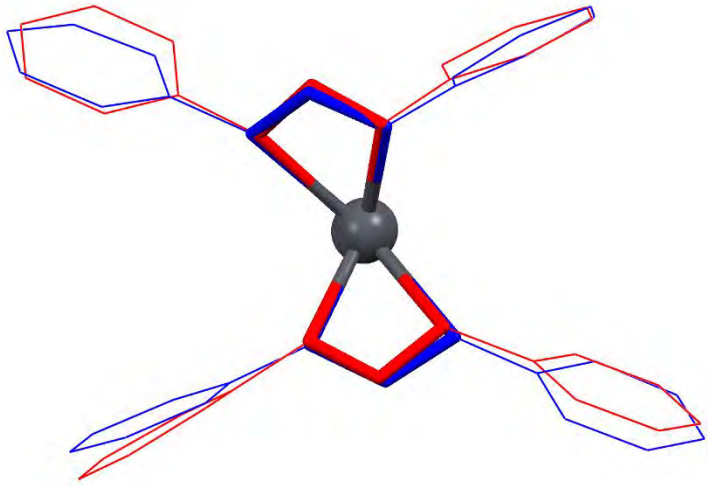

Figure 5.7 Structure overlay of **28** (red) and [Pb(Fiso)$_2$] (CSD code: GODWUS)[178] (blue) showing their geometrical similarities. Core structures are emphasised with thick bonds and isopropyl residues are omitted for clarity.

The distorted coordination geometry at the metal centre in **28** is consistent with hybridisation of the Pb(II) *s*- and *p*-valence orbitals as induced by coordination of the Dipp$_2$N$_3$ and thus in agreement with Bent's rule (*vide supra*) and fits the general trend described by Bock and co-workers in a comprehensive survey of lead coordination complexes reported in the Cambridge Structural Database.[182] This report surmises that low coordinate Pb(II) species, *i.e*. with coordination numbers between 2-5, bearing "hard" donor ligands exhibit metal non-bonding electron pairs with directional *p*-components leading them to occupy a vacant site on the metal centre.[182]

Highly strained divalent group 14 coordination geometries have also been observed for other more sterically demanding ligand systems and can cause considerable sterically-induced activation of the non-bonding valence electrons (*cf*. 2,6-terphenyl ligands popularised by Power and Robinson, Chapter 1 Sections 1.2). Under such conditions, comparable Sn(II) and Pb(II) complexes have displayed inter- or intramolecular E-H···M (E = B, C, N)[29,183,184] bond interactions either with small

molecules or through agostic interactions with the ligand scaffold, most notably with B-H substituents.[185] Thus, we further scrutinised the X-ray diffraction data of **28** for additional information regarding further indicators toward similar interactions (Figure 5.8).

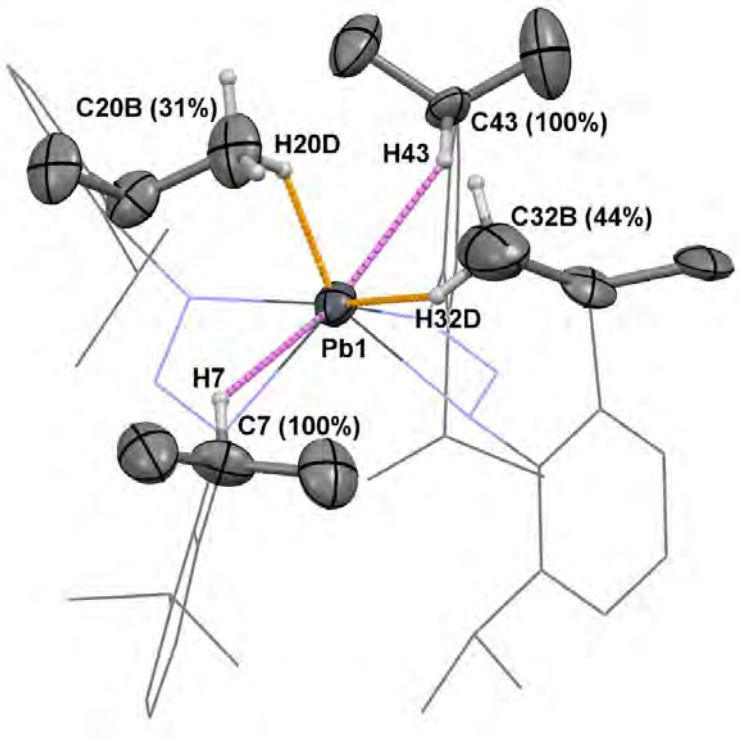

Figure 5.8 Possible agostic contacts of protons of two methyl (orange) and two methine (pink) groups with the Pb(II) metal centre in **28**. Chemical occupancies of the attached carbon atoms are shown in parentheses. Non-participating ligand framework and hydrogen atoms are depicted as wireframes or omitted for clarity. Selected distances (Å): Pb1···H20D: 2.0223(2), Pb1···C20B: 2.78(4), Pb1···H32D: 2.1837(3), Pb1···C32B: 2.92(6), Pb1···H7: 2.7890(4), Pb1···C7: 3.589(9), Pb1···H43: 2.7190(4), Pb1···C43: 3.606(8).

Careful examination of the rotational disorder of two of the eight Dipp isopropyl residues in the solid state structure of **28** reveals a C-H···Pb close contact, *i.e.* likely agostic interactions, to the methyl moieties (C20B and C32B with site occupancies of 31% and 44% respectively). The close facial approach of these methyl groups to the vacant

coordination site of the Pb(II) metal centre suggests an interaction between the non-bonding metal valence electrons of the AX_4E Pb(II) and the protons attached to C20B and C32B (Figure 5.8). Although the hydrogen atoms of these methyl groups (H20D and H32D) could not be located experimentally, despite efforts to do so, their modelled attachments to the anisotropically refined C20B and C32B place them within the sum of the van der Waals' radii of both Pb, H and Pb, C (3.22 Å, 3.72 Å respectively)[98] with an average Pb···H_{methyl} distance of 2.10 Å and average Pb···C_{methyl} distance of 2.85 Å. In addition to the methyl C-H···Pb interactions, longer contacts to the two opposing isopropyl methine protons (attached to C7 and C43), which also face the Pb(II) vacant site, are evident with average Pb···$H_{methine}$ and Pb···$C_{methine}$ distances of 2.75 Å and 3.60 Å respectively (both within combined van der Waals' radii). Interestingly, the latter methine interactions are also observed in the crystal structure of [Pb(Fiso)$_2$] with comparable metrics (Pb···H: 2.75 Å, Pb···C: 3.61 Å),[178] however further close contacts, such as those found for the methyl groups in **28**, are not present.

While Pb···E-H interactions have been reported (*vide supra*), Pb···H-C_{alkyl} interactions are uncommon.[70,183] The tentatively proposed solid state agostic interaction in **28** is likely relatively weak, since it poses no rotational barrier in solution at room temperature, *cf.* the ^{1}H NMR spectrum of **28**, which indicates that all isopropyl methyl protons are chemically equivalent without noticeable broadening (1.19 ppm in C_6D_6). This high degree of symmetry in solution is inconsistent with hindered rotation that would be expected upon formation of a robust agostic Pb···H-C interaction. The test of this hypothesis was deemed to be beyond the scope of this work and is the subject of future studies. To this end, future pursuits may include variable-temperature NMR spectroscopic studies to determine the presence of rotational barriers in solution.

5.2.4 Synthesis of [Pb(Dipp$_2$N$_3$)(HMDS)], ***29***

Since [Pb(HMDS)$_2$] was found to be suitable for the preparation of **28**, it was thought prudent to attempt to access the heteroleptic [Pb(Dipp$_2$N$_3$)(HMDS)] complex, **29**, by similar methods using one equivalent of Dipp$_2$N$_3$H instead of the two used to generate **28**. It was expected that **29** could act as a functional intermediate to complexes of the general form [Pb(Dipp$_2$N$_3$)(X)(NHC)] (Section 5.2.1, Scheme 5.2) through the ability of the HMDS co-ligand at the Pb(II) centre of **29** to deprotonate an equivalent of an imidazolium halide NHC precursor. Accordingly, this path is analogous to the *in situ* protolysis and metallation approach utilised in Chapter 4, Section 4.2.2.

The equimolar reaction of [Pb(HMDS)$_2$] with Dipp$_2$N$_3$H led to the expected colour change from a colourless to an orange solution (*cf*. orange colour change upon preparation of **28**). Removal of volatiles from the reaction mixture also afforded an orange, microcrystalline solid that was evaluated by ^{1}H NMR spectroscopy. The ^{1}H NMR spectrum (C_6D_6) of the crude vacuum dried reaction mixture indicates the presence of two species, one characterises as per the expected heteroleptic species [Pb(Dipp$_2$N$_3$)(HMDS)], **29**, and a second as compound **28** in a *ca*. 4:1 relative signal integral ratio of the isopropyl substituent resonances (Figure 5.9). Small amounts of the volatile [Pb(HMDS)$_2$] are also evident at high field (0.25 ppm).

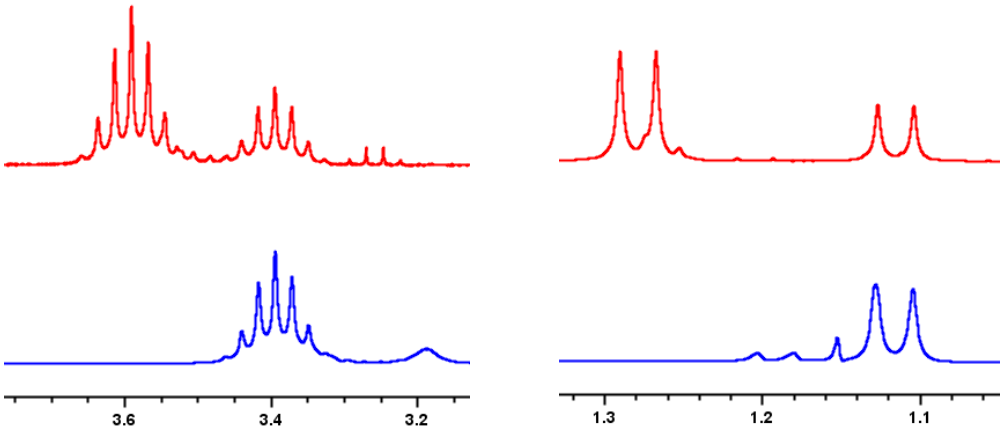

Figure 5.9 Excerpts from the ^{1}H NMR (C_6D_6) spectra showing the methine (left) and isopropyl methyl (right) resonances of the attempted preparation of **29** (red) and those of **28** (blue).

This suggests that the selective isolation of **29** from this reaction is impossible with respect to redistribution to the homoleptic products, particularly when reaction workups involve vacuum drying (volatile homoleptic [Pb(HMDS)$_2$)]). Furthermore, the high solubility of [Pb(HMDS)$_2$] likely also favours the formation of **28** and [Pb(HMDS)$_2$] from **29** in solution.

Indeed, attempts to recrystallise the crude product from a room temperature saturated hexane solution placed at -24 °C yielded only crystals that characterised as **28**. This marked instability in solution frustrated characterisation of **29** by X-ray crystallography and ^{13}C NMR. This kind of behaviour has also been documented for the Sn(II) complex when attempting to prepare [Sn(Dipp$_2$N$_3$)(HMDS)] from [Sn(HMDS)$_2$].[186]

*5.2.5 Attempted reaction of **29** with IMes·HCl*

As pure samples of **29** could not be obtained due to its inherent tendency to redistribute to homoleptic complexes, the installation of an IMes co-ligand through *in situ* protolysis of an imidazolium salt and metallation was still attempted with **28**. It was reasoned that

the triazenide could deprotonate an imidazolium C2 position under these conditions and still afford the desired [Pb(Dipp$_2$N$_3$)(Cl)(IMes)] complex, **30** (Scheme 5.4).

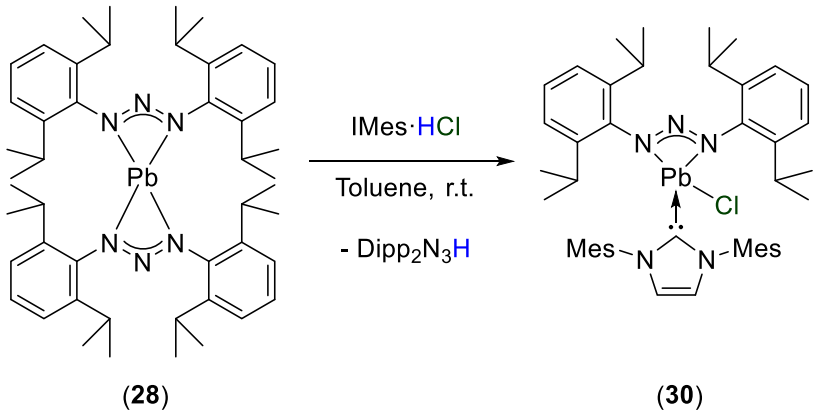

(**28**) (**30**)

Scheme 5.4 Attempted protolysis of IMes·HCl with **28** to access **30**.

Thus, the reaction of **28** with one equivalent of IMes·HCl was carried out in toluene with the gradual consumption of the solid IMes·HCl to give a less cloudy reaction mixture. Filtration after 18 hours and removal of volatiles from the filtrate *in vacuo* afforded an off-white microcrystalline solid, **31**.

The ^{1}H NMR spectrum (C_6D_6) of the crude solid, **31**, exhibits signals corresponding to alkyl signals of triazene and triazenide related compounds in roughly equimolar proportions as well as large amounts of unreacted **28** (*ca*. 50%), with broad septets at 3.34 ppm (triazene) and 3.87 ppm (triazenide), and doublets at 1.11 ppm (triazene) and 1.34 ppm (triazenide). Additionally, the presence of a single set of resonances attributable to an IMes species is also visible, marked by singlets at 6.75 (*m*-Ar*H*), 6.42 (4,5-C$_2$*H*$_2$), 2.13, and 2.05 (*o*- and *p*-CH$_3$) ppm. Interestingly, a broad singlet at 10.20 ppm is observed, where imidazolium C2-H resonances normally lie, with a relative signal integral half that of the above IMes resoances. This resonance is also distinct from the triazene NH resonance (9.36 ppm). Furthermore, the above triazene chemical shifts closely match

those of isolated $Dipp_2N_3H$ (C_6D_6), whereas the chemical shifts assigned to a triazenide species, distinct from **28**, are shifted downfield to both $Dipp_2N_3H$ and **28**.

To provide further information on the origin of the ^1H NMR data for **31**, single crystals were grown from the crude solid and found to be suitable for X-ray diffraction structural analysis (Figure 5.10). Interestingly, the molecular structure of this crystalline compound shows no inclusion of lead or chlorine, contrary to our expectations. Instead, **31** represents a unique example of an imidazolium triazenide ion pair, co-crystallised with its neutral IMes and $Dipp_2N_3H$ complements.

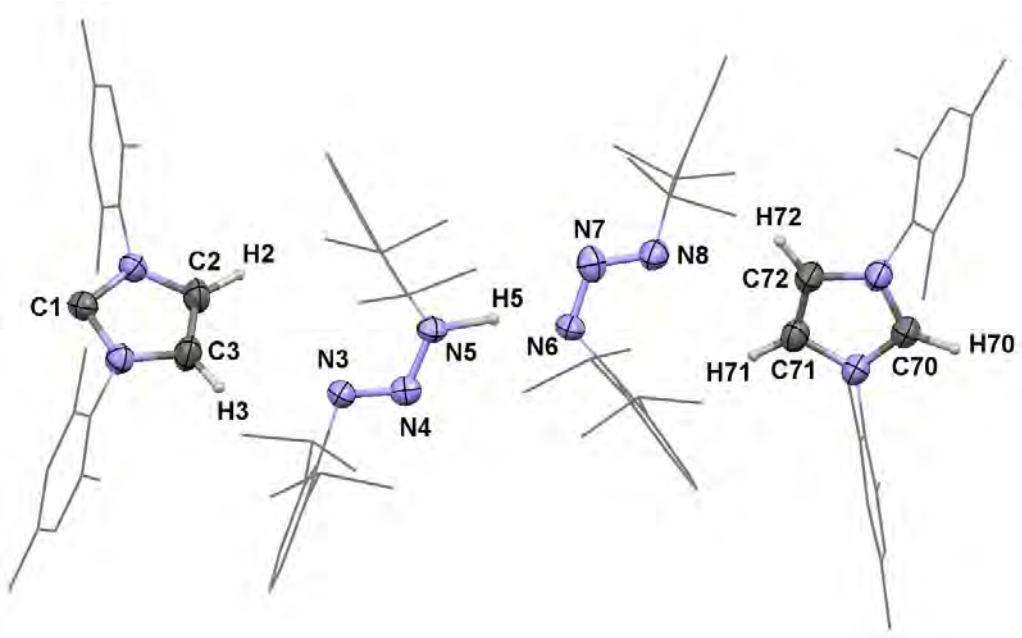

Figure 5.10 Molecular structure of the ion pair **31** shown with thermal ellipsoids of 50% probability. *N*-aryl substituents are shown as wireframes and hydrogen atoms, excepting those of the core imidazolyl and triazenyl functions, are omitted for clarity. Selected bond lengths (Å): N3-N4: 1.277(3), N4-N5: 1.334(3), N6-N7: 1.328(3), N7-N8: 1.276(3), N6···H5: 1550(16), C70-H70: 1.028(18), N8···H72: 2.54(3), N3···H3: 2.65(3), C1···H70: 2.33(2), and angles (°): N3-N4-N5: 115.3(2), N6-N7-N8: 115.7(2), N1-C1-N2: 100.9(2), N9-C70-N10: 107.8(3).

Compound **31** crystallises in the monoclinic space group $P2_1/c$ with one IMes, one IMes·H cation, one $Dipp_2N_3$ anion, one $Dipp_2N_3H$, and one molecule of toluene in asymmetric unit. A clear distinction can be made between the IMes·H imidazolium cation and the neutral IMes through measurement of the respective endocyclic N-C-N bond angles, whereby the IMes·H N-C-N bond angle is 107.8(3)° whilst the non-C2 protonated IMes exhibits a more acute angle of 100.9(2)°. Both are in good agreement with the metrics of the respective isolated entities, *e.g.* 101.4(2)° in IMes and 108.25(10)° in IMes·HCl. [100,187] The C2 proton of the IMes·H cation in **31** was located experimentally and refined isotropically. It exhibits a C-H bond length of 1.028(18) Å, which is longer than the analogous bond length in IMes·HCl (0.924(15) Å) [187] and possibly due to the close approach of the IMes carbenic carbon. However, the solution state room temperature ^{1}H NMR spectrum of **31** shows the coalescence of the IMes·H and IMes resonances to a single set of singlet resonances at 2.05, 2.13 ppm (*o*- and *p*-CH_3), and 6.42, 6.75 ppm (4,5-C$_2H_2$ and *m*-Ar*H*), it should be noted that these are distinct from those of free IMes in C_6D_6 (2.16, 6.48, 6.81 ppm in C_6D_6). We speculate that this signal coalescence may be due to rapid flux of the imidazolium C2 proton between each imidazolyl moiety (*cf.* $\mathbf{6^{Me}}$ Chapter 2, Section 2.3.3).

In contrast to the fluxional hydrogen placement observed within the $IMes_2H$ cation, both the solution and solid state data for the triazene and triazenide moieties are discernible. Notably, the experimentally derived location of the triazene NH proton (H5) from difference maps distinguishes it from the N6-N7-N8 triazenide anion. Further to this, the close approach of N8 to a 4,5-imidaozlyl proton (H72) of the IMes·H cation at a distance of 2.54(3) Å and 3.111(4) Å to its bound carbon (N8···C72) (sum of N, H and N, C van der Waals' radii: 2.75 and 3.25 Å respectively) suggests an interaction between an anionic nitrogen and the backbone proton of the imidazolium and thus supports our hypothesis

that N8 belongs to the triazenide anion. These metrics are comparable to the previously discussed bimca^{R}(H_2I), **5^{R}**, zwitterions (*cf.* bimca^{Me}(H_2I) average intermolecular N···H distance: 2.56 Å, Chapter 2, Section 2.3.1), which display similar intermolecular interactions. The intermolecular interactions observed in the asymmetric unit of **31** are also borne out in its supramolecular bonding arrangements, wherein the imidazolium C2 proton of one asymmetric unit is in close contact with the carbenic carbon of an IMes molecule of an adjacent asymmetric unit (H70···#C1: 2.33(2) Å) forming one dimensional close contact hydrogen-bridged polymers in the solid state (Figure 5.11).

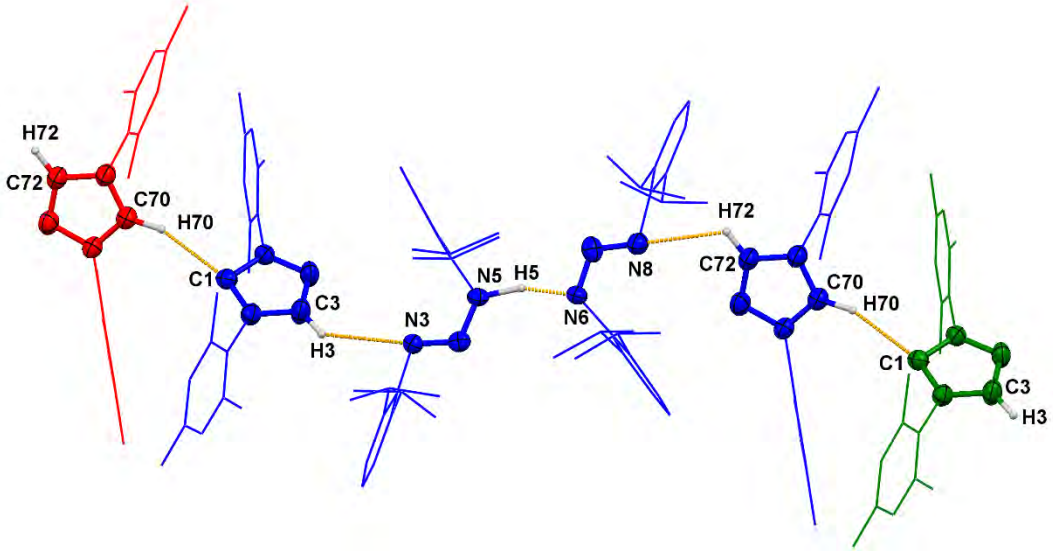

Figure 5.11 Supramolecular bonding interactions across three asymmetric units shown in red, blue, and green in the solid state packing of **31**. Selected distances (Å): C1···H70: 233(2), N3···H3: 2.65(3), N6···H5: 1550(16), N8···H72: 2.54(3), and angles (°): C1···H70-C70: 161(2), N3···H3-C3: 122(2), N6···H5-N5: 155(3), N8···H72-C72: 117.7(19).

Compound **31** possibly represents a salt metathesis elimination product from the reaction of [Pb(Dipp$_2$N$_3$)$_2$] and IMes·HCl where chloride is exchanged for Dipp$_2$N$_3$ triazenide to generate one equivalent of [IMes·H][Dipp$_2$N$_3$] (leaving one equivalent of **28** unreacted in

solution) wherein intermolecular proton transfer between these components accounts for the isolation of two protonated and to non-protonated components, as per the crystal structure of **31** (Scheme 5.5, A). Conversely, deprotonation of IMes·HCl by a triazenide ligand of **28**, as per our initial expectation, followed by imidazolium salt methathesis (as per A) and release of IMes from a transient [$PbCl_2$(IMes)] could also yield the same reaction outcome (Scheme 5.5, B), *i.e.* half an equivalent of each of **31**, **28**, and $PbCl_2$. The precipitation of $PbCl_2$ *via* either pathway is consistent with experimental observations and presumably provides a thermodynamic driving force for the formation of the remaining ^{1}H NMR spectroscopically visible products in the crude vacuum dried reaction mother liquor, *i.e.* **31** and **28**. However, at this stage it is unclear if the triazenide ligands of **28** are basic enough to deprotonate IMes·HCl.

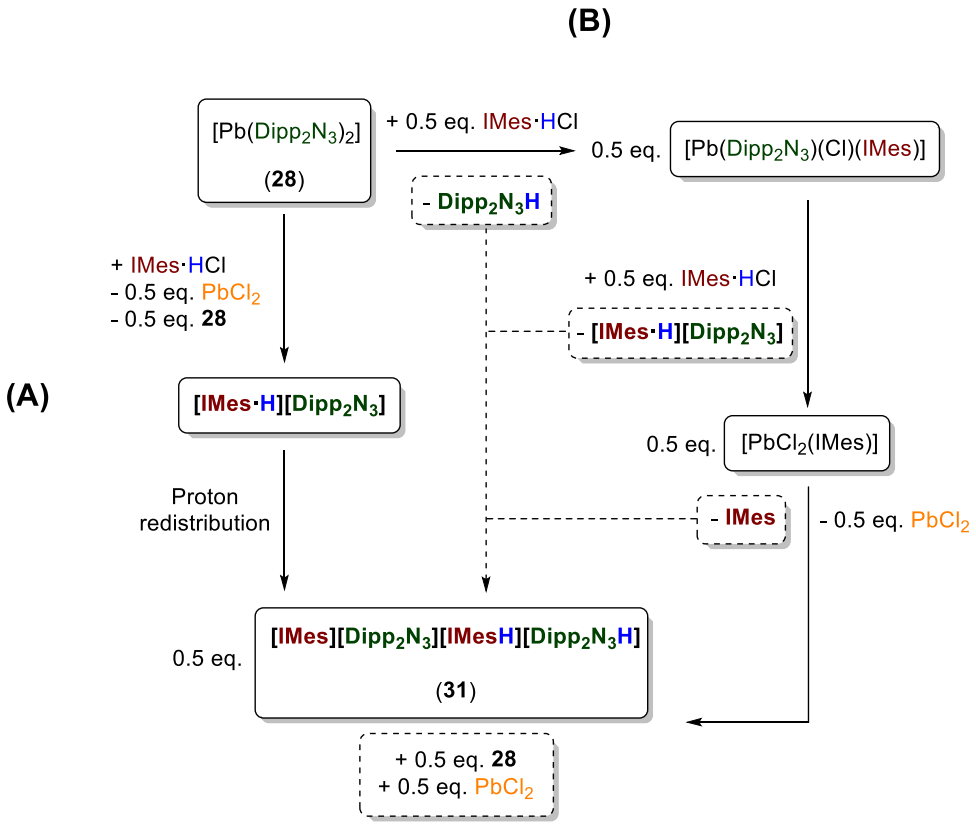

Scheme 5.5 Possible reaction path for forming **31** from the reaction of **28** with one equivalent of IMes·HCl.

5.2.6 NHC pre-coordination followed by triazene addition

Our synthetic strategy was changed to avoid the formation of **31** by attempting to form [Pb(HMDS)(Cl)(IMes)], **32**, through initial protolysis of an imidazolium salt with [Pb(HMDS)$_2$] followed by the addition of Dipp$_2$N$_3$H, with the ultimate goal being to prepare [Pb(Dipp$_2$N$_3$)(Cl)(IMes)], **30** (Scheme 5.6).

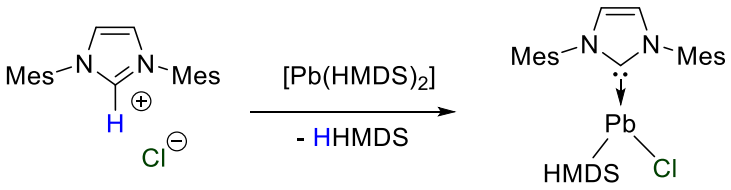

Scheme 5.6 Synthetic strategy for IMes coordination to Pb(II) *via* protolysis.

Thus, a hexane solution of [Pb(HMDS)$_2$] was added to an equimolar suspension of IMes·HCl in toluene to give a pale yellow reaction mixture that gradually cleared over 18 hours at room temperature. Removal of volatiles *in vacuo* gave an extremely moisture sensitive pale yellow solid, **32**. Successful deprotonation of IMes·HCl and the coordination of IMes is evidenced in the ^{1}H NMR (C_6D_6) spectrum of **32** by the disappearance of the C2-H singlet resonance (previously at 9.70 ppm in DMSO-*d*$_6$), and downfield shifting of the IMes ^{1}H NMR resonances at 6.77 ppm and 6.20 ppm, attributable to the mesityl aryl- and 4,5-imidazolyl protons respectively, relative to those of free IMes (C_6D_6) at 6.81 ppm and 6.47 ppm respectively. The appearance of a new singlet resonance at 0.23 ppm with a signal integral of 18 relative to the IMes associated resonances is attributable to a HMDS moiety, which is distinct from [Pb(HMDS)$_2$] (0.25 ppm). It was noted that complex **32** is extremely susceptible to protonation affording a colourless intractable solid upon decomposition, as noted during transfer of mother liquors containing **32** to fresh glassware. This frustrated attempts to isolate pure samples of **32** and thwarted its crystallographic characterisation. In light of the aims of

this study, *i.e*. accessing a [Pb(Dipp$_2$N$_3$)(Cl)(IMes)], **30**, this led us to pursue the use of **32** as a reagent *in situ* rather than attempting its isolation for subsequent reactions.

Thus, with **32** generated *in situ*, protolysis *via* step ii (Section 5.2.1, Scheme 5.2) was attempted. The addition of one equivalent of Dipp$_2$N$_3$H triazene to intermediate **32** proceeded without any visual indication of reaction, and filtration and recrystallisation of the filtrate led to the isolation of Dipp$_2$N$_3$H with near quantitative recovery. This suggests that no reaction takes place, presumably due to steric effects (Scheme 5.7).

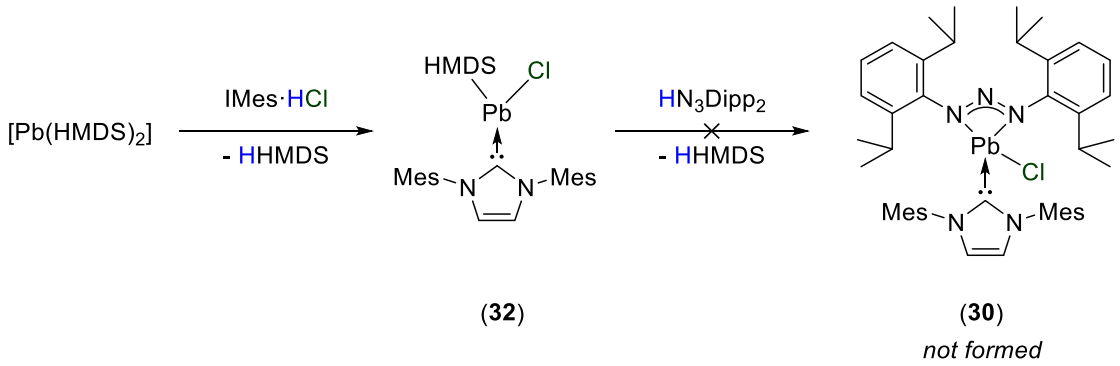

Scheme 5.7 Attempted *in situ* triazenide coordination to **32** to access **30**.

5.3 Development of a bulkier triazenide ligand

Installation of the relatively bulky IMes NHC donor with the N$_3$Dipp$_2$ triazenide proved to be challenging, likely due to a combination of steric and electronic effects. These outcomes compliment those from Chapter 4 concerning our efforts to access [Pb(bimca^{Me})X], which proved similarly challenging (Section 4.4). The use of strongly σ-donating bulky NHC ligands was thus discontinued at this stage and the use of smaller alkyl NHCs to address possible steric issues was not investigated. Instead, focus was directed toward the development of a bulkier triazenide ligand that could achieve higher degrees of steric shielding and, through either pendant arene coordination or low electron

donicity, afford stable [Pb(Ar'$_2$N$_3$)(X)] (Ar' = superbulky aryl, X = amide or halide) species for further study.

*5.3.1 Synthesis of Rock*N$_3$H*

The work of Niemeyer *et al*. provides an ideal strategy for accessing *N*,*N*'-unsymmetrical triazenides and presents the foundation for the synthesis of the target unsymmetrical proligand DmpN$_3$HDipp* (Rock*N$_3$H, **33**) (Scheme 5.8).[165]

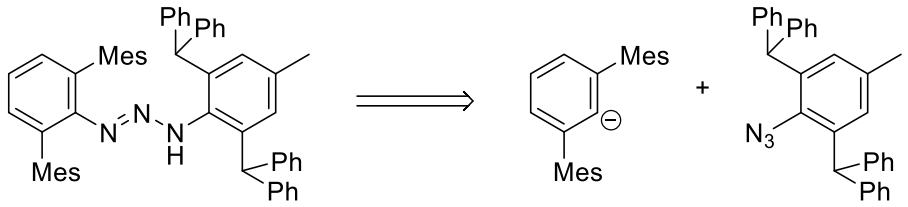

(**33**)

(i) (ii)

Scheme 5.8 (i) Target triazene, Rock*N$_3$H (**33**), (ii) Necessary Dmp$^-$ and Dipp*N$_3$ synthons.

The nitrogen substituents of Rock*N$_3$H were selected for their relative ease of access and handling, whilst also providing a platform for assessing the steric characteristics of a system that contained a relatively rigid and spatially imposing 2,6-dimesitylphenyl (Dmp) and a more flexible 2,6-bis(diphenylmethyl)-4-tolyl (Dipp*) moiety, both of which have been used to synthesise the respective symmetrical triazenides in the Cole group.[188,189] A representative synthesis of the symmetrical Dmp$_2$N$_3$H triazene, for example, is illustrated in Scheme 5.9.

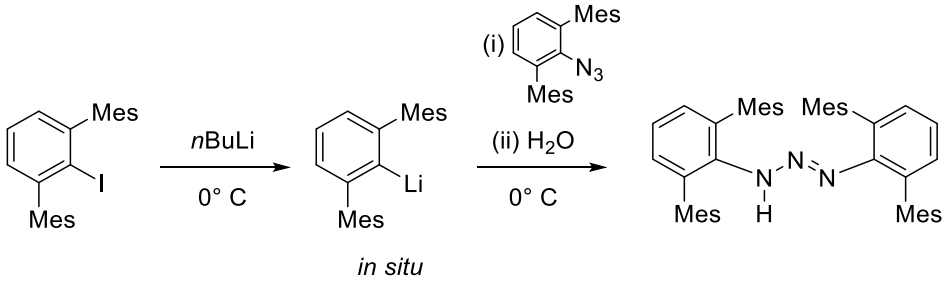

Scheme 5.9 Representative synthesis of the Dmp_2N_3H triazene.[188]

The preparation of the unsymmetrical Rock*N_3H system was anticipated to proceed in an analogous manner. For synthetic ease, DmpI and Dipp*N_3 precursors were chosen[6] rather than Dipp*I and $DmpN_3$ as the former (Dipp*I) co-elutes with both Dipp*NH_2 and Dipp*H making its preparation more arduous.[189]

5.3.2 DippN_3 preparation*

The Dipp*N_3 azide lends itself as a good synthetic equivalent for the Dipp* containing synthon as it may be prepared in good yields (79-96%) from the respective aniline through diazotisation and substitution. The aniline, Dipp*NH_2, can be prepared in bulk quantities from the high yielding (86%) reaction of *p*-toluidine and benzhydrol under Friedel-Crafts conditions (Scheme 5.10).[190]

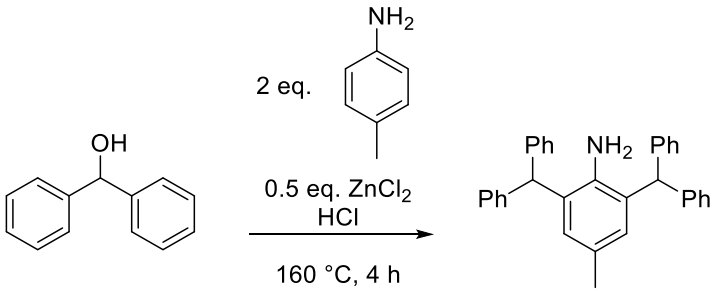

Scheme 5.10 Accessing Dipp*NH_2.[190]

[6] DmpI was synthesised in a convergent manner *via* a Grignard intermediate according to a literature procedure from commercially available starting materials (see experimental section for reference).

The Dipp* aniline was converted to the azide by oxidation through a Sandmeyer reaction, as adapted during previous studies in the Cole group,[189] using concentrated H_2SO_4 and sodium nitrite at -20 °C, to form the corresponding aryl diazonium salt, followed by nucleophilic substitution with sodium azide, warming to room temperature and extraction into diethyl ether. Dipp*N_3 of suitable purity for further reaction was obtained by recrystallisation of the diethyl ether extract from THF-diethyl ether (1:1) (Scheme 5.11).

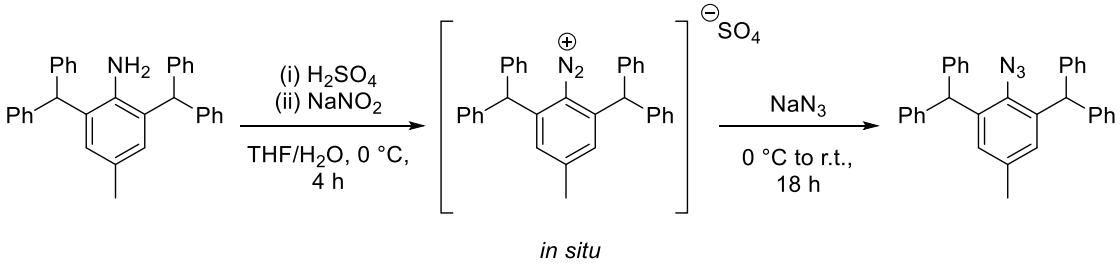

Scheme 5.11 Preparation of Dipp*N_3.

5.3.3 Synthesis of the unsymmetrical triazene

With both DmpI and Dipp*N_3 reagents in-hand, the synthesis of Rock*N_3H was attempted through Dmp carbanion addition to Dipp*N_3. The Dmp carbanion was generated from the reaction of *n*BuLi with DmpI in Et_2O at -78 °C, to form the corresponding aryllithium, and added directly to a THF solution of Dipp*N_3 at -78 °C. The reaction mixture was allowed to warm to room temperature over *ca*. 18 hours with stirring, at which point it was quenched with water leading to the precipitation of Rock*N_3H, **33**, as a creamy white solid. Neutralisation of the aqueous suspension (NH_4Cl), followed by extraction into diethyl ether, drying and filtration yielded a pale pink filtrate that deposited crystalline **33** as a colourless solid in excellent yield (94%) (Scheme 5.12).

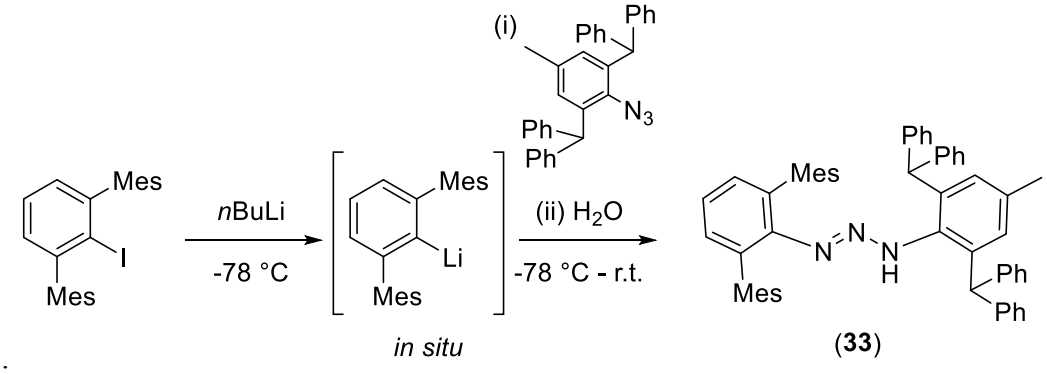

Scheme 5.12 Synthesis of the Rock*N_3H triazene.

The formation of triazene **33** is evidenced in its ^{1}H NMR (C_6D_6) spectrum, which exhibits a new broad singlet at 7.87 ppm and aryl multiplets that are representative of both the Dmp and Dipp* moieties, spanning chemical shift ranges from 6.90-6.76 ppm and 7.15-6.91 ppm respectively, in the anticipated signal integral ratios. These are complemented by methyl resonances in the alkyl region of the spectrum (mesityl methyl singlets at 2.20 ppm and 1.92 ppm, and Dipp* *p*-tolyl methyl at 1.79 ppm) and a benzhydryl singlet at 5.16 ppm which is shifted upfield relative to that of the Dipp*N_3 azide starting material (6.06 ppm in C_6D_6). It is noteworthy that no signal multiplication is apparent in the ^{1}H NMR spectrum of **33**, suggesting the absence of geometric isomers or rotational hindrance at the C-N and C-C biaryl bonds. Single crystals of **33** suitable for X-ray diffraction structure determination were grown from a saturated room temperature diethyl ether solution placed at 4 °C (Figure 5.12).

The triazene **33** crystallises in the monoclinic space group $P2_1/n$ with a full molecule in the asymmetric unit and an *E-anti* configuration[191-193] across the DmpN_3Dipp* scaffold. All non-hydrogen atoms were refined with anisotropic displacement parameters and all hydrogen atoms were located experimentally and refined isotropically.

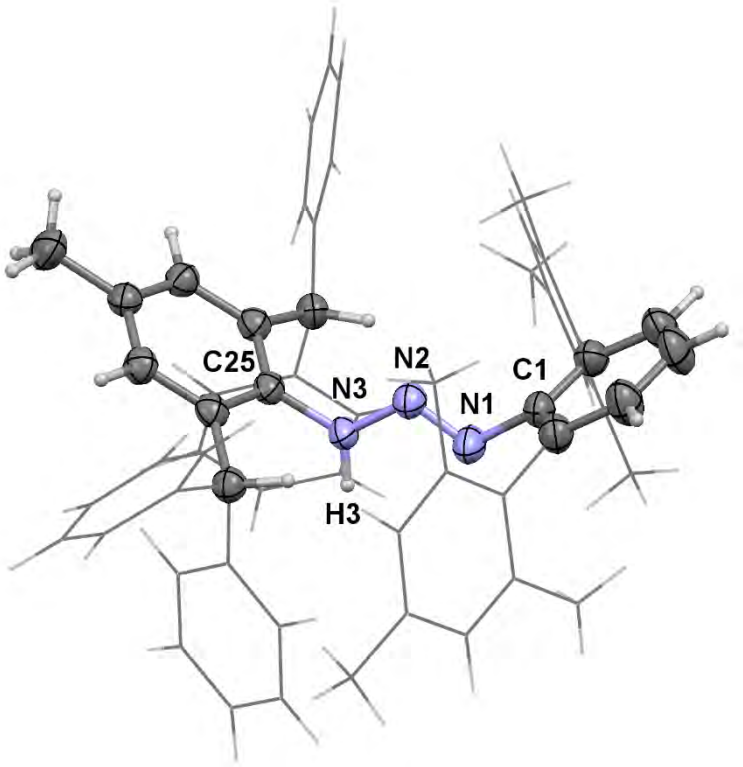

Figure 5.12 Molecular structure of **33** shown with thermal ellipsoids of 50% probability. Secondary arenes are shown as wireframes for clarity. Selected bond lengths (Å): N1-N2: 1.216(3), N2-N3: 1.351(3), N3-H3: 0.89(3), N1-C1: 1.438(3), N3-C25: 1.424(3), and angles (°): N1-N2-N3: 113.8(2), N2-N1-C1: 113.2(2), N2-N3-C25: 116.6(2).

The molecular structure of Rock*N_3H confirms incorporation of Dmp and Dipp* and exhibits metrics that are comparable to related *N*-2,6-terphenyl triazenes such as Dmp_2N_3H,[188] $Dipp*_2N_3H$,[189] and $DmpN_3HMes$ (Figure 5.3, Section 5.1.[167] For example, the N1-N2-N3 bond angle of 113.8(2)° in **33** is similar to that of $Dipp*_2N_3H$ (112.1(2)°) and $DmpN_3HMes$ (113.33(17)°), while that of Dmp_2N_3H is noticeably more acute at 109.78(12)°. Despite the different *N*,*N*'-substituents of **33**, its N-C bond lengths are similar (N1-C1: 1.438(3) Å and N3-C25: 1.424(3) Å) and are also in keeping with those measures in Dmp_2N_3H (average N-C: 1.408 Å) and $Dipp*_2N_3H$ (N-C: 1.434 Å). A

noteworthy feature of **33** that distinguishes it from the above symmetrical systems is its unequal N-N bond lengths (N1-N2: 1.216(3) Å and N2-N3: 1.351(3) Å). This disparity arises from the bond order of the respective nitrogen atoms N1 and N3 to N2, marked by the experimentally located proton attached to N3. This selective attachment is also observed in the solid state structure of $DmpN_3HMes$, which exhibits similar discrete N-N single- and double bonds (1.353(3) Å and 1.255(3) Å respectively). The absence of solid state disorder for the NH proton in **33** may be explained by the unsymmetrical *N*-substitution of **33**, wherein hydrolysis is likely regioselective with respect to the more electron rich Dipp* bound nitrogen relative to its more conjugated, electron withdrawing *N*-Dmp counterpart. Similar selectivity has also been noted in the preparations of other $DmpN_3HAr$ species.[167]

5.4 Assessing the steric demand of the RockN_3 ligand:*

5.4.1 Part One

Isolation of the new Rock*N_3H proligand permitted a standardised measurement of its steric bulk. The Tolman cone angle (θ) is often quoted for the quantification of steric demand of ligands and is best suited to symmetrical, conical, monodentate ligands such as substituted phosphines and η^5-cyclopentadienyls.[194] The assumptions drawn for these calculations inadequately characterise ligands with low rotational symmetry around the M-L bond, as is the case for many multidentate attachments, and do not transfer well to bidentate ligands such as triazenides.[194] Alternative methods that are able to take these characteristics into account have recently been presented.[195,196] For the purpose of this work the robust *G*-parameter calculation, outlined by Guzei *et al*. [196] has been chosen, as its methodology is independent of the M-L bond length and makes use of full metal

complex crystallographic data, permitting the close proximity and interleaving of ligand frameworks to be viewed as well.

Succinctly, the *G*-parameter method expresses the steric bulk of a given ligand as a percentage (*G*) of the area (*A*) subtended by the solid angle (*Ω*, Figure 5.13) of a ligand on a sphere of radius (*r*) centred on the metal of interest (M, Figure 5.13) relative to the total surface area of that sphere (Equation 5.1, Figure 5.13). This relationship is often visualised as a sphere of arbitrary radius with the atom of interest, imagined as a point light source, at its centre. The ligands on the central atom obstruct the "light" emanating from the central atom and cast a "shadow" on the walls of the surrounding sphere.

$$G = 100 \times \frac{A}{4\pi r^2}$$

Equation 5.1 The calculation of the *G*-parameter for a ligand at metal M.

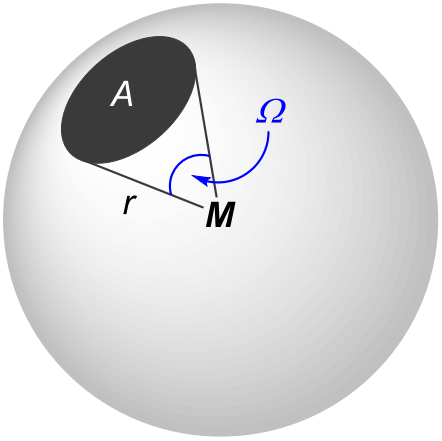

Figure 5.13 Graphical representation of the *G* parameter for a ligand at metal M.

The results of such calculations depend greatly on the metal centre as well as the attached ligands. For this reason standardised synthetic methods for comparing different ligands with invariant metal centres have been developed in the Cole group.[188] Previous work in our group, concerning a general approach to the measurement of steric parameters for

anionic bidentate *N*,*N'*-chelate ligands, has outlined dimethylaluminium complexes as an ideal means of standardising the results of these calculations.[188] Thus, the dimethylaluminium complex of Rock*N_3 was generated so that its *G*-parameter could be calculated and compared to those of other bulky ligands that we and others have reported.

5.4.2 Synthesis of [$AlMe_2$(RockN_3)], **34***

The complex [$AlMe_2$(Rock*N_3)], **34**, was prepared by the addition of a slight excess of $AlMe_3$ to a THF solution of Rock*N_3H at room temperature. After gas evolution had ceased, the volatiles were removed *in vacuo* (*NB:* $AlMe_3$ is volatile) to give a bright yellow treacly solid. Rhombic prisms of **34** suitable for single crystal X-ray diffraction structure determination (Figure 5.14) were acquired by recrystallisation of the crude reaction solid from a saturated room temperature hexane solution of **34** placed at 4 °C.

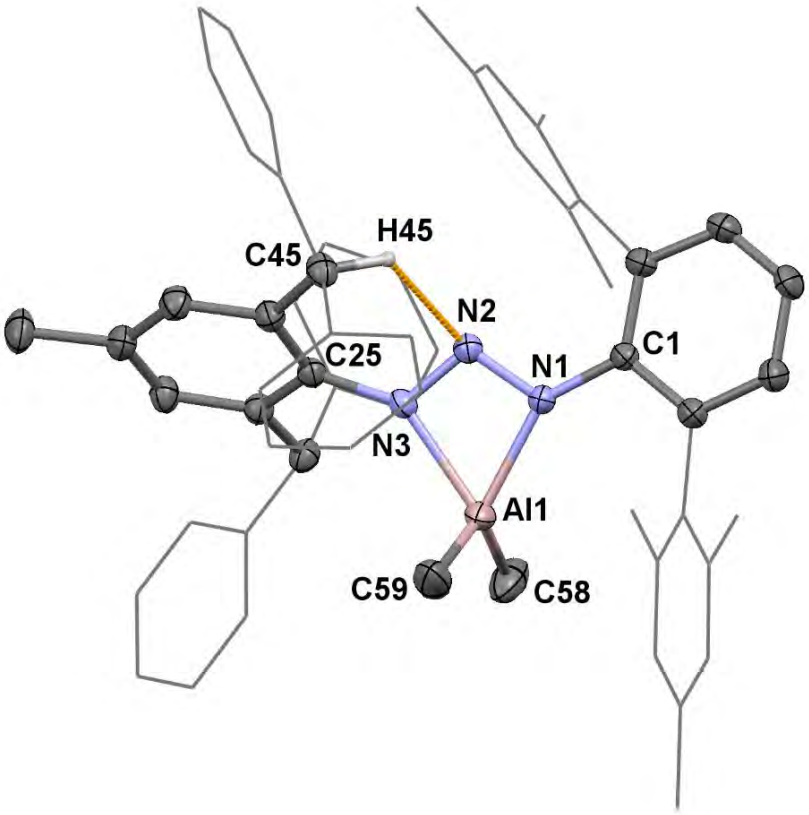

Figure 5.14 Molecular structure of [$AlMe_2$(Rock*N_3)], **34**, shown with thermal ellipsoids of 50% probability. Hydrogen atoms are omitted and secondary arenes are shown as wireframes for clarity. Selected bond lengths (Å): Al1-N1: 1.9497(15), Al1-N3: 2.0021(16), Al1-C58: 1.956(2), Al1-C59: 1.934(3), N1-N2: 1.322(2), N2-N3: 1.3036(19), N1-C1: 1.409(2), N3-C25: 1.417(2), N2···H45: 2.204(8), and angles (°): N1-Al1-N3: 64.07(6), C58-Al1-C59: 121.50(14), N1-Al1-C58: 117.14(11), N1-Al1-C59: 117.43(11), N3-Al1-C58: 115.72(10), N3-Al1-C59: 105.64(10), N3-N2-N1: 106.00(13), N2-N1-C1: 118.33(13), N2-N3-C25: 120.28(14)

Complex **34** crystallises in the triclinic space group $P\bar{1}$ with one molecule in the asymmetric unit. All atoms were located using experimentally derived electron density data, excepting the hydrogen atoms bound to one of the mesityl *p*-methyl groups, whilst

all non-hydrogen atoms were refined with anisotropic displacement parameters. The complex exhibits the bidentate coordination of one Rock*N_3 ligand and two methyl ligands to a heavily distorted tetrahedral aluminium. This distortion is marked by N1-Al1-N3 (AlN_2) and C58-Al1-C59 ($AlMe_2$) angles of 64.07(6)° and 121.50(14)° respectively, whereby the coordination geometry around Al1 is more appropriately described as pseudo-trigonal planar with respect to the methyl ligands and the Al,N1,N3 plane (Al1,N1,N3 plane-Al1-C58 angle of 123.305°, and Al1,N1,N3 plane-Al1-C59 angle of 114.055°). Additionally, the triazenide ligand scaffold is tilted noticeably to one side, subtending unequal angles between the C58,Al1,C59 plane to Al1-N1 vector (159.7°), and C58,Al1,59 plane to Al-N3 vector (136.1°). This tilt also leads to a slight discrepancy in the Al1-N1 or Al1-N3 bond lengths (1.9497(15) Å and 2.0021(16) Å respectively). A noteworthy intramolecular close contact between the bridgehead nitrogen, N2, and a benzhydryl proton (H45) of the Dipp* substituent is also apparent with a contact distance of 2.204(8) Å and C45-H45···N2 bond angle of 127.2(15)° (sum of van der Waals' radii for N and H 2.75 Å).

The unsymmetrical placement of the pendant aryl groups of the triazenide of **34** in the solid state is not mirrored by its solution state NMR data, in which the complex displays chemical shift and integration patterns consistent with free rotation about the C-C aryl bonds of both the Dmp and Dipp* moieties. This is observed in both ^{1}H and ^{13}C NMR (C_6D_6) spectra, suggesting that the aforementioned H-bonding interaction to the bridgehead nitrogen only manifests in the solid state. Furthermore, the ^{1}H NMR (C_6D_6) spectrum of **34** exhibits resonances shifted downfield by varying degrees relative to those of the neutral triazene precursor, as is characteristic of metallation. The most diagnostic of these resonances is the singlet at 6.09 ppm, attributable to the benzhydryl protons of the Dipp* moiety (*cf.* Rock*N_3H triazene; 5.16 ppm in C_6D_6), whilst a well-defined

singlet at -1.13 ppm may be assigned to the two equivalent methyl co-ligands bound to the aluminium centre.

5.4.3 Part Two

Since triazene **33** and its dimethylaluminium complex **34** represent hybrid compounds of the *N*,*N*'-symmetrical triazenides Dmp_2N_3 and $Dipp^*_2N_3$, a comparison of the steric parameters of $Rock^*N_3$ with these ligands was sought using the dimethylaluminium "steric probe" system. The Dmp_2N_3 ligated system, $[AlMe_2(Dmp_2N_3)]$, has been synthesised in the Cole group alongside a large catalogue of related $AlMe_2L$ (L = bulky *N*,*N*'-chelate) species,[188] however the synthesis of the corresponding $Dipp_2^*N_3$ analogue has not been attempted, making its preparation pertinent for structural comparison herein.

5.4.4 Synthesis of $[AlMe_2(Dipp^*_2N_3)]$, ***35***

It was reasoned that the complex $[AlMe_2(Dipp^*_2N_3)]$, **35**, could be prepared using an identical preparation to those of **34** and $[AlMe_2(Dmp_2N_3)]$, using $Dipp^*_2N_3H$. The triazene $Dipp^*_2N_3H$ was prepared and kindly provided by Dr Matt Gyton from the Cole group.

The addition of excess $AlMe_3$ to a THF solution of $Dipp^*_2N_3H$ at room temperature afforded a pale yellow reaction mixture that was stirred for 18 hours. Recrystallisation from hexane, after drying of the reaction mixture *in vacuo*, afforded the product as pale yellow needles that were found to contain a near 2:1:1 ratio of THF : hexane : **35** by ^1H NMR spectroscopy (C_6D_6). These proved to be of insufficient quality for single crystal X-ray diffraction study, however upon drying at 80 °C (*NB*: colour change from straw yellow to bright yellow) further recrystallisation from a room temperature saturated hexane solution placed at 4 °C afforded large, bright yellow THF-free blocks of **35** suitable for single crystal X-ray diffraction structure determination (Figure 5.15).

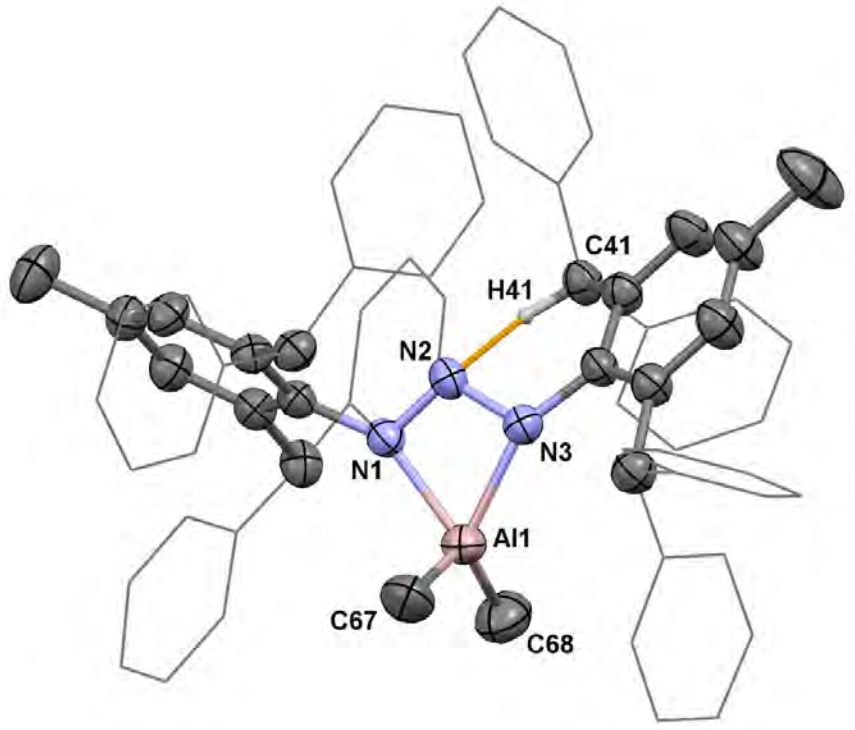

Figure 5.15 Molecular structure of [$AlMe_2(Dipp_2{*}N_3)$], **35**, shown with thermal ellipsoids of 50% probability. Hydrogen atoms are omitted and secondary arenes are shown as wireframes for clarity. Selected bond lengths (Å): Al1-N1 1.976(2), Al1-N3: 1.960(2), Al1-C58: 1.946(4), Al1-C59: 1.936(3), N1-N2: 1.300(3), N2-N3: 1.320(3), N1-C1: 1.430(3), N3-C25: 1.430(3), N2···H45: 2.23(3), and angles (°): N1-Al1-N3: 64.80(8), C58-Al1-C59: 122.25(18), N1-Al1-C58: 104.57(12), N1-Al1-C59: 116.00(14), N3-Al1-C58: 117.82(14), N3-Al1-C59: 115.98(14), N3-N2-N1: 107.28(19), N2-N1-C1: 114.22(19), N2-N3-C25: 113.0(2)

Similar to **34**, [$AlMe_2(Dipp{*}_2N_3)$], **35**, crystallises in the triclinic space group $P\bar{1}$ and displays comparable solid state metrics to **34**, with one unique molecule of **35** and a heavily disordered partial occupancy hexane molecule in the asymmetric unit, the latter could not be refined with satisfactory anisotropic displacement parameters nor could it be masked using the OLEX 2 masking function and was refined isotropically. All non-hydrogen atoms of **35** were refined with anisotropic displacement parameters, and

hydrogen atoms were placed in calculated positions (riding model), excepting the methine proton (H41) bound to C41, which was located using difference maps and exhibits a close contact (2.23(3) Å) to the bridgehead nitrogen (N2) of the triazenide moiety (sum of H, N van der Waals radii: 2.75 Å. *cf*. similar interaction Dipp* moiety in **34**: 2.204(8) Å). Likewise, the Al1 metal centre of **35** displays a pseudo-trigonal planar geometry with a C67-Al1-C68 bond angle of 122.24(18)°, Al1,N1,N3 plane to Al1-C67 angle of 114.7°, and Al1,N1,N3 plane to Al1-C67 angle of 121.2°. Despite the overall symmetry of the *N*-substituents across the N_3 donor, unlike those in **34**, there is a near identical tilt in the metallacycle (AlN_3) with respect to the $AlMe_2$ plane like that observed in **34**. This tilt contrasts the rigid and symmetrical orientations of the Dmp groups in the Dmp_2N_3 complex and likely arise from inclusion of the flexible Dipp* moiety in **34** and **35**.

Complex **35** behaves similarly to **34** in solution, as evidenced by its ^{1}H NMR spectrum (C_6D_6). For example, the methine to bridgehead nitrogen contact, displayed in its solid state structure, is not evident in the room temperature ^{1}H NMR spectrum of **35**, which exhibits a single set of Dipp* resonances, suggesting there is substantial mobility of the benzhydryl moieties in solution and that the N···H-C interaction is unstable in solution. Likewise, the methyl derived ^{1}H NMR singlet at -0.80 ppm, and relative signal integral of 6, is the most upfield shifted resonance in the ^{1}H NMR spectrum of **35** (-1.13 ppm in **34**). The corresponding ^{13}C resonance of the methyl co-ligands appears at -9.95 ppm in its ^{13}C NMR spectrum, as verified by a ^{1}H-^{13}C HSQC experiment (-9.73 ppm in **34**).

5.4.5 Part Three

With crystallographic data for **34**, **35**, and [$AlMe_2(Dmp_2N_3)$] in-hand, it was possible to compare the relative steric parameters of the triazenide ligands in these complexes. Thus, solid *G* calculations were carried out employing the crystallographic data for **34** (Figure

5.16) and **35** (Figure 5.17). The results of these calculations and salient solid state metrics are summarised for **34**, **35**, and [$AlMe_2(Dmp_2N_3)$] in Table 5.1 below.

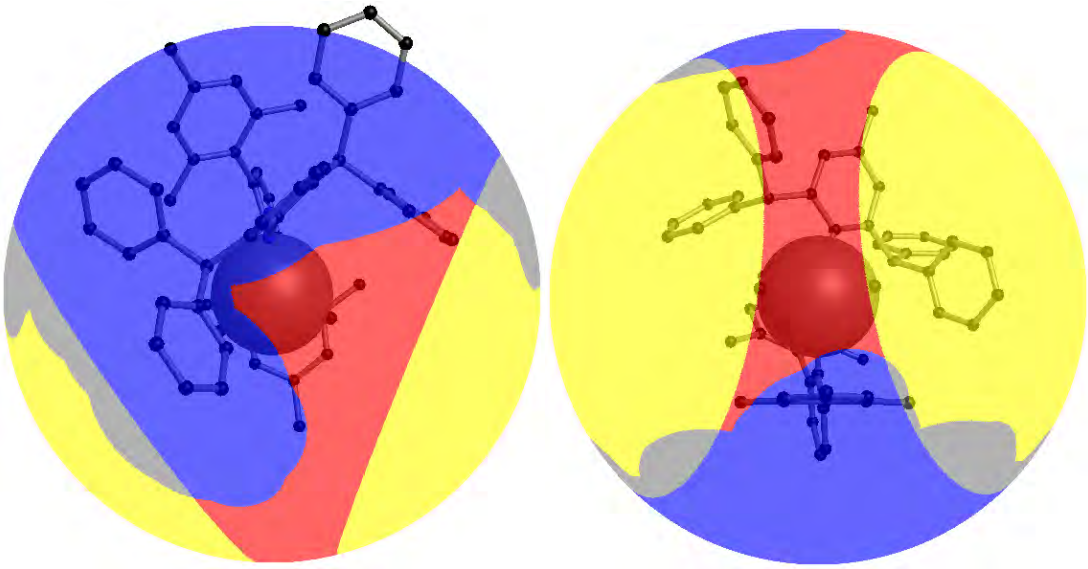

Figure 5.16 Solid angle illustration of **34** where the area cast by Ω of the Rock*N_3 ligand is coloured in blue, methyl co-ligands in yellow, and unshielded regions in red. Regions of overlap appear in grey.

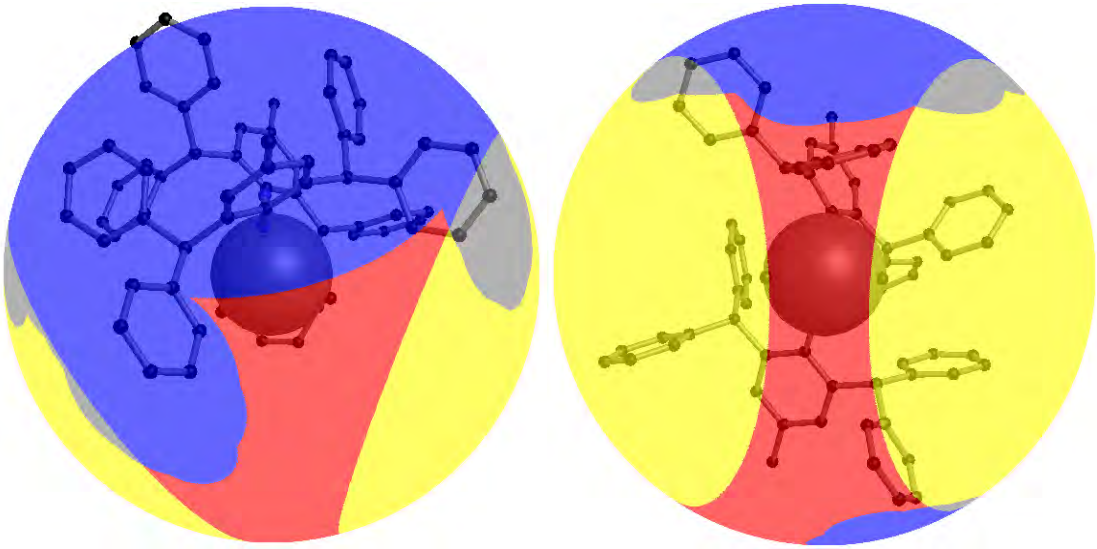

Figure 5.17 Solid angle illustration of **35** where the area cast by Ω of the Dipp*$_2N_3$ ligand is coloured in blue, methyl co-ligands in yellow, and unshielded regions in red. Regions of overlap appear in grey.

Metric	34	35	[AlMe$_2$(Dmp$_2$N$_3$)]
$G_{triazenide}$ (%)	62.1	57.8	63.4
NNN angle (°)	106.00(13)	107.28(19)	104.6(6)
Avg. N-Al (Å)	1.9759	1.968	1.969
C-Al-C (°)	121.50(14)	122.25(18)	118.5(4)
Avg. Al-C (Å)	1.945	1.941	1.951

Table 5.1 Comparison of solid *G* calculations and structural metrics for the triazenide ligands in **34**, **35**, and [AlMe$_2$(Dmp$_2$N$_3$)].

From the metrics presented in Table 5.1 it is apparent that all three triazenide ligand systems share comparable coordination metrics and Al-N and Al-C bond lengths that are statistically invariant across this series. Likewise, the triazenide N-N-N and C-Al-C angles in these complexes do not vary considerably from **34** to **35**, but some reduction is observed for [AlMe$_2$(Dmp$_2$N$_3$)]. This may be viewed as a consequence of the more electron withdrawing *N*-aryls overall, or steric enlargement. With respect to the latter, comparison of the solid *G*-parameter across **34**, **35**, and [AlMe$_2$(Dmp$_2$N$_3$)] highlights that while all three exhibit steric shielding that is substantially greater than the less bulky Dipp$_2$N$_3$ ligand in [AlMe$_2$(Dipp$_2$N$_3$)] (41.91%),[197] and greater than that of Dipp$_2$NacNac in [AlMe$_2$(Dipp$_2$NacNac)] (54.94%),[198] the Dipp* species in **34** and **35** demonstrates smaller profiles, perhaps due to the increased dexterity of Dipp* *vs*. Dmp. Thus, the Dmp$_2$N$_3$ triazenide shows the greatest amount of steric shielding around the aluminium metal centre with Dipp*$_2$N$_3$ the least.

5.5 Heavy metal RockN_3 coordination*

The preceding steric evaluation of the Rock*N_3 in its dimethylaluminium complex (**34**), in particular its substantially greater steric bulk relative to $Dipp_2N_3$, prompted us to apply it to lead(II) chemistry. This began with attempts to isolate a synthetically useful [Pb(Ar*$_2N_3$)X] precursor, such as [Pb(Ar'$_2N_3$)(HMDS)] (Ar' = bulky aryl). It was reasoned that the greater steric demand of the Rock*N_3 ligand would disfavour the problematic ligand redistribution processes observed during the attempted isolation of [Pb($Dipp_2N_3$)(HMDS)], **29**, which led to the homoleptics **28** and [Pb$(HMDS)_2$] upon reaction workup (Section 5.2.4).

*5.5.1 Reaction of [Pb$(HMDS)_2$] with **33** with 1:1 reaction stoichiometry*

The addition of one equivalent of [Pb$(HMDS)_2$] to a THF solution of **33** at room temperature afforded a bright orange reaction mixture that was stirred for 18 hours. Filtration and drying *in vacuo* yielded **36** as an extremely soluble bright orange treacly solid (hexane or THF; *ca*. 0.3 g mL^{-1} at room temperature). Recrystallisation of vacuum dried **36** from a room temperature saturated hexane solution placed at -24 °C afforded amorphous **36** as a precipitate. Concentration of the bright orange hexane supernatant to incipient crystallisation afforded a second crop of **36** upon standing at 4 °C as bright orange rhombohedral blocks suitable for single crystal X-ray diffraction structure determination (Figure 5.18).

Complex **36** crystallises in the tetragonal space group *P*4/*n* with one unique molecule of **36** and a molecule of partial occupancy disordered hexane in the asymmetric unit. The disorder and occupancy of the latter could not be refined satisfactorily. All non-hydrogen atoms were refined with anisotropic displacement parameters and hydrogen atoms were

placed in calculated positions (riding model) excepting the benzhydryl proton H45, which was located from difference maps and refined isotropically.

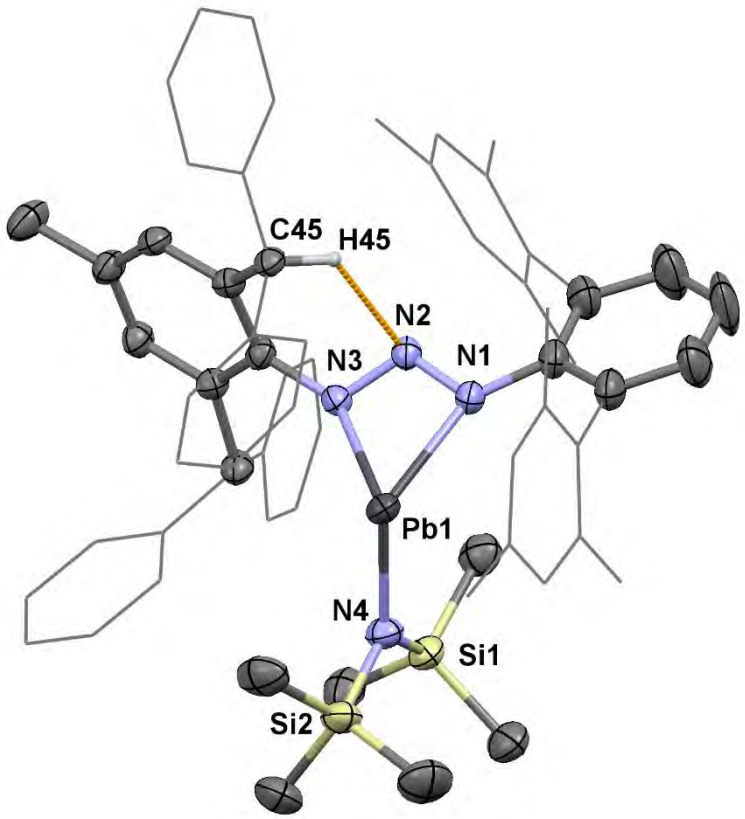

Figure 5.18 Molecular structure of [Pb(Rock*N_3)(HMDS)], **36**, shown with thermal ellipsoids of 50% probability. Hydrogen atoms are omitted and secondary arenes are shown as wireframes for clarity. Selected bond lengths (Å): Pb1-N1: 2.452(4), Pb1-N3: 2.475(4), Pb1-N4: 2.246(4), N1-N2: 1.304(6), N2-N3: 1.298(6), N2···H45: 2.47(6), and angles (°): N4-Pb1-N1: 110.70(16), N4-Pb1-N3: 103.27(16), N3-N2-N1: 109.8(4), Si1-N4-Si2: 120.1(3).

The molecular structure of **36** confirms its composition as the heteroleptic species [Pb(Rock*N_3)(HMDS)] with both Rock*N_3 and HMDS ligands at the Pb(II) centre. This confirms our hypothesis that the steric encumbrance posed by the Rock*N_3 ligand can stymie homoleptic ligand redistribution, as per [Pb($Dipp_2N_3$)(HMDS)], **29**. The

intraligand interactions in **36** are unlike those of the dimethylaluminium complexes **34** and **35**. For example, the bridgehead nitrogen (N2) in **36** does not lie in-plane with N1, N3 and Pb1. Instead it is forced out in an envelope-like manner, subtending a N1,N2,N3 plane to N1,Pb1,N3 plane angle of 20.5°, similar to that observed in **28** (average 'buckling' angle: 23.1°). This buckling accommodates a close contact between N2 and the benzhydryl proton H45 (N2···H45: 2.47(6) Å), which is similar to those in **34** and **35** (sum of H, N van der Waals radii: 2.75 Å).

The presence of the Pb(II) lone electron pair is also apparent from the bent coordination of the triazenide with respect to the HMDS co-ligand. For example, the Pb1,N1,N3 plane subtends an angle of 108.6° to the Pb1-N4 vector, which is 8° more open than the Pb1,N1,N3 plane to Pb1,N4,N6 plane angle in homoleptic **28** (100.6°) and likely results from the steric buttressing of Rock*N_3 and HMDS about the Pb(II).

A curious feature of **36** relative to the $Dipp_2N_3$ structure, **28**, is the extension of the Pb-$N_{triazenide}$ bonds despite a decrease in nominal coordination number at the metal centre (average Pb-N in **36**: 2.46 Å, *vs*. that in **28**: 2.38 Å). One possible rationale for this is the noticeable proximity of one Dipp* pendant phenyl ring and one mesityl function of the Dmp moiety to Pb1. Closer examination of these intramolecular distances reveals likely Pb···aryl interactions with Pb1···$centroid_{arene}$ distances of 3.374(2) Å (Dipp*) and 3.251(3) Å (Dmp), and Pb1···$centroid_{arene}$ to arene plane normal angles of 6.51° (Dipp*) and 15.14° (Dmp) (Figure 5.19). These moieties are thus facially oriented toward the vacant coordination site on Pb1, suggestive of an interaction between the non-bonding valence Pb(II) valence electrons and the LUMO of the coordinated arenes, as noted for other low valent *p*-block π-coordinated systems such as tin(II).[199]

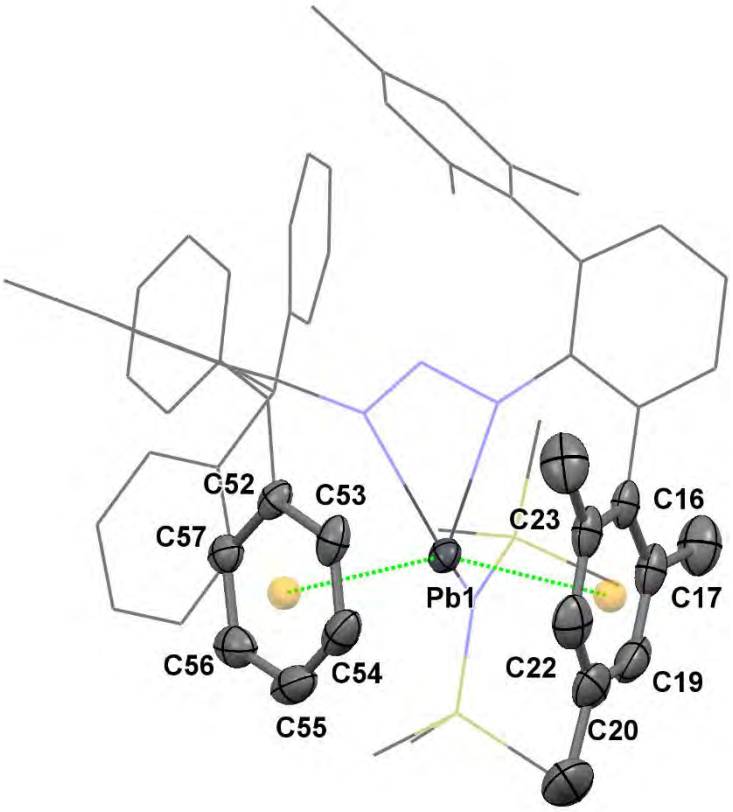

Figure 5.19 Molecular structure of **36** highlighting Pb···arene interactions (dashed green), centroids shown in orange, non-participating ligand framework shown as wireframes and hydrogen atoms omitted for clarity. Selected distances (Å): C16,C17,C19,C20,C22,C23 centroid···Pb1: 3.251(3), C52,C53,C54,C55,C56,C57 centroid···Pb1: 3.374(2), and angles (°): C16,C17,C19,C20,C22,C23 centroid···Pb1 to C16,C17,C19,C20,C22,C23 plane normal: 15.14, C52,C53,C54,C55,C56,C57 centroid···Pb1 to C52,C53,C54,C55,C56,C57 plane normal: 6.51.

Indeed, such interactions have precedence, albeit sparce for Pb(II), in the literature.[200-202] In 2010 Zukerman-Schpector and co-workers conducted a comprehensive survey of the Cambridge Structural Database and concluded that Pb···aryl interactions occur in *ca.* 3% of structures that contain Pb(II) and an arene.[203] The definition of a Pb···aryl interaction for the purpose of this survey is that the Pb···centroid$_{arene}$ distance be no more than the

sum of the arene ring half-thickness (1.7-1.9 Å)[204] and the van der Waals radius of lead(II) (2.02 Å), *i.e.* a sum of 3.72-3.92 Å.[98] This threshold was complemented by the additional condition that the angle between the Pb-centroid$_{arene}$ vector and the vector normal to the arene plane be no greater than 20°. Regarding these conditions for Pb$\cdots\pi$ interactions, **36** exhibits metrics that fit this definition well.

This interaction is not borne out in solution as determined by a room temperature ^{1}H NMR spectrum (C_6D_6) of **36**, wherein the Dmp and Dipp* moieties exhibit a degree of symmetry that is inconsistent with a persistent Pb$\cdots$arene interaction, as deduced by the chemical shift and integration patterns of the methyl singlet resonances in the alkyl region of the ^{1}H NMR spectrum. The resonances at 1.71 (Dipp* *p*-tolyl), 2.08, 2.14, and 2.34 ppm (Dmp CH_3) exhibit a signal integral ratio of 3:6:6:6 relative to the singlet of the two chemically equivalent Dipp* benzhydryl protons at 6.15 ppm. The signal integral pattern of the Dmp methyl singlets and Dipp* benzhydryl singlet, assigned with ^{1}H-^{1}H TOCSY experiments, suggest rotational locking of the Dmp mesityl:primary aryl axis that does not necessitate a Pb$\cdots$Dmp or Pb$\cdots$Dipp* interaction in solution. Such a persistent π-donor interaction would be expected to generate either five or six inequivalent methyl environments (with respect to Dmp, five if non-coordinated mesityl is free to rotate) with signal integral ratios of either 1:2:1:1:1 or 1:1:1:1:1:1, as opposed to the three environments observed in **36**, at room temperature, with a 1:1:1 signal integral ratio. The simplicity of the remaining ligand associated ^{1}H NMR signals, for example a single Dipp* benzyhydryl singlet (6.15 ppm) and single HMDS resonance (0.14 ppm), suggest that these substituents are likewise symmetrically oriented with respect to the Dmp group and that the observed shift and integration pattern of the Dmp moiety result from a plane of symmetry (*S*) that orthogonally bisects the Dmp primary aryl (Figure 5.20). The aryl ^{13}C NMR resonances of both Dmp and Dipp* substituents display chemical shift patterns that

are consistent with the above observation in addition to similar planes of symmetry that bisect the primary (*S1*) and secondary (*S2, S3*) arenes of the Dipp* moiety. These give rise to 12 signals, *vs*. 8 for a freely rotating Dipp* substituent (Figure 5.20). In combination with the degrees of freedom of the Dmp group, a total of 22 aryl ^{13}C resonances are observed in the ^{13}C NMR spectrum of **36**.

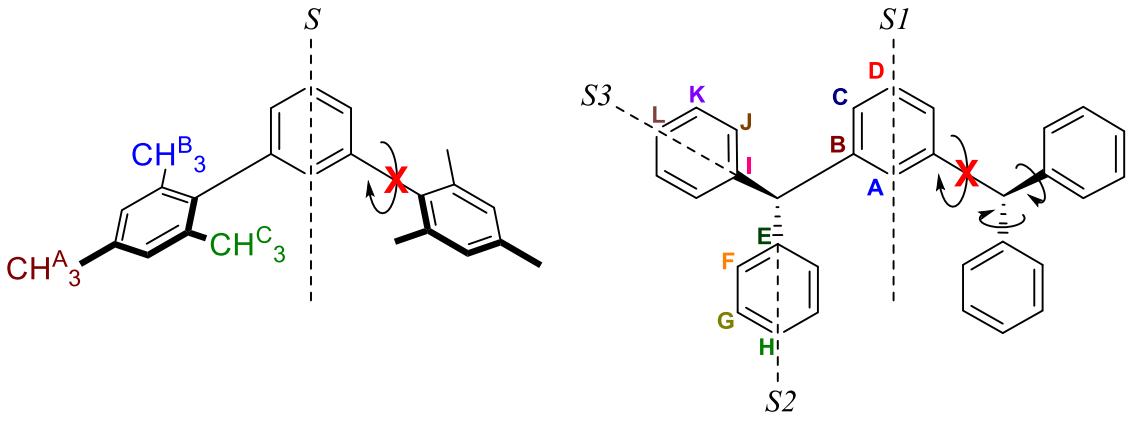

Figure 5.20 Solution state symmetry of the Dmp and Dipp* moieties in **36** as deduced from ^{1}H (left) and ^{13}C NMR data (right) highlighting three inequivalent ^{1}H methyl proton environments on Dmp and 12 inequivalent ^{13}C aryl carbon environments on Dipp*.

Complex **36** is stable with respect to homoleptic ligand redistribution in solution, unlike its $Dipp_2N_3$ relative **29**. We attribute this stability to the high degree of steric buttressing of the ligand substituents evident in the solid state and in solution. Indeed, when the reaction of $[Pb(HMDS)_2]$ with **33** was carried out with 2:1 triazene to $[Pb(HMDS)_2]$ stoichiometry, ^{1}H NMR (C_6D_6) spectroscopy revealed the outcome to be a 1:1 ratio of **36** and **33**. Complex **36** could be cleanly extracted into hexane in which **33** has poor solubility. This outcome firmly endorses our supposition that the ligand redistribution of **36** to form the bis(triazenide) complex is disfavoured due to steric effects.

5.6 Conclusions

This chapter showcases our efforts to bolster the triazenide chemistry of underdeveloped lead(II) heteroleptics with a view to facilitating later projects that address some of the pitfalls exposed during our bimca^{R} Pb(II) studies in Chapter 4 and the pilot study using $Dipp_2N_3$ in this chapter. Despite being preliminary in nature, this work has produced the first structurally authenticated Pb(II) triazenides and established that ligand redistribution to afford homoleptic complexes represents a major impediment to the preparation of complexes bearing triazenides with moderately large *N*-substituents, *i.e.* 2,6-diisopropylphenyl. This led us to develop a new, unsymmetrical, superbulky 2,6-terphenyl *N*-substituted triazene; Rock*N_3H.

The steric bulk of this new ligand was quantified by means of a dimethylaluminium probe and establishment of its *G*-parameter, following methods established in our group.[188] These calculations place the *G*-parameter of the Rock*N_3 between those of the related Dipp*$_2N_3$ and Dmp_2N_3 ligands. Application of the protolytic metallation pathway developed in Chapter 4 permitted the isolation of the new Pb(II) heteroleptic complex [Pb(Rock*N_3)(HMDS)], **36**, which is stable with respect to the above homoleptic ligand redistribution due to steric buttressing of the large *N*-substituents, which result in conformational locking in solution. This complex and the method by which it was prepared provide a promising foundation for future Pb(II) reactivity projects.

5.7 Experimental

General methods

$Dipp_2N_3H$,[174] IMes·HCl[187,205], DmpI,[206] and Dipp*NH_2[190] were synthesised and purified according to literature procedures.

*2:1 Reaction of $Dipp_2N_3H$ with $[Pb(HMDS)_2]$ to form **28***

A colourless hexane (10 mL) solution of $Dipp_2N_3H$ (0.21 g, 0.57 mmol) was added to an orange hexane stock solution of $[Pb(HMDS)_2]$ (2.1 mL, 0.29 mmol, 0.14 M) resulting in an orange reaction mixture that was stirred for 18 h. Filtration and removal of reaction volatiles *in vacuo* afforded **28** as an orange powder (0.23 g, 83%). Large rectangular blocks suitable for single crystal X-ray diffraction structure determination were grown from a saturated room temperature solution of **28** in hexane, placed at 4 °C. Microanalyses of crystalline samples of **28** returned values that are consistent with the inclusion of one equivalent of hexane as per the solid structure of **28** (*cf.* Section 5.2.3). ^{1}H NMR (300 MHz, C_6D_6): δ 1.19 (d, $^3J_{HH}$ = 7.05 Hz, 48H, *i*Pr-C*H*$_3$), 3.41 (sept, $^3J_{HH}$ = 7.05 Hz, 8H, *i*Pr-C*H*), 7.00-7.19 (m, 12H, aryl-*H*). ^{13}C NMR (75 MHz C_6D_6): δ 22.64 (s, *i*Pr-*C*H$_3$), 28.91 (s, *i*Pr-*C*), 123.11, 123.57, 127.09, 144.08 (s, aryl-*C*). Calcd. for $C_{48}H_{68}N_6Pb$, **28**: C, 61.57; H, 7.32; N, 8.98. Calcd. for **28**·C_6H_{14}: C, 63.43; H, 8.08; N, 8.22. Found: C, 63.82; H, 7.93; N, 9.05. IR (Nujol mull on NaCl plates, cm^{-1}): 1934 (*w*, *sh*), 1865 (*w*, *sh*), 1798 (*w*, *sh*), 1186 (*m*, *sh*), 1097 (*m*, *sh*), 1019 (*m*, *sh*), 935 (*w*, *sh*), 799 (*m*, *sh*), 753 (*m*, *sh*), 665 (*w*, *sh*). Mp: 141-143 °C (dec.).

*1:1 Reaction of $Dipp_2N_3H$ with $[Pb(HMDS)_2]$ to form **29***

A colourless hexane solution (20 mL) of $Dipp_2N_3H$ (0.50 g, 1.4 mmol) was added to an orange hexane stock solution of $[Pb(HMDS)_2]$ (9.8 mL, 1.4 mmol, 0.14 M) to immediately afford an orange reaction mixture that was stirred for 18 h. Filtration and removal of reaction volatiles afforded a treacly orange solid that characterised as a mixture of **28** and **29** by ^{1}H NMR spectroscopy. Complex **29** was found to be unstable with respect to redistribution in solution to form the homoleptics **28** and $[Pb(HMDS)_2]$. Large square blocks grown from a room temperature saturated hexane solution of the vacuum dried reaction product placed at 4 °C characterised as **28** by single crystal X-ray

diffraction methods. ^{1}H NMR (300 MHz C_6D_6, with omission of minor component signals of **28** and [Pb(HMDS)$_2$]): δ 0.14 (s, 18H, SiMe$_3$), 1.28 (d, $^{3}J_{HH}$ = 7.14 Hz, 24H, *i*Pr-C*H*$_3$), 3.59 (sept, $^{3}J_{HH}$ = 7.14 Hz, 4H, *i*Pr-C*H*), 7.00-7.32 (m, 6H, aryl-*H*).

Attempted preparations of [Pb(Dipp$_2$N$_3$)Cl(IMes)], ***30***

Method (i): Reaction of ***28*** *with IMes·HCl to afford* ***31***

Solid IMes·HCl (0.23g, 0.69 mmol) was added portionwise to a stirred orange solution of **28** (0.502 g, 0.69 mmol) in THF (60 mL) at room temperature. The reaction mixture was stirred for 18 h, during which time it gradually paled to yellow and a suspended solid formed. Filtration and removal of volatiles *in vacuo* yielded **31** as a yellow solid. Recrystallisation from a saturated solution of **31** in toluene at 50 °C afforded pale yellow plates of **31** suitable for single crystal X-ray diffraction structure determination upon cooling to room temperature. ^{1}H NMR (300 MHz, C_6D_6): δ 1.11 (d, $^{3}J_{HH}$ = 6.90 Hz, 12H, Dipp$_2$N$_3$H *i*Pr-C*H*$_3$), 1.34 (br d, 12H, Dipp$_2$N$_3$ *i*Pr-C*H*$_3$), 2.05 (s, 24H, IMes *o*-C*H*$_3$), 2.13 (s, 12H, IMes *p*-C*H*$_3$), 3.34 (sept, $^{3}J_{HH}$ = 6.90 Hz, 2H, Dipp$_2$N$_3$H *i*Pr-C*H*), 3.87 (br sept, 2H, Dipp$_2$N$_3$ *i*Pr-C*H*), 6.42 (s, 4H, IMes 4,5-C$_2$*H*$_2$), 6.75 (s, 8H, IMes *m*-aryl-*H*), 7.00-7.27 (m, 12H, Dipp$_2$N$_3$ + Dipp$_2$N$_3$H aryl-*H*), 9.36 (br s, 1H, Dipp$_2$N$_3$*H*), 10.20 (br s, 1H, IMes·*H*). Acquisition of ^{13}C NMR data was hampered by poor solubility. Further characterisation of compound **31** was frustrated due to the presence of inseparable impurities present in the bulk reaction product (*cf.* presence of **28**, see Section 5.2.5).

Method (ii): in situ prepared ***32*** *and Dipp$_2$N$_3$H*

An orange hexane stock solution of [Pb(HMDS)$_2$] (6.3 mL, 0.80 mmol, 0.14 M) was added to a toluene (20 mL) slurry of IMes·HCl (0.30 g, 0.80 mmol) at room temperature to afford an orange reaction mixture that was stirred for 18 h. During this time the reaction mixture gradually darkened from amber to red, at which point a hexane solution (10 mL) of Dipp$_2$N$_3$H (0.28 g, 0.80 mmol) was added and the clear reaction mixture was stirred

for a further 18 h. Filtration of the reaction mixture, followed by removal of volatiles from the filtrate afforded a solid mixture that characterised as **32** and $Dipp_2N_3H$ by ^1H NMR spectroscopy. ^1H NMR (300 MHz, C_6D_6, with omission of resonances of $Dipp_2N_3H$): δ 0.23 (s, 18H, $SiMe_3$), 3.12 (s, 6H, IMes *p*-CH_3), 3.33 (s, 12H, IMes *o*-CH_3), 6.20 (s, 2H, IMes 4,5-C_2H_2), 6.77 (s, 4H, IMes *m*-aryl-*H*). ^{13}C NMR (75 MHz, C_6D_6, with omission of resonances of $Dipp_2N_3H$): δ 2.48 (s, $SiMe_3$), 18.21 (s, IMes-CH_3), 21.06 (s, IMes-CH_3), 122.51 (s, 4,5-IMes-*C*), 129.57, 134.75, 135.65, 138.85 (s, IMes-aryl-C), 2-IMes-*C* not observed.

Synthesis of DippN_3*

Concentrated sulfuric acid (3.7 mL, 68 mmol) was added dropwise to a colourless suspension of Dipp*NH_2 (10.0 g, 22 mmol) in a THF/water mixture (2:1, 200 mL) at -20 °C followed by the dropwise addition of a cold (4 °C) aqueous solution (50 mL) of $NaNO_2$ (1.9 g, 27 mmol) to afford a dark orange slurry that was stirred mechanically and maintained below 0 °C for 5h, whereupon an aqueous solution (50 mL) of NaN_3 (27 mmol, 1.8 g) was added dropwise and the reaction mixture was warmed to room temperature over 18 h, during which it effervesced and paled from a dark brown to a light pink suspension. Extraction of the precipitate into diethyl ether (3 x 75 mL) followed by washing with brine (3 x 25 mL), drying (anhydrous $MgSO_4$), and removal of volatiles *in vacuo* afforded crude Dipp*N_3. Recrystallisation from the minimum amount of a THF/diethyl ether mixture (1:1, *ca*. 50 mL) afforded Dipp*N_3 as off-white needles (7.2 g, 68%). ^1H NMR spectroscopic and melting point data are in agreement with previous studies of this compound in our group.[189] ^1H NMR (300 MHz, C_6D_6): δ 1.77 (s, 3H, Ar-CH_3), 6.06 (s, 2H, Ph_2CH), 6.84 (s, 2H, Ar-*H*), 6.97-7.14 (m, 22H, Ar-*H*). Mp: 132-134 °C (dec.), 149-152 °C (melts, effervesces).

Reaction of DmpLi with DippN_3 to form Rock*N_3H, **33***

A hexane stock solution of *n*Butyl lithium (5.5 mL, 8.6 mmol, 1.6 M) was added to a suspension of DmpI (3.8 g, 8.6 mmol) in diethyl ether (30 mL) at -78 °C to afford a colourless suspension. Dropwise addition of a solution of Dipp*N_3 (4.0 g, 8.6 mmol) in THF (70 mL) at -78 °C over 30 min afforded a clear orange reaction mixture that was warmed to room temperature over 18 h. The dark amber reaction mother liquor was added dropwise to water (100 mL) to afford an off-white suspension that was neutralised with a saturated aqueous solution of NH_4Cl. The suspension was extracted into diethyl ether (3 x 50 mL), dried (anhydrous $MgSO_4$), filtered and concentrated by slow evaporation under N_2(g) flow to yield colourless rectangular plates of **33** suitable for single crystal X-ray diffraction structure determination (6.3 g, 94%). Microanalyses of **33** returned values consistent with the inclusion of half an equivalent of THF, which is in agreement with ^{1}H NMR data of **33**. ^{1}H NMR (300 MHz, C_6D_6): δ 1.79 (s, 3H, Dipp* Ar-C*H*$_3$), 1.92 (s, 6H, Dmp *p*-C*H*$_3$), 2.20 (s, 12H, Dmp *o*-C*H*$_3$), 5.16 (s, 2H, Dipp* Ph_2C*H*), 6.76-6.90 (s, 4H, Dmp Ar'-*H*), 6.91-7.15 (m, 25H, overlapping Dipp* and Dmp Ar,Ar'-*H*), 7.87 (br s, 1H, N_3*H*). ^{13}C NMR (75Hz, C_6D_6): δ 21.03 (s, Dmp Ar'-*C*H$_3$), 21.25 (s, Dmp Ar'-*C*H$_3$), 21.27 (s, Dipp* Ar-*C*H$_3$), 51.64 (s, Dipp* Ph_2*C*H), 126.51, 128.62, 128.78, 128.88, 129.22, 129.77, 129.88, 129.97, 130.09, 134.70, 136.28, 136.78, 137.18, 137.21, 142.99 (s, Ar,Ar'-*C*). Remaining aryl ^{13}C resonance is likely obscured by the C_6D_6 solvent resonance and could not be located. Calcd. for $C_{57}H_{53}N_3$, **33**: C, 87.76; H, 6.85; N, 5.39. Calcd. for **33**·0.5 THF: C, 86.83; H, 7.04; N, 5.15. Found: C, 86.31; H, 6.92; N, 5.30. IR (Nujol mull on NaCl plates, cm^{-1}): 2729 (*w*, *sh*), 2126 (*w*, *sh*), 1950 (*w*, *sh*), 1880 (*w*, *sh*), 1810 (*w*, *sh*), 1724 (*w*, *sh*), 1612 (*m*, *sh*), 1580 (*m*, *sh*), 1377 (*m*, *sh*), 1304 (*m*, *sh*), 1250 (*w*, *sh*), 1215 (*m*, *sh*), 1174 (*m*, *sh*), 1076 (*m*, *sh*), 1031 (*m*, *sh*), 766 (*m*, *sh*). Mp: 152-153 °C (dec.).

*Synthesis of [AlMe$_2$(Rock*N$_3$)], **34**, and [AlMe$_2$(Dipp*$_2$N$_3$)], **35** from AlMe$_3$ and Ar'$_2$N$_3$H*

Dimethylaluminium complexes **34** and **35** were synthesised commensurately. A representative synthesis for **34** is given below.

A toluene stock solution of AlMe$_3$ (0.46 mL, 0.91 mmol, 2.0 M) was added in excess to a colourless solution of **33** (0.20 g, 0.26 mmol) in THF (70 mL) at room temperature and stirred for 18 h, during which time the reaction mixture gradually turned yellow and exhibited a yellow fluorescence under long wave UV light. Filtration followed by removal of volatiles afforded a treacly yellow solid that was recrystallised from a saturated room temperature solution in hexane placed at 4 °C affording **34** as large bright yellow rectangular blocks suitable for single crystal X-ray diffraction structure determination (0.17 g, 80%). ^{1}H NMR (400 MHz, C$_6$D$_6$): δ -1.13 (s, 6H, Al(C*H*$_3$)$_2$), 1.58 (s, 3H, Dipp* Ar-C*H*$_3$), 2.07 (s, 12H, Dmp *o*-C*H*$_3$), 2.14 (s, 6H, Dmp *p*-C*H*$_3$), 6.09 (s, 2H, Dipp* Ph$_2$C*H*), 6.74-7.20 (m, 29H, overlapping Dipp* and Dmp Ar,Ar'-*H*). ^{13}C NMR (100 MHz, C$_6$D$_6$): δ -9.73 (s, Al(*C*H$_3$)$_2$), 20.93 (s, Dipp* Ar-*C*H$_3$, 21.22 (s, Dmp Ar'-*C*H$_3$), 21.42 (s, Dmp Ar'-*C*H$_3$), 50.52 (s, Dipp* Ph$_2$*C*H), 125.79, 126.65, 128.59, 128.98, 130.35, 130.92, 131.14, 133.53, 136.07, 136.84, 137.32, 137.92, 139.50, 140.42, 144.58 (s, Ar,Ar'-*C*). Remaining aryl ^{13}C resonance is likely obscured by the C$_6$D$_6$ solvent resonance and could not be located. Calcd. for C$_{59}$H$_{58}$N$_3$Al: C, 84.75; H, 6.99; N, 5.03. Found: C, 84.73; H, 7.24; N, 5.16. IR (Nujol mull on NaCl plates, cm^{-1}): 2729 (*w*, *sh*), 1970 (*w*, *sh*), 1949 (*w*, *sh*), 1880 (*w*, *sh*), 1810 (*w*, *sh*), 1767 (*w*, *sh*), 1612 (*m*, *sh*), 1580 (*w*, *sh*), 1303 (*w*, *sh*), 1260 (*m*, *sh*), 1216 (*w*, *sh*), 1174 (*m*, *sh*), 1076 (*m*, *sh*), 1031 (*m*, *sh*), 850 (*m*, *sh*), 803 (*w*, *sh*), 774 (*m*, *sh*), 765 (*m*, *sh*), 740 (*m*, *sh*), 702 (*m*, *sh*). Mp: 202 – 203 °C (dec.), 233 – 235 °C (melts), > 255 °C (effervesces).

*[AlMe$_2$(Dipp*N$_3$)]*

35 retained solvent more readily than **34** and microanalysis samples returned values that are consistent with the inclusion of one equivalent of THF despite heating the sample to 80 °C under vacuum for 1 h. Large rectangular blocks of **35** suitable for single crystal X-ray diffraction structure determination were recrystallised from hexane using vacuum dried crystals of inferior quality. ^{1}H NMR (400 MHz, C_6D_6): δ -0.80 (s, 6H, Al(C*H*$_3$)$_2$), 1.93 (s, 6H, Ar-C*H*$_3$), 6.43 (s, 4H, Ph$_2$C*H*), 7.03-7.27 (m, 44H, aryl-*H*). ^{13}C NMR (100 MHz, C_6D_6): δ -9.95 (s, Al(*C*H$_3$)$_2$), 21.13 (s, Ar-*C*H$_3$), 51.51 (s, Ph$_2$*C*H), 126.67, 128.69, 130.25, 132.01, 139.43, 140.21, 143.49, 144.32 (s, aryl-*C*). Calcd. for $C_{68}H_{60}N_3Al$, **35**: C, 86.32; H, 6.39; N, 4.04. Calcd. for **35**·THF: C, 84.92; H, 6.73; N, 4.13. Found: C, 84.95; H, 6.44; N, 4.16. IR (Nujol mull NaCl plates, cm^{-1}): 2729 (*w*, *sh*), 1950 (*w*, *sh*), 1888 (*w*, *sh*), 1807 (*w*, *sh*), 1765 (*w*, *sh*), 1677 (*w*, *sh*), 1581 (*m*, *sh*), 1323 (*w*, *sh*), 1293 (*w*, *sh*), 1255 (*m*, *sh*), 1228 (*m*, *sh*), 1182 (*w*, *sh*), 1077 (*m*, *sh*), 1031 (*m*, *sh*), 1003 (*w*, *sh*), 968 (*w*, *sh*), 917 (*w*, *sh*), 858 (*m*, *sh*), 767 (*m*, *sh*), 745 (*m*, *sh*), 697 (*m*, *sh*), 666 (*m*, *sh*). Mp: 276-279 °C (dec.).

*1:1 Reaction of [Pb(HMDS)$_2$] with **33** to afford [Pb(Rock*N$_3$)(HMDS)]*

A hexane stock solution of [Pb(HMDS)$_2$] (9.4 mL, 1.3 mmol, 0.14 M) was added to a colourless solution of **33** (1.0 g, 1.3 mmol) in THF (50 mL) to afford a clear orange reaction mixture that was stirred for 18 h, during this time it gradually brightened. Filtration and removal of volatiles afforded a treacly orange residue that was recrystallised from the minimum amount of hexane (*ca*. 3 mL) placed at -24 °C yielding amorphous **36** as a bright orange solid. Concentration of the supernatant to incipient crystallisation afforded a second crop of **36** upon standing at 4 °C as bright orange rhombohedral blocks suitable for single crystal X-ray diffraction (combined yield: 1.2 g, 79%). ^{1}H (400 MHz, C_6D_6): δ 0.14 (s, 18H, SiMe$_3$), 1.72 (s, 3H, Dipp* Ar-C*H*$_3$), 2.08 (s,

6H, Dmp Ar'-C*H*$_3$), 2.14 (s, 6H, Dmp Ar'-C*H*$_3$), 2.34 (s, 6H, Dmp Ar'-C*H*$_3$), 6.15 (s, Dipp* Ph$_2$C*H*), 6.70-7.24 (m, 29H, overlapping Dmp and Dipp* Ar,Ar'-*H*). ^{13}C (100 MHz, C_6D_6): δ 7.09 (s, $SiMe_3$), 20.98 (s, Dmp Ar'-*C*H$_3$), 21.26 (s, Dipp* Ar-*C*H$_3$), 21.81 (s, Dmp Ar'-*C*H$_3$), 22.45 (s, Dmp Ar'-*C*H$_3$), 50.84 (s, Dipp* Ph$_2$*C*H), 124.67, 126.52, 126.67, 128.45, 128.60, 128.71, 129.62, 130.05, 130.33, 130.51, 131.69, 133.86, 135.32, 135.73, 136.30, 137.40, 138.47, 139.06, 144.49, 145.77, 147.07, 147.71 (s, Ar,Ar'-*C*). Calcd. for $C_{63}H_{70}N_4Si_2Pb$: C, 65.99; H, 6.15; N, 4.89. Found: C, 66.60; H, 6.40; N, 4.48. IR (Nujol mull on NaCl plates, cm^{-1}): 1944 (*w*, *sh*), 1882 (*w*, *sh*), 1806 (*w*, *sh*), 1753 (*w*, *sh*), 1600 (*m*, *sh*), 1580 (*m*, *sh*), 1408 (*m*, *sh*), 1377 (*w*, *sh*), 1179 (*w*, *sh*), 1076 (*w*, *sh*), 849 (*m*, *sh*), 801 (*m*, *sh*), 772 (*w*, *sh*), 702 (*w*, *sh*), 672 (*m*, *sh*). Mp: 137-140 °C (dec.).

References

1. S. Aldridge, A. J. Downs, *The Group 13 Metals Aluminium, Gallium, Indium and Thallium: Chemical Patterns and Peculiarities*, Vol. **2011**. (John Wiley & Sons, Ltd: Chichester, UK).
2. W. Kutzelnigg, *Angew. Chem. Int. Ed.*, **1984**, 23, 272.
3. Y. Mizuhata, T. Sasamori, N. Tokitoh, *Chem. Rev.*, **2009**, 109, 3479.
4. H. Yamamoto (Ed.), K. Oshima (Ed.), *Main Group Metals in Organic Synthesis*, Vol. **2004**. (Wiley-VCH: Michigan, USA).
5. P. P. Power, *Nature*, **2010**, 463, 171.
6. S. T. Liddle, D. P. Mills, *Dalton Trans.*, **2009**, 5592.
7. A. Torvisco, K. Ruhlandt-Senge, *Top. Organomet. Chem.*, **2013**, 45, 1.
8. M. Stender, A. D. Phillips, R. J. Wright, P. P. Power, *Angew. Chem. Int. Ed.*, **2002**, 41, 1785.
9. C. A. Caputo, J. Koivistoinen, J. Moilanen, J. N. Boynton, H. M. Tuononen, P. P. Power, *J. Am. Chem. Soc.*, **2013**, 135, 1952.
10. T. A. Schmedake M. Haaf, B. J. Paradise, R. West, *Can. J. Chem.*, **2000**, 78, 1526.
11. D. W. Stephan, *Dalton Trans.*, **2009**, 3129.
12. Y. Peng, M. Brynda, B. D. Ellis, J. C. Fettinger, E. Rivard, P. P. Power, *Chem. Commun.*, **2008**, 6042.
13. Y. Peng, B. D. Ellis, X. Wang, P. P. Power, *J. Am. Chem. Soc.*, **2008**, 130, 12268.
14. C. M. Mömming, E. Otten, G. Kehr, R. Fröhlich, S. Grimme, D. W. Stephan, G. Erker, *Angew. Chem. Int. Ed.*, **2009**, 48, 6643.
15. A. Jana, G. Tavčar, H. W. Roesky, M. John, *Dalton Trans.*, **2010**, 39, 9487.
16. Y. Peng, B. D. Ellis, X. Wang, J. C. Fettinger, P. P. Power, *Science*, **2009**, 325, 1668.

17. Y. Jung, M. Brynda, P. P. Power, M. Head-Gordon, *J. Am. Chem. Soc.*, **2006**, 128, 7185.

18. S. K. Mandal, H. W. Roesky, *Acc. Chem. Res.*, **2012**, 45, 298.

19. G. H. Spikes, J. C. Fettinger, P. P. Power, *J. Am. Chem. Soc.*, **2005**, 127, 12232.

20. P. P. Power, M. M. Olmstead, D. Phillips, A. F. Richards, *J. Am. Chem. Soc.*, **2003**, 125, 3204.

21. P. P. Power, B. E. Eichler, *J. Am. Chem. Soc.*, **2000**, 122, 8785.

22. G. J. Kubas, *Metal Dihydrogen and s-Bond Complexes: Structure, Theory and Reactivity*, Vol. **2001**. (Kluwer Academic: New York, USA).

23. P. J. Davidson, M. F. Lappert, *Chem. Commun.*, **1973**, 317.

24. M. J. S. Gynane, D. H. Harris, M. F. Lappert, P. P. Power, P. Rivière, M. Rivière-Baudet, *Dalton Trans.*, **1977**, 2004.

25. A. Sekiguchi, R. Kingo, M. A . Ichinohe, *Science*, **2004**, 305, 1755.

26. A. D. Phillips, R. J. Wright, M. M. Olmstead, P. P. Power, *J. Am. Chem. Soc.*, **2002**, 124, 5930.

27. P. P. Power, L. Pu, B. Twamley, *J. Am. Chem. Soc.*, **2000**, 122, 3524.

28. N. J. Hardman, R. J. Wright, A. D. Phillips, P. P. Power, *J. Am. Chem. Soc.*, **2003**, 125, 2667.

29. M. Stürmann, M. Weidenbruch, K. W. Klinkhammer, F. Lissner, H. Marsmann, *Organometallics*, **1998**, 17, 4425.

30. M. Weidenbruch, J. Schlaefke, A. Schäfer, K. Peters, H. G. von Schnering, H. Marsmann, *Angew. Chem. Int. Ed.*, **1994**, 33, 1846.

31. P. Jutzi, H. Schmidt, B. Neumann, H.-G. Stammler, *Organometallics*, **1996**, 15, 741.

32. W. A. Herrmann, M. Denk, J. Behm, W. Scherer, F. -R. Klingan, H. Bock, B. Solouki, M. Wagner, *Angew. Chem. Int. Ed.*, **1992**, 31, 1485.

33. S. M. Mansell, R. H. Herber, I. Nowik, D. H. Ross, C. A. Russell, D. F. Wass, *Inorg. Chem.*, **2011**, 50, 2252.

34. D. Heitmann, T. Pape, A. Hepp, C. Mück-Lichtenfeld, S. Grimme, F. E. Hahn, *J. Am. Chem. Soc.*, **2011**, 133 11118.

35. R. S. Grev, *Adv. Organomet. Chem.*, **1991**, 33, 125.

36. P. P. Power, *Chem. Commun.*, **2003**, 2091.

37. J. R. Su, X. W. Li, R. C. Crittendon, G. H. Robinson, *J. Am. Chem. Soc.*, **1997**, 119, 5471.

38. N. C. Norman, *Periodicity and the s- and p-Block Elements*, Vol. **1994**. (Oxford Science Publications: Oxford, UK).

39. Z. Zhu, X. Wang, Y. Peng, H. Lei, J. C. Fettinger, E. Rivard, P. P. Power, *Angew. Chem. Int. Ed.*, **2009**, 48, 2031.

40. E. Rivard, P. P. Power, *Dalton Trans.*, **2008**, 4336.

41. N. J. Hardman, B. Twamley, P. P. Power, *Angew. Chem. Int. Ed.*, **2000**, 39, 2771.

42. L. W. Pineda, V. Jancik, K. Starke, R. B. Oswald, H. W. Roesky, *Angew. Chem. Int. Ed.*, **2006** 45, 2602.

43. H. W. Roesky, A. Jana, C. Schulzke, A. Döring, *Angew. Chem.*, **2009**, 121, 1126.

44. M. Gärtner, H. Görls, M. Westerhausen, *Synthesis*, **2007**, 725.

45. R. J. Errington, *Advanced Practical Inorganic and Metalorganic Chemistry*, Vol. **1997**. (Blackie Academic & Professional: London, UK).

46. M. S. Hill, D. J. Liptrot, C. Weetman, *Chem. Soc. Rev.*, **2016**, 45, 972.

47. S. O. Hauber, F. Lissner, G. B. Deacon, M. Niemeyer, *Angew. Chem. Int. Ed.*, **2005**, 44, 5871.

48. H. S. Lee, S. O. Hauber, D. Vindus, M. Niemeyer, *Inorg. Chem.*, **2008**, 47, 4401.

49. K. Ruhlandt-Senge, J. J. Ellison, R. J. Wehmschulte, F. Pauer, P. P. Power, *J. Am. Chem. Soc.*, **1993**, 115, 11353.

50. S. Krieck, H. Gorls, M. Westerhausen, *Organometallics*, **2010**, 29, 6790.

51. A. G. M. Barrett, M. R. Crimmin, M. S. Hill, G. Kociok-Köhn, D. J. MacDougall, M. F. Mahon, P. A. Procopiou, *Organometallics*, **2008**, 27,

52. L. Bourget-Merle, M. F. Lappert, J. R. Severn, *Chem. Rev.*, **2002**, 102, 3031.

53. N. D. Coombs, A. Stasch, A. Cowley, A. L. Thompson, S. Aldridge, *Dalton Trans.*, **2008**, 332.

54. V. C. Gibson, S. K. Spitzmesser, A. J. P. White, D. J. Williamsa, *Dalton Trans.*, **2003**, 2718.

55. G. T. Plundrich, H. Wadepohl, L. H. Gade, *Inorg. Chem.*, **2016**, 55, 353.

56. M. Moser, B. Wucher, D. Kunz, F. Rominger, *Organometallics*, **2007**, 26, 1024.

57. F. Ortu, G. J. Moxey, A. J. Blake, W. Lewis, D. L. Kays, *Chem. Eur. J.*, **2015**, 21, 6946.

58. M. Westerhausen, *Angew. Chem.*, **2008**, 120, 2215.

59. S. P. Green, C. Jones, A. Stasch, *Science*, **2007**, 318, 1754.

60. S. J. Bonyhady, S. P. Green, C. Jones, S. Nembenna, A. Stasch, *Angew. Chem.*, **2009**, 48, 2973.

61. C. Jones, A. Stasch, *Top. Organomet. Chem.*, **2013**, 45, 73.

62. Y. Xie, H. F. Schaefer III, E. D. Jemmis, *Chem. Phys. Lett.*, **2005**, 402, 414

63. S. J. Bonyhady, D. Collis, G. Frenking, N. Holzmann, Jones C, A. Stasch, *Nat. Chem.*, **2010**, 2, 865.

64. X. Weng, L. Andrews, S. Tam, M. E. DeRose, M. E. Fajardo, *J. Am. Chem. Soc.*, **2003**, 125, 9218.

65. L. Andrews, X. Wang, *Science*, **2003**, 299, 2049.

66. D. Franz, T. Szilvasi, E. Irran, S. Inoue, *Nat. Commun.*, **2015**, 6, 10037.

67. D. Neculai, H. W. Roesky, A. Mirela Neculai, J. Magull, B. Walfort, D. Stalke, *Angew. Chem. Int. Ed.*, **2002**, 41, 4294.

68. S. Schulz, H. W. Roesky, H. J. Koch, G. M. Sheldrick, D. Stalke, A. Kuhn, *Angew. Chem. Int. Ed.*, **1993**, 32, 1729.

69. V. Jancik, M. M. M. Cabrera, H. W. Roesky, R. Herbst-Irmer, D. Neculai, A. M. Neculai, M. Noltemeyer, H. G. Schmidt, *Eur. J. Inorg. Chem.*, **2004**, 3508.

70. As determined by a survey of the Cambridge Structural Database v. 5.37 with updates for September 2016.

71. A. Ecker, H. Schnöckel, *Z. Anorg. Allg. Chem.*, **1998**, 624, 813.

72. W. Clegg, N. C. Norman, N. L. Pickett, *Acta Crystallogr., Sect. C: Cryst. Struct. Commun.*, **1994**, 50, 36.

73. S. J. Black, D. E. Hibbs, M. B. Hursthouse, C. Jones, K. M. Abdul Malik, N. A. Smithies, *Dalton Trans.*, **1997**, 4313.

74. A. El-Hellani, J. Monot, R. Guillot, C. Bour, V. Gandon, *Inorg. Chem.*, **2013**, 52 506.

75. S. A. Cramer, F. L. Sturgill, P. P. Chandrachud, D. M. Jenkins, *Dalton Trans.*, **2014**, 43, 7687.

76. R. J. Baker, M. L. Cole, C. Jones, M. F. Mahon, *Dalton Trans.*, **2002**, 1992.

77. M. Arrowsmith, M. S. Hill, D. J. MacDougall, M. F. Mahon, *Angew. Chem. Int. Ed.*, **2009**, 48, 4013.

78. M. Arrowsmith, M. S. Hill, G. Kociok-Köhn, *Organometallics*, **2009**, 28, 1730.

79. M. Arrowsmith, A. Heath, M. S. Hill, P. B. Hitchcock, G. Kociok-Köhn, *Organometallics*, **2009**, 28, 4550.

80. M. R. Crimmin, M. S. Hill, *Top. Organomet. Chem.*, **2013**, 45, 191.

81. A. Baishya, M. Kr. Barman, T. Peddarao, S. Nembenna, *J. Organomet. Chem.*, **2014**, 769, 112.

82. J. R. Lachs, A. G. M. Barrett, M. R. Crimmin, G. Kociok-Köhn, M. S. Hill, M. F. Mahon, P. A. Procopiou, *Eur. J. Inorg. Chem.*, **2008**, 4173.

83. S. K. Furfari, PhD Thesis, *UNSW Australia*, Sydney, Australia, **2014**.

84. A. Seyboldt, B. Wucher, S. Hohnstein, K. Eichele, F. Rominger, K. W. Törnroos, D. Kunz, *Organometallics*, **2015**, 34, 2717.

85. E. Jürgens, K. N. Buys, A. T. Schmidt, S. K. Furfari, M. L. Cole, M. Moser, F. Rominger, D. Kunz, *New J. Chem.*, **2016**, 40, 9160.

86. Y. Liu, M. Nishiura, Y. Wang, Z. Hou, *J. Am. Chem. Soc.*, **2006**, 128, 5593.

87. S. Kajigaeshi, T. Kakinami, H. Yamasaki, S. Fujisaki, T. Okamoto, *Bull. Chem. Soc. Jap.*, **1988**, 61, 600.

88. Y. S. Vygodskii, E. I. Lozinskaya, A. S. Shaplov, K. A. Lyssenko, M. Y. Anitpin, Y. G. Urman, *Polymer*, **2004**, 45, 5031.

89. S. Cha, M. Ao, W. Sung, B. Moon, B. Ahlström, P. Johansson, Y. Ouchi, D. Kim, *Phys. Chem. Chem. Phys.*, **2014**, 16, 9591.

90. M. Bielawski, D. Aili, B. Olofsson, *J. Org. Chem.*, **2008**, 73, 4602.

91. D. Kalyani, N. R. Deprez, L. V. Desai, M. S. Sanford, *J. Am. Chem. Soc.*, **2005**, 127, 7331.

92. M. Zhu, N. Jalalian, B. Olofsson, *Synlett*, **2008**, 4, 592.

93. Y. Fujiwara Y. Makioka, T. Kitamura, *J. Organomet. Chem.*, **2000**, 611, 509.

94. T. Lv, Z. Wang, J. You, J. Lan, G. Gao, *J. Org. Chem.*, **2013**, 78, 5723.

95. F. G. Bordwell, G. E. Drucker, H. E. Fried, *J. Org. Chem.*, **1981**, 46, 632.

96. R. W. Alder, P. R. Allen, S. J. Williams, *Chem. Commun.*, **1995**, 1267.

97. R. S. Moorhouse, G. J. Moxey, F. Ortu, T. J. Reade, W. Lewis, A. J. Blake, D. L. Kays, *Inorg. Chem.*, **2013**, 52, 2678.

98. M. Mantina, A. C. Chamberlin, R. Valero, C. J. Cramer, D. G. J. Truhlar, *Phys. Chem. A*, **2009**, 113, 5806.

99. M. S. Hill, P. B. Hitchcock, R. Pongtavornpinyo, *Dalton Trans.*, **2005**, 273.

100. A. J. Arduengo, H. V. R. Dias, R. L. Harlow, M. Kline, *J. Am. Chem. Soc.*, **1992**, 114, 5530.

101. S. A. Mungur, S. T. Liddle, C. Wilson, M. J. Sarsfield, P. L. Arnold, *Chem. Commun.*, **2004**, 2738.

102. M. Brendel, J. Wenz, I. V. Shishkov, F. Rominger, P. Hofmann, *Organometallics*, **2015**, 34, 669.

103. M. S. Hill, G. Kociok-Köhn, D. J. MacDougall, *Inorg. Chem.*, **2011**, 50, 5234.

104. H. B. Mansaray, M. Kelly, D. Vidovic, S. Aldridge, *Chem. Eur. J.*, **2011**, 17, 5381.

105. Y. Wang, Y. Xie, M. Y. Abraham, P. Wei, H. F. Schaefer III, P. v. R. Schleyer, G. H. Robinson, *J. Am. Chem. Soc.*, **2010**, 132 14370.

106. A. Jana, R. Azhakar, G. Tavčar, H. W. Roesky, I. Objartel, D. Stalke, *Eur. J. Inorg. Chem.*, **2011**, 3686.

107. M. J. Asay, S. P. Fisher, S. E. Lee, F. S. Tham, D. Borchardt, V. Lavallo, *Chem. Commun.*, **2015**, 51, 5359.

108. R. D. Shannon, *Acta Cryst.*, **1976**, A32, 751.

109. P. S. Tanner, D. J. Burkey, T. P. Hanusa, *Polyhedron*, **1995**, 14, 331.

110. J. M. Boncella, C. J. Coston, J. K. Cammack, *Polyhedron*, **1991**, 10, 769.

111. M. Rauch, S. Ruccolo, J. P. Mester, Y. Rong, G. Parkin, *Chem. Sci.*, **2016**, 7, 142.

112. N. Kuhn, M. Schulten, R. Boese, D. Blaser, *J. Organomet. Chem.*, **1991**, 421, 1.

113. I. Nieto, F. Cervantes-Leeb, J. M. Smith, *Chem. Commun.*, **2005**, 3811.

114. U. Wannagat, H. Autzen, H. Kuckertz, H. J. Wiemar, *Z. Anorg. Allg. Chem.*, **1972**, 894, 254.

115. Y. Tang, L. N. Zakharov, W. S. Kassel, A. L. Rheingold, R. A. Kemp, *Inorg. Chim. Acta*, **2005**, 358, 2014.

116. L. Lopardi Franco, M. Vieira de Almeida, L. F. Rocha e Silva, P. P. Ribeiro Vieira, A. M. Pohlit, M. Siqueira Valle, *Chem. Biol. Drug. Des.*, **2012**, 79, 790.

117. W. Klemm, K. Beyetsdorfer, J. Orysckewitsch, *Z. anorg. allg. Chem.*, **1948**, 256, 25.

118. L. M. Engelhardt, B. S. Jolly, P. C. Junk, C. L. Raston, B. W. Skelton, A. H. White, *Aust. J. Chem.*, **1986**, 39, 1337.

119. M. Veith, T. Kirs, V. Huch, *Z. Anorg. Allg. Chem.*, **2013**, 639, 312.

120. F. M. Elms, G. A. Koutsantonis, C. L. Raston, *Chem. Commun.*, **1995**, 1669.

121. O.T. Beachley, S.H.L. Chua, M.R. Churchill, R.F. See, *Organometallics*, **1992**, 11, 1486.

122. A. J. Arduengo, H. V. R. Dias, J. C. Calabrese, F. Davidson, *J. Am. Chem. Soc.*, **1992**, 114, 9724.

123. M. L. Cole, S. K. Furfari, M. Kloth, *J. Organomet. Chem.*, **2009**, 694, 2934.

124. M. Wu, A. M. Gill, L. Yunpeng, L. Falivene, L. Yongxin, R. Ganguly, L. Cavallo, F. García, *Dalton Trans.*, **2015**, 44, 15166.

125. C. D. Abernethy, M. L. Cole, C. Jones, *Organometallics*, **2000**, 19, 4852.

126. A. J. Downs, C. R. Pulham, *Chem. Soc. Rev.*, **1994**, 23, 175.

127. L. L. Cao, E. Daley, T. C. Johnstone, D. W. Stephan, *Chem. Commun.*, **2016**, 52, 5305.

128. R. S. Ghadwal, H. W. Roesky, R. Herbst-Irmer, P. G. Jones, *Z. Anorg. Allg. Chem.*, **2009**, 635, 431.

129. W.-C. Shih, C.-H. Wang, Y.-T. Chang, G. P. A. Yap, T.-G. Ong, *Organometallics* **2009**, 28, 1060.

130. A. R. Kennedy, R. E. Mulvey, S. D. Robertson, *Dalton Trans.*, **2010**, 39 9091.

131. R. J. Baker, C. Jones, M. Kloth, D. P. Mills, *New J. Chem.*, **2004**, 28, 207.

132. T. Jurca, K. Dawson, I. Mallov, T. Burchell, G. P. A. Yap, D. S. Richeson, *Dalton Trans.*, **2010**, 39, 1266.

133. S.Tang, J.Monot, A.El-Hellani, B.Michelet, R.Guillot, C.Bour, V.Gandon, *Chem. Eur. J.*, **2012**, 18, 10239.

134. P. J. Ogren, L. Steenhoek, K. S. Greve, W. C. Hutton, *J. Inorg. Nucl. Chem.*, **1975**, 37, 293.

135. A. Castineiras, W. Hiller, J. Strahle, M. R. Bermejo, M. Gayoso, *An. Quim. Ser. B*, **1986**, 82, 282.

136. M. L. Cole, A. J. Davies, C. Jones, *Dalton Trans.*, **2001**, 2451.

137. B. Wrackmeyer, *Prog. Nucl. Magn. Reson. Spectrosc.*, **1979**, 12, 227.

138. A. R. Leverett, A. I. McKay, M. L. Cole, *Dalton Trans.*, **2015**, 44, 498.

139. M. L. Cole, D. E. Hibbs, C. Jones, N. A. Smithies, *Dalton Trans.*, **2000**, 545.

140. M. L. Cole , C. Jones , M. Kloth, *Inorg. Chem.*, **2005**, 44, 4909.

141. H. Bürger, J. Cichon, U. Goetze, U. Wannagat, H. J. Wismar, *J. Organomet. Chem.*, **1971**, 33, 1.

142. J. Lorberth, P. Krommes, *J. Organomet. Chem.*, **1977**, 131, 415.

143. R. S. P. Turbervill, J. M. Goicoechea, *Aust. J. Chem.*, **2013**, 66, 1131.

144. J. B. Waters, J. M. Goicoechea, *Dalton Trans.*, **2014**, 43, 14239.

145. P. A. Rupar, V. N. Staroverov, P. J. Ragogna, K. M. Baines, *J. Am. Chem. Soc.*, **2007**, 129, 15138.

146. S. Gründemann, A. Kovacevic, M. Albrecht, J. W. Faller, R. H. Crabtree, *J. Am. Chem. Soc.*, **2002**, 124, 10473.

147. C. Y. Tang, W. Smith, D. Vidovic, A. L. Thompson, A. B. Chaplin, S. Aldridge, *Organometallics*, **2009**, 28, 3059.

148. M. Chen, Y. Wang, R. J. Gilliard, P. Wei, N. A. Schwartz, G. H. Robinson, *Dalton Trans.*, **2014**, 43, 14211.

149. M. Uzelac, A. Hernán-Gómez, D. R. Armstrong, A. R. Kennedy, E. Hevia, *Chem. Sci.*, **2015**, 6, 5719.

150. G. Schnee, O. Nieto Faza, D. Specklin, B. Jacques, L. Karmazin, R. Welter, C. S. López, S. Dagorne, *Chem. Eur. J.*, **2015**, 21, 17959.

151. B. Wucher, PhD Thesis, *Eberhard Karls Universität Tübingen*, Tübingen, Germany, **2011**.

152. Y. Yamaguchi, T. Kashiwabara, K. Ogata, Y. Miura, Y. Nakamura, K. Kobayashic, T. Ito, *Chem. Commun.*, **2004**, 2160.

153. K. C. Thimer, S. M. I. Al-Rafia, M. J. Ferguson, R. McDonald, E. Rivard, *Chem. Commun.*, **2009**, 7119.

154. J. Clayden, S. A. Yasin, *New J. Chem.*, **2002**, 26, 191.

155. A. L. Balch, D. E. Oram, *Organometallics*, **1988**, 7, 155.

156. M. Weidenbruch, A. Stilter, K. Peters, H. G. v. Schnering, *Z. Anorg. Allg. Chem.*, **1996**, 622, 534.

157. S. M. I. Al-Rafia, A. C. Malcolm, S. K. Liew, M. J. Ferguson, E. Rivard, *J. Am. Chem. Soc.*, **2011**, 133, 777.

158. S. M. I. Al-Rafia, A. C. Malcolm, S. K. Liew, M. J. Ferguson, R. McDonald, E. Rivard, *Chem. Commun.*, **2011**, 47, 6987.

159. S. M. I. Al-Rafia, O. Shynkaruk, S. M. McDonald, S. K. Liew, M. J. Ferguson, R. McDonald, R. H. Herber, E. Rivard, *Inorg. Chem.*, **2013**, 52, 5581.

160. L. Hosford Jones, R. S. McDowell, M. Goldblatt, *Inorg. Chem.*, **1969**, 8, 2349.

161. F. T. Edelmann, A. F. Hill (Ed.), M. J. Fink (Ed.), *Advances in Organometallic Chemistry*, Vol. 57, **2008**. (Academic Press: USA).

162. P. J. Bailey, S. Pace, *Coord. Chem. Rev.*, **2001**, 214, 91.

163. H. S. Lee, S. O. Hauber, D. Vinduš, M. Niemeyer, *Inorg. Chem.*, **2008**, 47, 4401.

164. S. G. Minasiana, J. Arnold, *Chem. Commun.*, **2008**, 4043.

165. S. O. Hauber, F. Lissner, G. B. Deacon, M. Niemeyer, *Angew. Chem. Int. Ed.*, **2005**, 44, 5871.

166. W. W. Hartman, J. B. Dickey, *Organic Syntheses*, Vol. 14, **1934**. (John Wiley & Sons, Inc.: London, UK).

167. S. G. Alexander, M. L. Cole, C. M. Forsyth, S. K. Furfari, K. Konstas, *Dalton Trans.*, **2009**, 2326.

168. H. Zhu, J. Chai, H. Fan, H. W. Roesky, C. He, V. Jancik, H. G. Schmidt, M. Noltemeyer, W. A. Merrill, P. P. Power, *Angew. Chem. Int. Ed.*, **2005**, 44, 5090.

169. A. Hinz, A. Schulz, A. Villinger, J. M. Wolter, *J. Am. Chem. Soc.*, **2015**, 137, 3975.

170. H. A. Bent, *Chem. Rev.*, **1961**, 61, 275.

171. F. Weinhold, C. L. Landis, *Valency and Bonding: A Natural Donor-Acceptor Perspective*, Vol. **2005**. (Cambridge University Press: Cambridge, UK).

172. J. Y. Chen W. Li, W. Q. Xu, E. X. He, S. Z. Zhan, D. R. Cao, *Inorg. Chem. Commun.*, **2011**, 14, 916.

173. E. M. Matson, W. P. Forrest, P. E. Fanwick, S. C. Bart, *Organometallics*, **2013**, 32, 1484.

174. A. G. M. Barrett, M. R. Crimmin, M. S. Hill, P. B. Hitchcock, G. Kociok-Köhn, P. A. Procopiou, *Inorg. Chem.*, **2008**, 47, 7366.

175. F. A. Cotton, G. W. Rice, J. C. Sekutowski, *Inorg. Chem.*, **1979**, 18, 1143.

176. E. Hartmann, J. Strähle, *Z. Naturforsch. B: Chem. Sci.*, **1988**, 43, 525.

177. W. Li, Y. L. Liu, J. Liu, H. Zhang, S. Z. Zhan, T D. R. Cao, *Transition Met. Chem.*, **2011**, 36, 255.

178. C. M. Forsyth A. Stasch, C. Jones, P. C. Junk, *New J. Chem.*, **2008**, 32, 829.

179. P. B. Hitchcock, M. F. Lappert, A. V. Protchenko, *Chem. Commun.*, **2005**, 951.

180. W.-P. Leung, C.-W. So, Y.-S. Wu, H.-W. Li, T. C. W. Mak, *Eur. J. Inorg. Chem.*, **2005**, 513.

181. C. Bazzicalupi, A. Bencini, S. Biagini, A. Bianchi, E. Faggi, C. Giorgi, M. Marchetta, F. Totti, B. Valtancoli, *Chem. Eur. J.*, **2009**, 15, 8049.

182. L. Shimoni-Livny, J. P. Glusker, C. W. Bock, *Inorg. Chem.*, **1998**, 37 1853.

183. G. Mahmoudi, A Bauzá, A. Frontera, *Dalton Trans.*, **2016**, 45, 4965.

184. K. Izod, C. Wills, W. Clegg, R. W. Harrington, *Organometallics*, **2009**, 28, 2211.

185. K. Izod, W. McFarlane, C. Wills, W. Clegg, R. W. Harrington, *Organometallics*, **2008**, 27, 4386.

186. M. L. Cole, A. R. Leverett, *unpublished data from the Cole group, UNSW Australia*,

187. M. L. Cole, P. C. Junk, *CrystEngComm*, **2004**, 6, 173.

188. A. I. McKay, PhD Thesis, *UNSW Australia*, Sydney, Australia, **2015**.

189. M. R. Gyton, PhD Thesis, *UNSW Australia*, Sydney, Australia, **2015**.

190. G. Berthon-Gelloz, M. A. Siegler, A. L. Spek, B. Tinant, J. N. H. Reek, I. E. Markó, *Dalton Trans.*, **2010**, 39, 1444.

191. R. S. Cahn, C. Ingold, V. Prelog, *Angew. Chem. Int. Ed.*, **1966**, 5, 385.

192. V. Prelog, G. Helmchen, *Angew. Chem. Int. Ed.*, **1982**, 21, 567.

193. P. C. Junk, M. L. Cole, *Chem. Commun.*, **2007**, 1579.

194. T. L. Brown, K. J . Lee, *Coord. Chem. Rev.*, **1993**, 128, 89.

195. H. Clavier, S. P. Nolan, *Chem. Commun.*, **2010**, 46, 841.

196. I. A. Guzei, M. Wendt, *Dalton Trans.*, **2006**, 3991.

197. M. L. Cole, A. J. Davies, C. Jones, P. C. Junk, A. I. McKay, A. Stasch, *Z. Anorg. Allg. Chem.*, **2015**, 641, 2233.

198. B. Qian, D. L. Ward, M. R. Smith, *Organometallics* **1998**, 17, 3070.

199. E. R. T. Tiekink, J. Zukerman-Schpektor, *CrystEngComm*, **2009**, 11, 2701.

200. M. C. Kuchta, G. Parkin, *New J. Chem.*, **1998**, 22, 523.

201. R. J. Alvarado, J. M. Rosenberg, A. Andreu, J. C. Bryan, W.-Z. Chen, T. Ren, K. Kavallieratos, *Inorg. Chem.*, **2005**, 44, 7951.

202. J. P. H. Charmant, M. F. Haddow, F. E. Hahn, D. Heitmann, R. Fröhlich, S. M. Mansell, C. A. Russell, D. F. Wass, *Dalton Trans.*, **2008**, 6055.

203. E. R. T. Tiekink, J. Zukerman-Schpector, *Aust. J. Chem.*, **2010**, 63, 535.

204. C. Janiak, *Dalton Trans.*, **2000**, 3885.

205. L. Hintermann, *Beilstein J. Org. Chem.*, **2007**, 3, 1.

206. C. J. F. Du, H. Hart, K. K. D. Ng, *J. Org. Chem.*, **1986**, 51, 3162.

Appendix 1 – General experimental considerations

A1.1 General methods

All synthetic manipulations were performed under strict exclusion of air and moisture through standard Schlenk and glove box techniques unless otherwise specified. All glassware was oven dried before being flame dried under vacuum to remove residual water prior to use. All solvents required for air sensitive reactions were dried, degassed and stored for use under an inert gas atmosphere. Diethyl ether, DME, THF, hexane, and toluene were distilled from sodium benzophenone ketyl and stored over 3 Å molecular sieves. Fluorobenzene was distilled from calcium hydride and stored over 3 Å molecular sieves. THF-d_8 was dried over sodium chunks, distilled under vacuum, and stored over 3 Å molecular sieves prior to use. Air sensitive solid reagents or those used in air sensitive manipulations were vacuum dried to remove absorbed moisture and stored under an atmosphere of high purity argon in a Saffron Scientific Alpha or MBRAUN LABmaster glove box. $TlCl_3$ and $PbCl_2$ from chemical suppliers were dried with excess thionyl chloride followed by extraction into THF (see Chapter 3, Section 3.9) or washing with copious amounts of hexane, respectively. Commercially obtained $SnCl_2{\cdot}(H_2O)_2$ was dried with acetic anhydride and washed with copious amounts of hexane. Organolithium reagents were decanted into J. Youngs valved flasks under argon and standardised according to literature procedures.[A207] NMR scale reactions were mixed by sonication, manual inversion, or mechanical inversion by fastening the sample tubes to the rotary joint of a rotary evaporator set to slow rotation.

A1.2 NMR spectroscopic characterisations

^{1}H and ^{13}C NMR spectra were recorded on either a Bruker Avance DPX 250 (^{1}H: 250.13 MHz, ^{13}C: 62.90 MHz), Bruker Avance DPX 300 (^{1}H: 300.30 MHz, ^{13}C: 75.52 MHz),

Bruker Avance III 300 (^{1}H: 300.17 MHz, ^{13}C: 75.48 MHz), Bruker Avance III 400 (^{1}H: 400.13 MHz, ^{13}C: 100.62 MHz), or Bruker Avance III 600 (^{1}H: 600.16 MHz, ^{13}C: 150.92 MHz) spectrometer at 298 K, unless otherwise stated. All spectra were recorded as solutions in either benzene-d_6 (C_6D_6), chloroform-d_1 ($CDCl_3$), dichloromethane-d_2 (CD_2Cl_2), dimethylsulfoxide-d_6 (DMSO-d_6), or tetrahydrofuran-d_8 (THF-d_8) and the chemical shifts were referenced to residual non-deuterated solvent peaks.[A208] Chemical shifts (δ) are reported in parts per million (ppm) and are typically accurate to ± 0.01 ppm for ^{1}H and ± 0.05 ppm for ^{13}C. Coupling constants ($^{n}J_{XY}$) are reported in Hertz (Hz). Multiplicities are denoted as singlet (s), doublet (d), triplet (t), quartet (q), septet (sept) or multiplet (m) and prefixed broad (br) where applicable.

The following two-dimensional NMR techniques were routinely used for the assignment of organic and organometallic compounds: COSY (Correlation Spectroscopy), TOCSY (Total Correlation Spectroscopy), NOESY (Nuclear Overhauser Effect Spectroscopy), HSQC (Heteronuclear Single Quantum Coherence) and HMBC (Heteronuclear Multiple Bond Correlation). All NMR spectra were processed using the Bruker Topspin software suite.

A1.3 Infrared spectroscopic characterisations

Infrared spectra were prepared as Nujol mulls on sodium chloride plates or potassium bromide discs and the spectra (4,000 to 400 cm-1) were recorded on a Nicolet Avatar 320 FTIR spectrometer. Spectra were typically obtained in 16 scans with a resolution of 4 cm^{-1}. Absorbances are reported in wavenumbers (cm^{-1}) and the intensity of the absorbance is denoted as strong (*s*), medium (*m*) or weak (*w*) and prefixed broad (*br*) or sharp (*sh*) where applicable.

A1.4 Single crystal X-ray diffraction structure analysis

All crystallographic characterisations were carried out on a Bruker APEX II diffractometer with a Bruker Quazar Multilayer Optics MoKα X-ray micro source (λ = 0.71073 Å), and an Apex II CCD detector. All datasets were corrected for absorption using SADABS.[A209] Unit cell parameters were optimised upon completion of data collection using all collected frames. Structure solution and refinement was carried out using the SHELX or OLEX suite of programs[A210,211] with the graphical user interface OLEX 2.[A211] Crystallographic information files (.cif) of each structurally characterised compound discussed herein are made available as digital copies on the attached "Special Features" DVD.

A1.5 Melting point and Elemental analysis characterisations

Melting point samples of air sensitive compounds were prepared in a glove box and determined using a Gallenkamp MPD350 melting point apparatus in sealed glass capillaries under high purity argon and are uncorrected. Decomposition points are given for samples for which melting was not observed. Microanalyses were conducted at the Campbell Microanalytical Laboratory, University of Otago, Dunedin, New Zealand, the Microanalytical Unit, Research School of Chemistry, Australian National University, Canberra, Australia, or The Chemical Analysis Facility, Macquarie University, Sydney, Australia.

Appendix 2 – Crystallographic data for Chapters 2 to 5

A2.1 Chapter 2

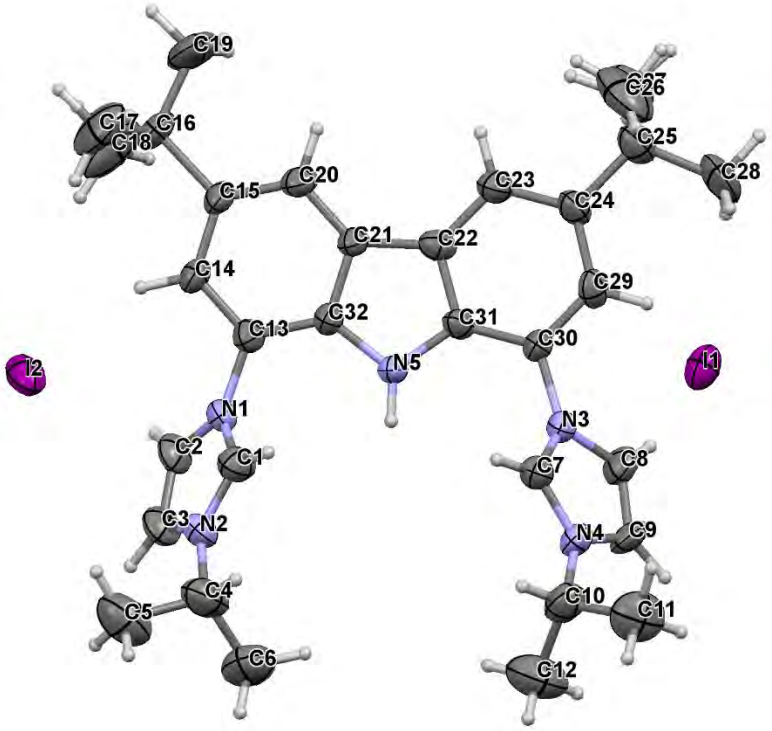

Hbimca^{iPr}(2HI), **4^{iPr}**

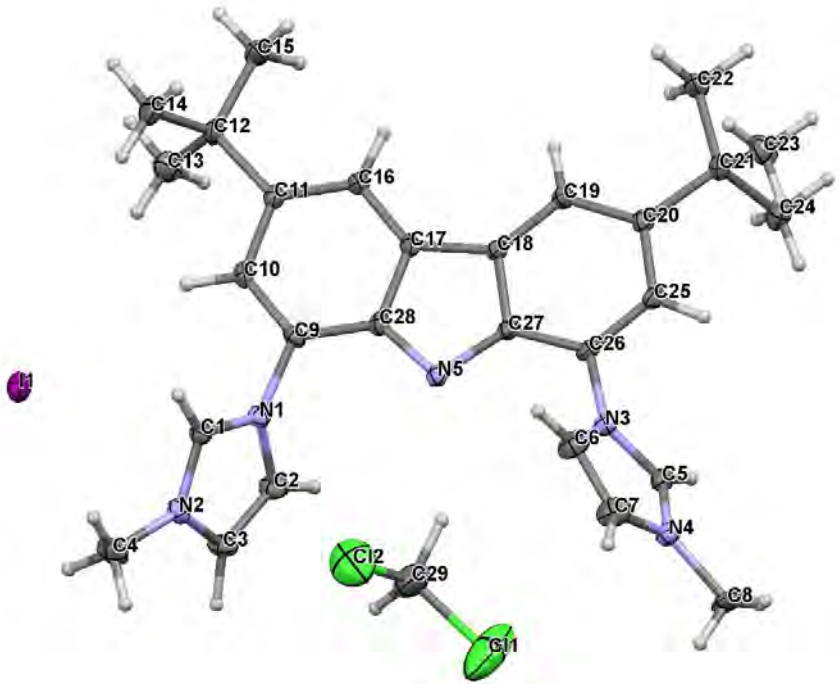

Bimca^{Me}(H_2I), **5^{Me}**

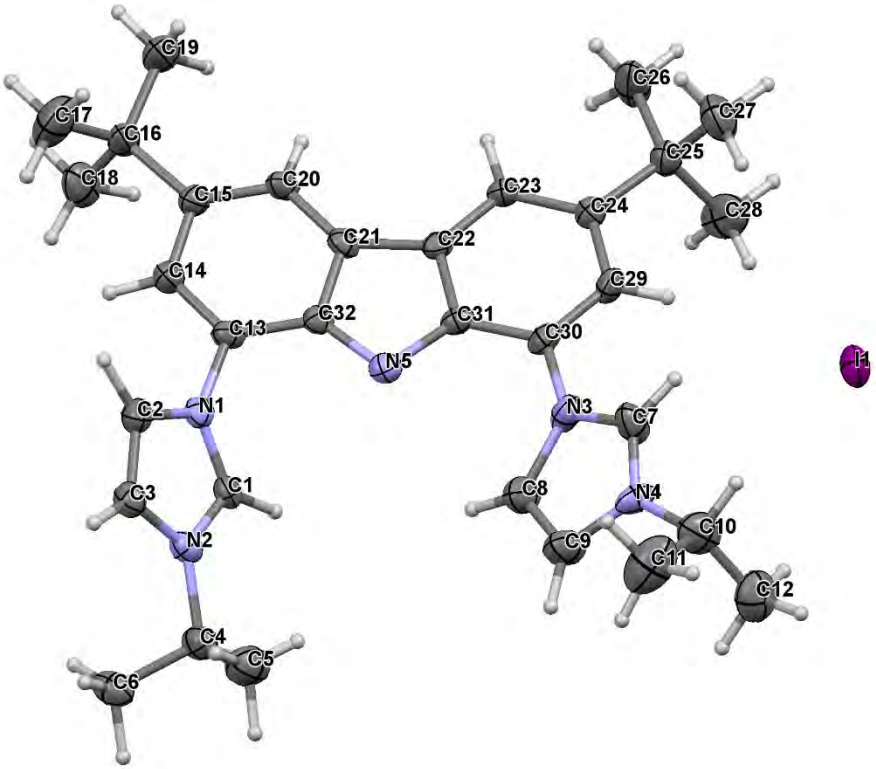

Bimca^{iPr}(H_2I), **5^{iPr}**

Parameter	bimca^{iPr}(2HI), 4^{iPr}	bimca^{Me}(H_2I)·DCM, 5^{Me}	bimca^{iPr}(H_2I)·PhF, 5^{iPr}
Empirical formula	$C_{32}H_{43}I_2N_5$	$C_{29}H_{36}Cl_2IN_5$	$C_{38}H_{47}FIN_5$
Formula weight	751.51	652.43	719.71
Temperature (K)	150(2)	150(2)	150(2)
Crystal system	triclinic	monoclinic	monoclinic
Space group	$P\bar{1}$	$P2_1/c$	$C2/c$
a (Å)	11.373(6)	13.4207(7)	26.258(3)
b (Å)	18.404(10)	24.3539(14)	8.8701(11)
c (Å)	23.130(12)	9.5113(5)	32.127(4)
α (°)	69.63(2)	90.00	90.00
β (°)	80.26(2)	106.905(2)	103.233(4)
γ (°)	76.44(2)	90.00	90.00
Volume (Å^3)	4392(4)	2974.4(3)	7284.0(14)
Z	4	4	8
ρ_{calc} (g cm^{-3})	1.137	1.457	1.313
μ (mm^{-1})	1.453	1.283	0.917
F(000)	1504.0	1328.0	2976.0
2Θ (°)	4.9 to 52.74	3.18 to 54.26	3.18 to 52.14
Refl. collected	71205	36311	18571
Independent refl.	17526	6568	7113
R_{int}	0.0774	0.0315	0.0418
Parameters	783	478	511
Goof on F^2	1.015	1.103	1.034
R_1	0.0638	0.0365	0.0665
wR_2 (all data)	0.2130	0.1094	0.1716
Description	Elongated blocks	Square plate	Square plate
Colour	Colourless	Pale yellow	Pale yellow

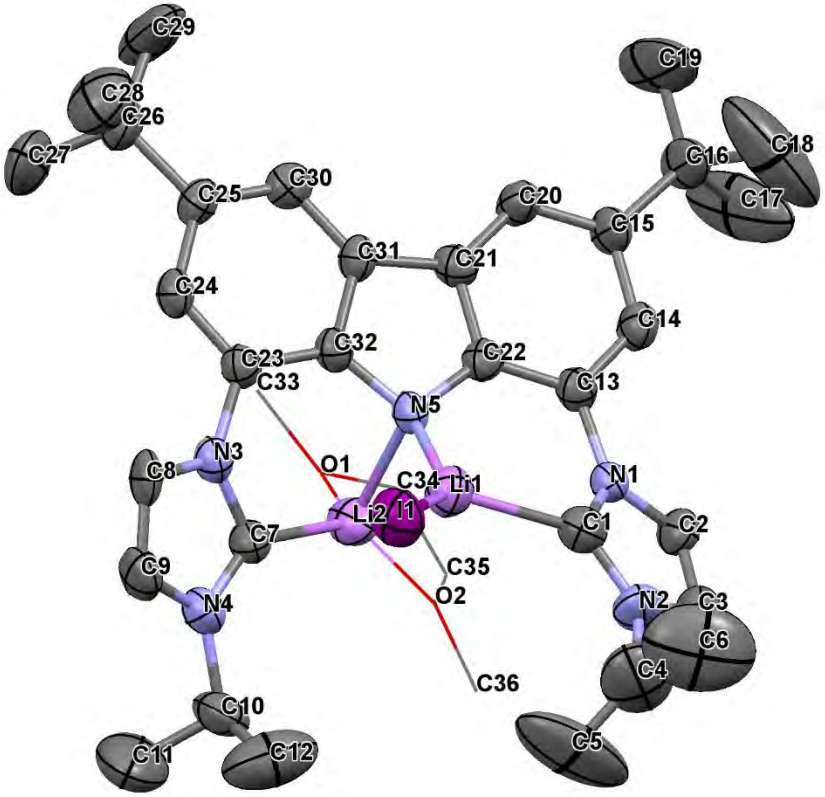

[Li(bimca^{iPr})·LiI(DME)], Li**7^{iPr}**·LiI(DME)

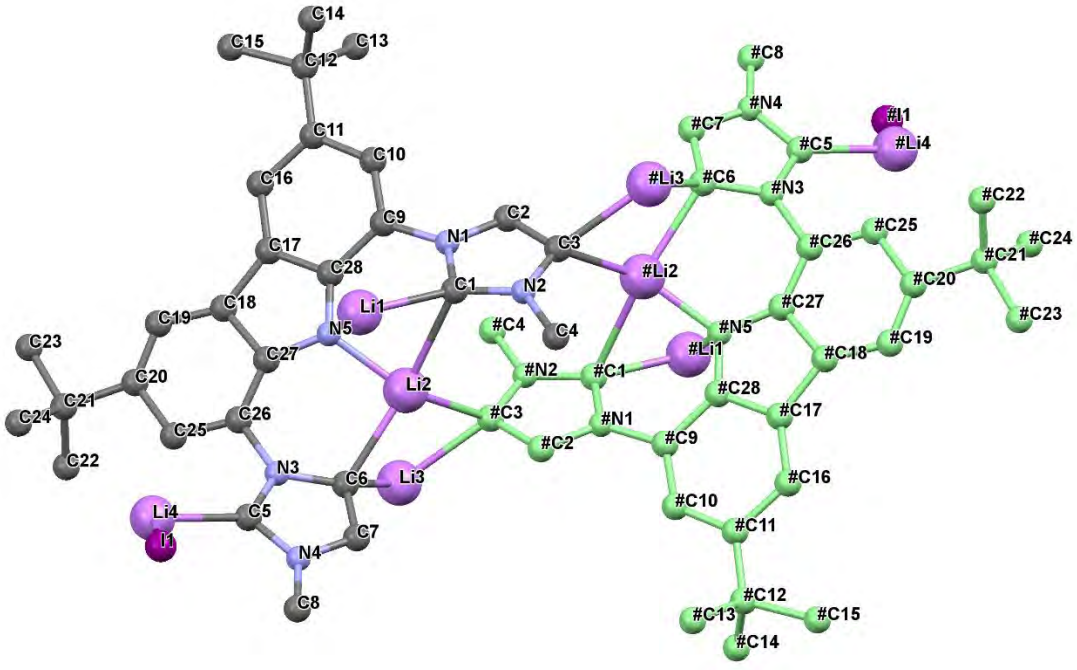

[{Li$_4$(bimca$^{'Me}$)I}$_2$], **8**

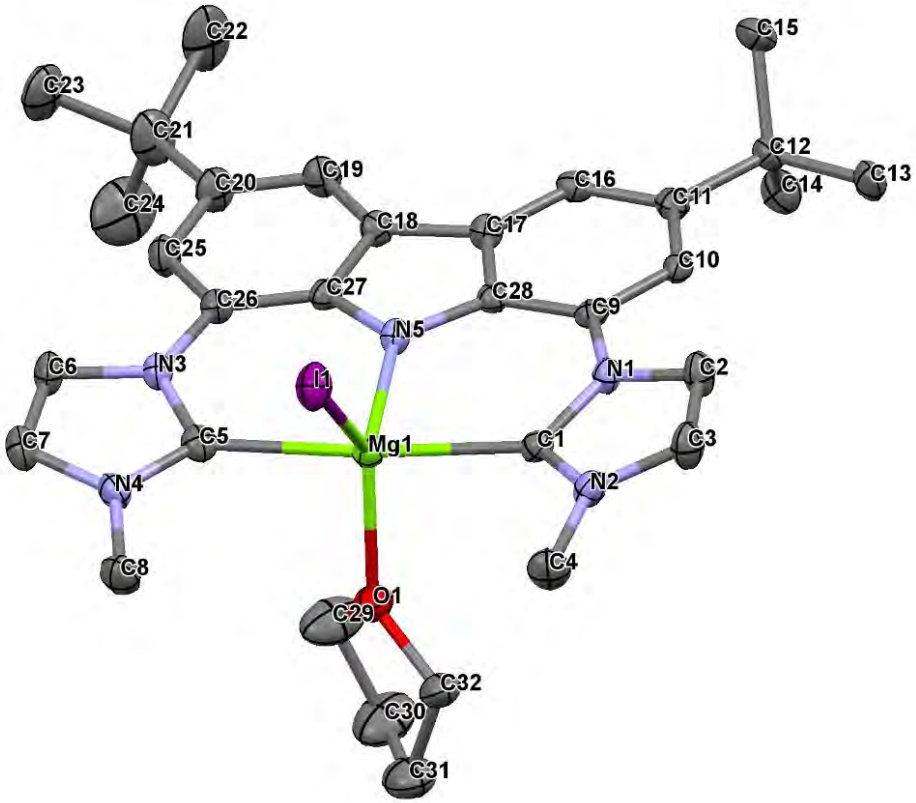

[Mg(bimca^{Me})I(THF)], **9^{Me}**

Parameter	$Li7^{iPr}$·LiI(DME)	[{$Li_4(bimca^{Me})I$}$_2$], 8	[Mg($bimca^{Me}$)I(THF)], 9^{Me}
Empirical formula	$C_{36}H_{50}ILi_2N_5O_2$	$C_{52}H_{78}ILi_4N_5O_6$	$C_{32}H_{40}N_5IMgO$
Formula weight	722.59	1023.85	661.90
Temperature (K)	150(2)	150(2)	150(2)
Crystal system	monoclinic	triclinic	orthorhombic
Space group	*C*2/*c*	$P\bar{1}$	*Pbca*
a (Å)	29.213(9)	12.7253(16)	17.7023(6)
b (Å)	13.853(4)	15.949(2)	10.7871(4)
c (Å)	22.665(7)	19.175(3)	35.0474(14)
α (°)	90	75.621(10)	90.00
β (°)	103.529(14)	70.746(6)	90.00
γ (°)	90	68.568(7)	90.00
Volume (Å^3)	8918(5)	3383.7(8)	6692.5(4)
Z	8	2	8
ρ_{calc} (g cm^{-3})	1.0763	1.005	1.314
μ (mm^{-1})	0.748	0.513	1.006
F(000)	2981.7	1076.0	2720.0
2Θ (°)	2.86 to 61.06	2.28 to 61.82	5 to 54
Refl. collected	55868	56221	114799
Independent refl.	11284	17986	7185
R_{int}	0.1047	0.6906	0.0755
Parameters	425	361	504
Goof on F^2	0.964	0.805	1.033
R_1	0.0662	0.1740	0.0352
wR_2 (all data)	0.2578	0.5742	0.1149
Description	Plate	Plate	Hexagonal plate
Colour	Colourless	Pale yellow	Pale yellow

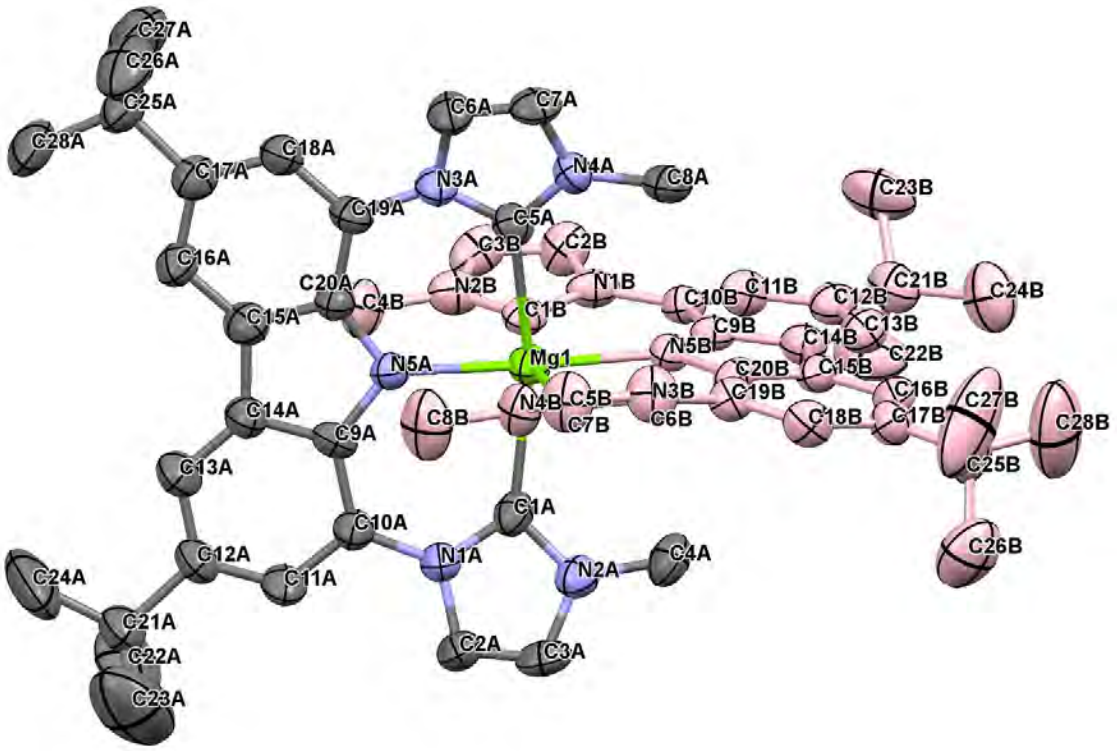

[Mg(bimca^{Me})$_2$], **10^{Me}**

Parameter	$[Mg(bimca^{Me})_2]$, 10^{Me}
Empirical formula	$C_{56}H_{64}MgN_{10}$
Formula weight	1045.69
Temperature (K)	150(2)
Crystal system	monoclinic
Space group	$P2_1/n$
a (Å)	19.377(3)
b (Å)	11.1456(13)
c (Å)	27.556(3)
α (°)	90
β (°)	100.676(9)
γ (°)	90
Volume (Å^3)	5848.3(12)
Z	4
ρ_{calc} (g cm^{-3})	1.188
μ (mm^{-1})	0.083
F(000)	2248.0
2Θ (°)	3.008 to 54.184
Refl. collected	91692
Independent refl.	12818
R_{int}	0.3338
Parameters	693
Goof on F^2	0.780
R_1	0.0944
wR_2 (all data)	wR_2 = 0.2748
Description	Hexagonal plate
Colour	Pale yellow

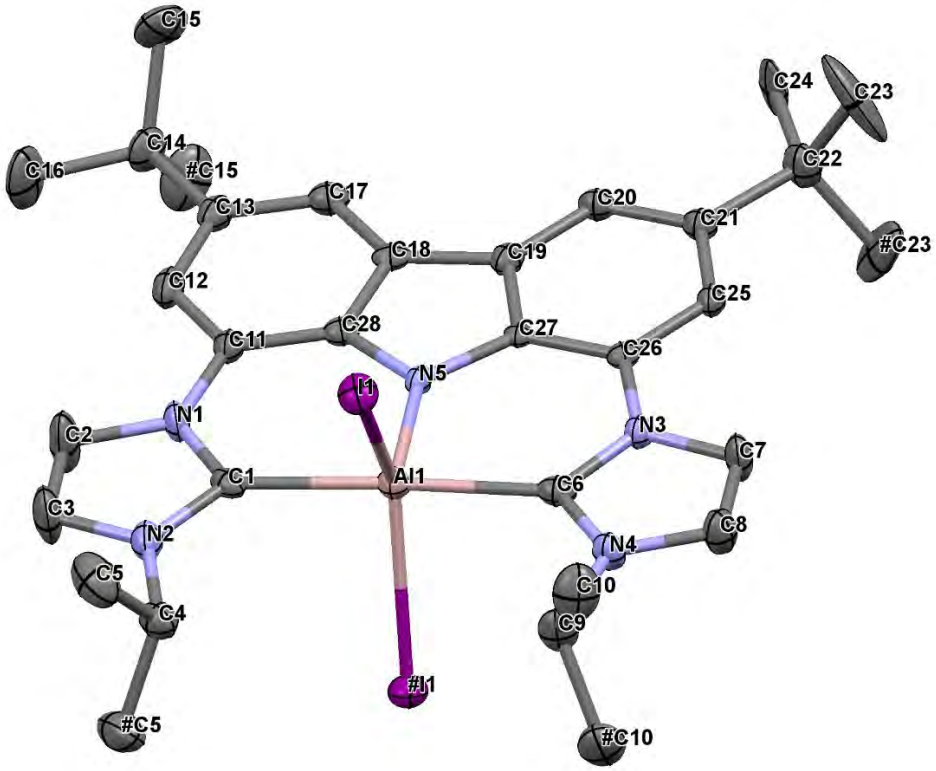

[Al(bimca^{iPr})I$_2$], **11^{iPr}**

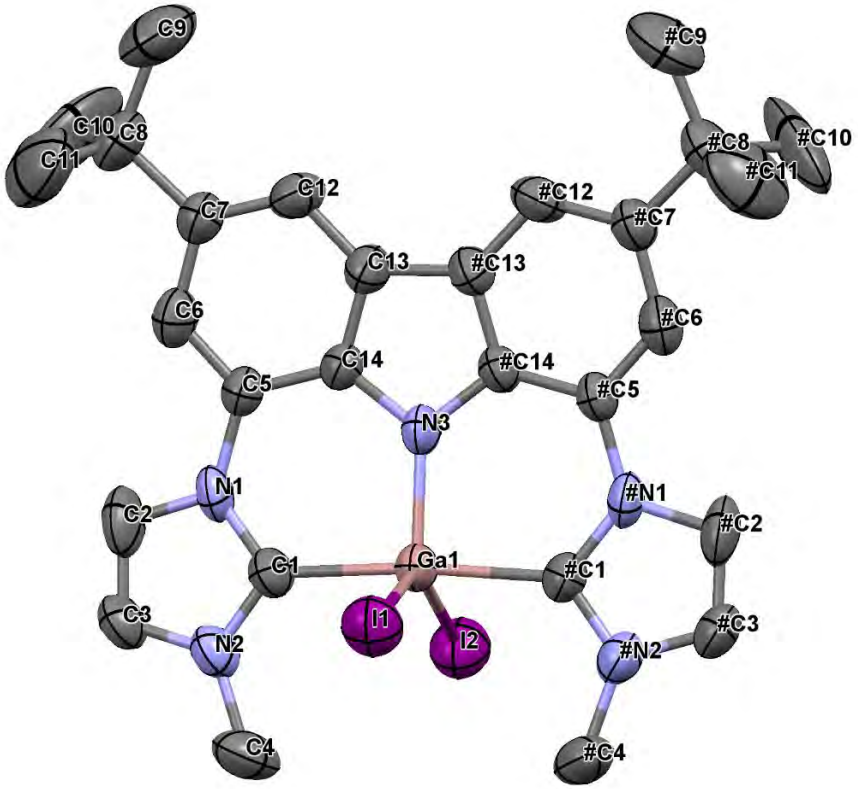

[Ga(bimca^{Me})I$_2$], **12^{Me}**

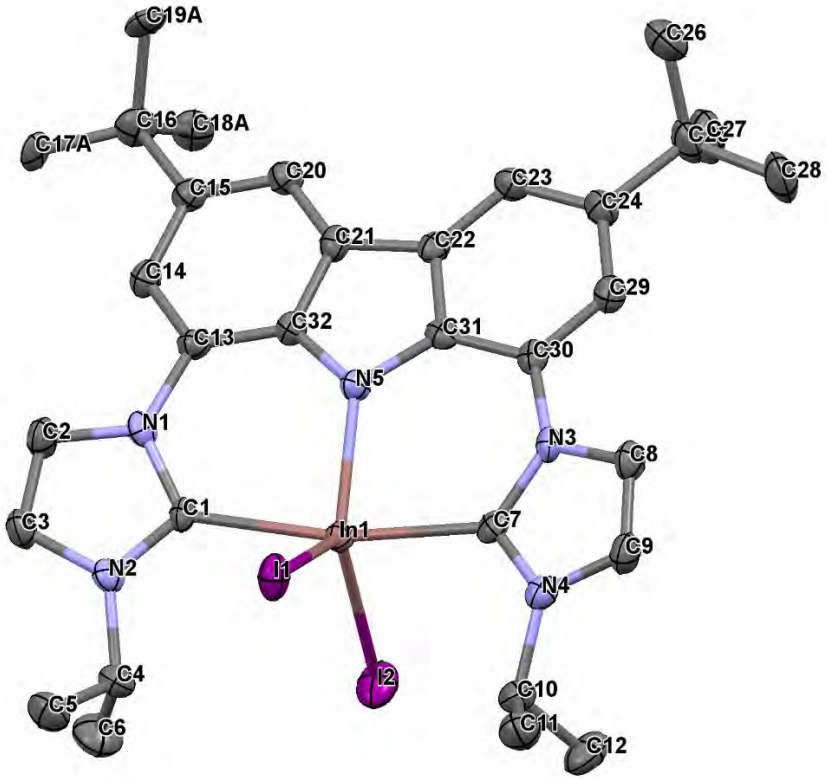

[In(bimca^{iPr})I_2], **13^{iPr}**

Parameter	[Al(bimca^{iPr})I$_2$]·PhF, **11^{iPr}**	[Ga(bimca^{Me})I$_2$], **12^{Me}**	[In(bimca^{iPr})I$_2$]·2PhF, **13^{iPr}**
Empirical formula	$C_{38}H_{42}AlFI_2N_5$	$C_{28}H_{32}GaI_2N_5$	$C_{44}H_{50}F_2I_2InN_5$
Formula weight	868.55	762.11	1055.51
Temperature (K)	150(2)	150(2)	150(2)
Crystal system	orthorhombic	monoclinic	monoclinic
Space group	*Pnma*	*C*2/*m*	*P*2$_1$/*n*
a (Å)	27.8695(15)	17.067(3)	9.3893(3)
b (Å)	9.3812(4)	16.305(2)	14.6938(5)
c (Å)	14.7912(7)	20.386(3)	31.6935(12)
α (°)	90.00	90.00	90.00
β (°)	90.00	104.088(5)	92.083(2)
γ (°)	90.00	90.00	90.00
Volume (Å^3)	3867.2(3)	5502.3(14)	4369.7(3)
Z	4	4	4
ρ_{calc} (g cm^{-3})	1.492	0.920	1.604
μ (mm^{-1})	1.686	1.636	1.998
F(000)	1732.0	1488.0	2088.0
2Θ (°)	4.02 to 52	2.06 to 58.52	3.06 to 54.08
Refl. collected	19321	26222	71413
Independent refl.	4036	7582	9498
R_{int}	0.0485	0.0495	0.0371
Parameters	337	173	593
Goof on F^2	1.025	0.975	1.083
R_1	0.0308	0.0702	0.0455
wR_2 (all data)	0.0782	0.2488	0.1218
Description	Hexagonal plate	Hexagonal plate	Hexagonal plate
Colour	Pale amber	Pale beige	Pale yellow

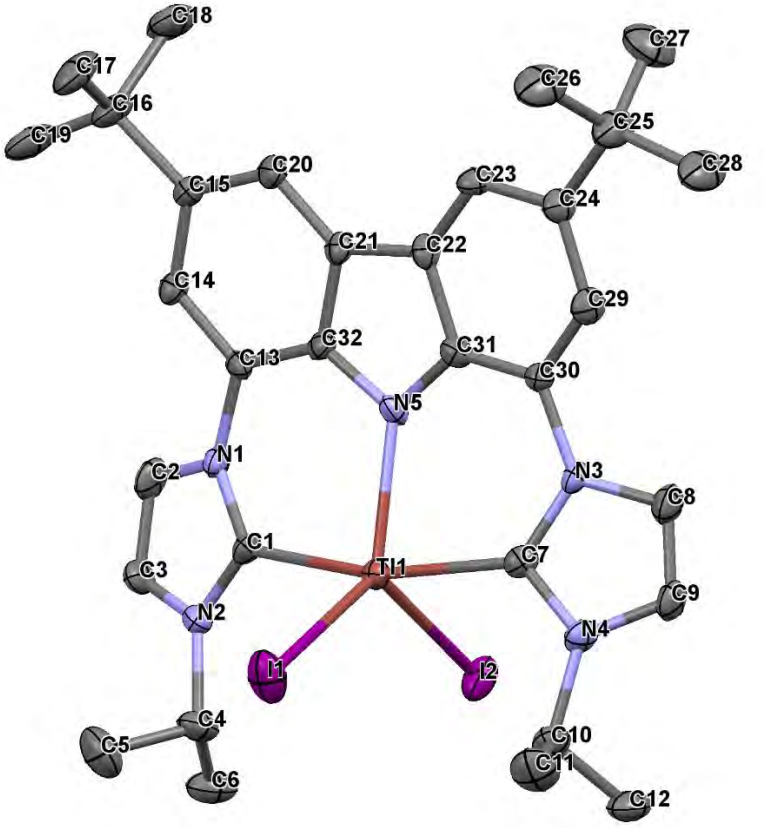

[Tl(bimca^{iPr})I$_2$], **14^{iPr}**

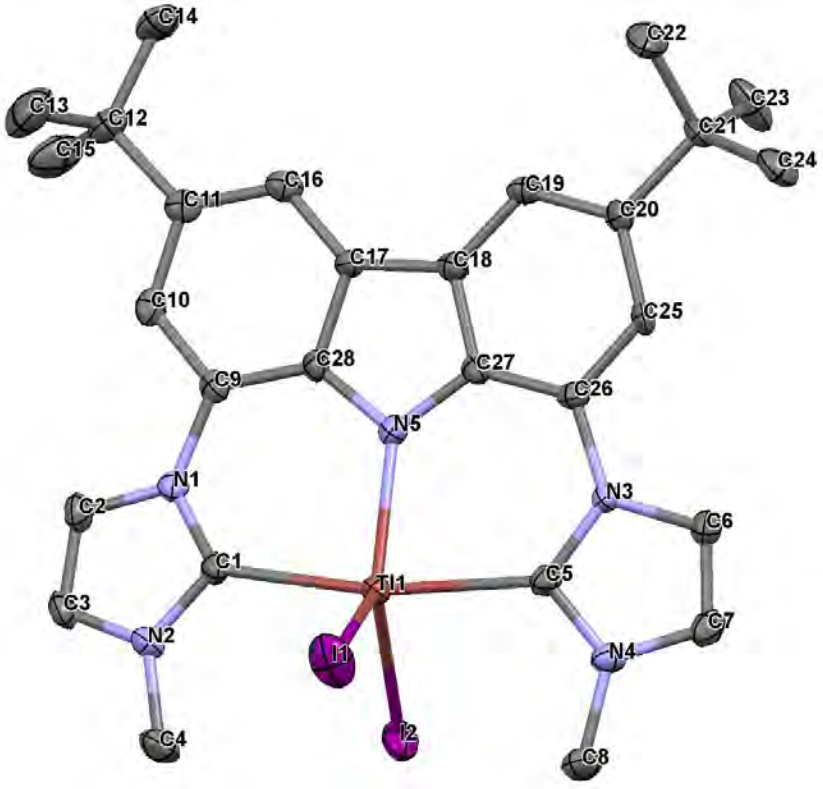

[Tl(bimca^{Me})I$_2$], **14^{Me}**

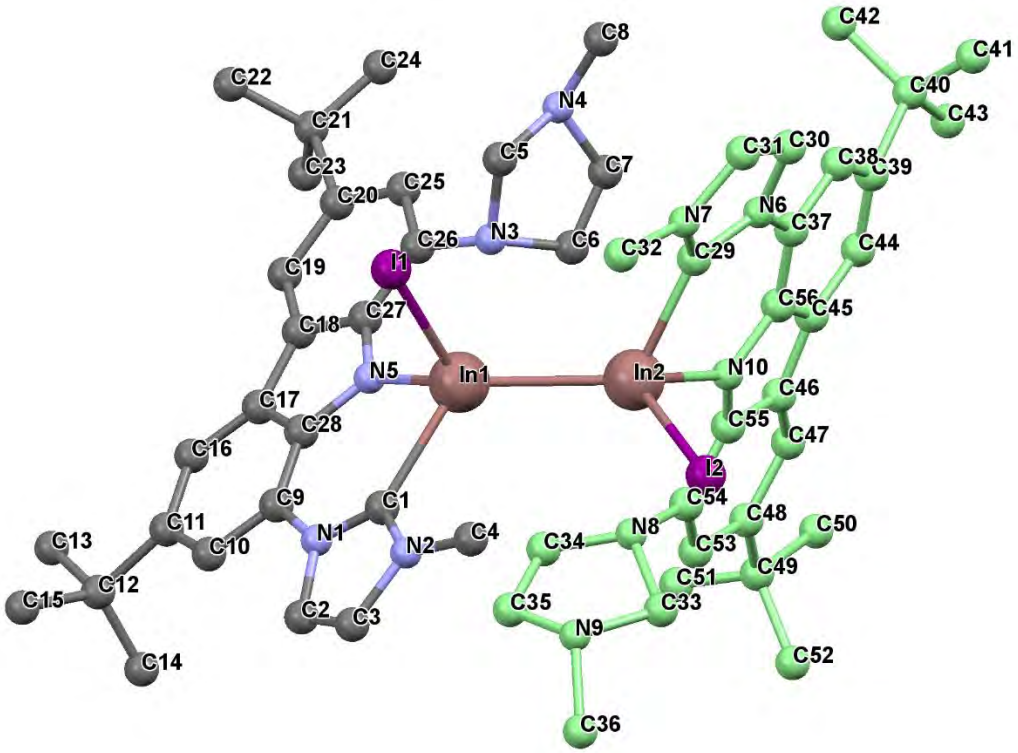

[{In(bimca'^{Me}HH)I}$_2$], **17**

Parameter	[Tl(bimca^{iPr})I$_2$]·PhF, 14^{iPr}	Tl(bimca^{Me})I$_2$]·2THF, 14^{Me}	In(II) dimer, 17
Empirical formula	$C_{38}H_{45}FI_2N_5Tl$	$C_{36}H_{48}I_2N_5O_2Tl$	$C_{56}H_{68}N_{10}I_2In_2$
Formula weight	1048.96	1040.96	1392.06
Temperature (K)	150(2)	150(2)	150(2)
Crystal system	monoclinic	triclinic	triclinic
Space group	$P2_1/n$	$P\bar{1}$	$P\bar{1}$
a (Å)	9.3886(7)	11.8479(10)	18.430(5)
b (Å)	14.6770(10)	12.9898(12)	19.794(5)
c (Å)	31.661(2)	13.1729(12)	20.435(5)
α (°)	90.00	92.110(4)	100.334(13)
β (°)	91.321(3)	108.385(4)	98.142(16)
γ (°)	90.00	99.628(4)	110.122(17)
Volume (Å^3)	4361.6(5)	1888.0(3)	6717(3)
Z	4	2	8
ρ_{calc} (g cm^{-3})	1.597	1.831	1.377
μ (mm^{-1})	5.152	5.950	1.646
F(000)	2016.0	1004.0	2740.0
2Θ (°)	2.58 to 57.92	5.32 to 50	2.08 to 54.2
Refl. collected	41641	17390	101563
Independent refl.	11420	6570	28254
R_{int}	0.0531	0.0419	0.5829
Parameters	464	423	539
Goof on F^2	1.146	1.041	0.944
R_1	0.0551	0.0289	0.1535
wR_2 (all data)	0.1522	0.0671	0.5339
Description	Hexagonal plate	Hexagonal plate	Amygdaloidal
Colour	Orange	Orange	Brown

A2.3 Chapter 4

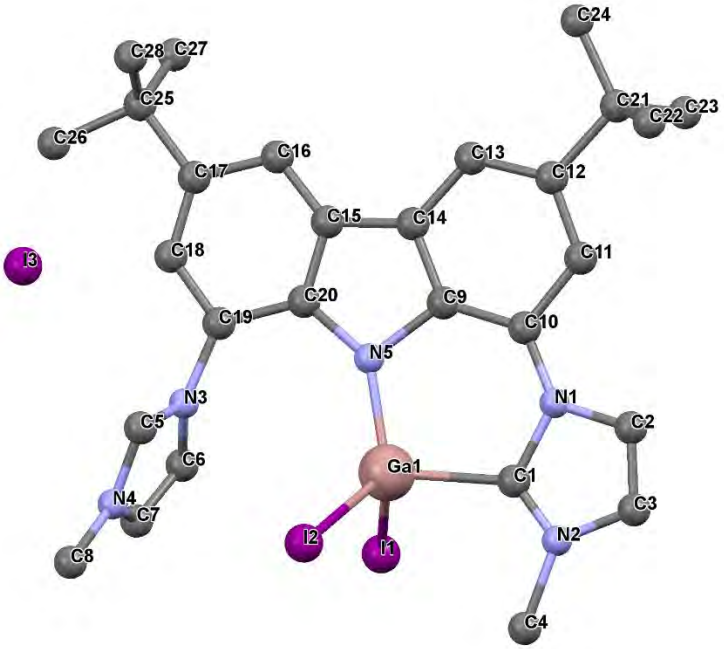

[Ga(bimca'^{Me}H)I_2][I], **22^{Me}**

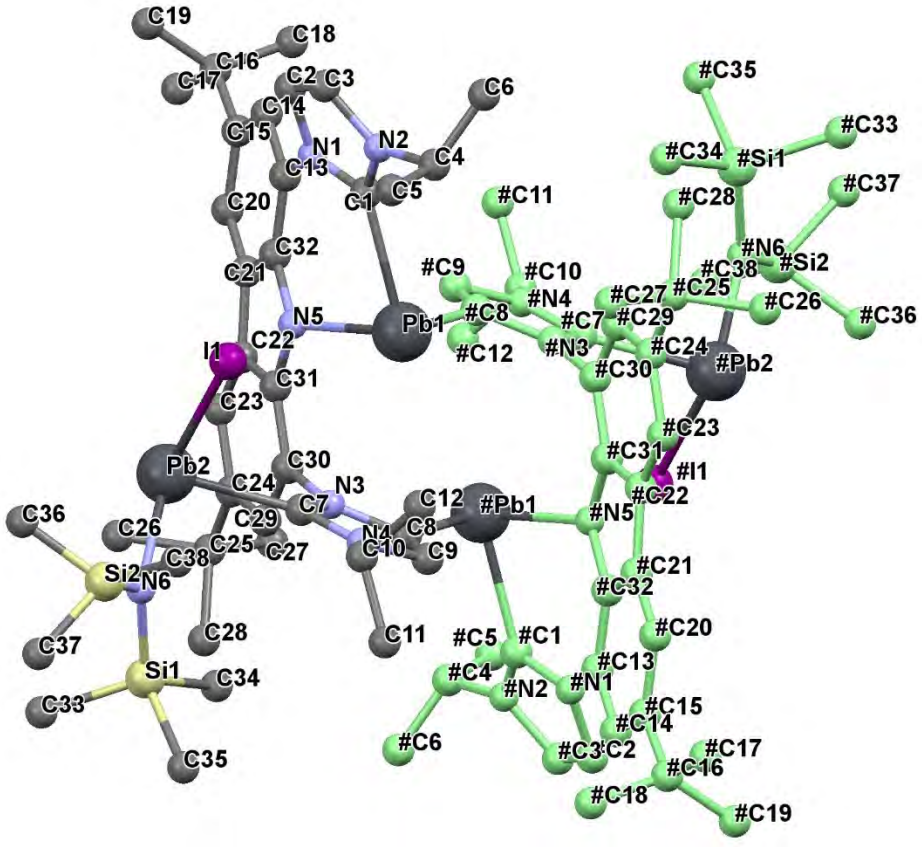

[{Pb_2(bimca'^{iPr})(HMDS)I}$_2$], **27^{iPr}**

Parameter	[Ga(bimca^{Me}H)I$_2$][I], 22^{Me}	Pb(II) dimer, 27^{iPr}
Empirical formula	$C_{28}H_{33}GaI_3N_5$	$C_{76}H_{114}N_{12}I_2Si_4Pb_2$
Formula weight	1041.19	2390.78
Temperature (K)	150(2)	150(2)
Crystal system	triclinic	monoclinic
Space group	$P\bar{1}$	$C2/c$
a (Å)	9.069(2)	38.945(5)
b (Å)	13.242(3)	14.9080(16)
c (Å)	16.990(5)	22.079(3)
α (°)	93.114(17)	90.00
β (°)	103.522(16)	123.777(8)
γ (°)	100.867(15)	90.00
Volume (Å^3)	1938.0(8)	10655(2)
Z	2	16
ρ_{calc} (g cm^{-3})	1.784	1.490
μ (mm^{-1})	3.135	6.963
F(000)	1010.0	4576.0
2Θ (°)	3.8 to 61.1	2.52 to 57.56
Refl. collected	21554	20853
Independent refl.	11059	10217
R_{int}	0.3668	0.2223
Parameters	177	244
Goof on F^2	0.978	0.759
R_1	0.1344	0.0950
wR_2 (all data)	0.3700	0.2719
Description	Plate	Plate
Colour	Colourless	Pale yellow

A2.4 Chapter 5

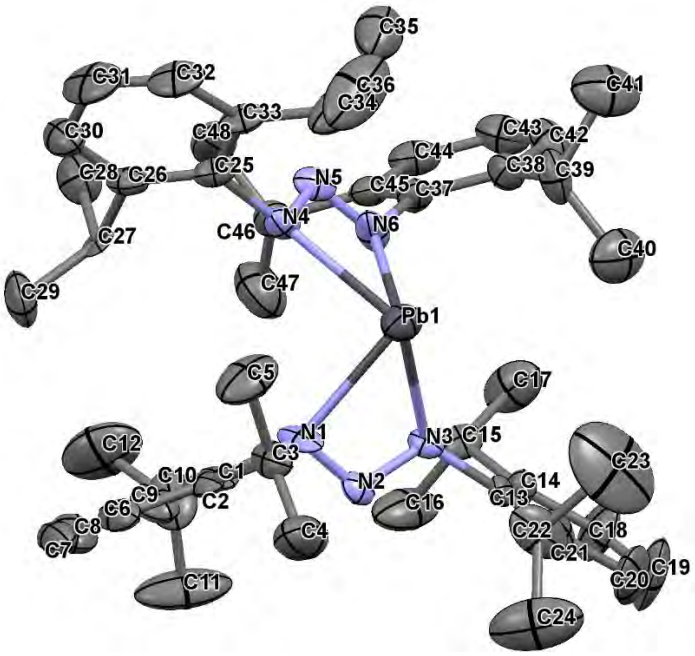

$[Pb(Dipp_2N_3)_2]$, **28**

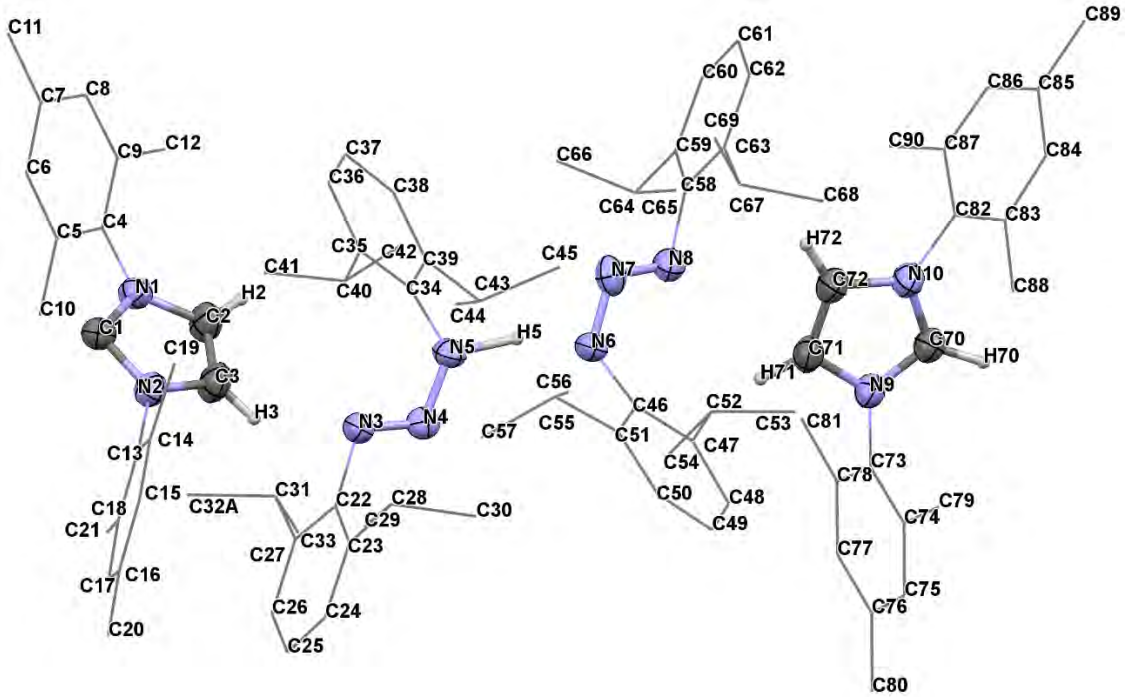

$[IMes][Dipp_2N_3H][Dipp_2N_3][IMes(H)]$, **31**

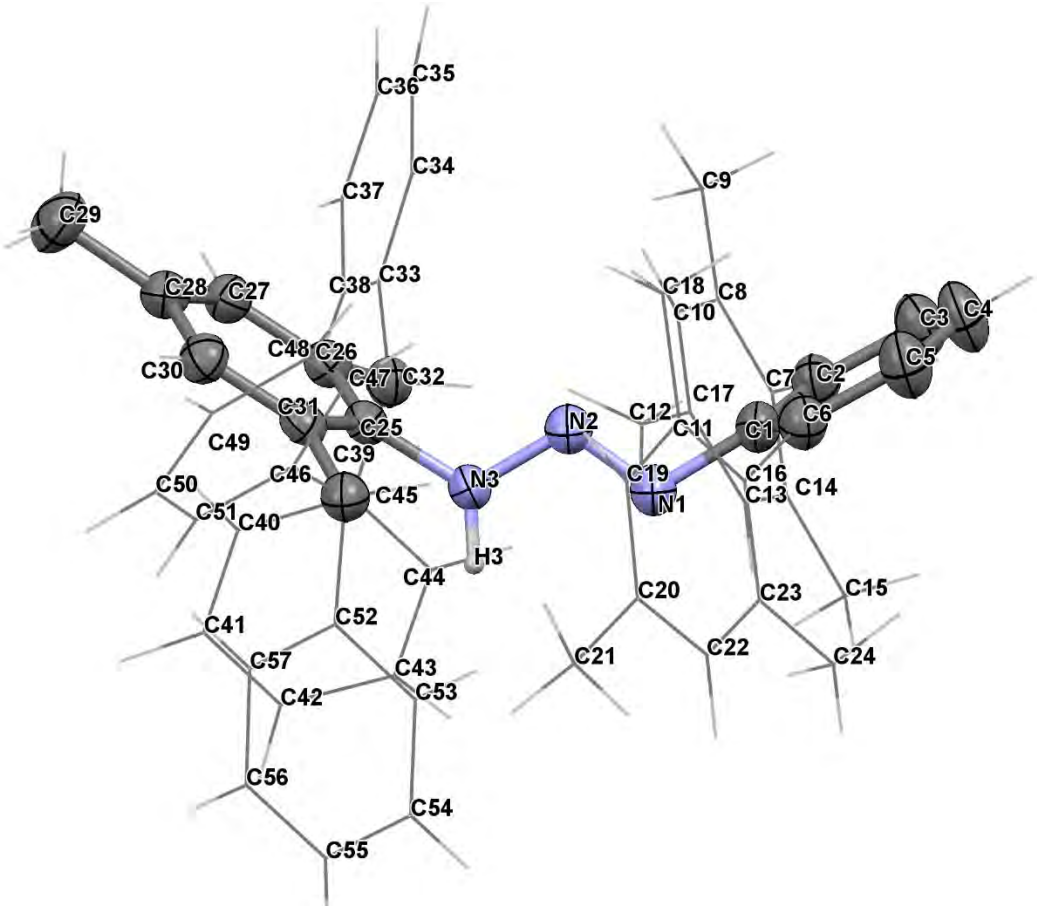
C36
C35
C34
C37
C29
C9
C28
C27
C38
C33
C18
C8
C10
C3
C4
C48
C26
C5
C30
C47
C32
C7
C2
C17
C31
C12
C6
C25
N2
C11
C1
C49
C39
C19
C16
C50
C46
N3
C13
C14
C45
N1
C51
C40
H3
C44
C20
C23
C15
C41
C52
C21
C22
C24
C57
C43
C42
C53
C56
C54
C55

Rock*N_3H, **33**

Parameter	[Pb(Dipp$_2$N$_3$)$_2$], 28	31·Toluene	Rock*N$_3$H, 33
Empirical formula	$C_{48}H_{68}N_6Pb$	$C_{97}H_{126}N_{10}$	$C_{57}H_{53}N_3$
Formula weight	936.27	1432.07	780.02
Temperature (K)	150(2)	150(2)	150(2)
Crystal system	monoclinic	monoclinic	monoclinic
Space group	$P2_1/c$	$P2_1/c$	$P2_1/n$
a (Å)	14.6229(8)	22.160(2)	10.5970(13)
b (Å)	16.3348(9)	19.2476(19)	24.772(4)
c (Å)	20.6588(12)	21.202(2)	17.603(2)
α (°)	90	90	90.00
β (°)	109.608(3)	100.849(6)	104.316(5)
γ (°)	90	90	90.00
Volume (Å^3)	4648.4(5)	8881.9(16)	4477.4(10)
Z	4	4	4
ρ_{calc} (g cm^{-3})	1.338	1.071	1.157
μ (mm^{-1})	3.667	0.063	0.067
F(000)	1920.0	3112.0	1664.0
2Θ (°)	2.956 to 61.146	4.422 to 61.22	4.06 to 50
Refl. collected	75948	118673	29173
Independent refl.	14181	24414	7848
R_{int}	0.0963	0.1163	0.0919
Parameters	688	1016	753
Goof on F^2	1.058	0.945	1.021
R_1	0.0781	0.0739	0.0607
wR_2 (all data)	0.2646	0.2636	0.1766
Description	Block	Block	Block
Colour	Orange	Colourless	Colourless

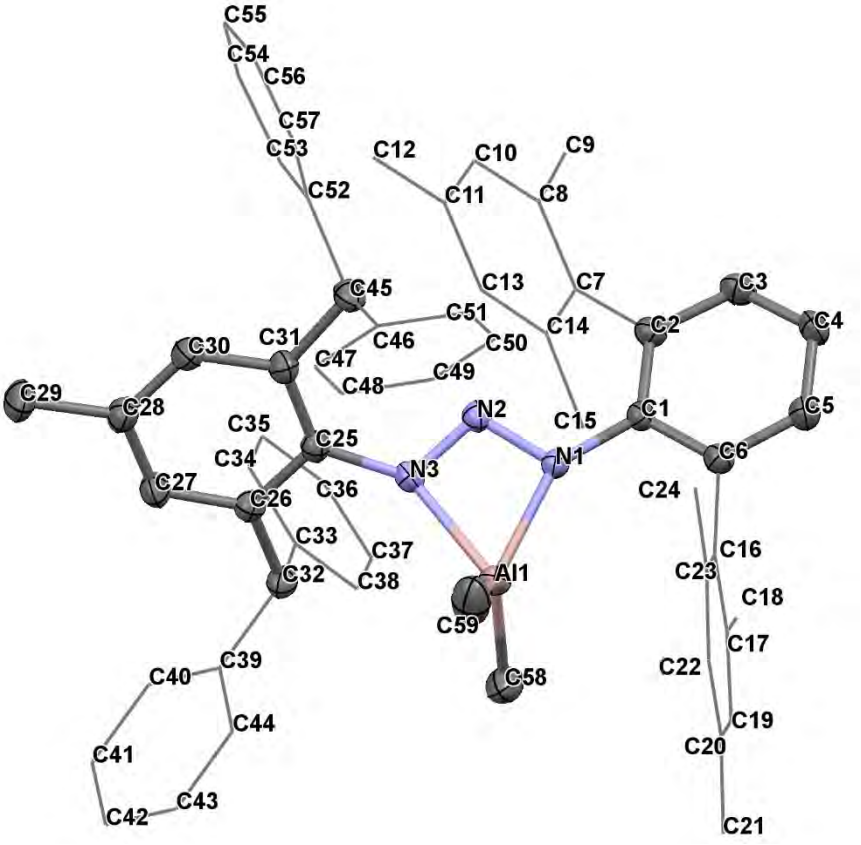

[AlMe$_2$(Rock*N$_3$)], **34**

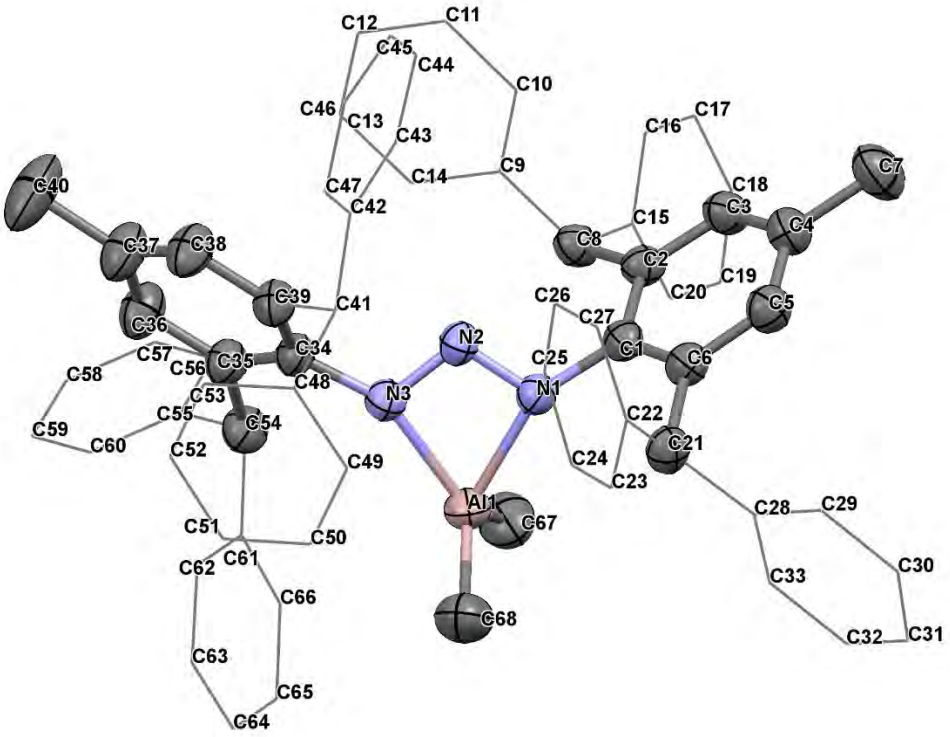

[AlMe$_2$(Dipp*$_2$N$_3$)], **35**

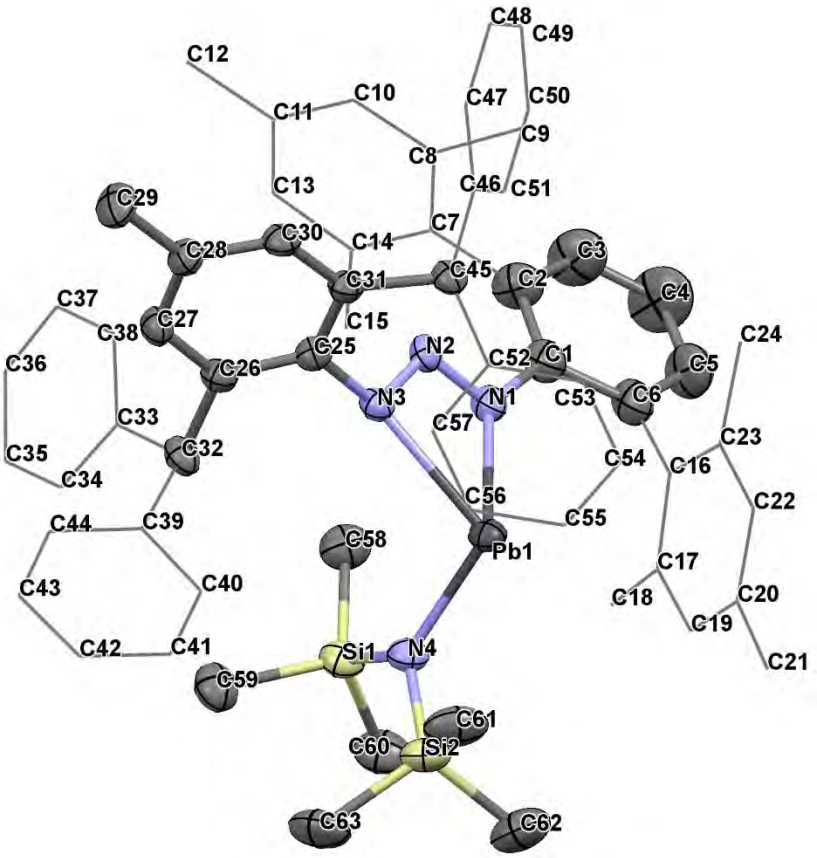

[Pb(Rock*N_3)(HMDS)], **36**

Parameter	[AlMe$_2$(Rock*N$_3$)], 34	[AlMe$_2$(Dipp*$_2$N$_3$)], 35	[Pb(Rock*N$_3$)(HMDS)], 36
Empirical formula	$C_{59}H_{58}AlN_3$	$C_{68}H_{60}AlN_3$	$C_{63}H_{70}N_4PbSi_2$
Formula weight	836.06	962.30	1146.60
Temperature (K)	150(2)	150(2)	150(2)
Crystal system	triclinic	triclinic	tetragonal
Space group	$P\bar{1}$	$P\bar{1}$	$P4/n$
a (Å)	12.156(3)	10.9317(4)	30.4242(18)
b (Å)	13.239(3)	12.8249(5)	30.4242(18)
c (Å)	15.814(4)	21.0420(8)	13.7971(10)
α (°)	81.255(11)	97.176(2)	90.00
β (°)	85.823(11)	96.680(2)	90.00
γ (°)	72.979(12)	94.698(2)	90.00
Volume (Å^3)	2404.1(10)	2893.11(19)	12771.0(14)
Z	2	2	8
ρ_{calc} (g cm^{-3})	1.155	1.105	1.193
μ (mm^{-1})	0.083	0.077	2.717
F(000)	892.0	1036.0	4688.0
2Θ (°)	5.76 to 54.74	4.46 to 54.08	1.9 to 54.08
Refl. collected	33555	47455	309171
Independent refl.	10361	12577	14003
R_{int}	0.0769	0.0615	0.0784
Parameters	789	657	648
Goof on F^2	1.047	1.042	1.153
R_1	0.0573	0.0847	0.0466
wR_2 (all data)	0.1741	0.2915	0.1577
Description	Rhomboid	Rhomboid	Rhomboid
Colour	Yellow	Yellow	Orange

Appendix 3 – Publications in support of this thesis

A3.1 Journal article

E. Jürgens, K. N. Buys, A. T. Schmidt, S. K. Furfari, M. L. Cole, M. Moser, F. Rominger, D. Kunz, "Optimised Synthesis of Monoanionic Bis(NHC)-Pincer Ligand Precursors and their Li-Complexes," *New J. Chem.*, **2016**, 40, 9160.

A3.2 Oral presentations

K. N. Buys, "Pincer Ligands to Study *s*- and *p*-Block Metals," *29th Reactive Organometallics Symposium*, (24.6.**2016**), UNSW Australia, Sydney, Australia.

A3.3 Conference papers

K. N. Buys, M. L. Cole, D. Kunz, "Using Bis-NHC Pincer Ligands to Study *s*- and *p*-block Halides and Hydrides," *42nd International Conference on Coordination Chemistry*, (3-8.7.**2016**), Brest, France.

K. N. Buys, M. L. Cole, D. Kunz, "Using Bis-NHC Pincer Ligands to Study *s*- and *p*-block Halides and Hydrides," *9th Australian Organometallics Discussion Meeting*, (8-11.12.**2015**), University of Sydney, Sydney, Australia.

M. L. Cole, D. Kunz, K. N. Buys, S. K. Furfari "Towards the Use of Pincer Ligands to Stabilise Main Group Hydrides," *8th Australian Organometallics Discussion Meeting*, (22-25.7.**2014**), James Cook University, Townsville, Australia.

A4 Appendix references

A1. T. R. Hoye, B. M. Eklov, M. Voloshin, *Org. Lett.*, **2004**, 6, 2567.

A2. G. R. Fulmer, A. J. M. Miller, N. H. Sherden, H. E. Gottlieb, A. Nudelman, B. M. Stoltz, J. E. Bercaw, K. I. Goldberg, *Organometallics*, **2010**, 29, 2176.

A3. G. M. Sheldrick *SADABS, A program for area detector absorption correction*, Bruker Analytical X-Ray-Division: Madison, Wisconsin, USA, 2008.

A4. G. M. Sheldrick, *Acta Crystallogr., Sect. A: Found. Crystallogr.*, **2008**, 64, 112.

A5. O. V. Dolomanov, L. J. Bourhis, R. J. Gildea, J. A. K. Howard, H. Puschmann, *J. Appl. Cryst.*, **2009**, 42, 339.